

U.S. DEPARTMENT OF COMMERCE
National Technical Information Service

AD-A024 271

HANDBOOK FOR FORECASTERS IN THE MEDITERRANEAN
WEATHER PHENOMENA OF THE MEDITERRANEAN BASIN;
PART 1. GENERAL DESCRIPTION OF THE METEOROLOGICAL
PROCESSES

NAVAL ENVIRONMENTAL PREDICTION RESEARCH FACILITY

NOVEMBER 1975

UNCLASSIFIED

SECURITY CLASSIFICATION OF THIS PAGE (When Data Entered)

REPORT DOCUMENTATION PAGE		READ INSTRUCTIONS BEFORE COMPLETING FORM
1. REPORT NUMBER ENVPREDRSCHFAC Technical Paper No. 5-75	2. GOVT ACCESSION NO.	3. RECIPIENT'S CATALOG NUMBER
4. TITLE (and Subtitle) Handbook for Forecasters in the Mediterranean; Weather Phenomena of the Mediterranean Basin; Part 1: General Description of the Meteorological Processes	5. TYPE OF REPORT & PERIOD COVERED	
7. AUTHOR(s) Elmar R. Reiter	6. PERFORMING ORG. REPORT NUMBER	
9. PERFORMING ORGANIZATION NAME AND ADDRESS Environmental Prediction Research Facility, Naval Postgraduate School Monterey, CA 93940	8. CONTRACT OR GRANT NUMBER(s)	
11. CONTROLLING OFFICE NAME AND ADDRESS Naval Air Systems Command Department of the Navy Washington, D.C. 20361	10. PROGRAM ELEMENT, PROJECT, TASK AREA & WORK UNIT NUMBERS ENVPREDRSCHFAC WU 055:2-2	
14. MONITORING AGENCY NAME & ADDRESS (if different from Controlling Office)	12. REPORT DATE November 1975	
	13. NUMBER OF PAGES 339	
	15. SECURITY CLASS. (of this report) UNCLASSIFIED	
16. DISTRIBUTION STATEMENT (of this Report) Approved for public release; distribution unlimited.		
17. DISTRIBUTION STATEMENT (of the abstract entered in Block 20, if different from Report)		
18. SUPPLEMENTARY NOTES Qualified requestors may obtain additional copies from the Defense Documentation Center. All others should apply to the National Technical Information Service.		
19. KEY WORDS (Continue on reverse side if necessary and identify by block number) Mediterranean Sea Jet streams Meteorology Orographic effects Climatology Weather regimes Meteorological phenomena Cyclone tracks		
20. ABSTRACT (Continue on reverse side if necessary and identify by block number) An overview of the interacting meteorological processes that affect Mediterranean weather systems on a regional and local basis is presented in Part 1 of the <u>Handbook for Forecasters in the Mediterranean</u> , a document intended to meet the needs of both operational and research meteorologists for working information and source materials. This first part		

DD FORM 1473

EDITION OF 1 NOV 68 IS OBSOLETE

UNCLASSIFIED

REPRODUCED BY
NATIONAL TECHNICAL
INFORMATION SERVICEU.S. DEPARTMENT OF COMMERCE
SPRINGFIELD, VA. 22161

SECURITY CLASSIFICATION OF THIS PAGE (When Data Entered)

UNCLASSIFIED

SECURITY CLASSIFICATION OF THIS PAGE(When Data Entered)

19. Key Words (continued)

Cyclogenesis
Wind regimes
Mesoscale phenomena
Diurnal effects
Clear air turbulence

Atmospheric refraction
Dust storms
Small scale phenomena
Meteorological scales
interaction

20. Abstract (continued)

comprises five major sections and eight appendixes with a comprehensive list of references. Among the subjects addressed are: geography and wind systems of the Mediterranean region; the concept of meteorological scales; present knowledge of large scale flow, jet stream interactions, orographic influences, and regional weather regimes and types; important local wind regimes such as the mistral, bora, etesian and sirocco; mesoscale phenomena, including diurnal effects; and areas of atmospheric physics relevant to an understanding of Mediterranean weather regimes including such small scale processes as clear air turbulence, air-sea interactions, and electromagnetic and acoustic refraction. Extensive climatological information is presented throughout the text. Selected meteorological relationships are examined in full mathematical treatments in the appendixes. Listings of pertinent meteorological units, conversion formulas and scales are provided.

ACQUISITION FOR	
NTIS	<input checked="" type="checkbox"/>
DDC	<input type="checkbox"/>
U.S.A.	<input type="checkbox"/>
BY	
DIST.	
Dist.	
A	

UNCLASSIFIED

SECURITY CLASSIFICATION OF THIS PAGE(When Data Entered)

LIST III: Item Nos. 2, 4, 5, 6, 8, and 11.

LIST V: Item Nos. 1 and 2.

LIST VII: Item Nos. 1, 3, 4, 5, 6, and 11.

LIST VIII: Item No. 1.

LIST IX: Item No. 2.

LIST XI:: Item Nos. 1 and 2.

LIST XII: Item Nos. 4 and 5.

LIST XIII: Item Nos. CAN-3 and 13, DEN-1, ENG-1, 2, 5, 10, and 11, FIN-1, FRA-1, 3, and 5, GER-1, 2, and 3, ISR-1, ITL-1, 2, and 5, NET-1, 2, and 3, NOR-1 and 3, SWE-1, 4, and 5, ALP-1, and TUR-1.

HANDBOOK FOR FORECASTERS
IN THE MEDITERRANEAN

WEATHER PHENOMENA OF THE MEDITERRANEAN BASIN

PART 1: GENERAL DESCRIPTION OF THE
METEOROLOGICAL PROCESSES

BY

ELMAR R. REITER

NOVEMBER 1975

ENVIRONMENTAL PREDICTION RESEARCH FACILITY
NAVAL POSTGRADUATE SCHOOL
MONTEREY, CALIFORNIA 93940

FOREWORD

This monograph on environmental forecasting in the Mediterranean was developed as a major part of the Environmental Prediction Research Facility's continuing effort to improve the quality of all types of forecasts issued for this area of the world.

As emphasized by Professor Reiter in his preface, it is intended that the information presented herein should continually respond to the current requirements of Fleet forecasters. Readers are therefore urged to submit to this Command their comments and suggestions regarding both the present content and additional topics that might merit discussion in subsequent sections.

I express my personal gratitude to Professor Reiter for undertaking a project of this magnitude during an already busy schedule. It will be readily apparent that this product of his effort is an important contribution to the literature of the meteorological sciences, and that it amply reflects his considerable expertise in the scientific fields addressed.

R. G. SHERAR
Captain, U.S. Navy

PREFACE

Weather prediction in the Mediterranean region, a demanding task even for the local forecaster, can often become a very frustrating experience for the "outsider" who may be unaware of the intricate and complex modifying effects that local topography can have on the region's synoptic-scale weather systems. It is intended that this volume shall serve as an informative primer and workbook for both the "outsider" and the local forecaster, inasmuch as it will discuss many of the complex details that affect Mediterranean weather systems on a regional and local basis.

This first part of the total monograph is divided into five major sections and eight appendixes, with a comprehensive list of references.

Section I describes and discusses general aspects of the Mediterranean region's geography and the wind systems that have prevailed in the area for centuries.

Section II explains the concept of meteorological scales; consideration of this section reveals, of course, that all scales of motion act in unison -- a difficult task for present computer models to handle, thus placing a heavy burden of interpretation on the regional meteorologist on land or aboard ship.

Section III, the focal point of this first part, explores our present knowledge of large-scale flow and weather regimes and types in the Mediterranean region.

Section IV discusses aspects of mesoscale phenomena.

Section V addresses both those areas of atmospheric physics of specific interest to military environmental specialists but beyond the scope of routine weather forecasts, and small scale processes (e.g., clear air turbulence) of interest mainly to aviation forecasters.

Certain meteorological relationships are examined in a full mathematical treatment in the appendixes. Although it was felt that this material should be available, it was decided to present it in appendix format to preclude unnecessary complication of the main text. The appendixes also contain extensive reference information, including a listing of pertinent meteorological units, conversion formulas and scales.

These sections and appendixes will subsequently be augmented by detailed examples and analyses of significant environmental events typical of the Mediterranean region. These future additions, intended to exemplify and emphasize the complex intermeshing of large- and small-scale circulation features, will be based on a variety of data sources, ranging from conventional synoptic surface and upper air observations to satellite imagery and numerical products. It is expected that this approach will enhance the output of computer models, and foster improvements in the models themselves by a feedback process.

Publication of this monograph is in loose-leaf format rather than textbook binding so that additions to it can be conveniently and easily accommodated. This format underscores the intention of the effort -- to provide a responsive, up-to-date and comprehensive information source for the Mediterranean forecaster.

Users of this volume are urgently requested to take part in its continuing development and expansion by providing significant inputs to it, based on their own information and experiences. Typical inputs might range from listings of baffling weather phenomena that have eluded standard forecasting skills and methods to information describing weather developments of special interest. Contributors may be assured that every effort will be made to reflect user inputs in the development of subsequent materials; these addenda will be collected, coordinated and prepared for publication by the Environmental Prediction Research Facility, Monterey, California. It is hoped that this updating process will maintain this monograph at a maximum level of usefulness for many years to come.

Special recognition is due to the staff of the Environmental Prediction Research Facility, especially to Dr. Yoshikazu Sasaki, Lieutenant Commander W. N. Bowman, Royal Navy, Mr. L. Robin Brody, and AGCS James Futtner, USN, for numerous contributions to, and improvements of, this monograph as it evolved during the past months; Dr. Willem van der Bijl, Department of Meteorology, Naval Postgraduate School, conducted a very careful and painstaking final review. Special thanks are extended to project editor Mr. Stephen Bishop; to the artists who prepared the illustrations and finalized production copy for printing, Mr. Mason Kidlen and Mr. Richard Clark; and to a most patient and efficient typist, Mrs. Winona Carlisle.

Gratitude is expressed to Captain W. L. Somervell, Jr., USN (Ret.), formerly commanding officer of the Navy Weather Research Facility, Norfolk, VA, for his contributions during the inception of this project. The subsequent support and leadership of two successive commanding officers of the Environmental Prediction Research Facility, Captain G. D. Hamilton, USN, and Captain R. C. Sherar, USN, is gratefully acknowledged.

Fort Collins, CO
November 1975

Elmar R. Reiter
Professor of Atmospheric Science
Colorado State University

CONTENTS

FOREWORD	iii
PREFACE	iv
I. REGIONAL GEOGRAPHY	I-1
A. INTRODUCTION	I-1
B. GEOGRAPHICAL FEATURES	I-1
C. TOPOGRAPHICAL FEATURES AND EFFECTS	I-5
II. SCALES OF METEOROLOGICAL PHENOMENA	II-1
III. LARGE SCALE WEATHER SYSTEMS	III-1
A. INTRODUCTION	III-1
B. JET STREAMS	III-3
C. LARGE SCALE OROGRAPHIC EFFECTS	III-48
D. REGIONAL MEDITERRANEAN WEATHER REGIMES	III-55
E. SIGNIFICANT CYCLONE OCCURRENCES	III-67
F. LARGE SCALE WIND REGIMES	III-75
G. ANNUAL TEMPERATURE VARIATION	III-98
H. ANNUAL PRESSURE VARIATION	III-109
I. PRECIPITATION	III-113
J. CLOUDINESS	III-124
K. FOG, HAZE AND VISIBILITY	III-126
IV. MESOSCALE WEATHER PHENOMENA	IV-1
A. CHANNELING AND CORNER EFFECTS	IV-1
B. DIURNAL EFFECTS	IV-2
V. SMALL SCALE PHENOMENA OF INTEREST TO THE MEDITERRANEAN FORECASTER	V-1
A. CLEAR AIR TURBULENCE (CAT) - A GENERAL REVIEW	V-1
B. MOUNTAIN WAVES AND CAT	V-14
C. AIR-SEA INTERACTIONS	V-19
D. SEA-SURFACE TEMPERATURE EFFECTS ON CYCLOGENESIS	V-20
E. REFRACTIVE INDEX PROBLEMS	V-21
REFERENCES	R-1
APPENDIX A - A THEORETICAL DESCRIPTION OF THE RELATIONSHIP BETWEEN JET STREAMS AND CYCLONE DEVELOPMENT AND MOVEMENT	A-1
APPENDIX B - BAROCLINICITY AND THERMAL WIND EQUATION	B-1
APPENDIX C - CONSERVATION OF ABSOLUTE ANGULAR MOMENTUM	C-1
APPENDIX D - POTENTIAL VORTICITY	D-1
APPENDIX E - INDIVIDUAL LARGE SCALE WEATHER TYPES WITH EXAMPLES	E-1
APPENDIX F - LIST OF STATIONS FOR WHICH CLIMATOLOGICAL DATA ARE AVAILABLE FROM WORLD-WIDE AIRFIELD SUMMARIES	F-1
APPENDIX G - NORMAL PRESSURE TENDENCIES AT SYNOPTIC HOURS IN THE MEDITERRANEAN	G-1
APPENDIX H - METEOROLOGICAL UNITS, CONVERSION FORMULAS AND SCALES	H-1

I. REGIONAL GEOGRAPHY

A. INTRODUCTION

The Mediterranean region is characterized by multinational as well as geographical and topographical complexities, with many peoples of strongly contrasting cultural backgrounds living in relatively close proximity to one another; Figure I A-1 shows the region's present political boundaries and the locations of major cities.

Figure I-A-2, a "three-dimensional" map illustrating both topographical relief and land mass configurations, shows the two main basins into which the Mediterranean -- the world's largest inland sea -- can be considered to be divided:

- (1) The Western Basin -- from Gibraltar to Italy
- (2) The Eastern Basin -- from Italy to the coast of Syria

The area between Corsica, Sardinia and Tunisia on the west and Greece and Cyrenaica on the east is sometimes referred to as the "Central Mediterranean."

B. GEOGRAPHICAL FEATURES

The complexity of the region may be seen in the many separate gulfs, "seas," straits and channels that must be known by the regional weather expert. In the west, the Strait of Gibraltar opens into the Alboran Channel (named after the tiny island of Alboran). To the northeast, the Gulf of Valencia is bounded on the south by the Balearic Islands (Ibiza, Mallorca and Menorca are the three major ones) and merges with the Gulf of Lion farther to the northeast. Moving eastward, the Gulf of Genoa on the northernmost shore of Italy extends into the Ligurian Sea. This sea is separated from the Tyrrhenian Sea by the islands of Elba (in the Tuscanian Archipelago), Corsica and Sardinia. The two important connections between these two seas are the Strait of Bonifacio between Corsica and Sardinia and the Strait of Corsica between Corsica and the island of Elba.

East of Italy is the long and narrow Adriatic Sea which opens into the Ionian Sea to the south. The Gulf of Taranto and the Gulf of Squillace are located under the "boot" of Italy. The Strait of Messina separates the mainland of Italy from Sicily and opens into the Gulf of Catania.

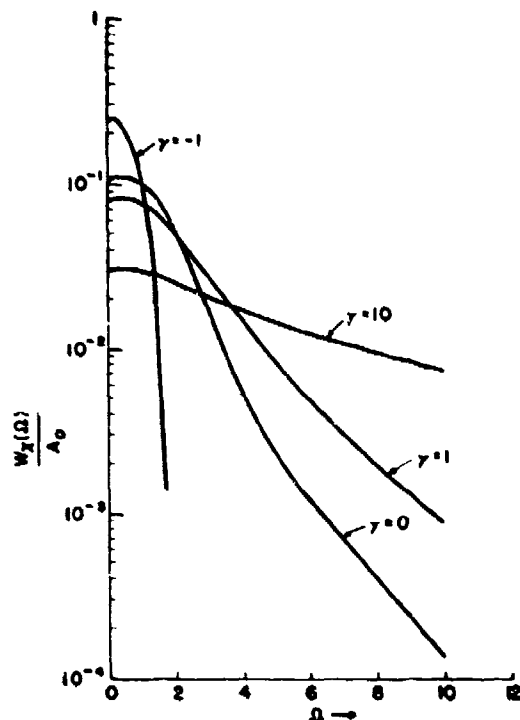


Figure 2. Temporal Frequency Spectrum of the Amplitude Fluctuations at the Center of a Laser Beam Propagating in Turbulence for the Case When $F = 10^{-7}$ and $a = 1$. Note that γ is positive when the beam is slewed in the direction opposite to V

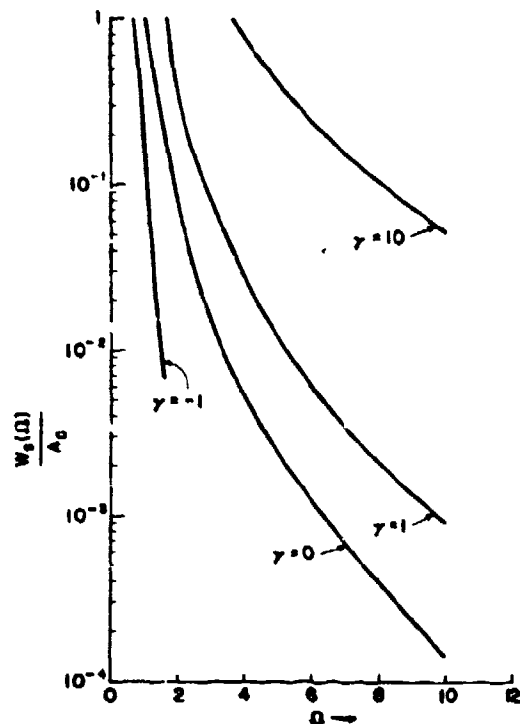


Figure 3. Temporal Frequency Spectrum of the Phase Fluctuations at the Center of a Laser Beam Propagating in a Turbulent Medium for the Case When $F = 10^{-7}$ and $a = 1$. Note that γ is positive when the beam is slewed in the direction opposite to V

$$\langle \chi^2 \rangle = \frac{1}{\pi} \int_{-\infty}^{\infty} W_{\chi}(\omega) d\omega$$

and

$$\langle S^2 \rangle = \frac{1}{\pi} \int_{-\infty}^{\infty} W_S(\omega) d\omega,$$

it does affect the shape of W_{χ} and W_S .

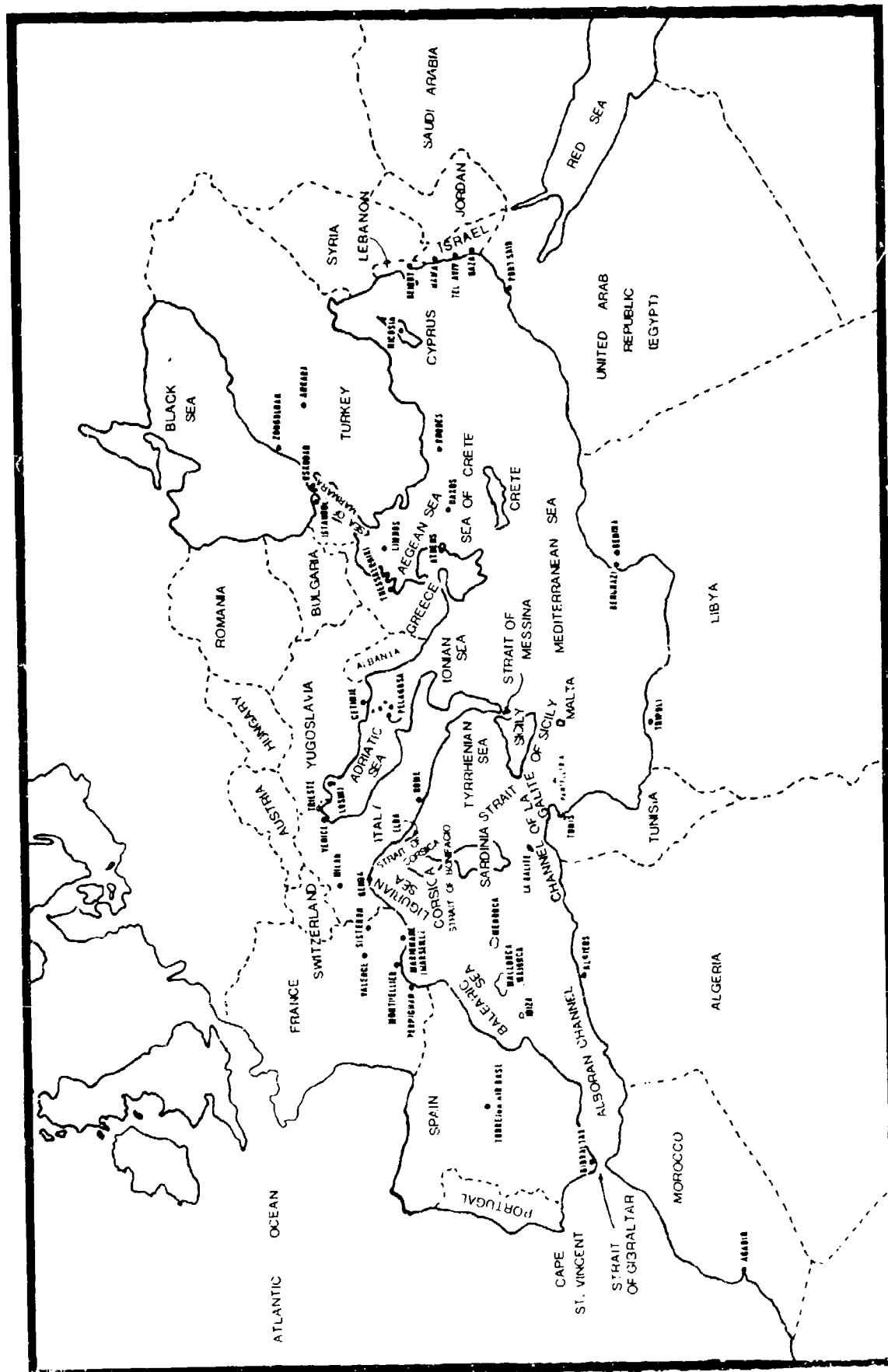


Figure I-A-1. Map of Mediterranean area with political boundaries and major cities.

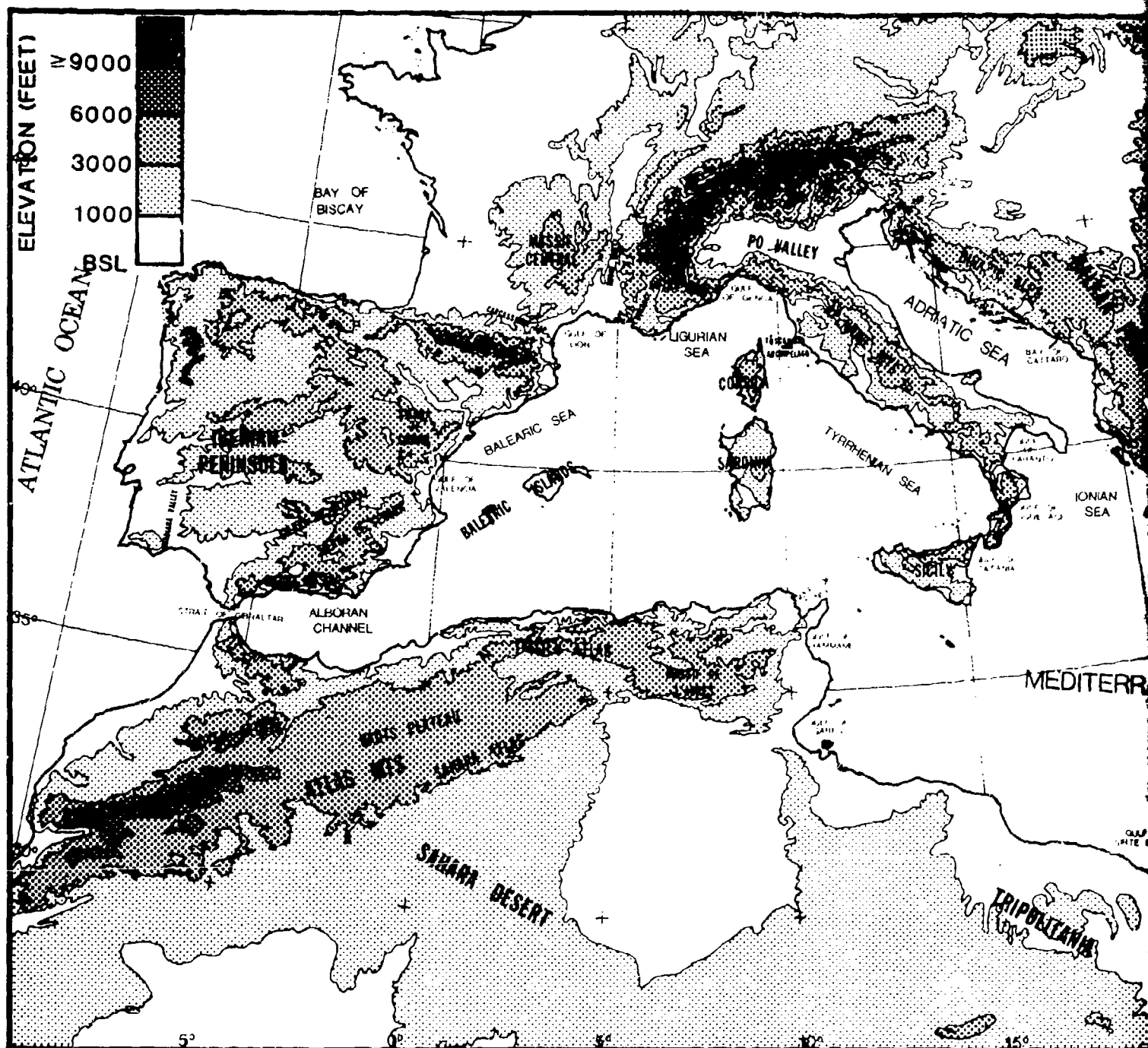
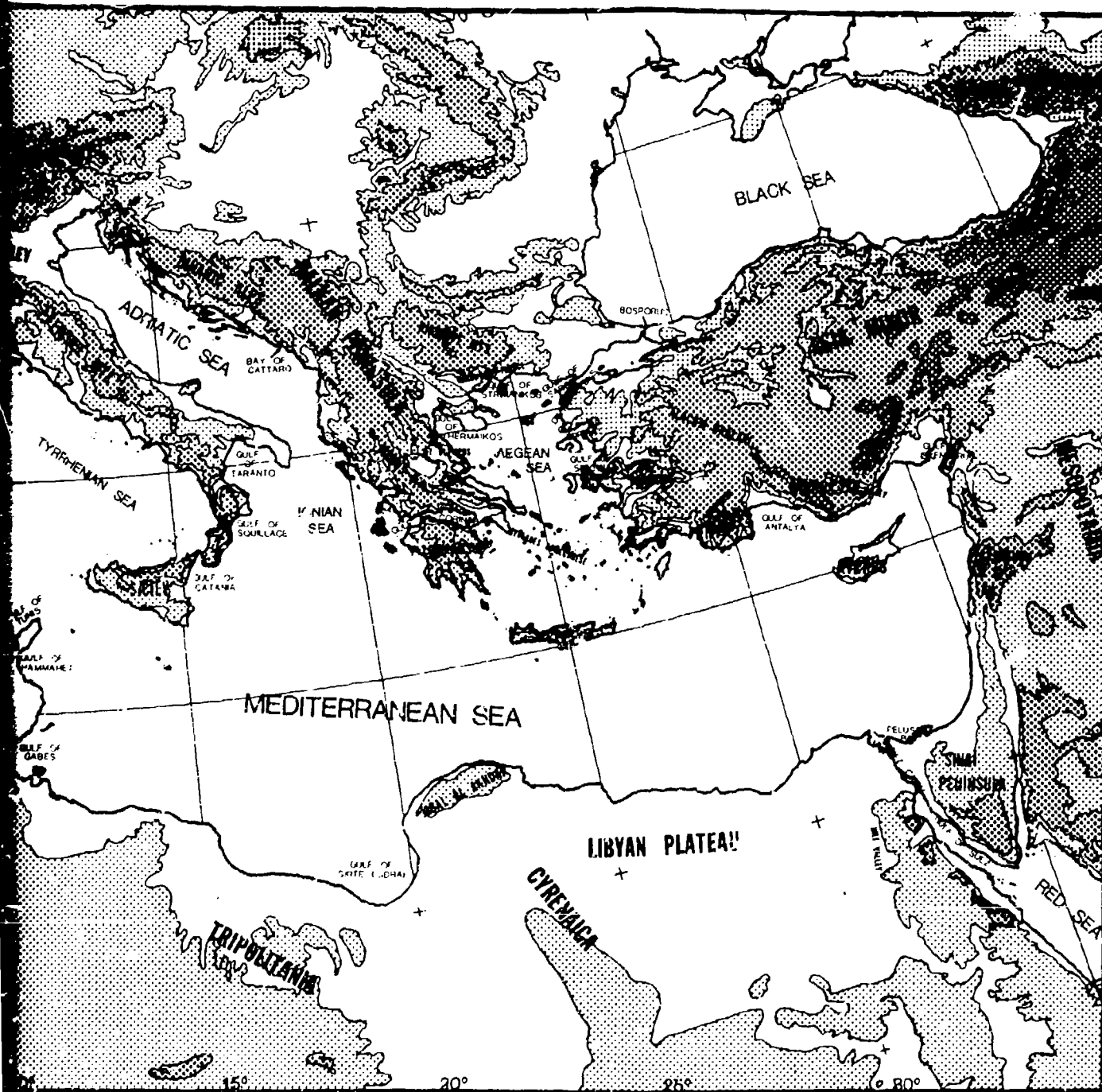


Figure I-A-2. "Three-dimensional" map showing of the Mediterranean area.



"e-dimensional" map showing the topography
an area.

The narrows between Sicily, Malta, Pantelleria and Tunis are known collectively as the Strait of Sicily. However, the area north of Tunis between the African mainland and the island of La Galite is known as the Channel of La Galite.

East of Tunis along the North African coast lie the Gulf of Tunis, Gulf of Hammamet, Gulf of Gabes, and Gulf of Sirte (or Sidra), and the Pelusium Bay (Khalig el Tina) east of Port Said.

Along the northern shores of the Eastern Basin, the Gulf of Corinth extends eastward from the Ionian Sea and bisects the peninsula of Greece. The Aegean Sea opens to the northeast into the Dardanelles and thence into the Sea of Marmara, the Bosphorus (with the cities of Istanbul and Uskudar along its shores), and the Black Sea.

The Cyclades, Sporades and Dodecanese Islands are sprinkled across the southern part of the Aegean Sea; Rhodes is the largest of these islands. The Sea of Crete extends between these island groups and the island of Crete.

Along the southern shores of Turkey are the Gulf of Antalya and the Gulf of Iskenderun to the northwest and northeast of Cyprus, respectively.

C. TOPOGRAPHICAL FEATURES AND EFFECTS

The topography behind the coastlines of the Mediterranean is similarly complex; it provides barriers against and openings toward air currents that bring extreme differences of air masses to play upon the region. Figure I-C-1 shows these barriers and gaps along an irregular line that runs approximately 100 miles inland from the coast. The listing of mountain ranges and gaps in Table I-C-1 may be compared with Figures I-A-2 and I-C-1.

The planetary boundary layer, friction layer, or Ekman layer, is the lowest region in the atmosphere, usually about 1000 m (3000 ft) thick above level terrain. In this layer, frictional drag of air along the rough surface of the earth causes a pronounced inflow across the isobars towards lower pressure. Theoretically, this departure of flow from the geostrophic wind (parallel to the isobars) is 45° at the earth's surface, diminishing to 0° at about 1000 m above ground. Over flat and smooth terrain the actual angle of departure of the winds from the direction of the isobars is usually less than 45° , more like 20 to 30° . In narrow mountain gaps, however, this angle may reach 90° , i.e., the air "falls" down the fall-line, almost like water.

Unfortunately, little is presently known about the vertical extent of the friction layer above mountain ranges, simply because radiosonde and pilot balloon stations tend to be located in the plains and broad valleys rather than atop inaccessible mountain peaks. For the sake of simplicity, and in the absence of contradictory evidence, it must be assumed that mountain ranges in excess of 1000 m elevation, when located near the seashore, will provide an

Table I-C-1. Mountain barriers and gaps in the Mediterranean basin.

NORTHERN COASTLINE (WEST TO EAST)		SOUTHERN COASTLINE (WEST TO EAST)	
MOUNTAIN BARRIERS	GAPS	MOUNTAIN BARRIERS	GAPS
SIERRA NEVADA	<i>Strait of Gibraltar</i>	ATLAS MOUNTAINS	<i>Strait of Gibraltar</i>
SIERRA DE GUDAR	Jucar Valley	MASSIF DE L'AURES	<i>Biskra Gap</i>
PYRENEES MOUNTAINS	Ebro Valley	TRIPOLITANIA	Gulf of Gabes
MASSIF CENTRAL	<i>Carcassone Gap</i>	JABAL AL AKHDAR	<i>Gulf of Sidra</i>
	<i>Rhone Valley</i>	LIBYAN PLATEAU	<i>Nile Valley, Suez Canal and Gulf of Suez</i>
ALPS OF THE DAUPHINE	<i>Durance Valley</i>	SINAI PENINSULA	Gaza
ALPS	Po Valley		Haifa
APENNINE MOUNTAINS	<i>Trieste Gap</i>	LEBANON MOUNTAINS	Gulf of Iskenderun
DINARIC MOUNTAINS	Gulf of Thermaikos Gulf of Strimonikos		
RHODOPE MOUNTAINS	<i>Gulf of Sarou bardanelles</i>		
ALACAM DAGLARI		<p>Note: The gaps identified by <i>italic typeface</i> in this table are those gaps below 1000 m elevation (marked in Figure I-C-1) through which the agrostrophic flow component can pass freely and at considerable strength into the Mediterranean Basin.</p>	
BOZ DAGLAR	Gulf of Antalya		
BEY DAGLARI	Goksu Valley		
TAURUS MOUNTAINS			
TAURUS MOUNTAINS	Gulf of Iskenderun		

effective obstacle against the ageostrophic flow (i.e., the flow down the pressure gradient and across the isobars) in the planetary boundary layer. Markings in Figure I-C-1 identify those gaps below 1000 m elevation through which the ageostrophic flow component can pass freely and at considerable strength into the Mediterranean basin. The same gaps are denoted by *italic typeface* in Table I-C-1.

The more prominent of these gaps are associated with the wind systems, named many centuries ago, that are shown schematically in Figure I-C-2; Table I-C-2 contains the definitions of these winds as given in the Glossary of Meteorology (Huschke, 1959). Further general descriptions of the more important of these wind systems are given in Section III-F. It will suffice here to point out that these winds are not steady, as are, for example, the trade winds. They occur only when an appropriate synoptic situation sets up the required pressure gradients which can drive the air flow through the mountain gap. Recognizing these weather situations in advance is one of the major tasks of the weather forecaster in the Mediterranean theater.

If the pressure gradients and the air flow component in the lower and middle troposphere directed perpendicular to a mountain range are strong enough to force the flow over the mountain rather than around it, strong and gusty winds on the lee side of the mountains will result. These winds are known as "foehn" winds and are similar to "chinook" winds in the North American Rockies (see Section III-F, para. 3). The forecaster will therefore have to direct his attention to the mountain ranges themselves as well as to the mountain gaps when assessing orographic effects. The topographic features shown in Figure I-C-1, and also the islands and groups of islands not included in this diagram, may act upon the atmospheric flow as:

- (1) Channeling effects of gaps and valleys
- (2) Corner effects of prominences
- (3) Barrier effects in flow that is forced over an obstacle

The possible combinations of these effects (see Section IV-A), given the complex terrain configurations shown in Figures I-A-2 and I-C-1, generate overwhelmingly intricate local forecasting problems. For many of them there are no cut-and-dried rules, so experience and intuition will have to guide the forecaster in the absence of objective prognostic techniques.

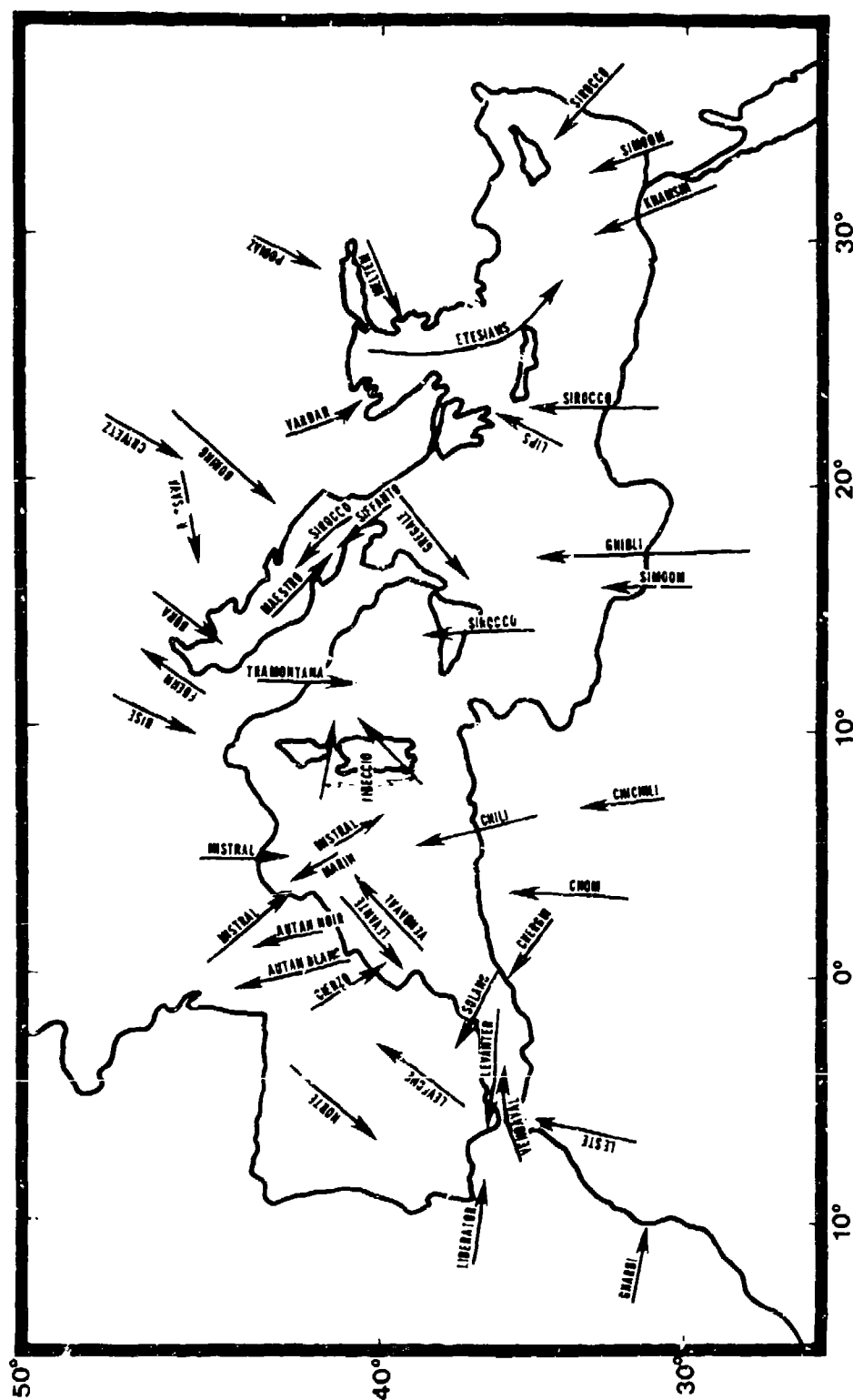


Figure I-C-2. Major wind systems in the Mediterranean region.

Table I-C-2. Definition of wind systems in the Mediterranean and surrounding regions (Huschke, 1959).

autan - (Also called *altanus*.) A strong southeast wind in south-central France, especially in Gascony and the upper Garonne River.

Near the Pyrenees the autan is very turbulent, growing in strength in the valleys. At Toulouse its average speed is 30 mph with gusts of 45 to 50 mph; it tends to be strongest at midday. It increases in speed up to a height of 1500 ft, above which it weakens and veers to the south. North of Toulouse it loses its special character and becomes an ordinary southeast wind.

There are two types. (a) The autan blanc brings fine, dry weather, cold in winter, hot in summer, as a result of the downslope motion imposed by the Pyrenees and the Southern Cevennes. It occurs with an anticyclone centered near Denmark or moving northeastward from the Azores. It lasts for two to four days in winter, but may persist for more than a week in summer, bringing severe drought and desiccating the vegetation. In Catalonia (northeastern Spain) a similar wind is called the *outo*. (b) The autan noir is less frequent and rarely lasts for more than two days; it is more humid and cloudy, bringing fog, rain or snow over high ground near the sea. As such, it is more like the *marin*, the name applied to the southeast wind out of the Cevennes where its maritime character predominates.

bise - (Also spelled *bize*.) A wind from north or northeast which blows in or from the mountain regions of France and Switzerland; similar to the *mistral* and *tramontana*. It is cold, moderately strong (especially in mountain regions), and generally dry.

The bise is most frequent in spring, when it usually brings fine bright weather, and in winter, when it may bring heavy clouds and falls of snow or hail (*bise noire* in Saone, *bise negre* in Aveyron), and snow whirlwinds in the mountains. It often persists for several days and brings damaging spring frosts. In Morvan the very dry bise in March is termed *hale* (drying wind) *de mars*. In the Drome valley south of Valence (southeast France) the name *bise brume* is given to a moist, mild and sometimes foggy wind from the northwest.

bize - Same as *bise*.

bochorno - A sultry wind (or sultry weather in general) in the Ebro valley of Spain, possibly a form of *sirocco*.

bora - A fall wind whose source is so cold that when the air reaches the lowlands or coast the dynamic warming is insufficient to raise the air temperature to the normal level for the region; hence it appears as a cold wind. The terms *borino* and *boraccia* denote a weak bora and strong bora, respectively.

The term was originally and still is applied (along with *karstbora*) to the cold northeast wind on the Dalmatian coast of Yugoslavia in winter when cold air from Russia crosses the mountains and descends to the relatively warm coast of the Adriatic. It is very stormy and squally, the squalls sometimes reaching 100 mph or more. F. Defant (*Compendium of Meteorology*, 1951, pp. 669-670) distinguishes between cyclonic bora (*bora scura*) with clouds and rain, covering the whole Adriatic and occurring with a depression over southern Adria, and the dry anticyclonic bora, with a powerful anticyclone over Central Europe extending over

Table I-C-2 (continued)

Dalmatia; the latter is very violent over the land but extends only a short distance out to sea. A local bora also occurs on the east coast of the Adriatic with an anticyclone over the Balkans. Defant states that the critical ground slope for the occurrence of bora is 1:100.

The term bora is now applied to similar winds in other parts of the world. Well known examples occur at Novorossiisk on the northern shore of the Black Sea, and in Novaya Zemlya (islands in the Russian Arctic). A squally katabatic wind at Alme Dagh in the Gulf of Iskenderun (E. Mediterranean Sea) is termed rageas (also ragne, ghaziyah). The Bulgarian term is buria.

See borasca.

boraccia - See bora.

borasca - (or borasco; also called bourrasque.) Literally, "little bora."
A thunderstorm or violent squall, especially in the Mediterranean.

bora scura - See bora.

borino - See bora.

bourrasque - Same as borasca.

camsin - Same as khamshin.

cers - A name for the mistral in Catalonia, Narbonne, and parts of Provence (southern France and northeastern Spain).

It is very violent and turbulent in the Aude Valley below Carcassone with gusts often reaching 50 to 55 mph. It is cold in winter, hot in summer, always dry and clear. A similar northerly wind in Spain is the cierzo.

chergui - An east or southeast desert wind in Morocco (North Africa), especially in the north. It is persistent, very dry and dusty, hot in summer, cold in winter. It blows with high pressure in the Mediterranean and the isobars running nearly parallel with the coast.

It is said to be most frequent in the forty days following July 11th or 12th, a period which is known as the Smaim (compare simoom).

chibli - Same as ghibli.

chichili - See chili.

chili - A warm, dry, descending wind in Tunisia resembling the sirocco. In southern Algeria it is called chichili.

chom - See sirocco.

cierzo - Spanish term for the mistral in the lower valleys of the Ebro. It occurs mainly in the autumn and early winter. Compare cers.

crivetz - (Also called krivu, crivat.) North to east winds in Rumania, especially a cold bora-like wind characteristic of the climate of Rumania. Crivetz may occur in any season, but is least frequent in June and July.

Table I-C-2 (continued)

cyclonic bora - (Also called bora scura.) See bora.

dramundan - See mistral.

düsenwind - (Literally "jet wind" or "blast wind.") The mountain-gap wind of the Dardanelles; a strong east-northeast wind which blows out of the Dardanelles into the Aegean Sea, penetrating as far as the island of Lemnos. It is caused by a ridge of high pressure over the Black Sea.

See Jet-effect wind.

eiszero - See sirocco.

etesians - The prevailing northerly winds in summer in the eastern Mediterranean and especially the Aegean Sea; basically similar to monsoon and equivalent to maestro of the Adriatic Sea.

According to the ancient Greeks, the etesians blow for forty days beginning with the heliacal rising of Sirius. They are associated (along with the seistan and shamal) with the deep low pressure area which forms in summer over northwest India. They bring clear skies and dry, relatively cool weather.

In Greece the etesian wind is locally named the sleeper. In Turkey it is the meltém. The Romans used the word also for the southwest monsoon of the Arabian Sea.

fall wind - A strong, cold, downslope wind. A fall wind differs from a föehn in that the air is initially cold enough so that it remains relatively cold despite adiabatic warming upon descent. It is a larger-scale phenomenon than the gravity wind (as usually defined), in that a fall wind prerequisites an accumulation of cold air at high elevations.

Fall winds are especially well developed as strong easterly winds on the coast of Norway, and for some distance inland; here they give a narrow strip of fine weather along the shore. They are also well developed on the northern coast of the Aegean Sea. At the southeastern tip of the rocky Hagion Oros Peninsula in Greece, Mt. Athos rises to 6670 ft and descends steeply to the sea; northerly winds are disturbed by this great mass and descend as the cold northeasterly Athos fall wind, often of gale force, extending several miles out to sea.

Good examples of fall winds are the bora, mistral, and vardar.

föehn - (Or föhn.) A warm, dry wind on the lee side of a mountain range, the warmth and dryness of the air being due to adiabatic compression upon descending the mountain slopes.

The föehn is characteristic of nearly all mountain areas. It is associated with cyclonic-scale motions, being produced only when the circulation is sufficiently strong and deep to force air completely across a major mountain range in a short period of time. The exact local nature of föehn winds, however, varies widely and depends upon the local topography, the strength of the basic flow across the mountain, the amount of moisture lost through precipitation on the windward side, conditions prior to the onset of the föehn, etc.

Table I-C-2 (continued)

The name originated in the Alps where it is best developed, especially as the south foehn on the northern slopes, and where south-north valleys open into plains or large east-west valleys, as at Innsbruck. In other mountain regions the foehn has a variety of local names: chinook of the Rocky Mountains; zonda of the Argentine (for a westerly foehn); puelche in the Andes (for an easterly foehn); ljuka in Carinthia (northwestern Yugoslavia); halny wiatr in Poland; austru in Romania; favogn in Switzerland. A northeasterly foehn descending the Massif Central of France and extending over the Garonne plain is locally called aspre. A dry wind from northwest descending the coastal hills in Majorca is named the sky sweeper. In New Zealand a foehn blowing from the New Zealand Alps onto the Canterbury plains is the Canterbury northwester.

See north foehn.

forano - A sea breeze of Naples, Italy.

gallego - A cold, piercing, northerly wind in Spain and Portugal.

gargal - See gregale.

gebli - Same as ghibli.

gharbi - A fresh westerly wind of oceanic origin in Morocco.

ghibli - (Also called chibli, gebli, gibleh, gibli, kibli.) A hot dust-bearing desert wind in Tripolitania similar to the foehn. In Morocco, the analogous gibleh is a hot dry wind from between southeast and south. It means "the direction in which one turns," i.e., the traditional direction of Mecca

See chili, khamsin, and sirocco.

gibleh - Same as ghibli.

gibli - Same as ghibli.

grècale - See gregale.

gregale - The Maltese and best known variant of a term for a strong northeast wind in the Central and Western Mediterranean and adjacent European land areas (stronger than the levante; compare levantera and lombarde). It occurs either with high pressure over central Europe or the Balkans and low pressure over Libya, when it may continue for up to five days, or with the passage of a depression to south or southeast, when it lasts only a day or two. It is most frequent in winter. The weather varies with the type of pressure distribution and the on-shore or off-shore direction of the wind. In Malta the gregale raises dangerous seas in the harbor.

Jet-effect wind - A wind which is increased in speed through the channeling of air by some orographic configuration such as a narrow mountain pass or canyon; a class of local winds. Examples of this effect are the düsenwind, and kossava winds.

See also mountain-gap wind.

Table I-C-2 (continued)

kamsin - Same as khamsin.

karstbora - The bora of the Yugoslavian coast.

katabatic wind - Any wind blowing down an incline; the opposite of anabatic wind. If the wind is warm, it is called a foehn; if cold, it may be a fall wind (such as the bora).

khannasseen - Same as khamsin.

khamsin - (Also spelled camsin, chamsin, kamsin, khamasseen, khamsin.) A dry, dusty and generally hot desert wind in Egypt and over the Red Sea. It is generally southerly or southeasterly, occurring in front of depressions moving eastward across North Africa or the southeastern Mediterranean.

The deep khamsins occur in spring with depressions traveling east-northeast across the northern Sahara. They are preceded by a heat wave lasting about three days, and followed by a dust storm. The passage of the depression is marked by a cold front bringing Mediterranean air and a sudden drop in temperature.

See ghibli, chili, sirocco.

khamsin - Same as khamsin.

kibli - Same as ghibli.

kosava - Same as kossava.

koschawa - Same as kossava.

kossava - (Also spelled kosava, koschawa.) A cold, very squally wind, descending from east or southeast in the region of the Danube "Iron Gate" through the Carpathians, continuing westward over Belgrade, thence spreading northward to the Rumanian and Hungarian borderlands and southward as far as Nish. In winter it brings temperatures down to below - 20°F and it is cool even in summer, when it is also dusty.

It usually occurs with a depression over the Adriatic and high pressure over southern Russia, a frequent situation in winter. It is usually explained as a Jet-effect wind through the Iron Gate, giving speeds well above the gradient, but J. Küttner ("Der Kosava in Serbien," Meteor., Z., 57: 1940, pp. 120-123) regards it rather as a katabatic wind intermediate between foehn and bora. The kossava has a marked diurnal variation with its maximum occurring between 0500 and 1000 local time.

krivu - Same as crivetz.

laveche - Same as leveche.

leste - Spanish nautical term for east wind. The name is given to a hot, dry, dusty easterly or southeasterly wind which blows from the Atlantic coast of Morocco out to Madeira and the Canary Islands. It is a form of sirocco and occurs in front of depressions advancing eastward.

levant - Same as levante.

Table I-C-2 (continued)

levant blanc - See levante.

levante - The Spanish and most widely used term for an east or northeast wind occurring along the coast and inland from southern France to the Strait of Gibraltar. It is moderate or fresh (not as strong as the gregale), mild, very humid, overcast and rainy; and occurs with a depression over the Western Mediterranean Sea. In summer it is rare and weak; in January it is inhibited by the Iberian anticyclone. It is most frequent from February to May and October to December.

A levant (French spelling) with fine weather is a levant blanc; in the Roussillon region of southern France (where, as along the Catalonian coast of Spain, it is called llevant) it often brings floods in the mountain streams. The levanter of the Strait of Gibraltar is a related phenomenon.

Compare leste, lombarde, levatera.

levanter - An English name for the levante, more specifically applied to winds in the Strait of Gibraltar and on the east coast of Spain. It blows from east or northeast with high pressure over Central Europe and a depression over the southwest Mediterranean. It is most frequent and strongest from October to December and February to May, and persists for two or three days.

levatera - A persistent east wind in the Adriatic, usually bringing cloudy weather.

Compare levante and gregale.

leveche - (Also spelled laveche.) A name for the sirocco in Spain. It is a hot, sand- and dust-laden wind from between southeast and southwest, that blows in front of a depression on the southeast coast of Spain but extends only a few miles inland.

lebeccio - Italian name for a southwest wind; used especially in northern Corsica for the west or southwest wind which blows throughout the year, and especially in winter when it is often stormy. On windward slopes it brings rain, with thunderstorms in summer and autumn. After crossing the mountains it is warm and dry, but may be very turbulent.

liberator - A name sometimes given the west wind through the Strait of Gibraltar.

Lips - The ancient Greek name for the southwest wind, which is the sea breeze in Athens.

On the Tower of the Winds it is represented by a bare-legged young man carrying a piece of a trireme. This may indicate either that the wind favored homecoming ships or that when stormy it caused wrecks. Today the name is applied to any hot wind, usually the sirocco.

llevant - See levante.

Table I-C-2 (continued)

lombarde - An easterly wind (from Lombardy) that predominates along the French-Italian frontier. It comes from the High Alps. In winter it is violent and forms snow drifts in the mountain valleys. In the plains it is gentle and very dry. It comes with an anticyclone over France and Central Europe, or with high pressure to the southeast of Europe and low pressure to the northwest along with falling pressure over western France.

maestro - A northwesterly wind with fine weather which blows, especially in summer, in the Adriatic; it is most frequent on the western shore, and is equivalent to the *etesians* of the Eastern Mediterranean. It is also found on the coasts of Corsica and Sardinia.

Compare *mistral*.

maistrau - See *mistral*.

maistre - See *mistral*.

mamatele - (Also called *mamaliti*, *mamatili*.) A light northwest wind of Sicily; a form of *mistral*.

manéofando - See *mistral*.

marin - A warm moist southeast wind from the sea on the French Mediterranean coast and in the Maritime Alps, especially frequent in spring and autumn. In the Rhone delta it blows also from the south.

The *marin* is associated with depressions which cross southern France or northern Spain and the Gulf of Lion. Generally, it is strong and regular, sometimes violent and turbulent in hilly country as the *ayalas* in the Massif Central; it is very humid, cloudy with hill fog, and often rainy (unless unaccompanied by fronts, when it is the *marin blanc*). The heavy rains, which may continue for one or two days on the mountain slopes, cause dangerous river floods. On the western slope of the Cevennes it becomes the *sutan*. In the southern Cevennes the *marin* is called the *aygalas*. On the coast of Catalonia (northeast Spain) and Roussillon (southern France) it is the *marinada* and generally occurs with a depression centered over or south of the Gulf of Gascony.

Compare *autan*, *sirocco*.

metém - 1. (Also spelled *metémi*.) A strong wind from the northeast or east which often sets in suddenly and blows during the day in summer on the Bulgarian coast and in the Bosphorus.

2. Turkish name for the *etesians*.

mistral - A north wind which blows down the Rhone valley south of Valence, France and into the Gulf of Lion. It is strong, squally, cold, and dry; the combined result of the basic circulation, a fall wind, and jet-effect wind. It blows from the north or northwest in the Rhone Delta, where it is strongest, from the northwest in Provence and from the northeast in the valley of the Durance below Sisteron.

A general *mistral* usually begins with the development of a depression over the Tyrrhenian Sea or Gulf of Genoa with an anticyclone advancing from the Azores to central France. It often exceeds 60 mph and reaches 85 mph in the lower Rhone valley and 50 mph at Marseilles, decreasing both

Table I-C-2 (continued)

to the east and west. It remains strong to a height of 2 to 3 km. In the absence of a strong pressure gradient, a weaker katabatic local mistral develops in the Rhone valley. A general mistral usually lasts for several days, sometimes with short lulls. It is most violent in winter and spring, and may do considerable damage.

The mistral has a variety of local names; *mangofango* in Provence; *sécaire*, *maistrau*, *maistre* or *magistral* in the Cevennes; *dramundan* in Perpignan; *cierzo* in Spain; *cers* in the Pyrenees, etc. South of Mont Ventoux a similar wind is named *bise*. A local west wind of mistral type which descends from Mt. Canigou to the plains of Roussillon is called *canigouenc*.

montagnère - See *tramontana*.

montagneuse - See *tramontana*.

mountain-gap wind - A local wind blowing through a gap between mountains.

This term was introduced by R.S. Scorer (Quart. J. R. Meteor. Soc., 61: 1952 pp. 53-61), for the surface winds blowing through the Strait of Gibraltar. When air stratification is stable, as it usually is in summer, the air tends to flow through the gap from high to low pressure, emerging as a "jet" with large standing eddies. The excess of pressure on the upwind side is attributed to a pool of cold air held up by the mountains.

Similar winds occur at other gaps in mountain ranges.

norte - The winter north wind in Spain.

north foehn - A foehn condition sustained by wind flow across the Alps from north to south.

The northern slopes are normally cooler than the southern slopes, and the dynamic warming is not often sufficient to overcome the difference of temperature. Hence a warm dry northerly wind of foehn-like character occurs less frequently than the south foehn. In the Italian Alps only eleven general north foehns were recorded between 1935 and 1943.

orsure - A stormy north to northeast wind in the Gulf of Lion.

outo - See *autan*.

ponente - A west wind on the Cote d'Azur (French Mediterranean coast), the northern Roussillon region, and Corsica. On the Cote d'Azur it is a weakened mistral and brings clear skies. In northern Roussillon it is the land breeze of early morning, changing to southeast during the day, and generally preceding the *tramontana*.

poriaz - Violent northeast winds on the Black Sea near the Bosphorus.

qibla - See *ghibli*.

raffiche - (Also called *refoli*). In the Mediterranean region, gusts from the mountains; violent gusts of the *bora*.

Table I-C-2 (continued)

rageas - See bora.

ragut - See bora.

refoli - Same as raffiche.

riefne - An intense storm of Malta in the Mediterranean.

sahel - A strong dust-bearing desert wind in Morocco.

simoom - (Many variant spellings). A strong, dry, dust-laden desert wind which blows in the Sahara, Palestine, Syria and the desert of Arabia. Its temperature may exceed 130°F and the humidity may fall below 10 per cent.

The name means "poison wind" and is given because the sudden onset of a simoom may cause heat stroke. This is attributed to the fact that the hot wind brings more heat to the body than can be disposed of by the evaporation of perspiration.

siffanto - A southwest wind of the Adriatic Sea; it is often violent.

sirocco - (Also spelled scirocco). A warm south or southeast wind in advance of a depression moving eastward across the southern Mediterranean Sea or North Africa. The air comes from the Sahara (as a desert wind) and is dry and dusty, but the term is not used in North Africa, where the natives call it chom (hot) or arifi (thirsty). In crossing the Mediterranean the sirocco picks up much moisture because of its high temperature, and reaches Malta, Sicily, and southern Italy as a very enervating, hot, humid wind. As it travels northward it causes fog and rain.

In some parts of the Mediterranean region the word may be used for any warm southerly wind, often of foehn type. In the extreme southwest of Greece a warm foehn crossing the coastal mountains is named sirocco di levante. There are a number of local variants of the spelling such as xaroco (Portuguese), Jaloque or xaloque (Spanish), xaloc or xalock (Catalonian). In the Rhone delta the warm rainy southeast sirocco is called eissero. On Zakynthos Island it is called lampaditsa.

See solano, zhibli, chili, simoon, leveche, marin.

sirocco di levante - See sirocco.

sleeper - See etesians.

solano - A southeasterly or easterly wind on the southeast coast of Spain in summer; usually an extension of the sirocco. It is hot and humid and sometimes brings rain; when dry it is dusty.

tarantata - A strong breeze from northwest in the Mediterranean region.

tramontana - A cold wind from the northeast or north, particularly on the west coast of Italy and northern Corsica, but also in the Balearic Islands and the Ebro Valley in Catalonia. Like the misral, it is associated with the advance of an anticyclone from the west following a depression over the Mediterranean. Weather is fine with occasional instability showers.

In Languedoc and Roussillon (southern France) a similar wind (tramontane) blows from the northwest; but the name is also applied to an invasion of polar air from the northwest, which is squally or tempestuous, dry and cold, except south of the Cevennes where it becomes foehn-like. This type occurs during the filling of a depression in the Gulf of Genoa and persists for eight to twelve days, mainly in winter and early spring;

Table I-C-2 (continued)

it rises to a peak at midday and weakens at night. On the Cote d'Azur and in eastern Provence, the tramontane is sometimes called the *montagnère* or *montagneuse*.

traversier - In the Mediterranean, dangerous winds blowing directly into port.

vardar - (Also called vardarac). A cold fall wind blowing from the northwest down the Vardar valley in Greece to the Gulf of Salonica. It occurs when atmospheric pressure over eastern Europe is higher than over the Aegean Sea, as is often the case in winter. It persists for two or three days with a mean velocity of 10 to 15 mph, rising to 35 mph in squalls. It is strongest where the Vardar River leaves the mountains, but it extends for some distance out to sea.

A similar wind, the Struma fall wind, blows in the Struma valley.

vardarac - Same as vardar.

vendaval - A stormy southwest wind on the southern Mediterranean coast of Spain and in the Strait of Gibraltar. It occurs with a low advancing from the west in late autumn, winter, or early spring, and is often accompanied by thunderstorms and violent squalls.

xaloch - (Or xaloque, xaroco). See sirocco.

II. SCALES OF METEOROLOGICAL PHENOMENA

In the previous section it was pointed out that many of the flow patterns of concern to the Mediterranean forecaster are of rather localized extent and are strongly influenced by the orography -- it is especially these local effects that make weather forecasting in the Mediterranean region exceedingly difficult. In general, the forecaster will have to be on the alert for the following four major effects:

- (1) Large-scale synoptic patterns:
 - (a) Their seasonal variations
 - (b) The effects of orography on the development of these patterns
 - (c) The effect of air-sea interaction on these patterns
- (2) Synoptic, orographic, and land-sea distribution effects on the flow within the planetary boundary layer which regulate some of the major wind systems enumerated in Table I-C-2 and described in the subsequent section. The flow in this layer is characterized by a sizeable ageostrophic wind component towards lower pressure, and forced flow over mountain barriers or through mountain gaps will have to be considered.
- (3) Diurnal variations of flow regimes due to the varying temperature contrast between land and water. Land-sea breeze regimes are the most outstanding manifestations of these diurnal effects. Mountain and valley breezes also are thermally forced with a diurnal cycle. Diurnal effects, to a certain extent, may influence the development of synoptic systems, by virtue of the rather complex diurnal pressure variations.
- (4) Small-scale effects produced by flow over and around obstacles, such as islands, mountains, etc.

In describing the various weather phenomena of the Mediterranean region, it is difficult to subdivide the discussion according to these four major effects. Therefore, it is intended to proceed in a more logical sequence of events that first addresses assessment of the large scale synoptic situation (Section III), then discusses mesoscale modulation (Section IV) and finally addresses small scale processes (Section V). Nevertheless, the forecaster should be aware of

the influences of these four effects, and should also bear in mind that all scales in the atmosphere are interactive -- no process stands alone. One example is clear air turbulence (a typical small-scale phenomenon, described in Section V), which occurs preferentially in or near jet streams (a phenomenon of synoptic-scale dimensions, described in Section III). Also, channeling effects produced by islands in the Aegean Sea are classified as mesoscale processes, yet they are most significant during the large-scale etesian wind regime. Extensive cross referencing has therefore been included throughout the sections to help the reader to better understand significant interactions.

III. LARGE SCALE WEATHER SYSTEMS

A. INTRODUCTION

During winter and spring, the Mediterranean region is characterized by extensive cyclonic activity. The Mediterranean climate thus has its rainy season during winter (see Section III-I). This low-pressure activity is brought about by a number of large-scale factors which are described in some detail in this section. Two of the most important of these are the interplay of the polar front jet stream (PFJ) and the subtropical jet stream (STJ) (see Section III-B, para. 5), and the effect of orography (see Section III-C, para. 2).

Cyclonic activity in the Mediterranean region is at its most intense during late winter and spring when blocking anticyclones are frequently observed over the eastern Atlantic (see Section III-D, para. 2). During these periods a quasi-permanent low-pressure trough in the mid-troposphere extends along the axis of the Mediterranean basin, as schematically indicated in Figure III-A-1, where the solid lines represent typical 500 mb contour lines. The blocking high often assumes the shape of the Greek letter Ω , from which it derives its name "Omega High." The trough line, frequently running the whole length of the Mediterranean basin, is conducive to cyclogenesis when vorticity maxima move into its region of influence.

Such vorticity maxima may be associated with wave disturbances traveling along the PFJ and rounding the blocking anticyclone from a northwesterly or northerly direction, leading to Genoa cyclogenesis (see Section III-E). These maxima may also be associated with the STJ which crosses the narrow "neck" of the high-pressure bridge that connects the blocking anticyclone with the subtropical high-pressure belt. Since this jet-stream branch tends to flow over North Africa south of the Atlas Mountains, the subsequently developing North African depressions are usually very difficult to trace because of the sparseness of upper-air and surface data in this region.

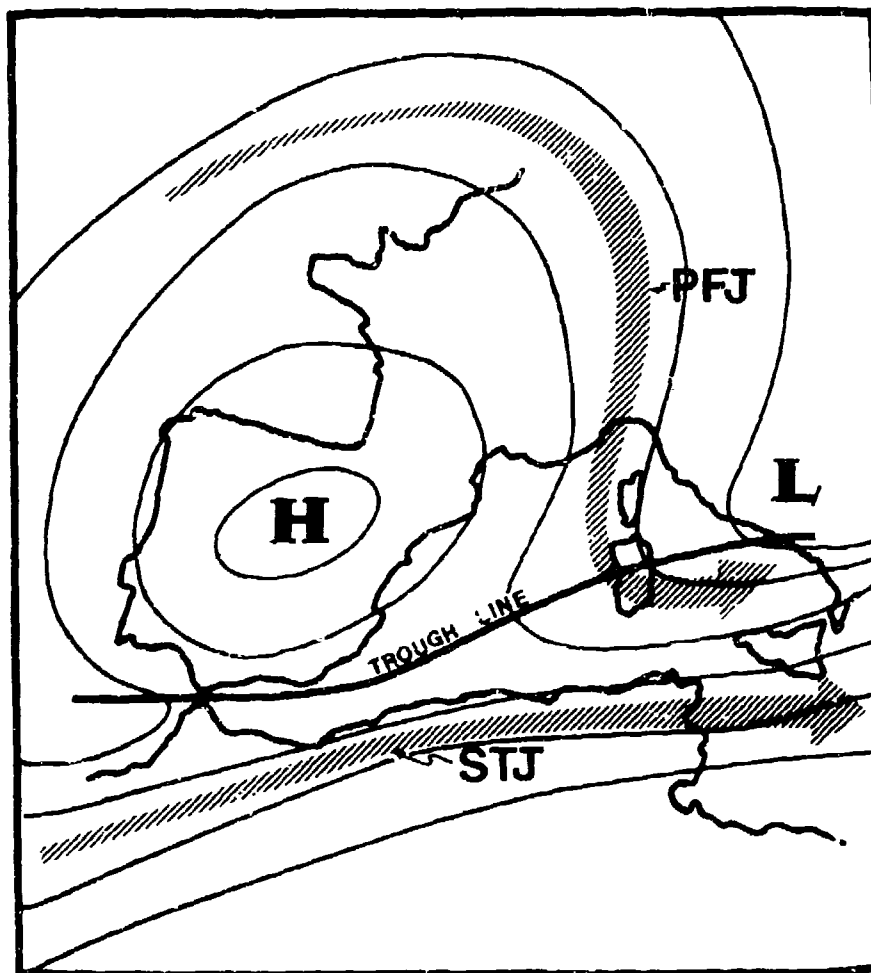


Figure III-A-1. Schematic diagram showing
Omega high and trough lines at 500 mb
and locations of jet streams.

B. JET STREAMS

1. Polar-Front and Subtropical Jet Streams

The development and movement of cyclones are generally dictated by the flow in the jet stream region (see Appendix A). In general, two prominent jet stream systems are found near the tropopause level during winter. The first is the subtropical jet stream (STJ), located at the northern edge of the tropical Hadley cell of meridional motion and overlying the subtropical high-pressure belt. The second is the polar front jet stream (PFJ) associated with the polar front and its wave disturbances. Figure III-B-1 depicts these jet stream patterns schematically; Figure III-B-2 shows the more complex behavior of mean meridional flow from actual data. The arctic front, wherever it appears, is also associated with a jet stream that is quite similar in behavior to the polar front jet.

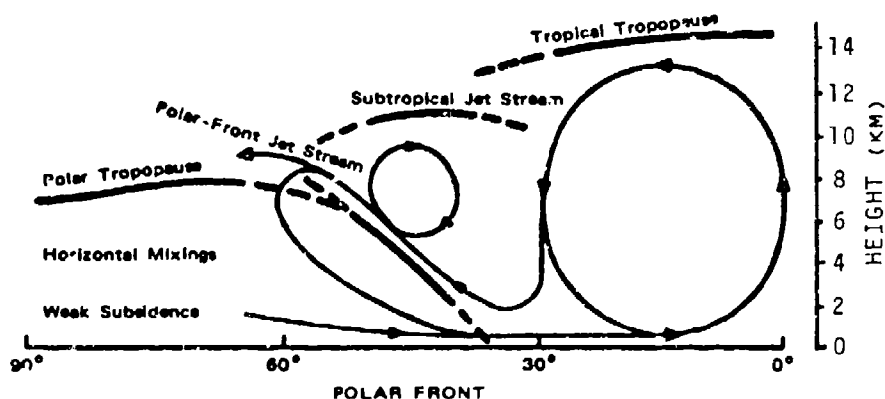


Figure III-B-1. Schematic diagram of the mean meridional circulation in the Northern Hemisphere during winter. Heavy lines indicate tropopause and the polar front (from Reiter, 1963).

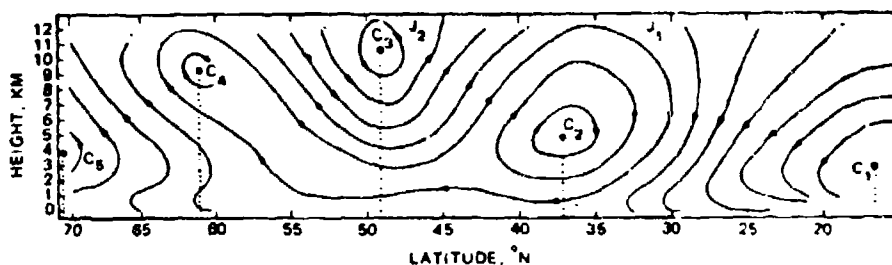


Figure III-B-2. Mean meridional circulation. Streamlines define the centers of the Hadley cell (C_1), of the Ferrel cell (C_2), of two cells of the upper troposphere (C_3 and C_4), and of a direct cell north of 65°N (C_5) (from Reiter, 1969).

The subtropical jet stream is usually found near the 12-km level (200 mb). Since subsidence prevails underneath it in the lower troposphere, frontal systems are not maintained, and the baroclinicity to which this jet stream owes its existence is restricted to the upper troposphere above 500 mb. It is well developed only during the cold season.

The polar front jet lies close to the 10-km level (300 mb), and wherever it is well developed a baroclinic zone (the polar front) extends throughout the depth of the troposphere (see Appendix B). A similar situation occurs with the arctic front jet (AFJ) and the baroclinic zone of the arctic front.

There are certain regions over which PFJ and STJ interact quite frequently, giving rise to very strong, combined jet maxima and cases of rapid cyclogenesis and severe weather. One such region is over Japan, one is over the United States, and one is over the southern Mediterranean area. These three regions coincide with the mean positions of jet maxima in the STJ belt. As shown in Figure III-B-3, this belt is usually deformed into a planetary 3-wave pattern.

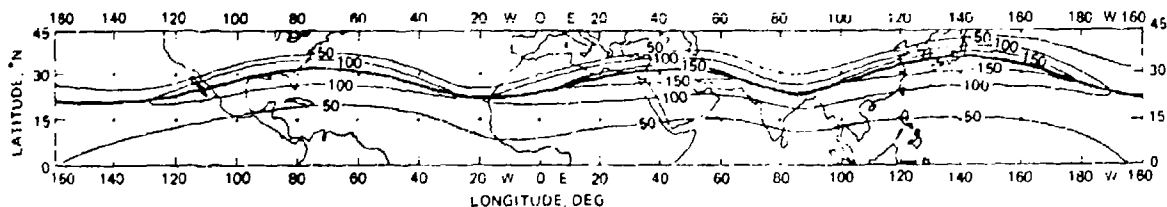


Figure III-B-3. Mean subtropical jet stream of the winter of 1955-1956. Isotach analysis at the 200-mb surface, with isotachs drawn at 50 kt intervals. The mean latitude of the jet axis is 27.5°N (from Reiter, 1969).

Unfortunately, no detailed analyses of the interaction between STJ and PFJ over the Mediterranean are presently available because of the lack of synoptic upper-air data over North Africa. It is known from special analyses of other data sources, however, that a well developed STJ does exist during winter and spring. Most of the time it stays south of the Atlas Mountains, except during periods of strong interaction with the PFJ and rapid cyclogenesis in the Mediterranean basin.

2. Cloud Bands and Jet Streams

Figure III-B-4 shows an analysis of cloud-drift vectors from the ATS satellite for 18 November 1967. Since the observed clouds were probably located in the middle troposphere the "winds" (actually cloud drifts) shown in this figure are characteristic of, say, the 400-500 mb layer rather than the jet stream level. This diagram indicates an anticyclonic jet maximum with clouds, and hence wind information, restricted to its south side, where ascending motions prevail because of upper speed divergence in the right rear quadrant of the jet. The position of this jet maximum is farther to the west than the climatological mean location indicated in Figure III-B-3, and such a westward shift of the Mediterranean wind maximum of the STJ is to be expected whenever a deep trough in the westerlies prevails over the East Atlantic off the Portuguese and African coasts.

Wind speeds cannot be estimated from APT- or NIMBUS-type satellites in the same manner as the ATS "winds" shown in Figure III-B-4. Efforts are presently underway to extract upper-atmospheric temperature and geostrophic flow patterns from satellite radiance data (Martin and Salomonson, 1970). A study by Lovill (1972) has shown that the location of jet maxima coincides with strong meridional gradients of the total ozone content in vertical air columns. This ozone content can also be measured from satellites. Operational applicability of such remote sensing techniques for a real-time diagnosis of the atmospheric temperature and wind fields is not yet possible. A qualitative assessment of jet stream location can, however, be made on many occasions. Cloud bands usually coincide well with the STJ position under the following conditions:

- (1) Extension of the band from equatorial into temperate latitudes, with orientation from SW to NE. Preferred regions of occurrence of such bands are: East Atlantic into West Africa (see Figure III-B-4); East Pacific into Baja California, Northern Mexico and Southern U. S.; East China Sea and Japanese Islands.
- (2) Streaky appearance of the cloud band, with a rather well-defined northern edge and a relatively cloud-free region extending along the cyclonic (northern) side of the cloud band.

- (3) Indication of a deep trough in the westerlies extending into low latitudes to the west of the observed cloud band.

If the three conditions cited above are met, one should expect winds in excess of 100 kt at 200 mb over the location of the northern edge of the cloud band. An example of a strong STJ over West Africa as seen in satellite pictures is shown in Figures III-B-5(a) and III-B-5(b). The wind maximum is most likely to occur in the apex of the anticyclonically curved flow around a high-pressure ridge (see Figure III-B-4) in agreement with the tendency of conservation of absolute angular momentum (see Appendix C).

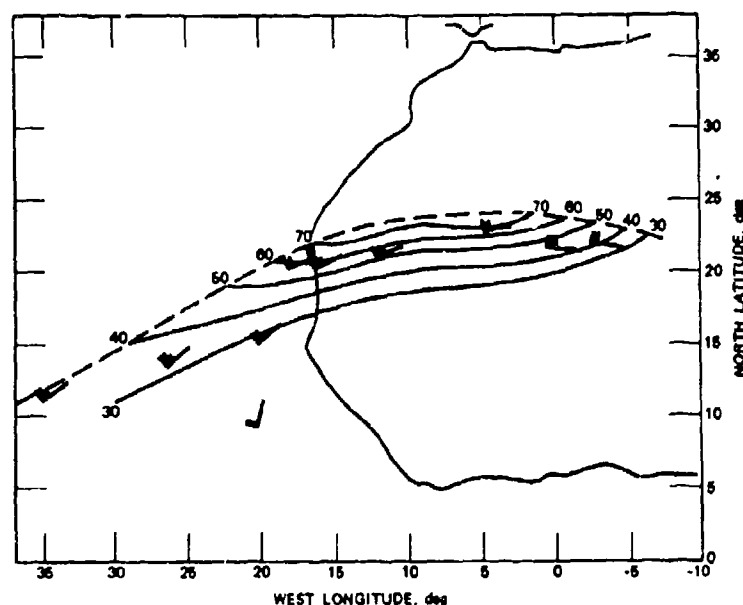
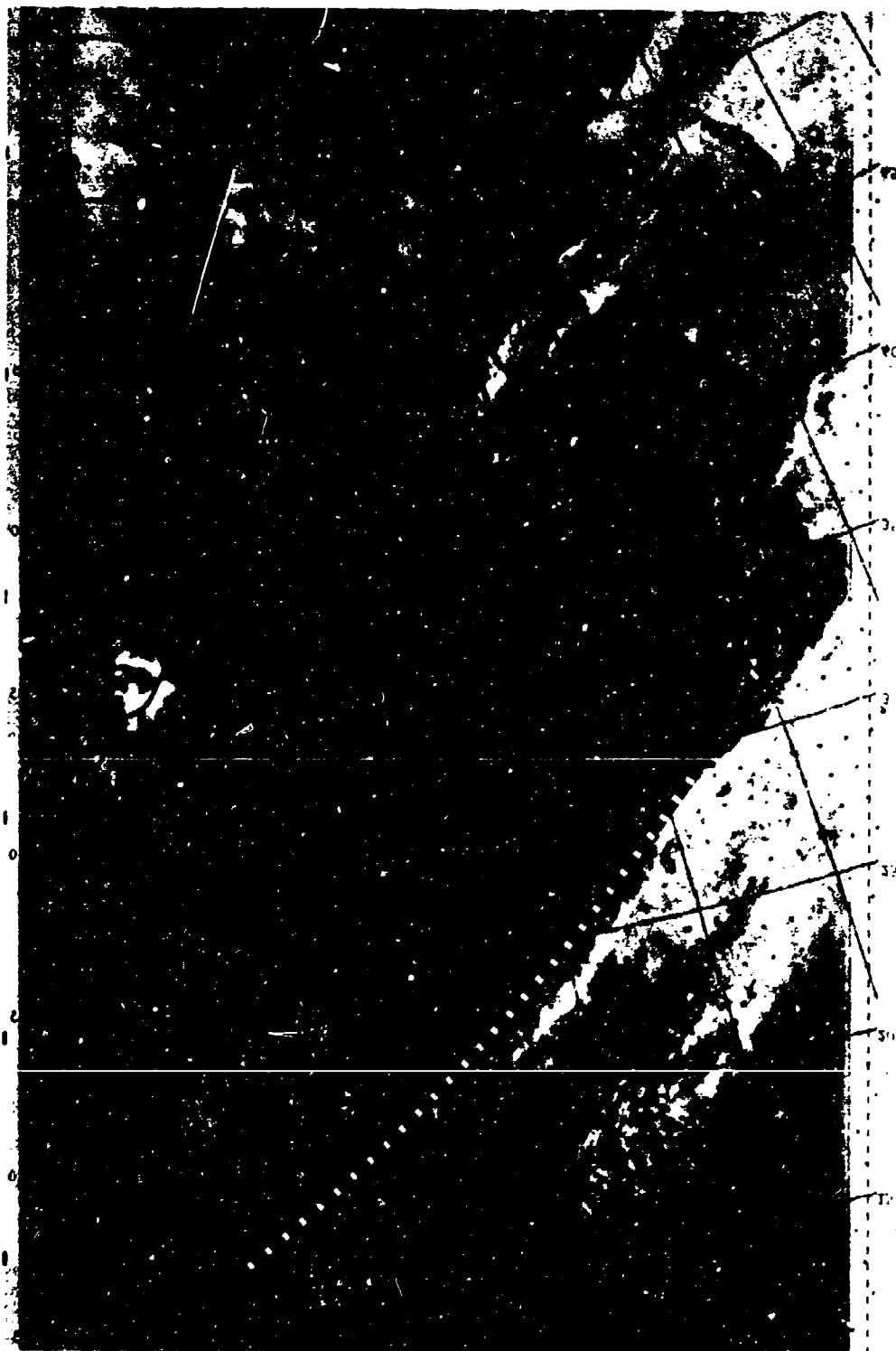


Figure III-B-4. Cloud-drift trajectory vector, 18 November 1967, derived from ATS satellite pictures. Isotachs in knots (from Reiter, 1972a).



Figure III-B-5. Cloud pattern associated with the STJ over the Sahara (dashed line): (a) DMSP high-resolution visual for 1141 GMT, 7 December 1974, and (b) DMSP IR for 0930 GMT 7 December 1974.



b

Figure III-B-5 (continued)

3. Horizontal Wind Shears

The horizontal wind shear on the anticyclonic side of this STJ jet maximum is expected to conform closely to "zero absolute vorticity" (see Appendix C), i.e.,

$$\frac{\Delta u}{\Delta y} = f \quad \text{III-B(1)}$$

where Δu is the change in the zonal wind velocity component (in cm sec^{-1}) measured over the meridional distance Δy (cm), f is the Coriolis parameter of that particular latitude (units: sec^{-1}). The values of the latter may be interpolated from Table III-B-1.

EXAMPLE: At latitude 25°N (Sahara Desert) a wind of 100 kt ($= 51.5 \text{ m sec}^{-1}$) should decrease by approximately 24 kt over a distance of 200 km:

$$\begin{aligned} \Delta y &= 200 \text{ km} = 2 \times 10^7 \text{ cm}; \\ f &= 0.6164 \times 10^{-4} \text{ sec}^{-1}; \\ \Delta u &= 0.6164 \times 10^{-4} \times 2 \times 10^7 \text{ cm sec}^{-1} = 1232.8 \text{ cm sec}^{-1} \\ &\approx 12.3 \text{ m sec}^{-1} \\ &\approx 24 \text{ kt.} \end{aligned}$$

With strong anticyclonic curvature, the decrease in wind speed will actually be somewhat less than in the example given above. The radius of streamline curvature in Figure III-B-4 is approximately 14° of latitude ($\approx 1.5 \times 10^8 \text{ cm}$). According to Eq. (6) in Appendix A, this yields an anticyclonic curvature vorticity of

$$\frac{v}{r_s} \approx -2 \times 10^{-5} \text{ sec}^{-1},$$

assuming an average value $V = 30 \text{ m sec}^{-1}$. (The minus sign results from a negative radius of anticyclonic curvature.) Hence, according to Eq. (6) in Appendix A, for zero absolute vorticity

$$\frac{\partial v}{\partial n} = +f + \frac{V}{r} = 0.4164 \times 10^{-4} \text{ sec}^{-1}$$

Taking, again, $\Delta n = 200 \text{ km}$, we arrive at $\Delta u = 832.8 \text{ cm sec}^{-1} \approx 8.3 \text{ m sec}^{-1} \approx 16 \text{ knots}$. This conforms reasonably well to the maximum horizontal shear conditions shown in Figure III-B-4.

Table III-B-1. Coriolis parameter, f , as a function of latitude (from List, 1958).

Latitude	$2\Omega \sin \phi$ (sec^{-1})	Latitude	$2\Omega \sin \phi$ (sec^{-1})
0°	0	50°	1.1172×10^{-4}
5	0.1271×10^{-4}	55	1.1947
10	0.2533	60	1.2630
15	0.3775	65	1.3218
20	0.4988	70	1.3705
25	0.6164	75	1.4087
30	0.7292	80	1.4363
35	0.8365	85	1.4529
40	0.9375	90	1.4584
45	1.0313		

Note: $f = 2\Omega \sin \phi$, where

ϕ = latitude

Ω = angular velocity of the earth = 7.292116×10^{-5} rad sec^{-1}

Examples of such maximum shears were given by Johnson (1964). Figure III-B-6 exhibits an example of average wind shears for three jet stream cases, together with a theoretical profile according to Eq. III-B (1). It appears that over a wide latitude band south of the jet maxima, the observed shears follow quite accurately the theoretical prediction. In Figure III-B-7, winds measured by Doppler radar on 24 January 1961 along an aircraft traverse over North Africa are plotted. Again, the wind profile conforms well to Eq. III-B (1). Near 10°N and near 24°N the critical wind shear of Eq. III-B (1) appears to have been exceeded locally. Such occasions also have been observed by Reiter (1963) near the PFJ over the United States. Such small departures from theory should not be viewed with great concern, however, because Eq. (1) in Appendix A contains a number of simplifying assumptions. (For more detail, see Reiter, 1963.)

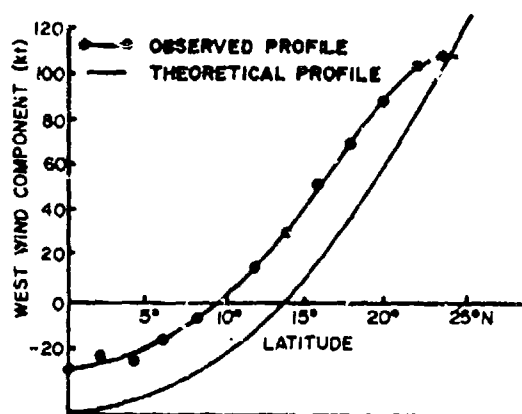


Figure III-B-6. Subtropical westerly jet stream: a mean westerly wind component profile (from Johnson, 1964).

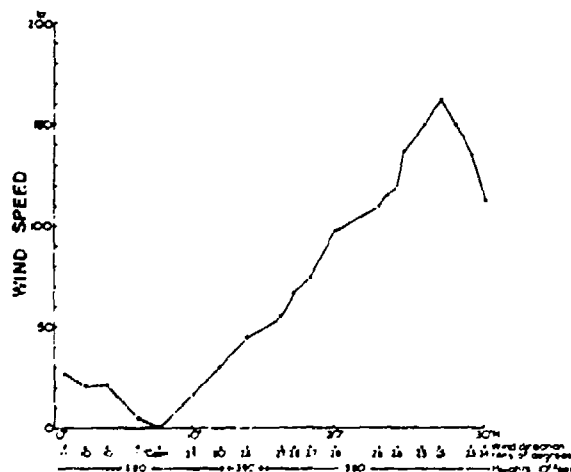


Figure III-B-7. Profile of wind speeds and directions measured during a flight across the subtropical jet stream, at longitudes near 25°E (from Johnson, 1964).

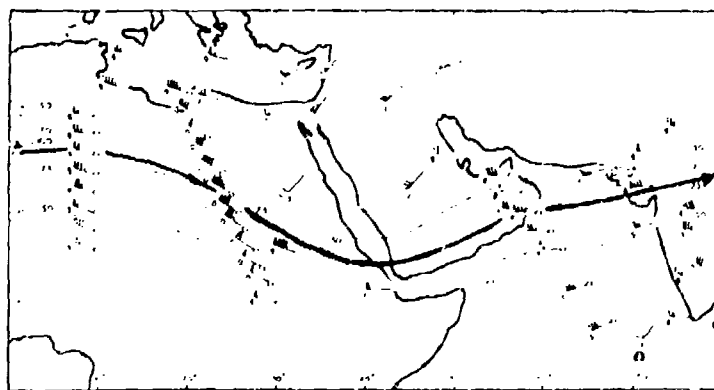


Figure III-B-8. 250-mb winds and 35,000-ft aircraft winds, 1200 GMT, 17 April 1968 (from Reiter, 1971).

A second example of an STJ maximum over North Africa is shown in Figure III-B-8. This time the winds were obtained from commercial aircraft (using Doppler equipment) on 17 April 1968 flying near the 250-mb level, i.e., slightly below the mean level of maximum wind in the STJ region. Again, the anticyclonic wind shears are close to those predicted in the example given above. This time the observed wind maximum was located only slightly to the west of the mean climatological position suggested by Figure III-B-3. However, a trough in the flow pattern is indicated over the Red Sea where a ridge is normally found. The weather pattern of 17 April 1968 was characterized by excessive rainfalls over the Red Sea, stimulated by the upper-level divergence in the left-front quadrant of the STJ maximum shown in Figure III-B-8.

4. Jet Stream Interaction

These two examples of an STJ over North Africa did not involve a pronounced interaction with the PFJ. Case studies of flow patterns under such interacting conditions require a denser radiosonde network such as that of the U.S.A. Figure III-B-9 shows a sequence of 250-mb isotach and isotherm patterns of the period 12 to 14 April 1962. The two jet stream systems, PFJ and STJ, interact strongly with each other during the time of pronounced surface cyclogenesis (after 12 April, 1200 GMT).

Figure III-B-10 comprises a sequence of surface weather charts containing the period of cyclogenesis. Cross-sections of potential temperature, wind speed and wind direction through this jet stream situation at 0001 GMT on 13 April, are shown in Figures III-B-12 and III-B-13 (Figure III-B-11 shows the locations of these cross-sections). There is a deep layer between approximately 300 and 200 mb in which the wind backs strongly with height. In the cold air, the wind direction is northwesterly. In the warm air above, the flow is from the west to southwest. This turning of wind with height may also be seen from the 250-mb isotach chart in Figure III-B-9 for 1200 GMT on 13 April 1962. Here it appears as though the winds were cornering around an extremely sharp trough line that trails off from the Great Lakes region towards the Texas-Mexico border.

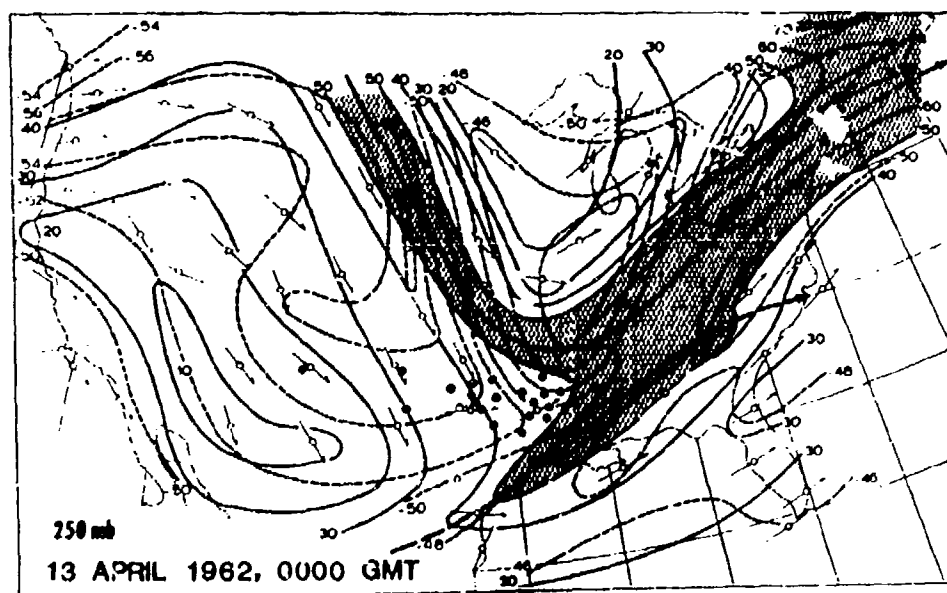
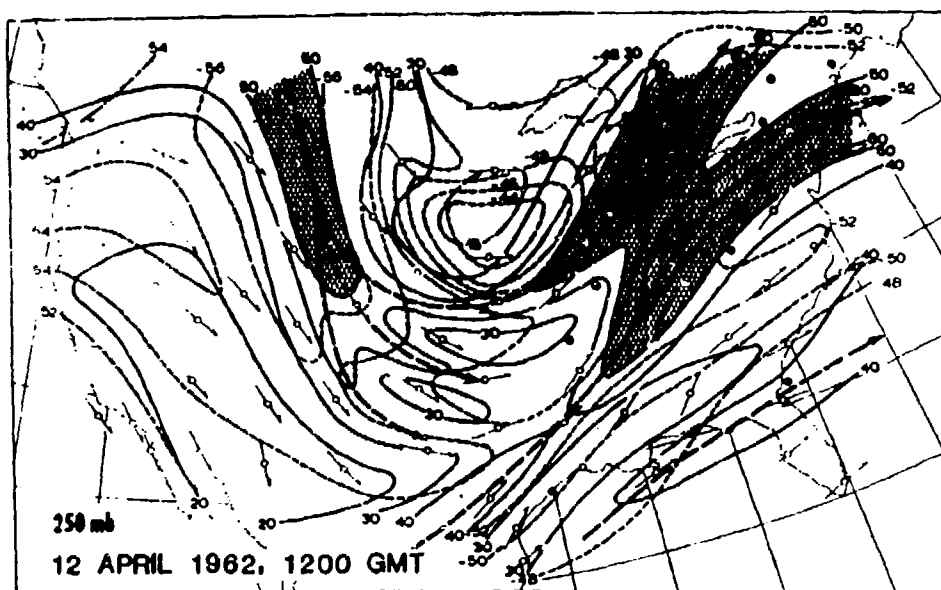


Figure III-B-9. Isotachs (solid lines, heavy numbers, m sec^{-1}) and isotherms (dashed lines, light numbers, centigrade) of the 250-mb surface for dates and times as indicated. Regions with speeds $> 50 \text{ m sec}^{-1}$ are shaded. Half-filled circles stand for reports with moderate CAT, heavy dots stand for severe CAT. (Numerous reports of light CAT have not been entered into this figure.) Jet axes indicated by heavy dashed lines and arrows (from Reiter and Nania, 1964).

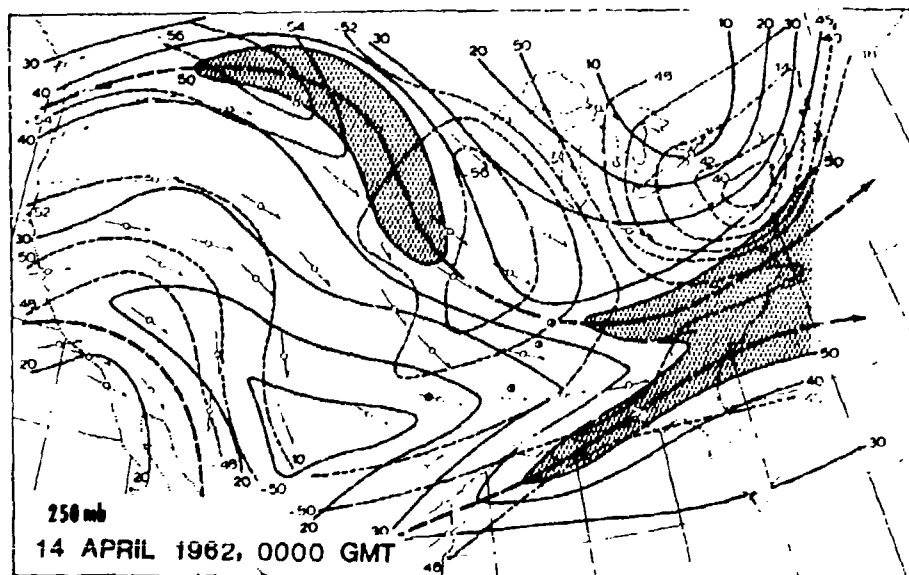
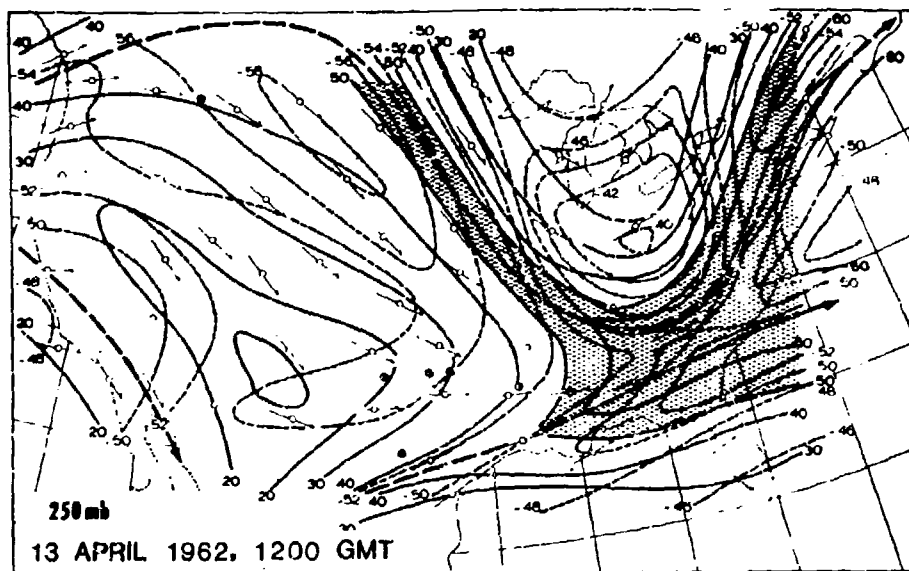


Figure III-B-9 (continued)

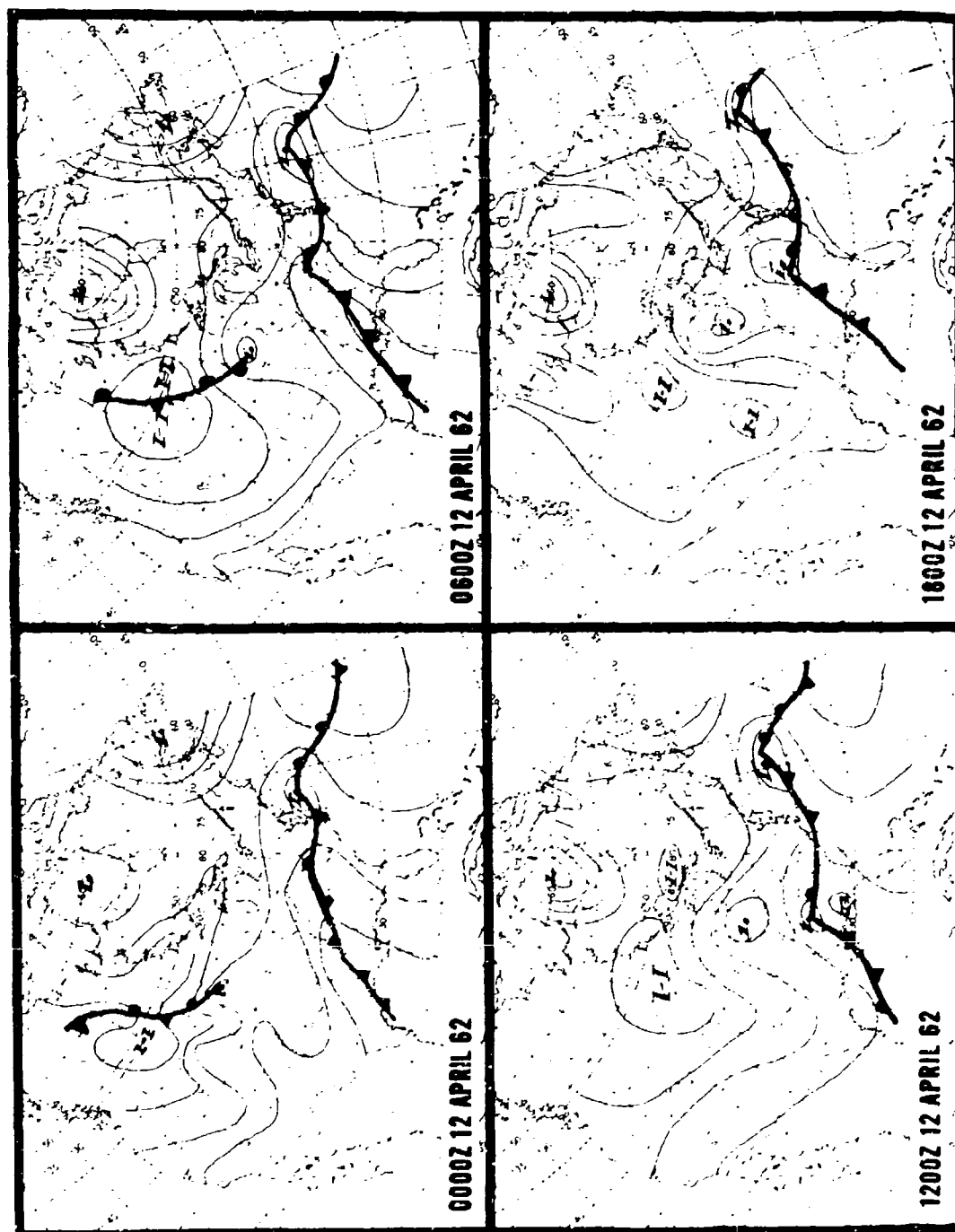


Figure III-B-10. Surface weather maps for the period 0000 GMT, 12 April 1962 through 1800 GMT, 14 April 1962 showing characteristic case of cyclogenesis with PFJ and STJ interaction.

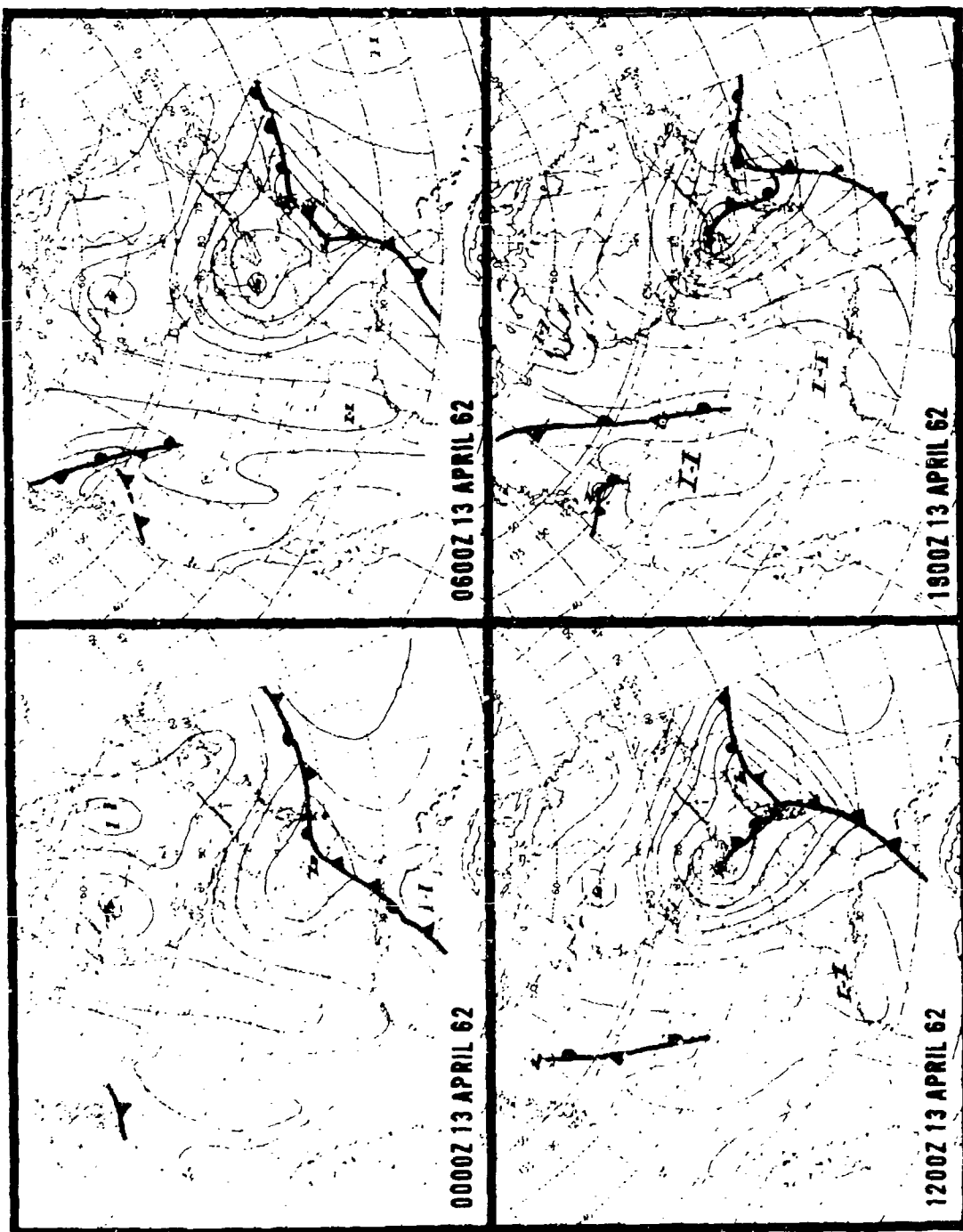


Figure III-B-10 (continued)

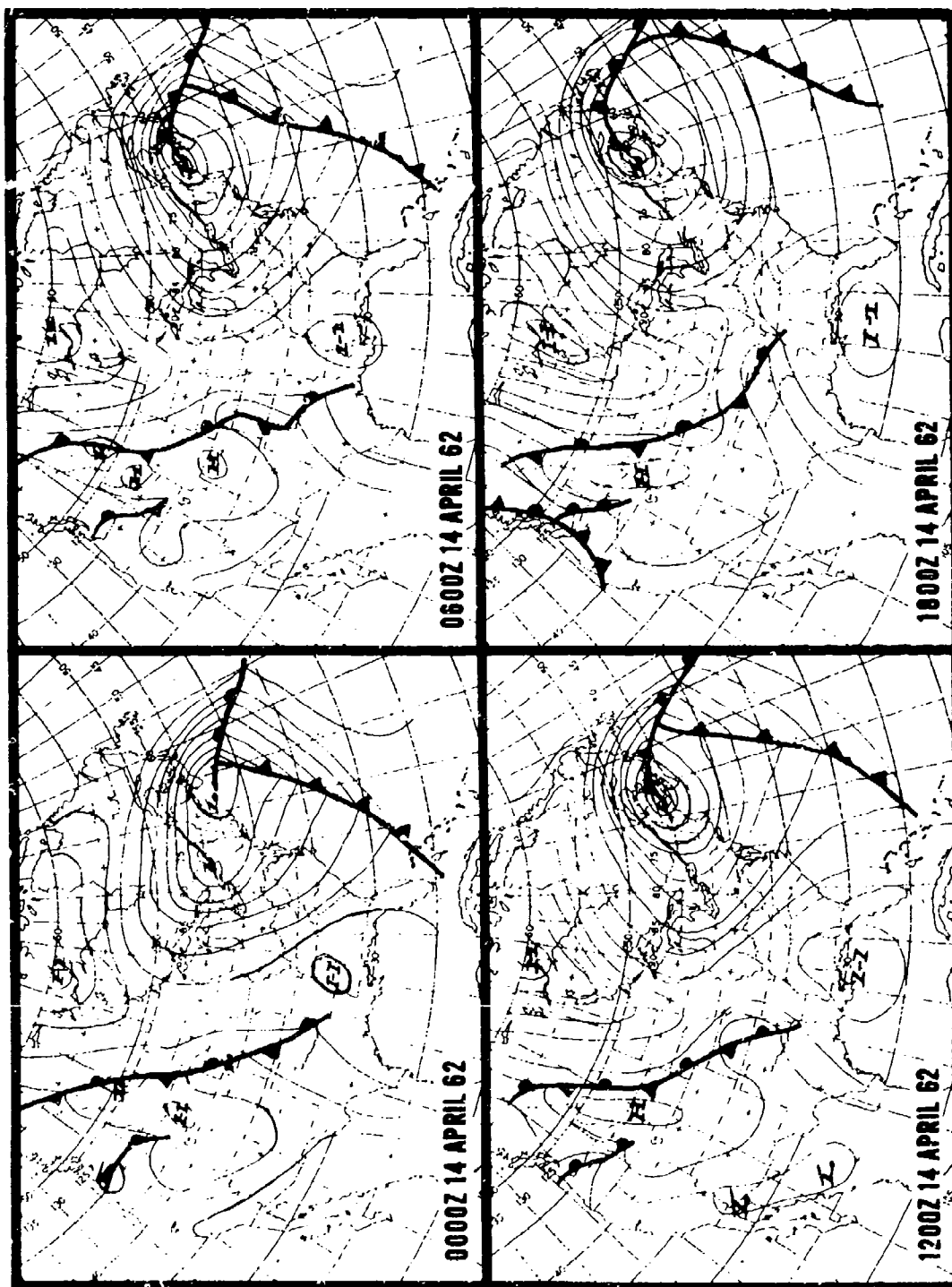


Figure III-B-10 (continued)

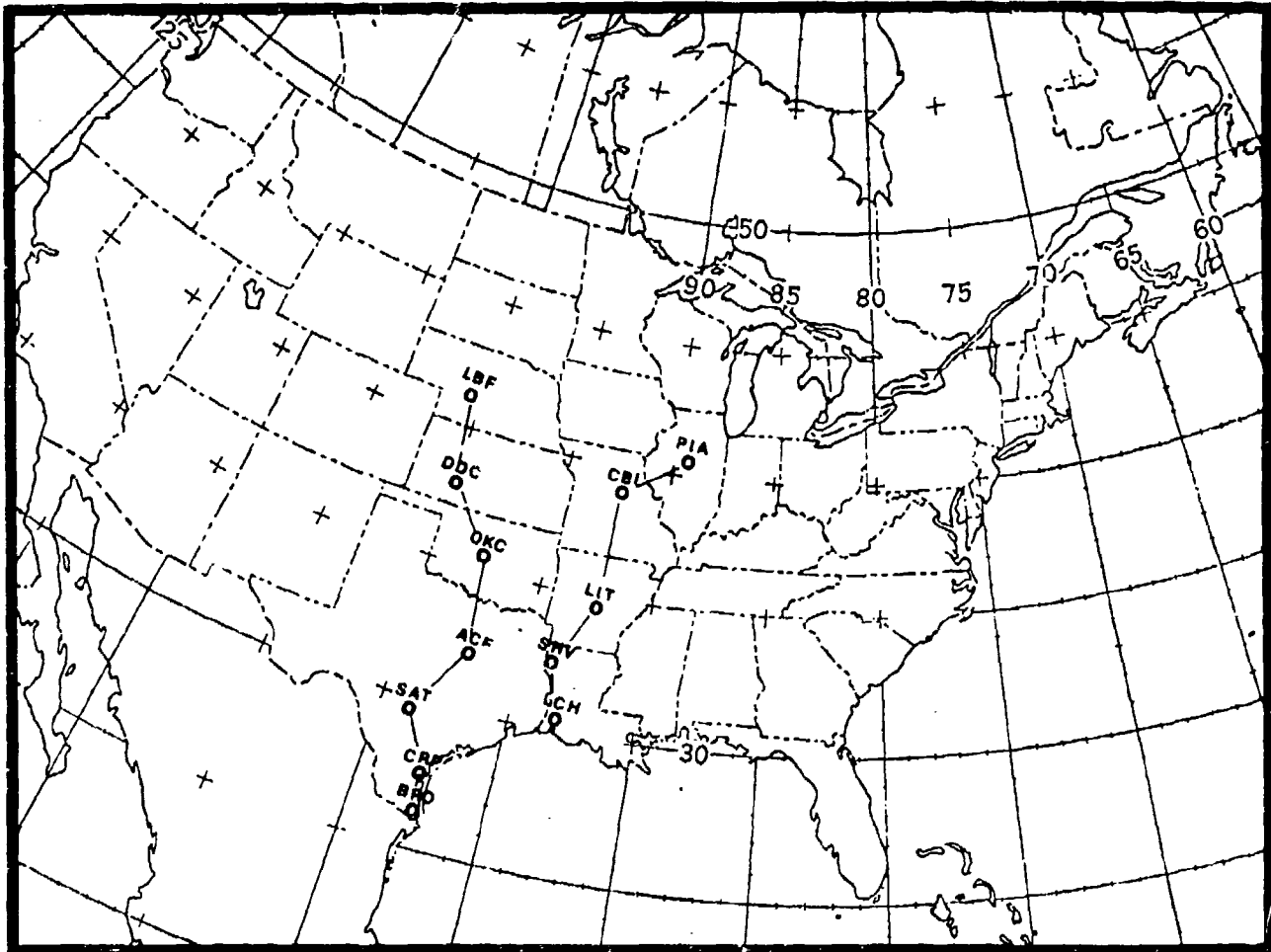
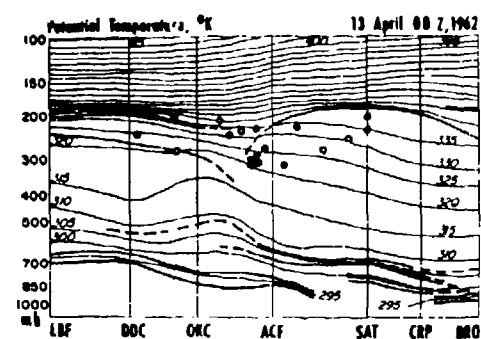
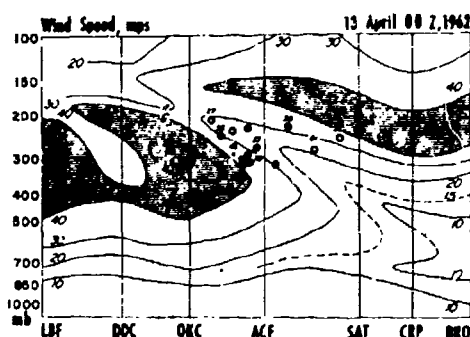


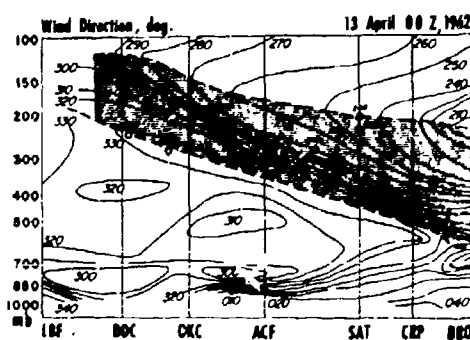
Figure III-B-11. Location of cross sections shown in Figures III-B-12 and III-B-13.



(a) Potential temperature (K); stable layers and tropopause are marked by heavy lines. CAT observations in the vicinity of the cross-sectional plane: open inner circles—light CAT; half-black inner circles—moderate CAT; black inner circles—severe CAT; the black portions of the outer rings indicate the time of the CAT observation (plus or minus 6 hours from map time shown by a black semi-circle to right or left of inner circle).



(b) Wind speeds (mps); aircraft wind reports are entered numerically next to CAT observations; x stands for wind report without turbulence; shaded: region with winds > 40 mps.



(c) Wind direction (degrees); maximum and minimum directions indicated by heavy dashed lines; shaded area marks region of strong turning of wind with height.

Figure III-B-12. Cross sections through the atmosphere from North Platte, Nebraska (LBF) to Brownsville, Texas (BRO), 13 April 1962, 0000 GMT (from Reiter and Nania, 1964).

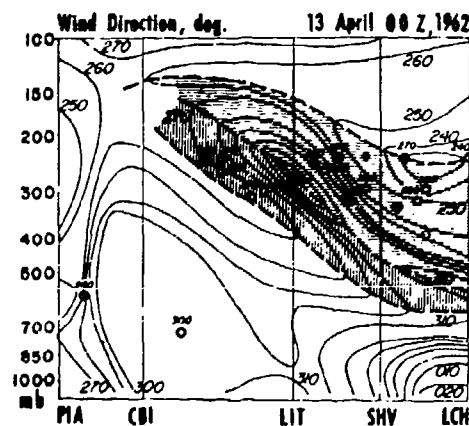
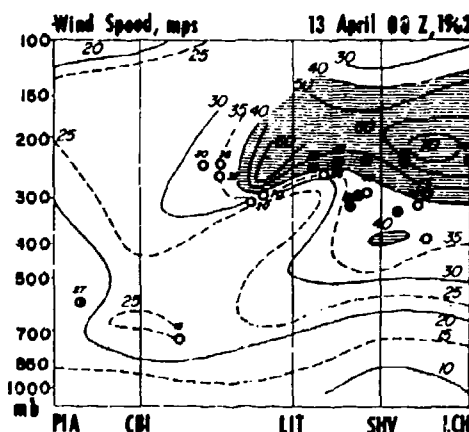
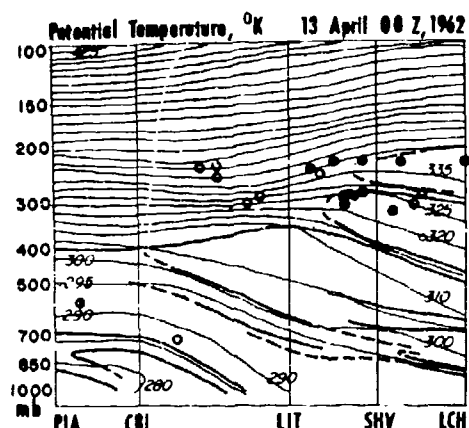


Figure III-B-13. Cross sections through the atmosphere from Peoria, Illinois (PIA) to Lake Charles, Louisiana (LCH), 13 April 1962, 0000 GMT. For explanation, see legend to Figure III-B-12 (from Reiter and Nania, 1964).

In reality, as Figures III-B-12c and III-B-13c show, the northern jet stream branch, identified with the PFJ, dips underneath the southwesterly STJ. This subsidence in the PFJ branch to the rear of the jet maximum gives rise to a cloud-free upper troposphere. The rising motion in the southwesterly current tends to produce a cirrus cloud shield (Figure III-B-14). This cloud shield extends from the STJ in the rear of the jet maximum to the PFJ in the front of the jet maximum, suggesting that the rising air currents from the southwest in the upper troposphere actually cross over the sinking currents from the northwest in the middle troposphere. The dotted jet axes in Figure III-B-9c actually take into account this "crossing over" of flow.

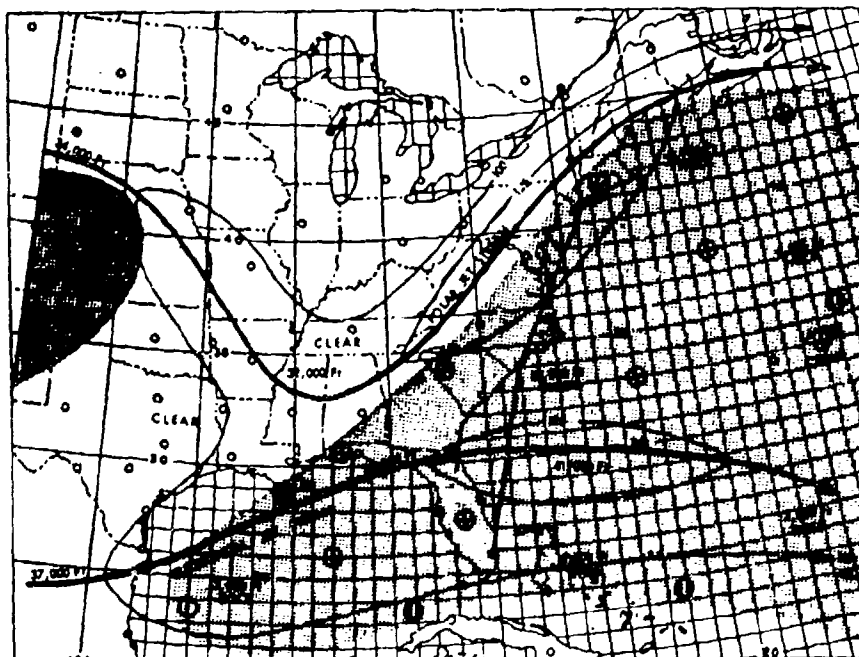


Figure III-B-14. Plan view of polar and subtropical jet streams with cirrus pattern. Jet cores - thick black lines; shaded areas - cirrus; height of maximum wind level of jet streams in thousands of feet; average thickness of cirrus in thousands of feet (from Reiter, 1972a).

The jet-stream interaction case presented here as an example was characterized by strong clear air turbulence (CAT), especially in the rear of the jet maximum where winds were backing strongly with height. These implications are discussed in Section V-A.

Even though the case illustrated above occurred over the United States, it is suspected that a similar interaction of PFJ and STJ occasionally takes place in the Mediterranean region. Especially, the cases of strong North African lows (see, e.g., Reiter, 1971, p. 100ff, case of 11-16 April 1967) or of intense Genoa cyclogenesis (ibid, p. 72ff, case of 17-19 February 1958) will have to be viewed in this context.

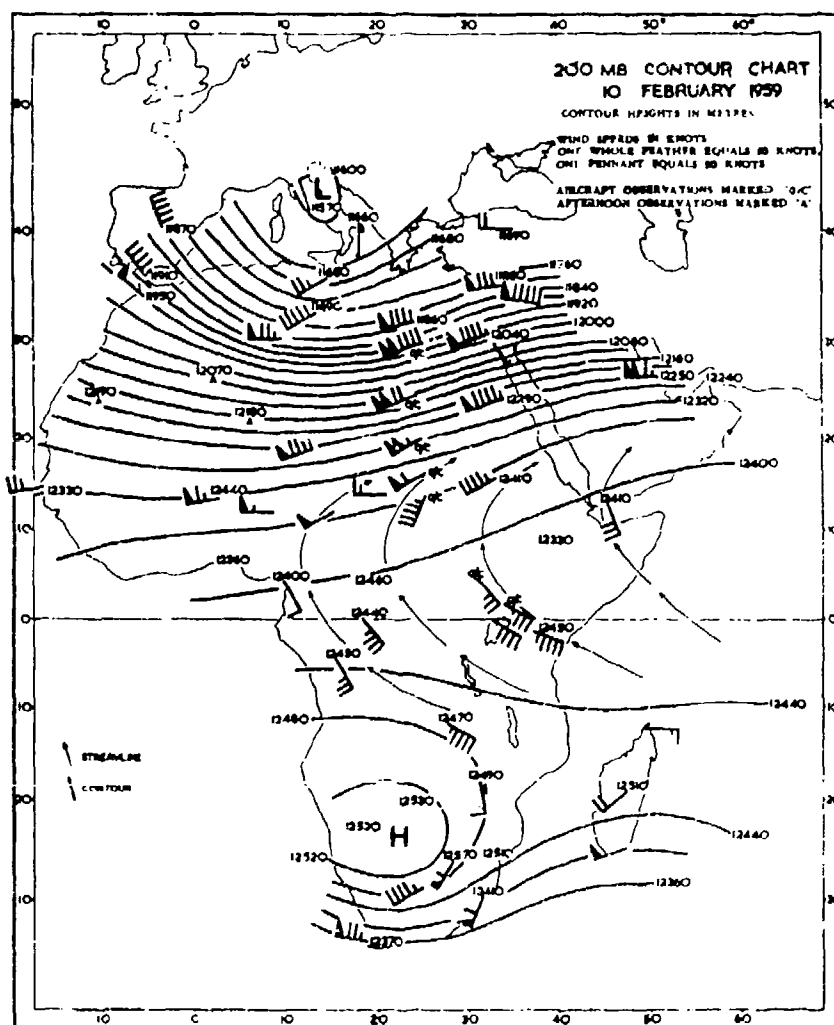


Figure III-B-15. 200-mb contour chart, 10 February 1959 (from Johnson, 1964).

A third case (10 February 1959) of an STJ over North Africa (Johnson, 1964) is shown in Figure III-B-15. This time the wind maximum is located over Egypt and Saudi Arabia, close to the climatological position of the mean wind maximum (see Figure III-B-3). The flow around the low pressure region over northern Italy and the anticyclonically curved streamlines over equatorial Africa (thin lines in Figure III-B-15) suggest that this jet maximum combined the flow in the PFJ and STJ as discussed above.

The foregoing examples have shown that the STJ is by no means a stationary phenomenon that could be described adequately by Figure III-B-3. Even though it does not behave as erratically as the PFJ, it undergoes daily variations due to traveling disturbances. These cause a shifting of trough and ridge locations, and perturbations in wind speeds and horizontal wind shears (see Figure III-B-16). Table III-B-2 shows these changing wind conditions through the relatively high values of standard deviation that prevail in the wind speeds of the STJ (see, e.g., the 200 mb level at Nicosia in this table (Sutcliffe, 1960a)). The paucity of upper-tropospheric wind data in subtropical and tropical latitudes makes forecasting the STJ a difficult task.

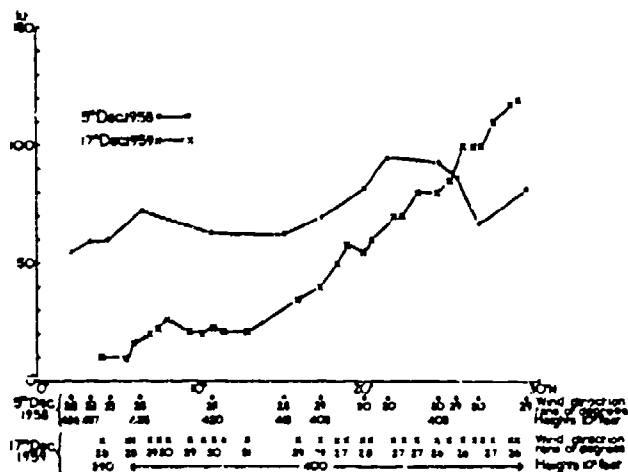


Figure III-B-16. Profiles of wind speeds measured during flights across the subtropical jet stream at longitudes near 25°E, 5 December 1958 and 17 December 1959 (from Johnson, 1964).

Table III-B-2. Upper wind and temperature characteristics
at four Mediterranean stations (from Sutcliffe, 1960a).

January						July				
mb	V	S	σ	T	sd	V	S	σ	T	sd
GIBRAL. AR										
100	295/18	23	18	-59	4.9	250/14	21	21	-64	3.2
150	300/20	28	26	-58	6.2	255/29	37	31	-59	3.0
200	310/19	33	34	-58	6.0	255/31	42	35	-52	3.1
300	320/15	39	43	-46	3.3	255/22	33	31	-36	3.7
500	315/13	30	33	-19	3.9	235/20	26	23	- 9	2.6
700	300/8	21	24	- 2	4.2	235/15	21	19	+11	2.2
850	280/5	18	21	+ 6	3.8	165/4	14	16	+21	3.4
MALTA										
100	275/31	34	23	-60	3.1	245/21	25	19	-65	3.4
150	270/40	45	31	-57	4.3	255/38	41	23	-58	3.0
200	270/40	51	41	-56	5.4	265/40	45	28	-49	3.1
300	280/28	52	52	-45	2.9	285/29	34	27	-34	3.6
500	290/17	35	37	-21	3.6	305/19	24	19	- 8	2.6
700	295/12	25	26	- 4	3.7	320/16	20	19	+ 9	2.8
850	275/10	21	22	+ 5	3.4	320/7	12	13	+19	3.1
BENINA (BANINAH)										
100	270/57	58	23	-63		200/17	21	19	-70	
150	265/76	79	22	-57		235/28	33	23	-60	
200	260/96	100	42	-54		245/31	34	24	-48	
300	260/85	91	45	-44		260/27	31	23	-29	
500	265/41	47	32	-19		315/21	26	13	- 5	
700	270/21	26	22	- 3		340/21	25	13	+11	
850	265/10	17	17	+ 5		355/13	16	11	+20	
NICOSIA										
100	270/45	47	22	-60	3.7	220/23	27	19	-69	2.9
150	275/62	66	32	-56	3.9	240/38	40	24	-58	2.9
200	275/70	76	44	-54	5.2	240/42	44	26	-45	2.5
300	275/59	70	51	-46	3.4	245/37	40	27	-26	2.3
500	275/31	38	32	-21	4.2	260/14	20	18	- 4	3.1
700	270/17	23	20	- 5	4.2	300/5	11	12	+11	2.4
850	265/6	14	15	+ 3	3.9	330/4	9	10	+21	2.7

V = Vector mean wind (kt)

σ = Vector standard deviation

T = Mean Temperature ($^{\circ}$ C)

S = Mean wind speed (kt)

sd = Standard deviation of temperature

5. Effects of Jet Streams on Cyclogenesis

In reference again to Figure III-B-3, it will be noted that the first and the third jet maxima in the STJ are located slightly downstream from regions of major cyclogenetic activity. The generation of cyclones in the lee of the Rocky Mountains is a phenomenon well known to the weather forecaster in the United States. The development of a trough in the westerlies in the lee of the mountains may be ascribed to the tendency of conservation of potential vorticity (see Appendix D and Section III-C, para. 1). The STJ wind maximum shown in Figure III-B-3 is actually located in a ridge, however. This seeming controversy may be explained by the fact that the STJ itself does not trigger frontal cyclogenesis along the polar front. It does interact with the PFJ, however, as soon as pronounced cyclogenesis in this region occurs; when such interaction takes place, the PFJ axis is curved cyclonically and the STJ axis is curved anticyclonically (see Figure III-B-9 for comparison). Thus, the STJ wind maximum over the United States may be viewed as a perturbation of the zonal flow in the upper troposphere at subtropical latitudes, caused by a trough and frequent cyclogenesis along the PFJ in the lee of the Rockies.

An analogy may be noted in the anticyclonically curved STJ wind maximum over Japan (Figure III-B-3) downstream from the East China Sea. In this region, frequent and strong cyclogenesis occurs along the polar front that separates the cold air sweeping around the barrier of the Himalayas and the Plateau of Tibet and the warm air originating over Southeast Asia.

Addressing the consideration of the STJ wind maximum in the Mediterranean region, Figure III-B-17 shows the frequency of cyclogenesis during January and February (Frank and Elliot, 1953). During the winter, the Gulf of Genoa is one of the most cyclogenetically active regions of the world. This is also expressed in older statistics by Petterssen (1956) (Figures III-B-18 and III-B-19).

This cyclogenetic activity has been ascribed by Godev (1971a) to the orographic effect of the Alps (see Appendix D, also Section III-C, para. 1) and to the concave shape of mountains and coastline in the Gulf of Genoa (see Section III-C, para. 2). In view of Figure III-B-3, it must also be concluded that this region of preferred cyclogenesis is in exactly the right position with respect to the Mediterranean STJ wind maximum which, in turn, may be explained as a resonant planetary wave between the two waves produced by the Rocky Mountains and the Himalayas. Thus, jet stream interaction is a likely contributing factor in cases of intense cyclogenesis in this region.

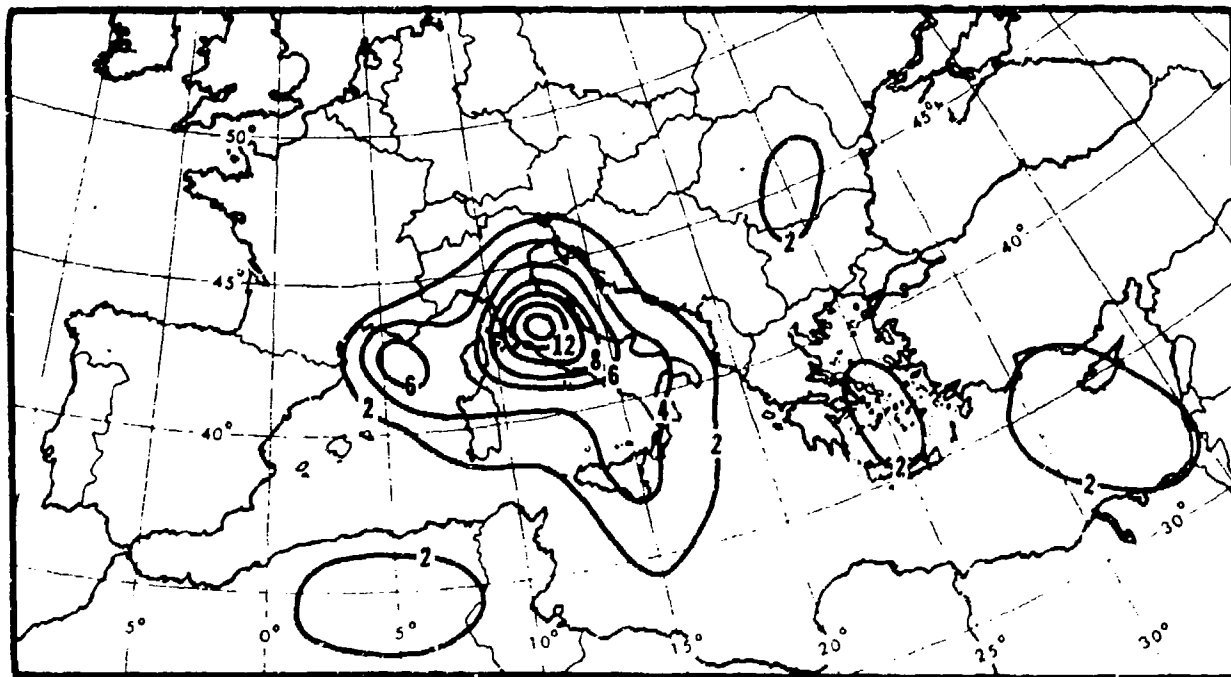
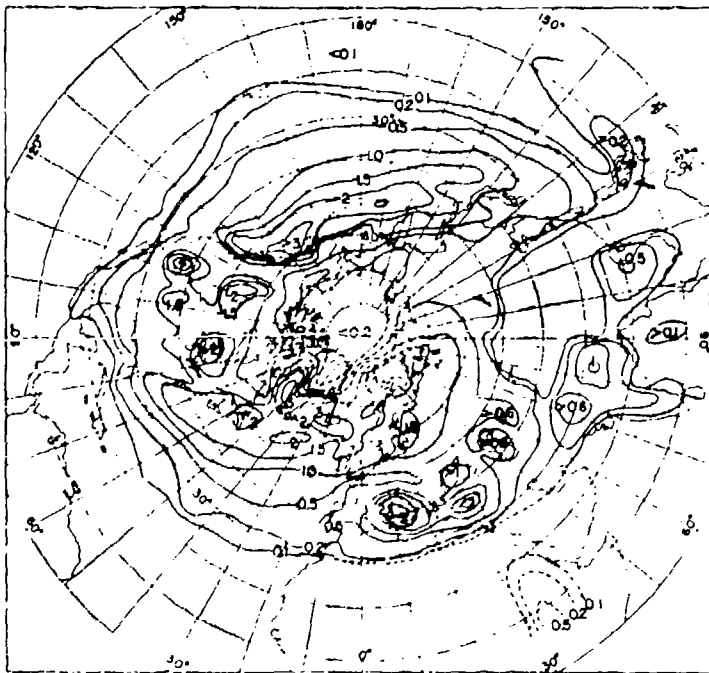
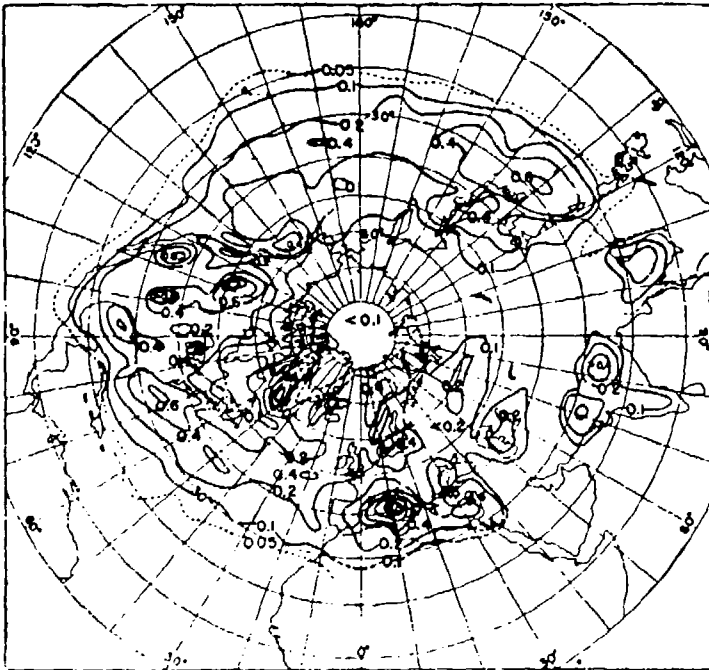


Figure III-B-17. Frequency of cyclogenesis, January-February
(from Frank and Elliott, 1953).

Figure III-B-3 depicts the Mediterranean and Japanese STJ wind maxima as the stronger two of the three. At the level of the PFJ (300 mb), the Mediterranean wind maximum of the winter season seems to be the weakest of the three. This may be inferred from Figure III-B-20 which shows the mean total kinetic energy (averaged for the months of January for the years 1950 to 1957, in units of $\text{kg m}^{-1} \text{sec}^{-2}$, and proportional to $\frac{\bar{v}^2}{2}$) and the eddy kinetic energy (proportional to $\frac{\overline{(v')^2}}{2}$, where v' indicates the departures of daily values of wind speed from the long-term January average, \bar{v}).



Actually, caution must be exercised in ascribing the wind maxima in Figure III-B-20 exclusively to the PFJ. Whereas the maxima over Japan and over the U.S. coincide well with the average position of the polar front jet stream, the maximum over North Africa and Saudi Arabia is too far south for the average location of the PFJ and corresponds better to the position of the STJ shown in Figure III-B-3. The reason for this apparent discrepancy is that the PFJ, due to varying weather patterns, migrates over a much wider latitude range over Europe than over the U.S. or Asia. Thus, it becomes a very fickle entity which tends to be "washed out" in the statistical averaging process and does not dominate the pattern of mean kinetic energy in Figure III-B-20. The eddy kinetic energy, on the other hand, shows relatively large values over Northern Europe and the Mediterranean region as well, again indicating the great day-to-day variability of the PFJ in this region. The STJ, in contrast, is rather stable and changes its position only slowly. Therefore, even at the 300-mb level (which is considerably below the level of maximum wind), it dominates the scene.

Summer kinetic energy distributions are illustrated in Figure III-B-21. The European jet maximum has all but disappeared. The STJ during the warm season cannot be identified any longer as a circum-hemispheric system, the reason for this being that the meteorological equator with its ascending mean air motion along the intertropical convergence zone (ITCZ) has shifted far into the Northern Hemisphere. This exposes the ensuing Hadley circulation to a relatively large Coriolis parameter. Dishpan experiments have shown that, with a relatively large rate of rotation (commensurate to a large Coriolis parameter), a hemispheric Hadley cell with a symmetric (three-) wave pattern is not capable of transporting the required amount of heat and absolute angular momentum poleward. The flow breaks down into an irregular wave regime.

During summer the cyclogenetically active region shifts from the Gulf of Genoa to the northwest (Figures III-B-22 and III-B-23). This is in agreement with a maximum of eddy kinetic energy, shown in Figure III-B-21, that indicates frequent traverses of PFJ maxima over the Bay of Biscay region.

Figures III-B-18, III-B-19, III-B-22 and III-B-23 provide a quick comparison between winter and summer conditions over the Mediterranean region, and a tie-in of this region with the weather patterns over the rest of the Northern Hemisphere. More recent statistics by Black (1969) allow us to follow the cyclogenetic activity over Europe and the Mediterranean on a month-by-month basis. Results are shown in Figure III-B-24 and are based upon statistics by Klein (1957).

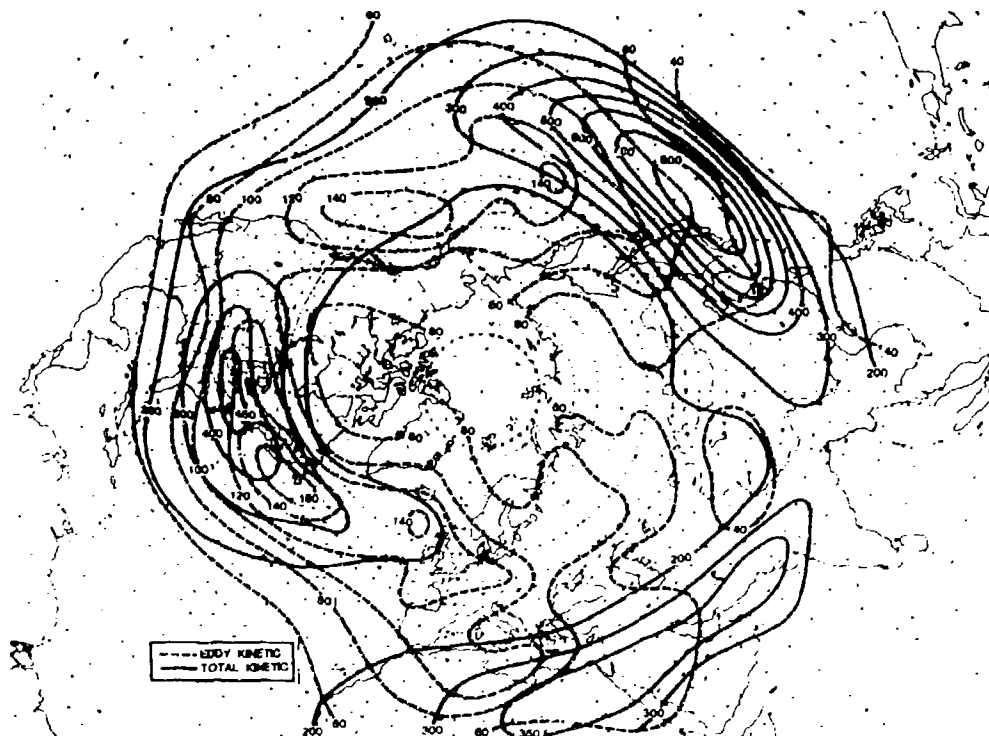


Figure III-B-20. Distribution of mean total (solid lines) and eddy kinetic energies (dashed lines) ($\text{kg m}^{-1} \text{sec}^{-2}$) at 300 mb for January (from Reiter, 1969).

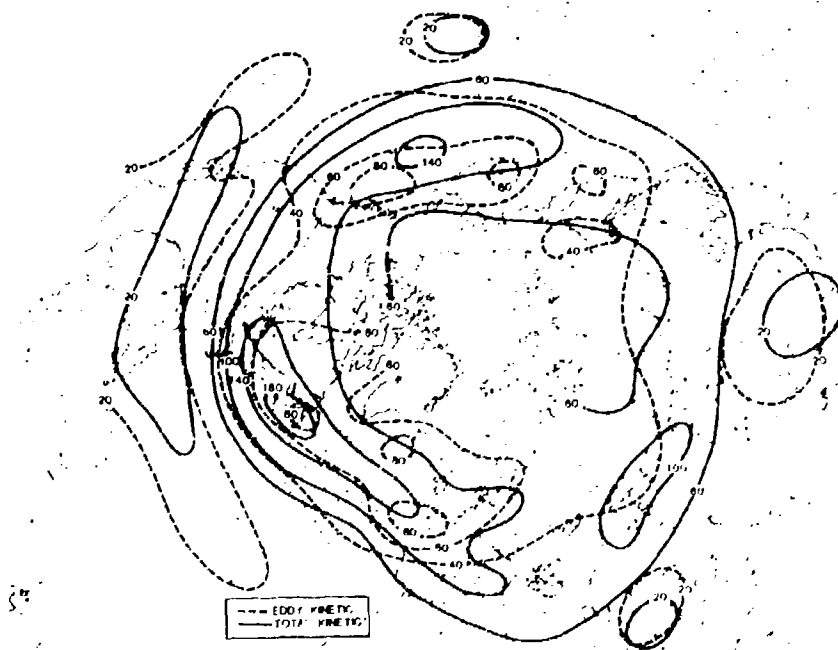
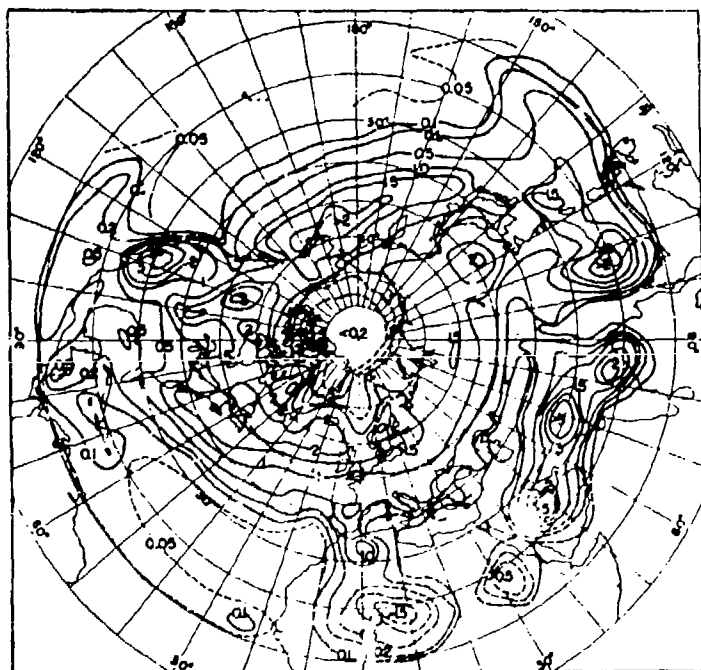
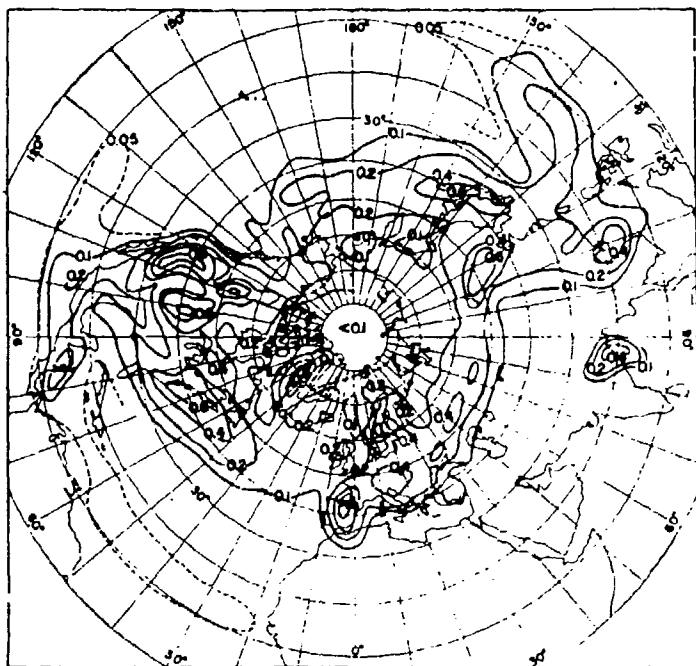


Figure III-B-21. Distribution of mean total (solid lines) and eddy kinetic energies (dashed lines), ($\text{kg m}^{-1} \text{sec}^{-2}$) at 300 mb for July (from Reiter, 1969).



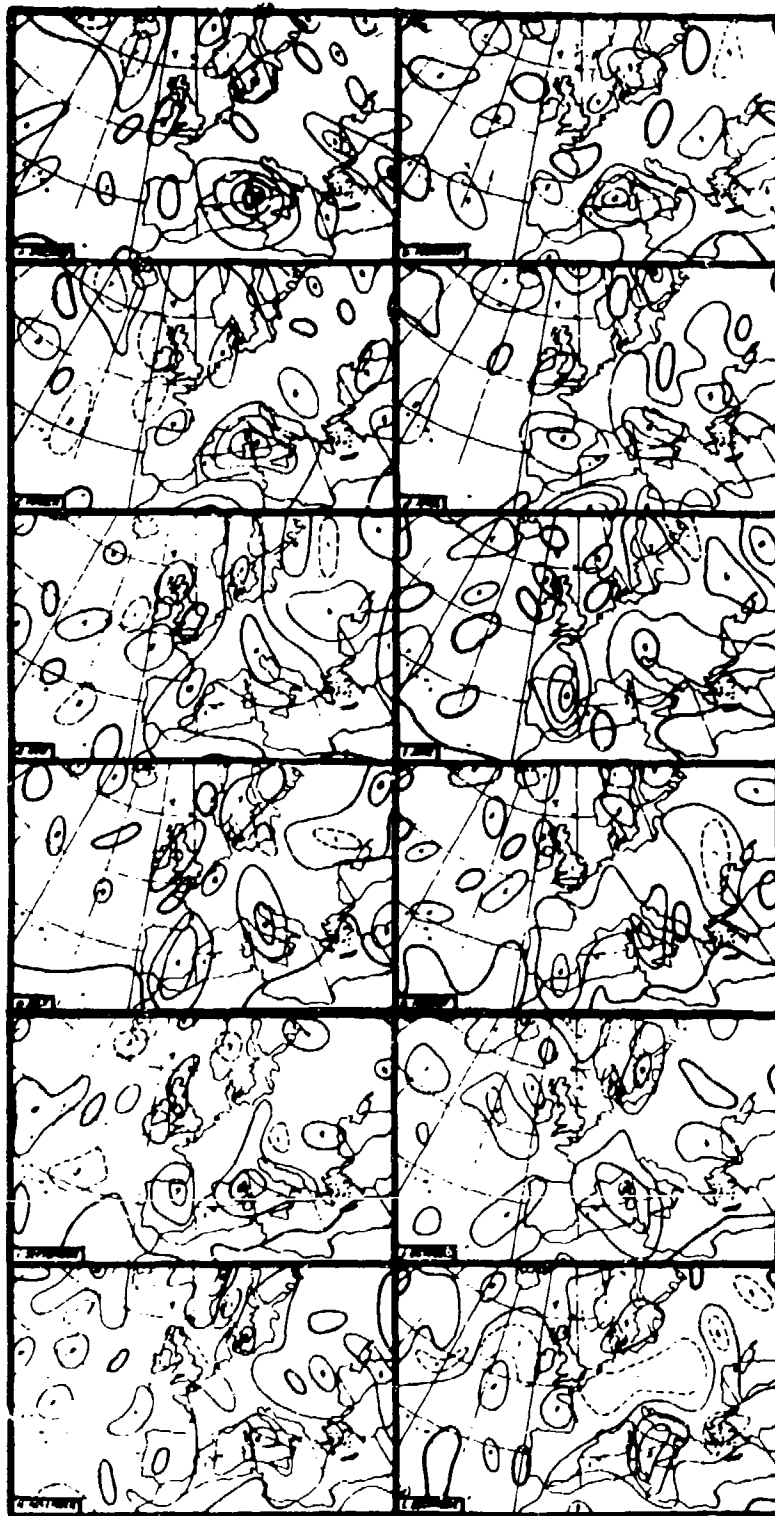


Figure III-B-24. Areas of cyclogenesis by month. Isopleths are at intervals of four with intermediate isopleths dashed. Zero isopleths are heavier (from Black, 1969).

The isopleths indicate, for each calendar month, the number of cyclones that originated within unit boxes over a 20-year period. Only the location of the low at 1230 GMT on the first day of its existence was considered. The frequencies were counted in boxes 5° latitude in length and of the varying widths listed in Table III-B-3. Since all boxes were roughly equal in area to a unit box 5° latitude by 5° longitude at 47°N, no further adjustment was made. In addition to the above-mentioned shift of cyclogenetic activity between winter and summer from the Gulf of Genoa to the northwest, Figure III-B-24 indicates the following interesting features:

- (1) North African depressions tend to form most frequently during March and April south of the Atlas Mountains.
- (2) During June and July there is a strong tendency for low-pressure systems to form over Spain (Iberian low). These systems have a tendency to become quasi-stationary because of the temperature contrast between the Iberian Peninsula and Atlantic and Mediterranean waters. Forecasting the slow movement of these depressions and their associated cloud and precipitation systems is a challenging but not always successful task.
- (3) Cyclogenesis in the Gulf of Iskenderun, especially during July, is in correlation with the occurrence of etesian winds in the Aegean Sea.

Unfortunately the analyses shown in Figure III-B-24 were constructed using an extremely coarse grid with resultant great loss of detail. Therefore, it was felt that a special study would be necessary to provide deeper insight into cyclogenesis within the Mediterranean region.

Two sets of surface pressure maps were used for the study, each made at six-hour intervals. The first, covering the period 1 January 1965 through 31 December 1969, was analyzed by the Air Ministry Meteorological Office at Malta. The second, covering the period 1 October 1972 through 31 July 1974 consisted of the high-resolution fields by Information Blending (FIB) analyses for the Mediterranean (FIB/SLP-MED) produced by Fleet Numerical Weather Central, Monterey, California.

In order to classify the cases of cyclogenesis, there first had to be a closed circulation visible on two consecutive charts. Second, this depression had to show some movement away from its place of origin -- a procedure which, hopefully, would exclude pure heat lows from the sample. Finally, due to manpower limitations, only those depressions which affected the weather in the Mediterranean were included; therefore, lows which remained over North Africa were not counted.

Table III-B-3. Width of 5° boxes in degrees longitude and miles (Klein, 1957).

Latitude (°N)	Width (°long.)	Width (miles)
05-09	3	206
10-14	3	203
15-19	4	265
20-24	4	257
25-29	4	247
30-34	4	235
35-39	4	221
40-44	5	257
45-49	5	236
50-54	5	213
55-59	6	227
60-64	8	260
65-69	9	244
70-74	12	257
75-79	15	234
80-84	24	232
Mean		237

Figure III-B-25 shows the locations where cyclogenesis was first observed for all the seasons of the year. The data were not analyzed with isopleths because of the smallness of the data sample (only about seven years). This figure clearly indicates, however, that the area of the Gulf of Genoa and northern Italy has the maximum occurrence of cyclogenesis in the Mediterranean region. It can also be seen that the maximum density moves from the relatively warm water of the Gulf of Genoa during the winter to the hot land regions during the summer. It should be pointed out that the results in Figure III-B-24 suggest that the area of maximum cyclogenesis is located much farther south in the winter (over Sardinia). The probable reason for this incorrect conclusion is the use of a too-coarse grid spacing. Another interesting difference between Figures III-B-24 and III-B-25 is the lack of cyclogenesis over the Iberian Peninsula in the summer in the recent study. This is likely caused by the exclusion of heat lows from the data shown in Figure III-B-25.

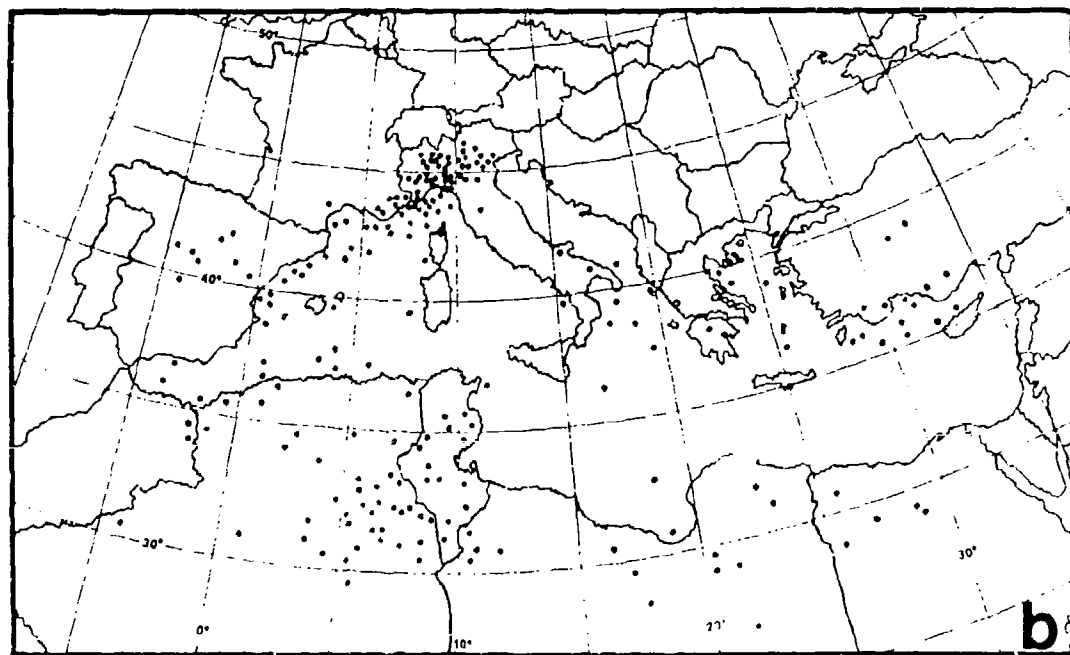
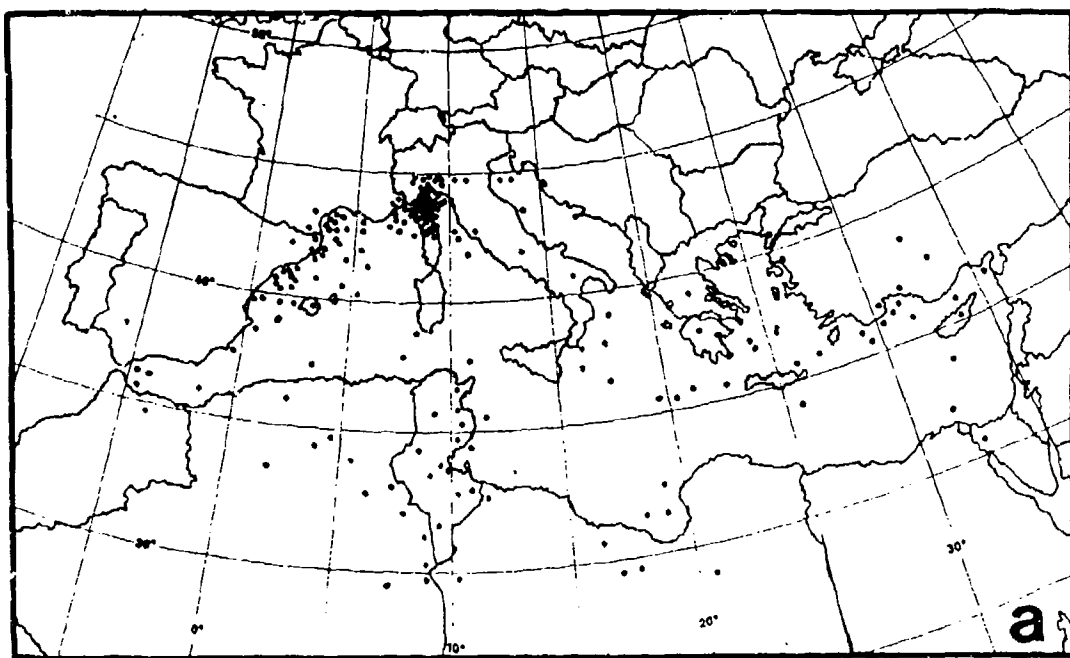


Figure III-B-25. Occurrence of cyclogenesis during the seasons indicated for periods 1 Jan 65 through 31 Dec 69 and 1 Oct 72 through 31 Jul 74 (see text) (a) Dec-Feb, (b) Mar-May, (c) June-Aug, and (d) Sept-Nov.

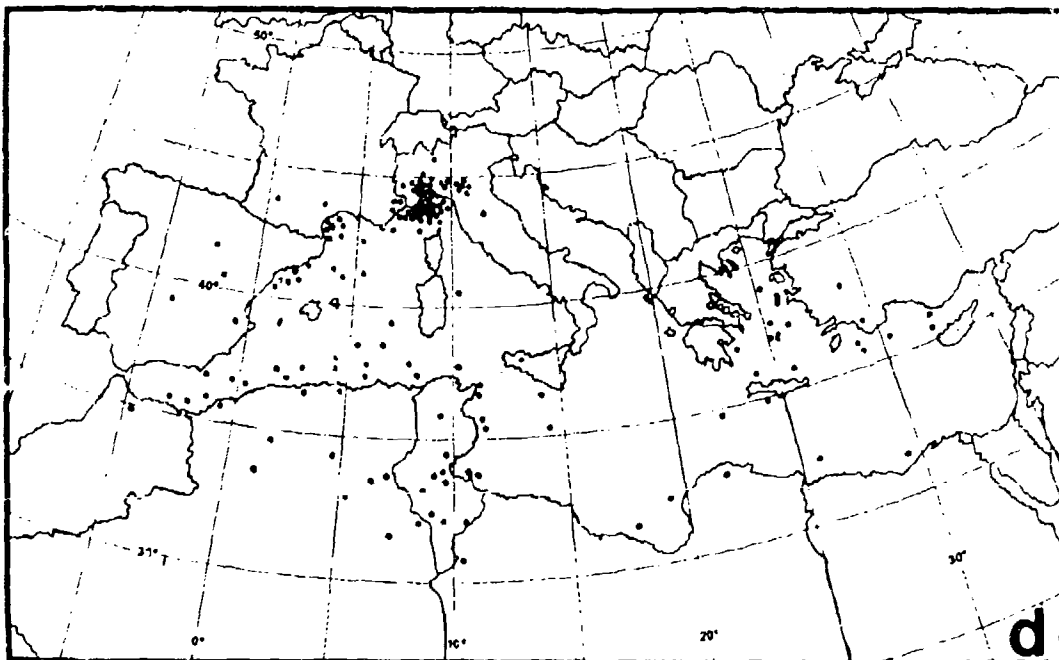
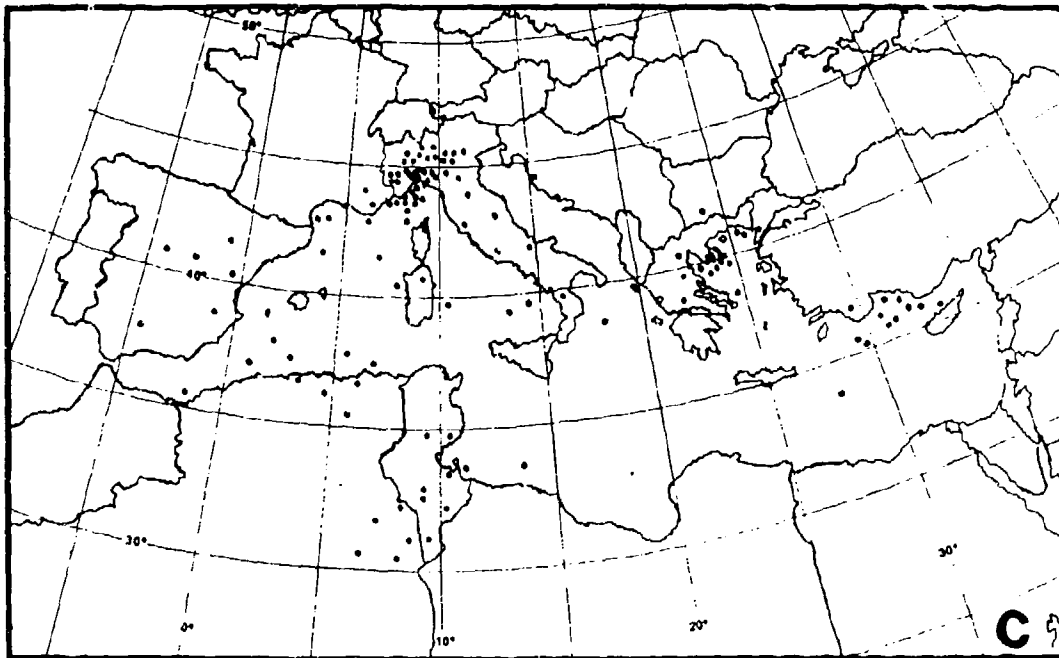


Figure III-B-25 (continued)

According to Figure III-B-23, the southern Sahara during summer is characterized by a relatively high frequency of cyclonic centers. These have to be classified as "heat lows" which are restricted to the lower half of the troposphere and cause the observed monsoonal weather patterns over tropical Africa. In the upper troposphere, anticyclonic conditions and outflow prevail over subtropical Africa. Along the northern rim of this upper-tropospheric anticyclone is found the westerly jet stream over Europe (Figure III-B-21). Along the southern edge of the anticyclone flows the tropical easterly jet stream (Figure III-B-26) with its wave disturbances. This tropical easterly jet (TEJ) is characteristic of the summer monsoon circulation over Southeast Asia, India, the Indian Ocean and Africa.

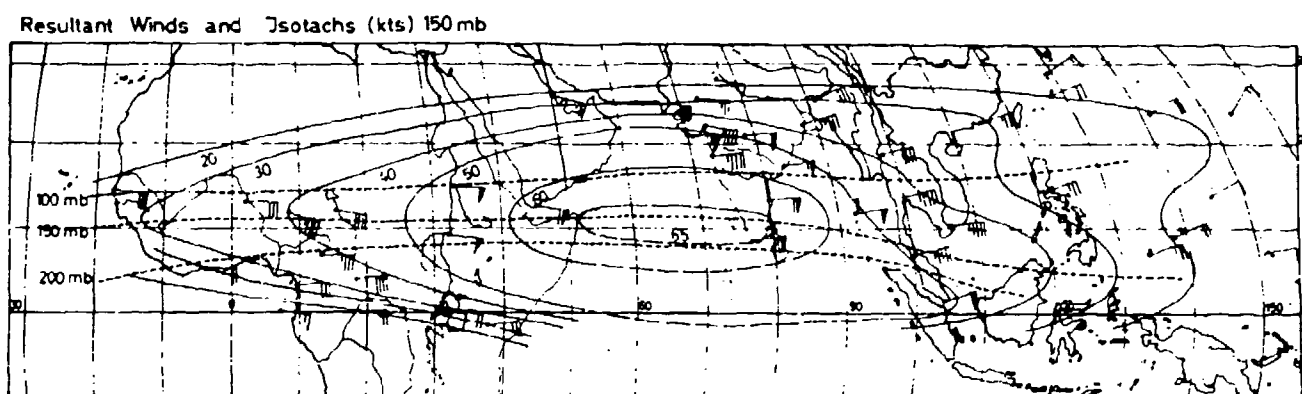


Figure III-B-26. Resultant winds and isotachs (kt) for 150 mb representative for July. Dashed lines indicate jet axis for 100 mb, 150 mb, and 200 mb (from Flohn, 1964).

6. Anticyclones and Jet Stream

The distribution of anticyclogenesis and anticyclones for winter and summer is shown in Figures III-B-27 through III-B-30. During the cold season, the Sahara south of the Atlas Mountains, Libya, and Egypt are the preferred regions in which the subtropical high-pressure belt resides. This is in agreement with the location of the STJ according to Figures III-B-2 and III-B-3. During summer the subtropical high-pressure activity shifts into the Mediterranean basin, stabilizing weather conditions there. The distribution shown in Figure III-B-30 also indicates the basic origination for the etesian wind regime (anticyclone maximum over the Black Sea) in the Eastern Mediterranean, which will be discussed in Section III-F, para. 4.

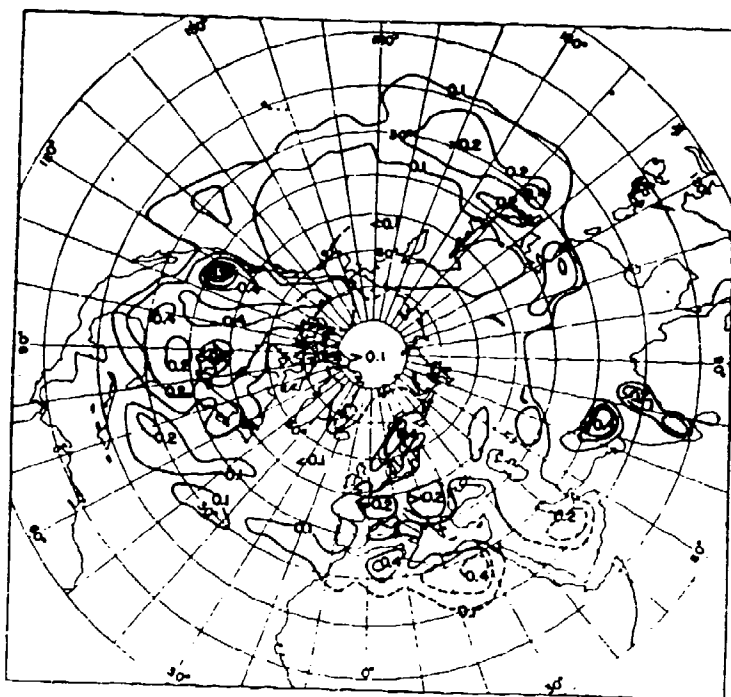


Figure III-B-27. Percentage frequency of occurrence of anticyclogenesis in squares of 100,000 km² in winter (1899-1939) (from Petterssen, 1956).

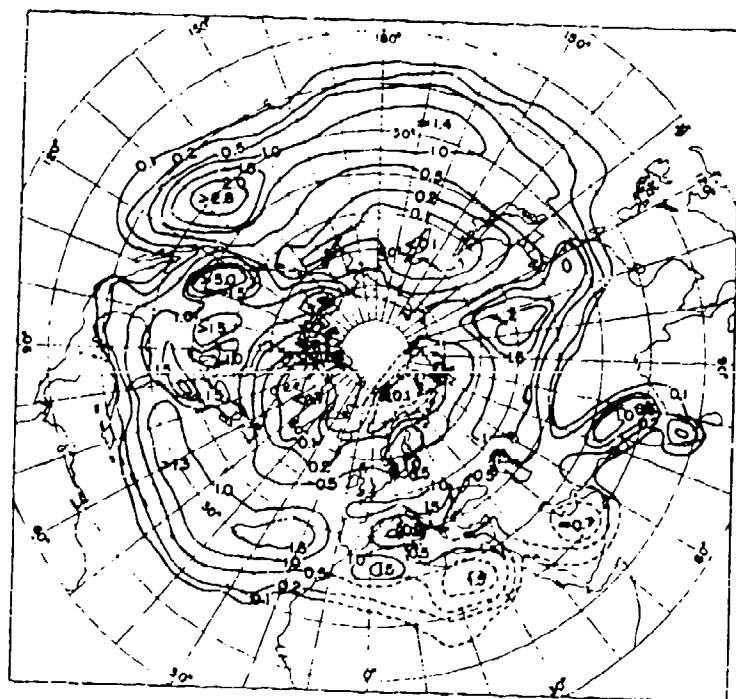


Figure III-B-28. Percentage frequency of centers of anticyclones in squares of 100,000 km² in winter (1899-1939) (from Petterssen, 1956).

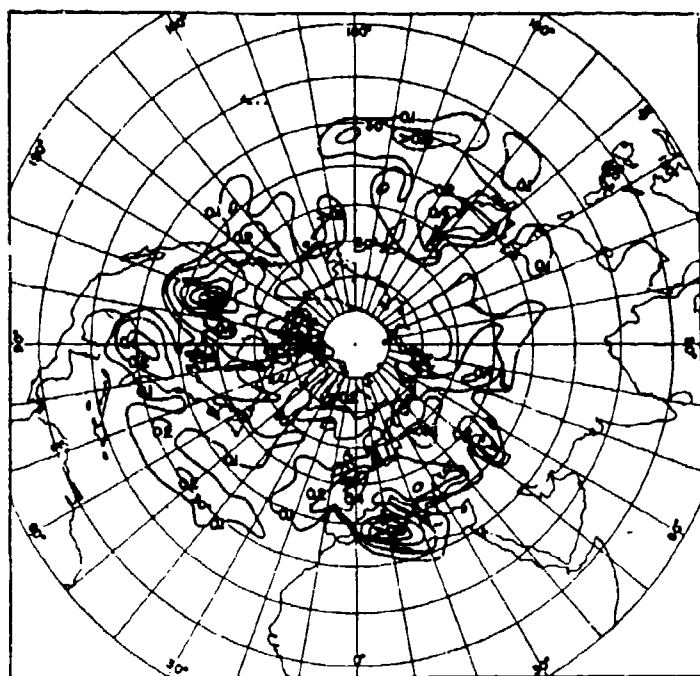


Figure III-B-29. Percentage frequency of occurrence of anticyclogenesis in squares of 100,000 km² in summer (1899-1939) (from Petterssen, 1956).

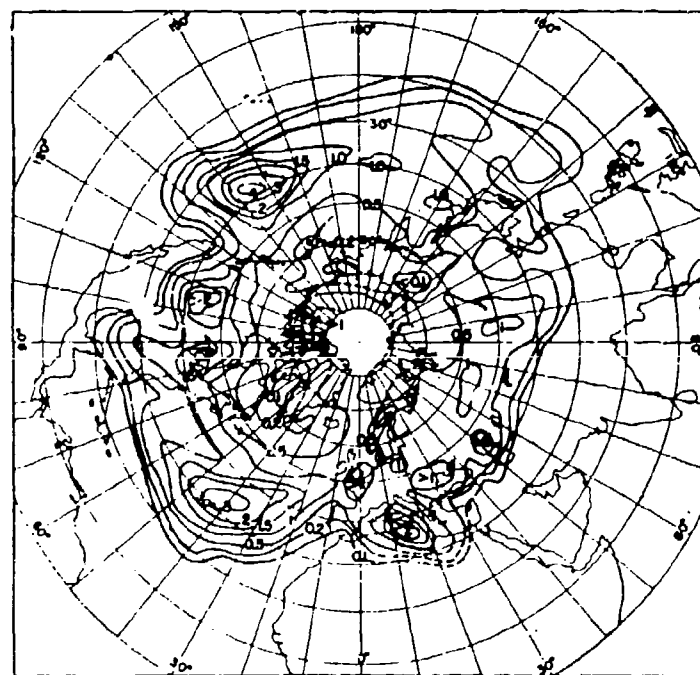


Figure III-B-30. Percentage frequency of centers of anticyclones in squares of 100,000 km² in summer (1899-1939) (from Petterssen, 1956).

The monthly progression of anticyclongenetic activity over Europe and the Mediterranean is shown in Figure III-B-31 (Black, 1969), which was constructed in a manner similar to that used for Figure III-B-24; this series of diagrams confirms the statements made in the preceding paragraph. March and April reveal frequency maxima of anticyclogenesis over North Africa. Together with the frequency maxima of cyclogenesis shown in Figure III-B-24, this indicates relatively unsettled weather conditions along the North African coastline during the spring transition season.

The variability of Mediterranean weather may also be deduced from Figures III-B-32 and III-B-33 which give the rate of alternation between cyclones and anticyclones (in percent) for winter and summer. This rate is computed as the frequency of cyclones divided by the frequency of anticyclones observed over a given location, multiplied by 100. It can be seen in these two diagrams that during winter the Mediterranean abounds with traveling disturbances, while in summer the same region is relatively quiescent.

A typical summer situation in the upper-tropospheric flow over North Africa is shown in Figure III-B-34 (Johnson, 1964). A weak westerly jet maximum appears along the northern edge of a high-pressure cell over Saudi Arabia. The TEJ is evident along the southern edge of this anticyclonic cell.

A comparison of Figure III-B-15 with Figure III-B-34 reveals the major differences between winter and summer that were noted briefly earlier. During winter the STJ flows over the surface location of the subtropical high-pressure belt. The ageostrophic inflow into the STJ from equatorial regions, postulated in the schematic cross section of Figure III-B-1 is quite clearly evident in Figure III-B-15 over central Africa. No closed anticyclonic cells are present in the upper troposphere on time-averaged weather charts over North Africa. The isobaric surfaces of the upper troposphere rise continuously from high latitudes towards the equator. In summer (Figure III-B-34), anticyclonic cells appear at the 200-mb level above the heat lows described in connection with Figure III-B-23. The cellular high-pressure pattern in subtropical latitudes, which characterizes the 200-mb chart of Figure III-B-34, prohibits a circum-hemispheric development of the STJ as suggested by Figure III-B-3 for winter. Only short segments and weak maxima, such as the one over the Eastern Mediterranean in Figure III-B-34, are evident.

Figures III-B-15 and III-B-34 showed the flow pattern for one characteristic day in each of the winter and summer seasons. Mean maps of the 300- and 100-mb surfaces lead to the same conclusions (Figure III-B-35 and III-B-36) (Sutcliffe, 1960a). Comparison of the mean vertical cross-sections of Figures III-B-37 and III-B-38 also reveals the disappearance of the westerly STJ during summer.

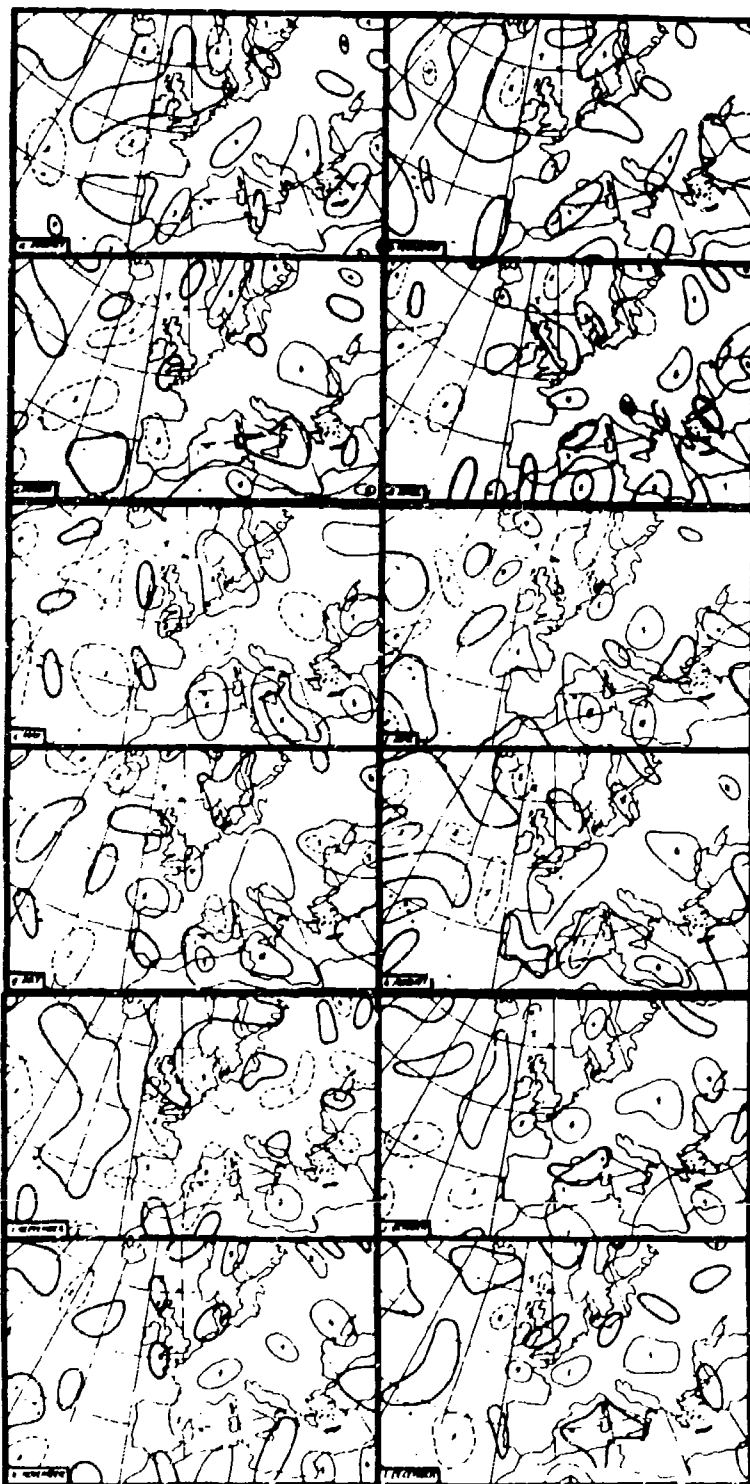


Figure III-B-31. Areas of anticyclogenesis by month. Isopleths are at intervals of four with intermediate isopleths dashed. Zero isopleths are heavier (from Black, 1969).

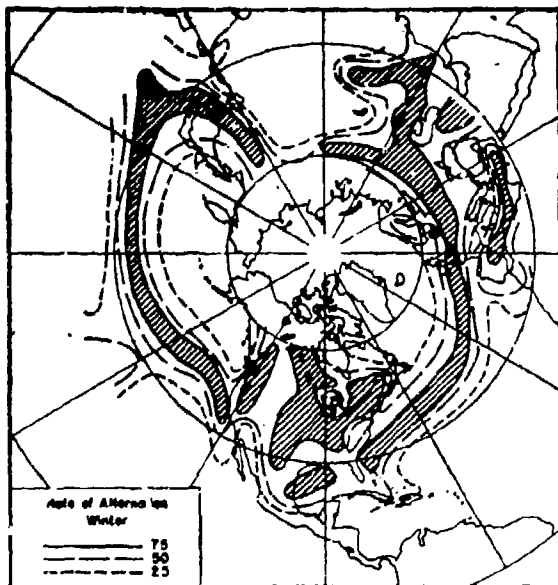


Figure III-B-32. Rate of alternation (percent) between cyclones and anti-cyclones in winter (from Petterssen, 1956).

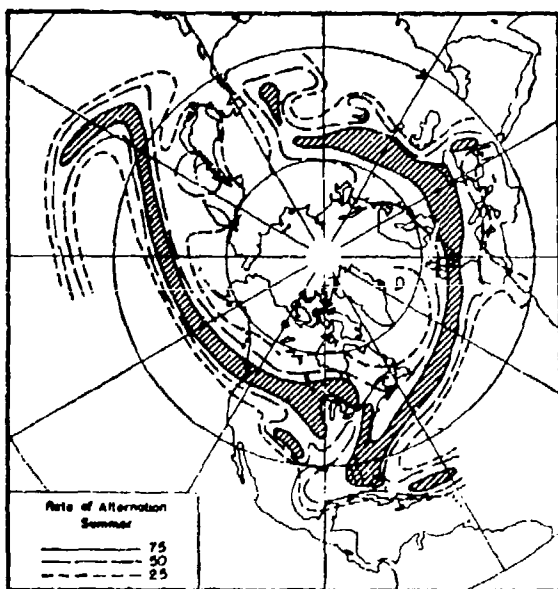


Figure III-B-33. Rate of alternation (percent) between cyclones and anti-cyclones in summer (from Petterssen, 1956).

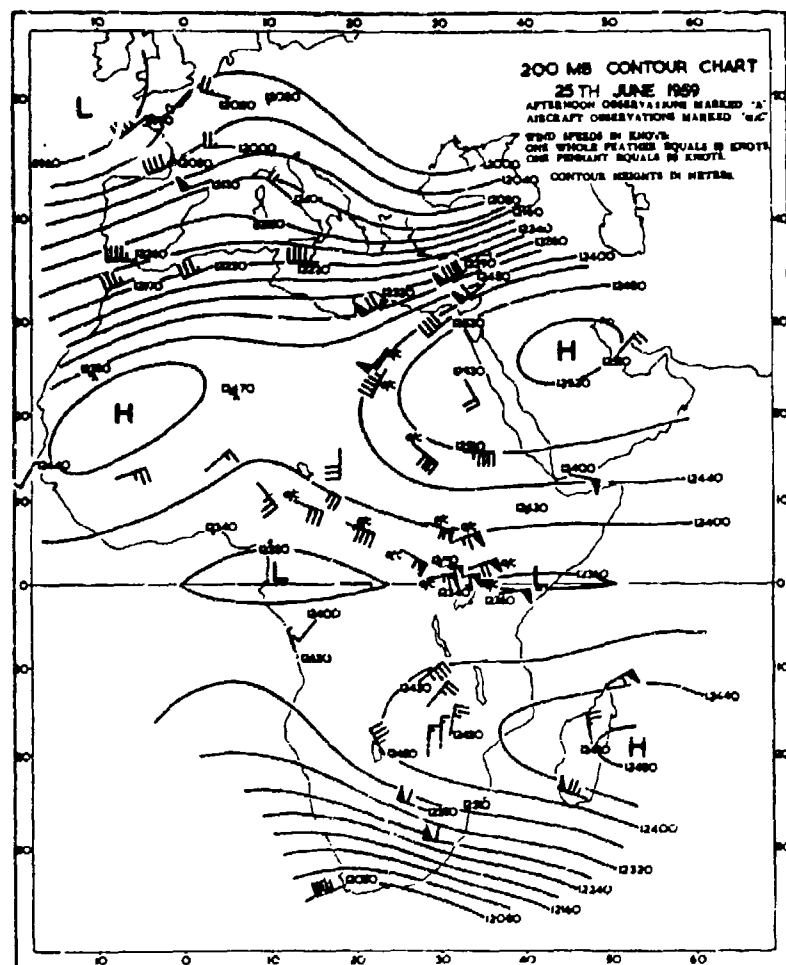


Figure III-B-34. 200-mb contour chart, 25 June 1959 (from Johnson, 1964).

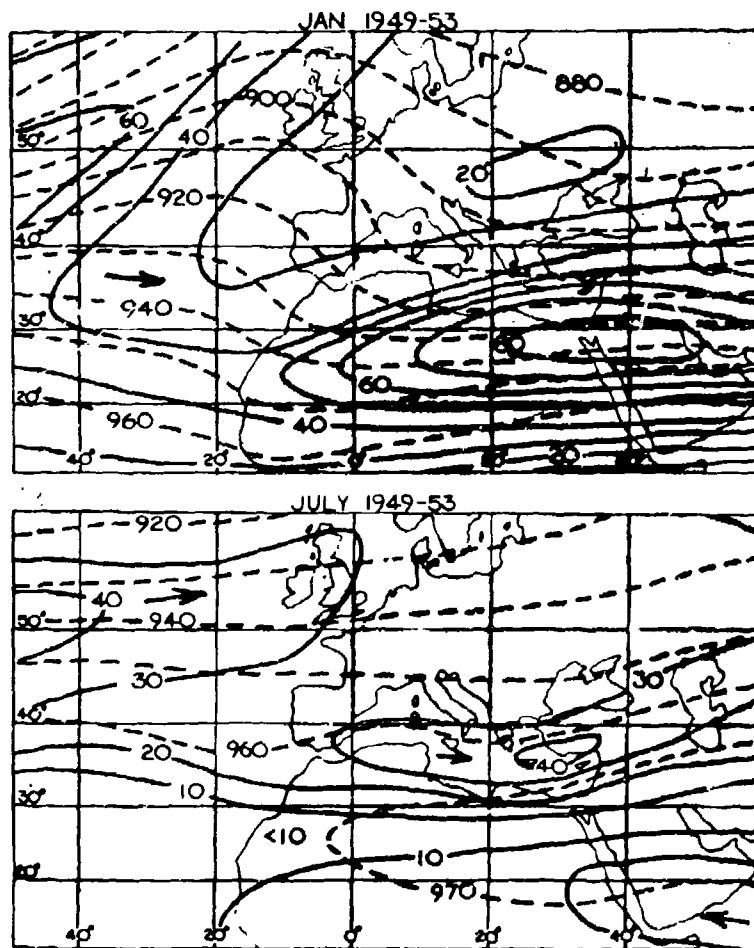


Figure III-B-35. Mean 300-mb contours (dashed lines) in geopotential decameters and isotachs (solid lines) in knots for January and July (from Sutcliffe, 1960a).

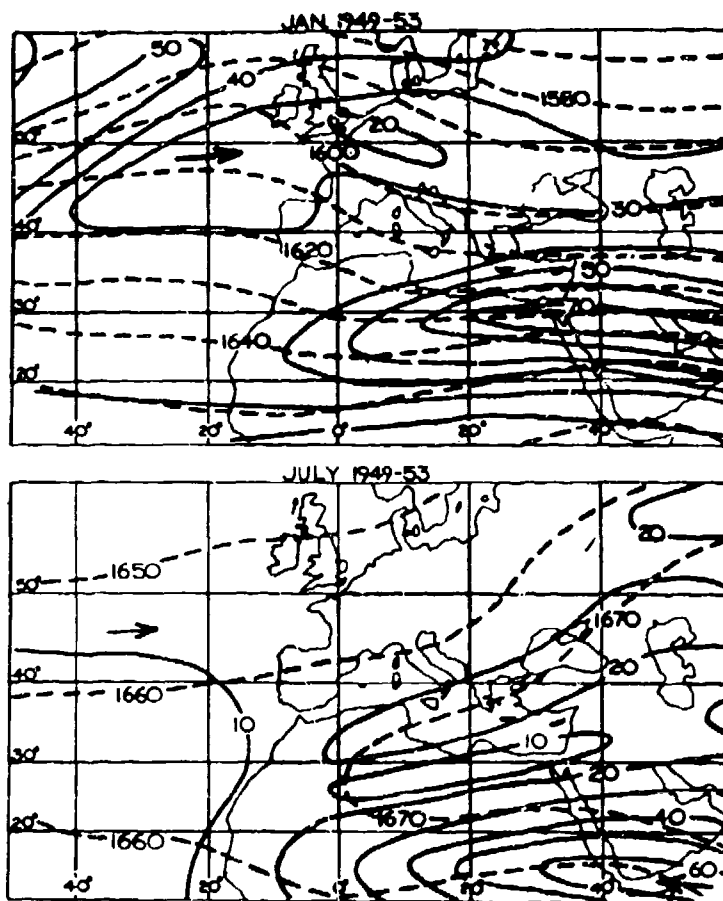


Figure III-B-36. Mean 100-mb contours (dashed lines) in geopotential decameters and isotachs (solid lines) in knots for January and July (from Sutcliffe, 1960a).

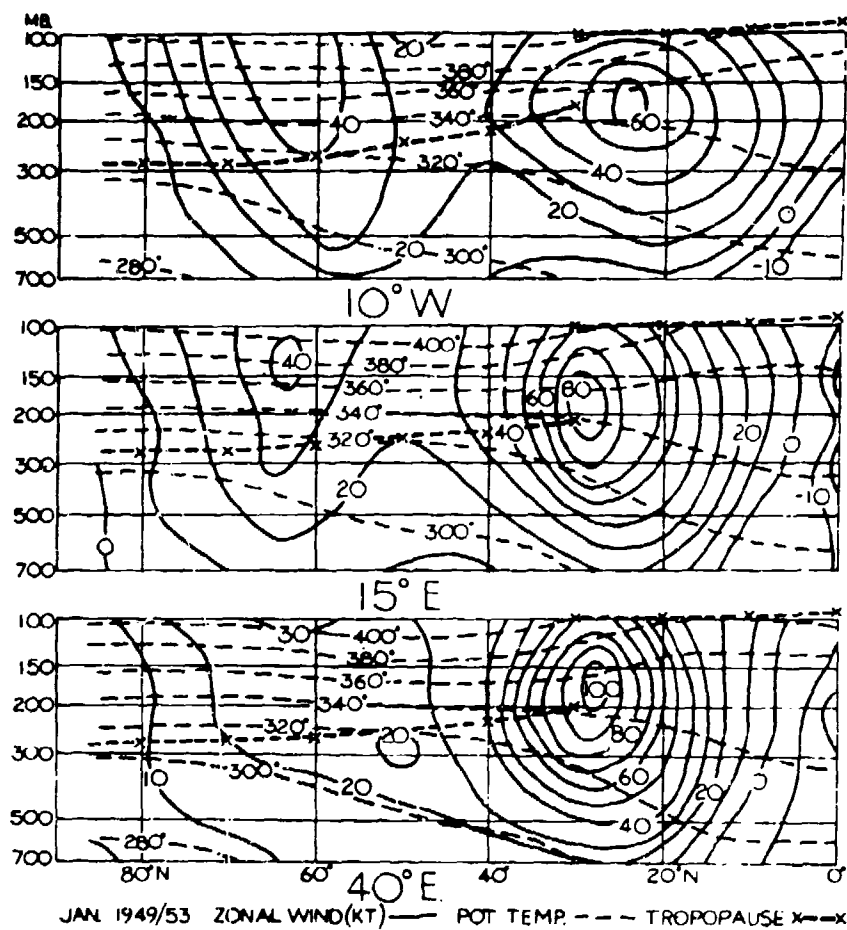


Figure III-B-37. Meridional cross sections for January (10°W, 15°E, and 40°E) (from Sutcliffe, 1960a).

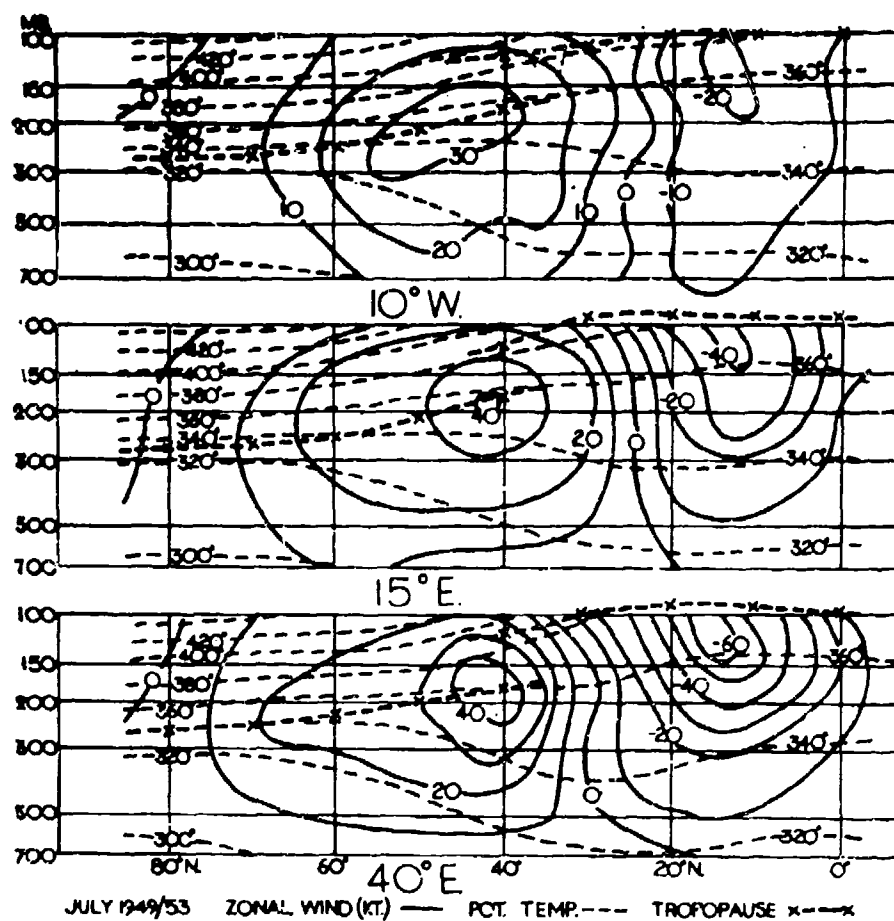


Figure III-B-38. Meridional cross sections for July (10°W, 15°E, and 40°E) (from Sutcliffe, 1960a).

C. LARGE SCALE OROGRAPHIC EFFECTS

Mountain ranges unfortunately do not occur in nature in such simple geometric forms as a step-function resembling a rectangular building block, or a sine-wave, or a bell-shaped Gaussian curve. In reality, the structure is one of a relatively large mountain massif upon which are superimposed individual mountain ridges, peaks, and valleys of smaller scale. The still smaller dimensions of boulders, trees, cliffs and sharp corners add to the general roughness of the terrain at scales commensurate to atmospheric turbulence. Thus, any consideration of orographic effects must allow for a wide variety of horizontal and vertical dimensions of the topographic features generally termed "mountains," as well as for their effects on the whole scale of atmospheric motions from planetary wave lengths to small-scale turbulence.

1. Effects on Planetary Waves

The effect of large orographic barriers on planetary flow patterns can be understood by considering the vorticity equation

$$\frac{d}{dt} (\zeta + f) = - D(\zeta + f). \quad \text{III-C(1)}$$

The left side of this equation represents the change with time of absolute vorticity. $\zeta (= \frac{\partial u}{\partial x} - \frac{\partial v}{\partial y})$ is the relative vorticity of an air parcel and f is the Coriolis parameter. $D (= \frac{\partial u}{\partial x} + \frac{\partial v}{\partial y})$ is the divergence of horizontal flow which can also be written as

$$D = - \frac{1}{\Delta p} \frac{d(\Delta p)}{dt}, \quad \text{III-C(2)}$$

where Δp is the thickness (in millibars) of the layer contained between two isentropic surfaces. For adiabatic motions, the flow within this layer will remain bounded by the same two isentropic surfaces.

Combining Eqs. III-C(1) and III-C(2) we can write

$$\frac{d}{dt} \frac{\zeta + f}{\Delta p} = 0. \quad \text{III-C(3)}$$

This means the quantity $\frac{\zeta + f}{\Delta p}$, called "potential vorticity" (see Appendix D), should be conserved for adiabatic flow over a mountain range.

Example 1: Westerly flow over a N-S oriented mountain range.

Consider the flow contained between two isentropic surfaces, one located in the lower troposphere, the other near the tropopause. The low-tropospheric flow will be forced over the mountain range, whereas the flow near tropopause level will remain nearly horizontal because it is restrained by the "lid" of a stable stratosphere. The thickness of the layer, as the flow approaches the mountain range, is Δp_1 . Over the ridge it is Δp_2 ($< \Delta p_1$) (Figure III-C-1). In the lee of the ridge the layer expands again, so that $\Delta p_3 > \Delta p_2$. Using Eq. III-C(3), it is found that, in order to conserve potential vorticity, the flow has to turn anticyclonically while Δp is shrinking on the windward side of the mountain range. On the lee side Δp increases and consequently the absolute vorticity ($\zeta + f$) also has to increase in order to keep the potential vorticity constant. Since the Coriolis parameter, f , is constant in zonal flow conditions, this means that the relative vorticity, ζ , has to increase. The streamlines turn cyclonically in the lee of the mountain range.

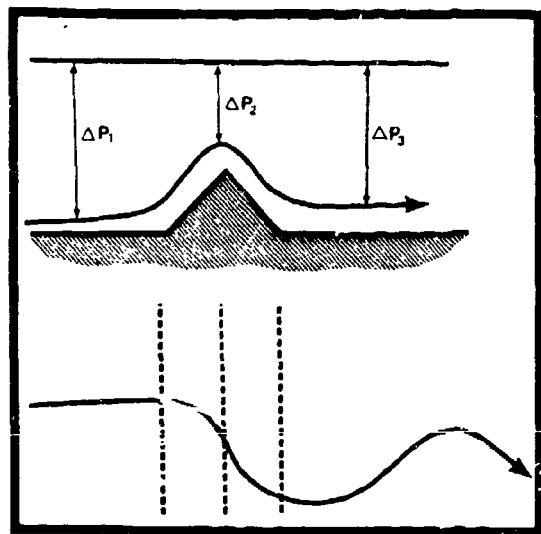


Figure III-C-1. Schematic diagram showing flow over a mountain ridge under conservation of potential vorticity. Upper diagram: Vertical cross section revealing the shrinking and stretching of the layer between two isentropic surfaces. Lower diagram: schematic streamline on a horizontal plane.

In agreement with this conclusion, rather persistent troughs are found in the westerly flow regime, especially during winter, in the lee of the Himalayas (over the East China Sea) and in the lee of the Rocky Mountains (over the midwestern United States). Cyclogenesis occurs frequently in these planetary troughs. Thus, the large orographic barriers exercise their influence on synoptic-scale disturbances.

The Pyrenees and Alps offer insufficient resistance to the mid-latitude westerlies to cause the generation of a quasi-permanent planetary-scale trough. Long-wave troughs in the European sector develop as a resonance phenomenon between the North American and Asian troughs. The European trough situations, therefore, are less stationary and less stable than the two orographically influenced planetary troughs.

Example 2: Northerly flow over an E-W oriented mountain range.

The considerations cited in Example 1 also apply to flow from the north: as it impinges upon the mountain range Δp decreases, consequently $(\zeta + f)$ also has to decrease in order to satisfy Eq. III-C(3). This decrease, however, is partially accomplished by a decrease in the Coriolis parameter, f , as air moves towards lower latitudes. Therefore ζ does not have to decrease as much as it had to in the case of westerly flow. This means that anticyclonic flow conditions along the northern slope of the E-W oriented mountain range (e.g., the Alps) are somewhat suppressed.

Along the southern slopes under northerly flow conditions Δp increases, therefore $(\zeta + f)$ should increase at the same rate. However, since f decreases along air trajectories from the north, the increase in ζ has to compensate for both the increase in Δp and the decrease in f . Enhanced cyclogenetic activity is to be expected in the lee of the mountain range. From this, one should expect that the region of northern Italy is conducive to pressure falls and cyclone formation when a northerly jet stream impinges upon the Alps. The Atlas Mountains should have a similar effect under northerly tropospheric flow.

Example 3: Southerly flow over an E-W oriented mountain range.

In southerly flow the Coriolis parameter, f , increases along an air trajectory. As Δp decreases under upslope wind conditions, ζ has to decrease in order to compensate for both the decrease in Δp and the increase in f . Pronounced anticyclonic conditions over the mountain range are to be expected.

Over the leeward slopes Δp increases again. This increase, however, is partially compensated by the increase in f . However, ζ does not have to increase by much, and lee cyclogenesis, as a consequence, is somewhat suppressed.

2. Effects on Cyclogenesis

Godev (1970, 1971a,b) developed an interesting theory using the quasi-geostrophic equations (unlike the theory in Section III-G, para. 1) which shows that concave terrain features, such as bays, are conducive to cyclone formation, whereas convex terrain features inhibit cyclogenesis. Figure III-C-2 shows generalized isohypses, \bar{z} , of the Alps, Italy, and the Balkan region. Figure III-C-3 gives the Laplacian of ground elevations, a parameter which influences the vertical velocity, $W_g(h)$, at the top of the planetary boundary layer:

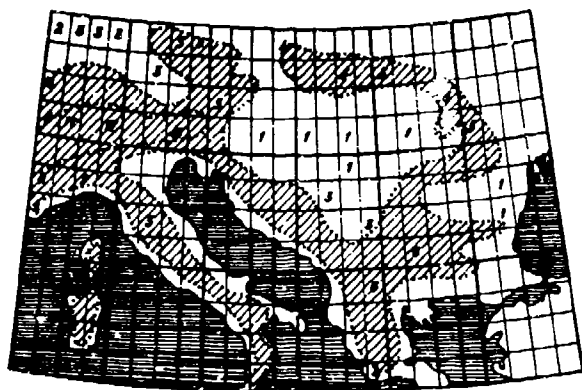


Figure III-C-2. Generalized isohypses giving the height of the mountains (38°-50°N, 6°-30°E). One unit is approximately 300 m (from Godev, 1970).

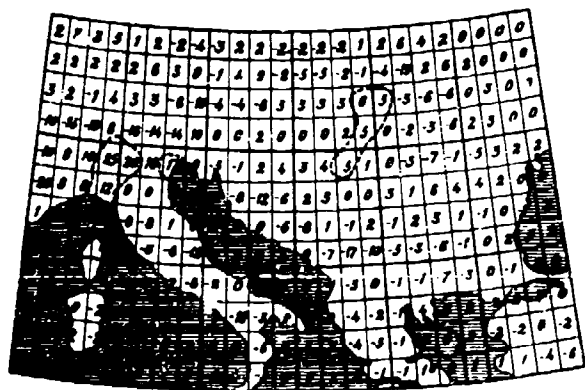


Figure III-C-3. The values of the Laplacian

$$\Delta z_0 = \left(\frac{\partial^2 z_0}{\partial x^2} + \frac{\partial^2 z_0}{\partial y^2} \right).$$

The horizontal step $L=300$ km is accepted as a unit of length. The dashed lines outline the regions with a large value of Δz_0 (from Godev, 1970).

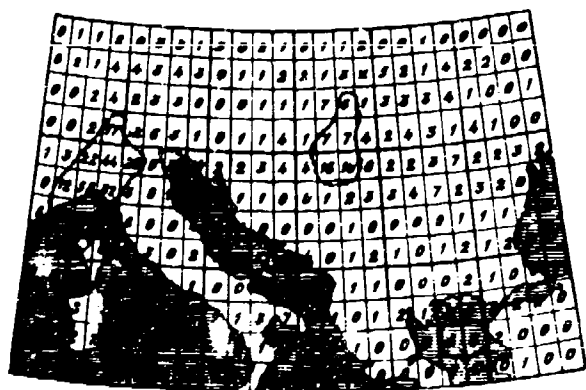


Figure III-C-4. Frequency distribution of depressions generated in the considered area. Dashed lines outline regions with a great number of generated cyclones (from Godev, 1970).

$$W_g(h) = - au_g^2 \left(\frac{\partial^2 \bar{z}_0}{\partial x^2} + \frac{\partial^2 \bar{z}_0}{\partial y^2} \right) - bu_g^2 \frac{\partial^2 \bar{z}_0}{\partial x \partial y} \quad \text{III-C(4)}$$

In this equation, a and b are constants, a being of the order of 10^4 sec and b being of the order of 1.8×10^4 sec. u_g is the geostrophic wind speed (along which the x-axis is oriented) at the top of the planetary boundary layer. The Laplacian (first term on the right side of Eq. III-C(4)) is independent of wind direction. The second term on the right side of Eq. III-C(4) depends on wind direction.

For $u = 20 \text{ m sec}^{-1}$ and $v^2 \bar{z}_0 = 10^{-8} \text{ m}^{-1}$, the Laplacian term in Eq. III-C (4) yields

$$au_g^2 v^2 \bar{z}_0 = 10^4 \times 400 \times 10^{-8} = 4 \text{ cm sec}^{-1}.$$

The contribution from the second term is significantly smaller than this.

Figure III-C-4 shows the number of cyclones generated in each grid square during the period 1951-1960, and the agreement between Figures III-C-3 and III-C-4 is remarkable.

3. Effects on Fronts

Outbreaks of polar cold air whose vertical depth does not exceed the height of a mountain range will effectively be blocked by such an orographic barrier. In this sense the Alps fend off a large number of cold outbreaks from the north, especially those which are associated with low-pressure disturbances whose centers adhere to a west-east track over Central Europe (England, Germany, Poland). This sheltering effect produces a much milder climate over the plains of northern Italy than would otherwise be expected at these latitudes.

The blocking of cold fronts along the northern rim of the Alps also has a dynamic effect upon cyclogenesis in northern Italy. The divergence patterns in the upper tropospheric jet stream flow, which are an important prerequisite to surface cyclogenesis, pass more or less unaffected over the mountain range. The pressure rise pattern associated with the inflow of cold air behind the cold front, however, is held back by the orographic barrier. This allows surface pressures to continue falling over northern Italy, leading to significant cyclogenesis (Hoinkes, 1951).

An example of strong cyclogenesis over northern Italy, enhanced by the blocking of a cold front, is given in Figures III-C-5, III-C-6 and III-C-7. As can be seen from these figures, the cold front actually invades northern Italy from the east. By the time the cold air arrives over the Po plains, it has lost most of its sting.

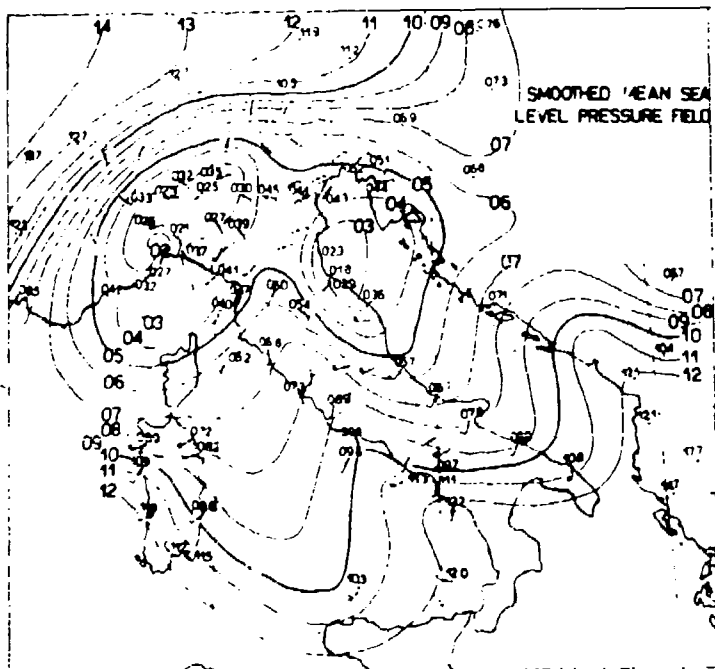


Figure III-C-5. Smoothed mean sea-level pressure field, 17-18 February 1958 (from Reiter, 1971).

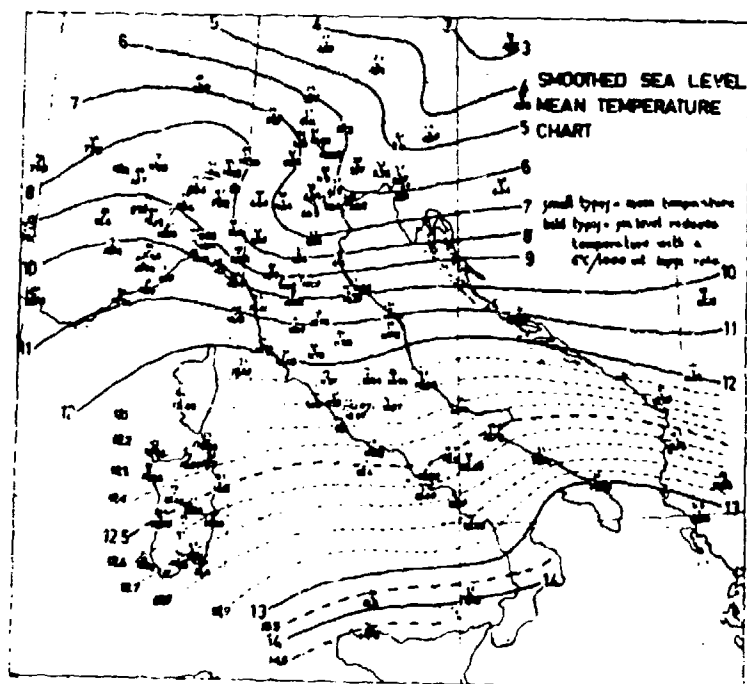


Figure III-C-6. Mean temperature reduced to sea level using the assumption of a lapse rate of $0.6^{\circ}\text{C}/100\text{ m}$, 17-18 February 1958 (from Reiter, 1971).

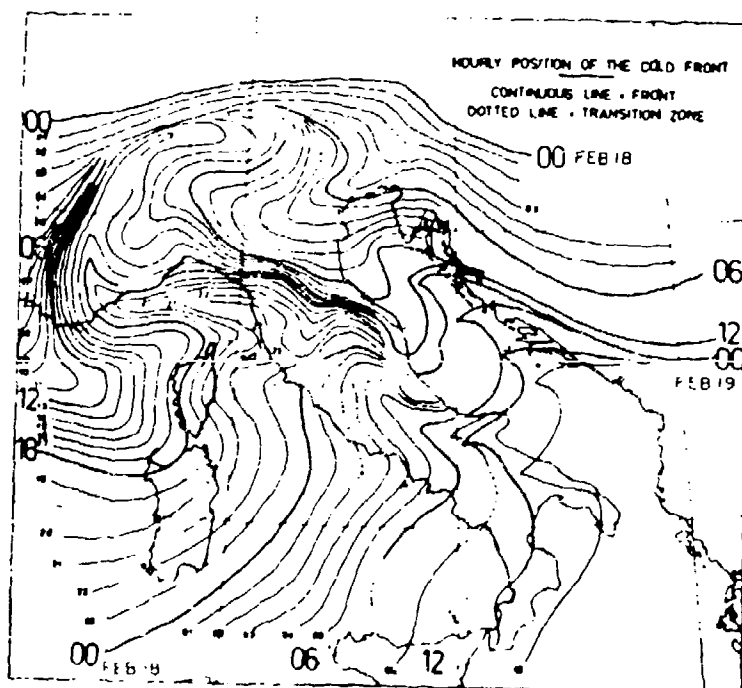


Figure III-C-7. Hourly positions of the cold front between 0000 GMT, 18 February 1958 and 1500 GMT, 19 February 1958 (from Reiter, 1971).

D. REGIONAL MEDITERRANEAN WEATHER REGIMES

1. Correlation Between Mediterranean Weather and European/Atlantic Weather Regimes.

The weather patterns in the Mediterranean region do not stand isolated; rather, they are dynamically controlled by events in the polar front zone and, especially in winter, in the subtropical zone. It was noted in Section III-B-4 that the polar front jet stream (PFJ) and the subtropical jet stream (STJ) interact with each other. Such interaction is especially pronounced where deep troughs in the westerlies extend into subtropical regions. Such trough development occurs especially during winter and spring in the Mediterranean region, often in conjunction with strong cyclogenesis in the Gulf of Genoa.

Before the advent of numerical forecasts, much research had been done, especially in Germany, aimed at categorizing European weather into various types whose behaviors could be used as forecasting tools whenever analog weather situations appeared on the weather maps. In the light of modern computer techniques, the forecasting applications of these "weather types" appear to be somewhat obsolete. Nevertheless they afford an overview, in rather general terms, of weather behavior and persistence statistics (Aerospace Science Div., 1968, and Hess and Brezowsky, 1969). The following is quoted from Aerospace Science Div., 1968:

"In 1941-1943 "A Calendar of the European Large Scale Weather Types" was prepared at the former Research Institute for Extended Weather Forecasting at Bad Homburg under the direction of W. Baur. The calendar was worked up by F. Hess and H. Nagel using data from the years 1881 through 1939. The term large-scale weather-type means an atmospheric condition which is more or less unchanged during a period of several days, for instance over Europe, as in this study.

The classification was amended several times due to the improvement in synoptic analysis and enlargement of the network of meteorological observations. These changes were partly described by F. Baur in the years 1946 through 1948 and were published by him before the release of the first revision of this work. Additional data were introduced into the study; data through 1957 are included in this revision. This revision represents an unbroken record of 86 years.

The circulation is classified into three types: zonal, mixed, and meridional flow. The following relationship exists between the type of circulation and the location of the surface subtropical high:

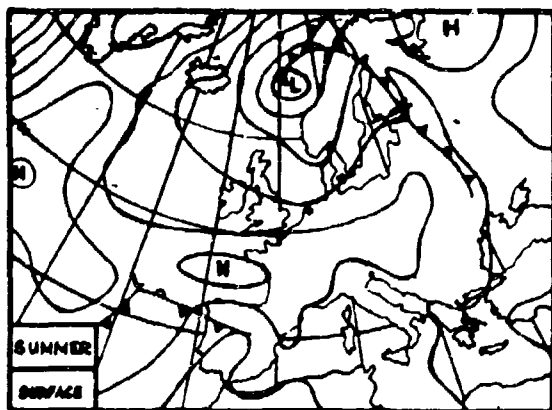
- a. General zonal flow -- the subtropical high is in its normal position near 35N.
- b. Mixed flow -- the subtropical high is displaced towards the north or northeast to approximately 50N.
- c. Meridional flow -- a well defined closed high lies between approximately 50-70N (blocking high).

To aid the forecaster to readily determine under which of the three types of circulation the current synoptic situation may fall, generalized surface and 500-mb models of these types have been reproduced (Figures III-D-1 to III-D-3). The first circulation type, zonal flow, is shown for both summer and winter conditions in Figure III-D-1. Figure III-D-2 shows mixed flow. Figure III-D-3 shows meridional flow for a blocking high, subtropical flow, trough and polar flow.

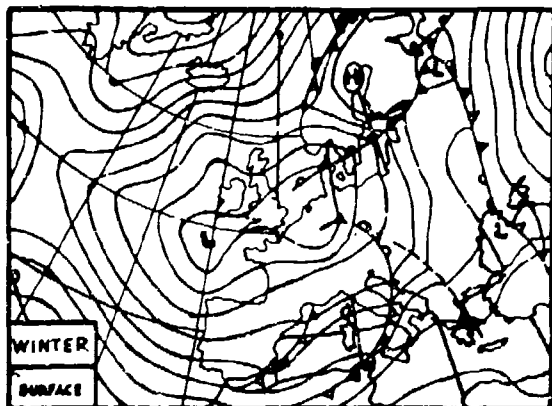
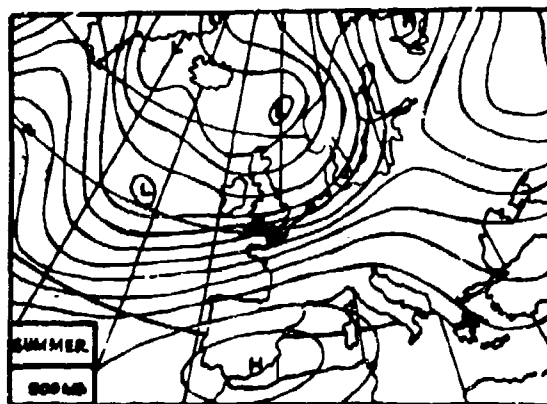
The general division of the circulation types is the basis for classification of the individual large scale weather types. Originally the notation used both upper and lower case letters to describe the circulation pattern; this paper uses only upper case in order to be compatible with teletype bulletin transmissions. The individual types are shown in Table III-D-1. Table III-D-2 shows the breakdown of weather types by general circulation types.

The sequence of meridional flow weather types begins with general northerly flow, followed by southerly flow and finally, easterly flow. The "northwesterly sloped trough" (WW) situation is the last meridional flow type and is related to the beginning of the classification of zonal flow. In the original publication by Baur there were 18 large scale weather types. However, while screening the weather types, the authors became aware of the important role which the curvature of the surface isobars plays. To distinguish the characteristic weather, the number of large scale weather types had to be increased to 25. As for the northeasterly flow (NE), the cases occurring in the cold months (October-May) have been classified as cyclonic and those of the warm months (June-September) as anticyclonic, since the polar air advection during the cold season is the main factor for the characteristic weather.

In determining the frequency of certain patterns, a break in steering was used as the main criterion. The same type with periods of different characteristic weather, however, was classified as an uninterrupted period of the same large-scale weather type. Generally, a large-scale type will exist for at least three days. In the case of a slow break in steering, one or two transitional days might occur. If they did not represent days with a typical flow, they were classified as a transitional type using the symbol UE."



a



b

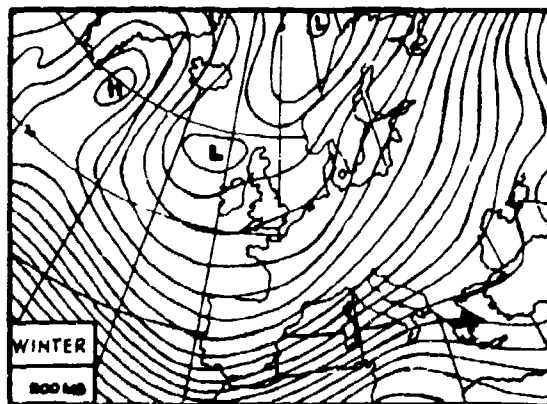


Figure III-D-1. Typical zonal type flow situation over Europe (a) summer (b) winter (from Aerospace Science Div., 1968).

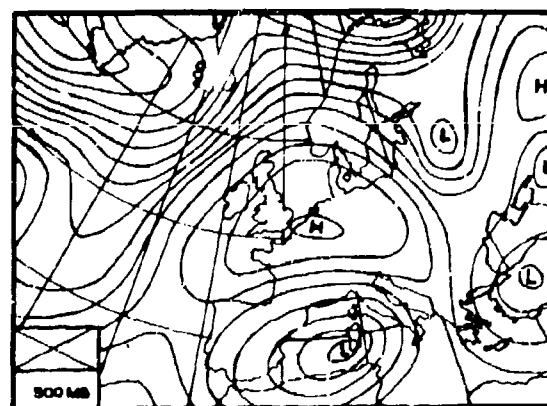
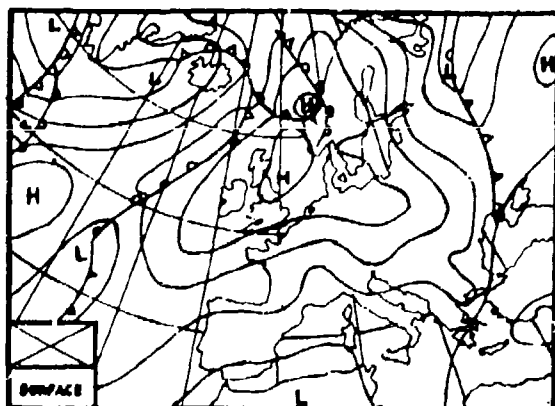
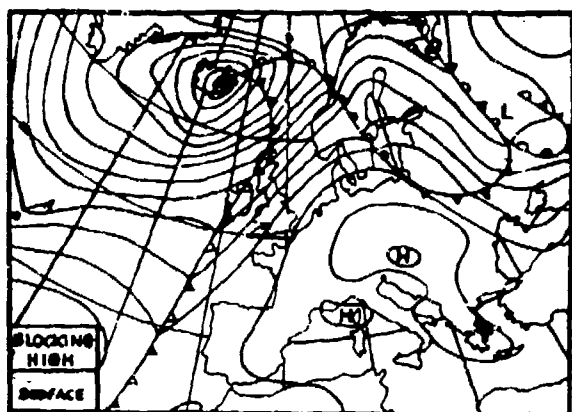
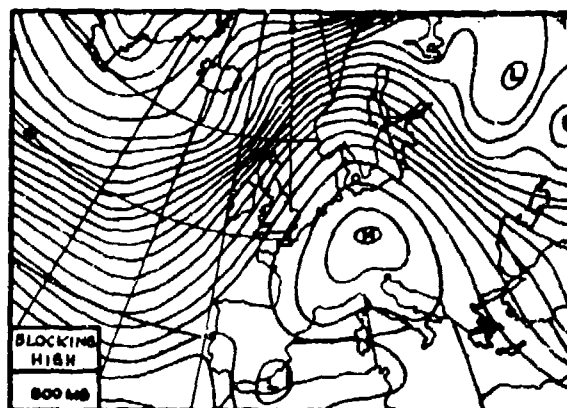


Figure III-D-2. Typical mixed type flow (from Aerospace Science Div., 1968).



a



b

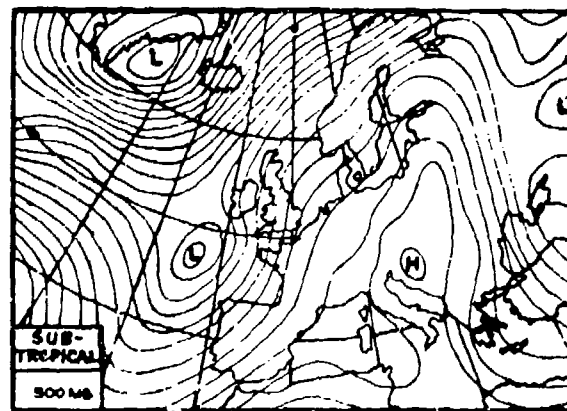
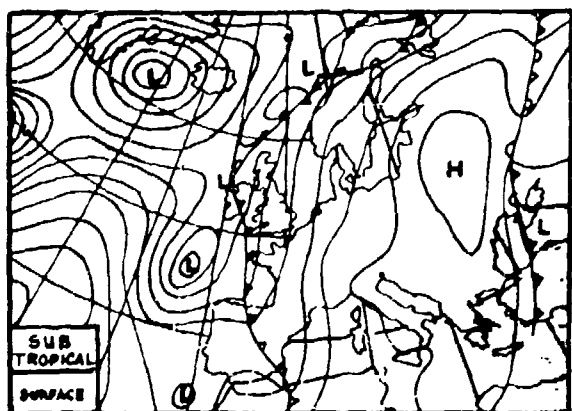
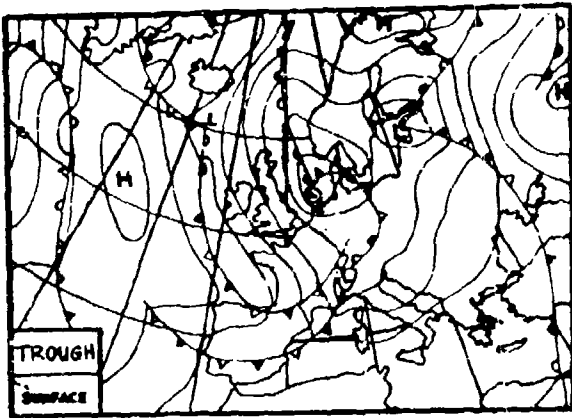
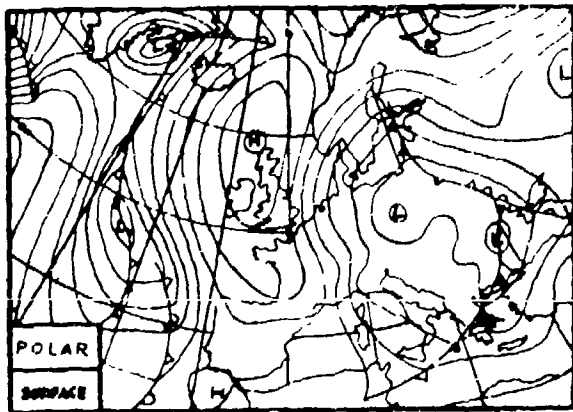
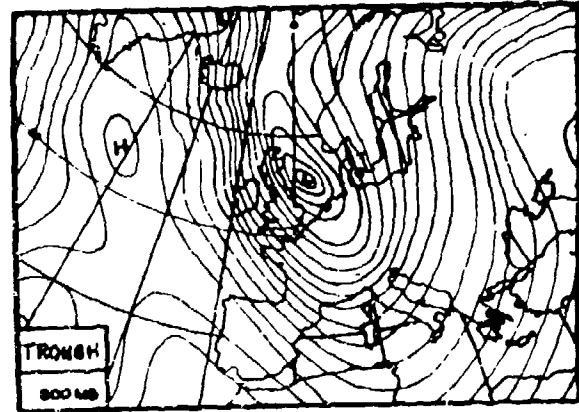


Figure III-D-3. Typical meridional type flow (a) blocking high over Central Europe, (b) subtropical flow over Central Europe, (c) trough over Central Europe, and (d) polar flow over Central Europe (from Aerospace Science Div., 1968).



c



d

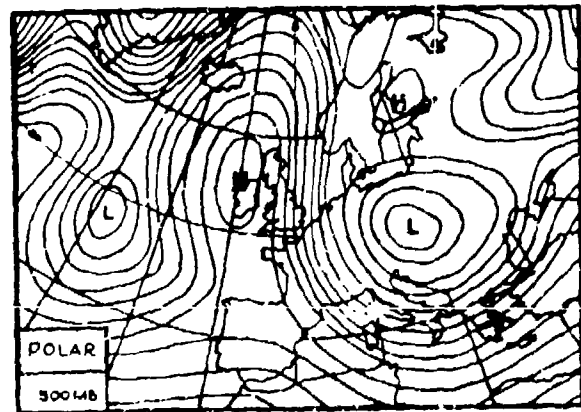


Figure III-D-3 (continued)

Table III-D-1. Catalog of European large scale weather types
(from Aerospace Science Div., 1968).

<u>CODE</u>	<u>DESCRIPTION</u>
WS	Cyclonic <u>w</u> esterly flow with a slight <u>s</u> outherly component
WA	<u>W</u> esterly flow, <u>a</u> nticyclonic
WZ	Cyclonic <u>w</u> esterly flow (<u>z</u> yklonal)
BM	<u>B</u> ridge of high pressure over Central Europe (<u>M</u> itteleuropa)
HM	Well-defined closed <u>h</u> igh over Central Europe (<u>M</u> itteleuropa)
SWA	<u>S</u> outh <u>w</u> esterly flow, <u>a</u> nticyclonic
SWZ	<u>S</u> outh <u>w</u> esterly flow, cyclonic (<u>z</u> yklonal)
NWA	<u>N</u> orth <u>w</u> esterly flow, <u>a</u> nticyclonic
NWZ	<u>N</u> orth <u>w</u> esterly flow, cyclonic (<u>z</u> yklonal)
HNA	Well-defined closed <u>h</u> igh over the <u>N</u> orwegian Sea (<u>a</u> nticyclonic over Central Europe)
HNZ	Well-defined closed <u>h</u> igh over the <u>N</u> orwegian Sea (cyclonic flow over Central Europe)
HB	Well-defined closed <u>h</u> igh over the <u>B</u> ritish Isles
NA	<u>N</u> ortherly flow, <u>a</u> nticyclonic
NZ	<u>N</u> ortherly flow, cyclonic (<u>z</u> yklonal)
TRM	<u>T</u> rough over Central Europe (<u>M</u> itteleuropa)
TR	Well-defined closed low (<u>T</u> ief) over the <u>B</u> ritish Isles
TRW	<u>T</u> rough over <u>W</u> estern Europe
SA	<u>S</u> outherly flow, <u>a</u> nticyclonic
SZ	<u>S</u> outherly flow, cyclonic (<u>z</u> yklonal)
SEA	<u>S</u> outhe <u>a</u> sterly flow, <u>a</u> nticyclonic
SEZ	<u>S</u> outhe <u>a</u> sterly flow, cyclonic (<u>z</u> yklonal)
HFA	Well-defined closed <u>h</u> igh over <u>F</u> ennoscandia (<u>a</u> nticyclonic flow over Central Europe)
HFZ	Well-defined closed <u>h</u> igh over Fennoscandia (cyclonic flow over Central Europe - low in SE)
HNFA	Well-defined closed <u>h</u> igh over the Norwegian Sea and Fennoscandia (<u>a</u> nticyclonic flow over Central Europe)
HNFZ	Same with cyclonic flow - low in SE
NE	<u>N</u> orthe <u>a</u> sterly flow
TM	Well-defined closed low (<u>T</u> ief) over Central Europe (<u>M</u> itteleuropa)
WW	West-Winkellage - northwesterly sloped trough
UE*	Transitional type <u>U</u> ebergaenge (due to slow break in steering)

* Code UE is not a weather type in the same sense as the other types listed in this table; it is of an interim transitional nature only.

Table III-D-2. The large scale weather types of Europe (from Aerospace Science Div., 1968).

GENERAL TYPE	SPECIAL TYPE	CODE	EXPLANATION
Nord	N Nordlage Hoch Nordmeer Hoch Britische Inseln Trog Mitteleuropa	NA,NZ* HNA,HNZ HB TRM	Northerly flow High over the Norwegian Sea High over the British Isles Trough over Central Europe
Nordwest	NW Nordwestlage	NWA,NWZ	Northwesterly flow
West	W Westlage	WA,WZ,WS	Westerly flow; S: southerly component
Sued	S Suedlage Tief Britische Inseln Trog Westeuropa	SA,SZ TB TRW	Southerly flow Low over British Isles Trough over Western Europe
Suedost	SE Suedostlage	SEA,SEZ	Southeasterly flow
Ost	E Hoch Fennoskandien Hoch Fennoskandien-Nordmeer	HFA,HFZ HNFA,HNFZ	High over Fennoscandia, anticyclonic, cyclonic flow over Central Europe High over Fennoscandia and the Norwegian Sea
Nordost	NE Nordostlage	NE	Northeasterly flow
Hoch Mitteleuropa	HM Hoch Mitteleuropa Zonale Hochdruckbruecke	HM BM	High over Central Europe Zonal ridge of high pressure
Hoch Kontinent	HK Hoch Mitteleuropa Zonale Hochdruckbruecke Suedwestlage, antizyklonal Suedlage Suedostlage Ostlage	HM BM SWA SA SEA HFA,HNFA	High over Central Europe Zonal ridge of high pressure Anticyclonic southwesterly flow Anticyclonic southerly flow Anticyclonic southeasterly flow Anticyclonic flow over Central Europe
Tief Mitteleuropa mit Vb-artiger Gleitaneordnung**	TM Tief Mitteleuropa Ostlage, zyklonal Suedostlage, zyklonal Nordmeerhochlage, zyklonal Nordostlage (Oct-May)	TM HFZ,HNFZ SEZ HNZ NE	Low over Central Europe Cyclonic easterly flow Cyclonic southeasterly flow High over Norwegian Sea, flow over Central Europe is cyclonic Northeasterly flow, winter season

*A: Anticyclonic flow, Z: Cyclonic flow.

**Vb weather type - upslope effect.

Examples of the individual large-scale weather types are given in Appendix E along with a synopsis of the accompanying weather. Tables giving the percentage frequency of days per month that particular weather types occur and the number of consecutive days per month that each type occurs are also given in Appendix E.

2. Blocking Anticyclones

A "blocking high" or "blocking anticyclone" is a high pressure system which is either stationary or moves only slowly relative to the west-east motion of the disturbances upstream. Thus it effectively "blocks" the progress of migratory cyclones and anticyclones.

The long planetary waves in the westerlies of temperate latitudes are effectively controlled by the two big mountain barriers: the Himalayas and the Rocky Mountains. Each of these two barriers has a tendency to generate a long-wave trough to its lee, i.e., over the China Sea and over the midwestern United States, respectively. Anticyclonic flow conditions prevail at the geographic longitude of the mountain range itself.

The mountain ranges of Europe are too small to exercise such drastic effects on the mid-latitude westerlies. On the other hand, the planetary long-wave pattern which develops over Europe in resonance with the pattern over East Asia and America quite often reaches a persistence in "blocking anticyclones" which, to the westerly flow, appears almost like a mountain barrier. Since there is no effective orographic "anchoring" of these blocking highs, their positions may vary from occasion to occasion, causing drastically different weather patterns to occur over Europe and the Mediterranean region. Out of the 29 weather types listed in Section III-D-1 and Appendix E, the 16 listed below show characteristics of a "blocking high"; figure numbers referenced are those in Appendix E.

TYPE	FIG. NO.	TYPE	FIG. NO.
HM	E-6	SEA	E-21
NWA	E-9	SEZ	E-22
NWZ	E-10	HFA	E-23
HNA	E-11	HFZ	E-24
HNZ	E-12	HNFA	E-25
HB	E-13	HNFZ	E-26
HA	E-14	HE	E-27
NZ	E-15	TM	E-28

This means that more than half of the typical weather patterns occurring in the European sector are characterized by a blocking high somewhere in this region. This is one of the reasons why European weather development is not easy to forecast. Blocking anticyclones can be stationary, slowly progressive, or slowly retrogressive, or they may collapse relatively quickly. Many of their features are well represented in barotropic forecasting models because, quite often, the anticyclonic flow conditions extend from the surface into the stratosphere. On the other hand, baroclinic disturbances have a drastic effect on these blocking highs, especially when they are about to break down.

According to a study by Rex (1950b), the greatest probability that blocking highs will occur in the European sector is between January and May (Figure III-D-4). Most of the blocking anticyclones develop west of the 0° meridian (Figure III-D-5). During the first week after the formation of the blocking ridge, there is a tendency for slight retrogression toward the west. Such retrogression will take place with warm advection on the west side of the ridge and cold advection on its east side. As the high pressure vortex becomes completely separated, a so-called omega block develops (see Figure III-A-1). The subtropical jet stream, although weak, flows across the narrow "neck" of this blocking ridge and joins with the polar front jet in the southwesterly flow to the east of this ridge. As the temperature advection patterns become less pronounced, a slight progression of the blocking ridge is usually observed.

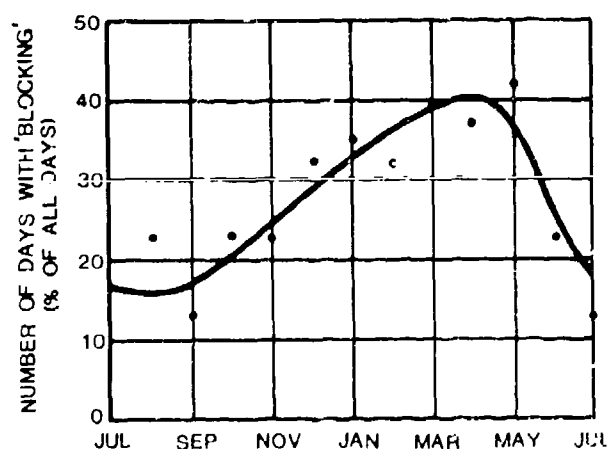


Figure III-D-4. Mean monthly number of days (in percent) on which blocking anticyclones are observed in the Atlantic sector (after Reiter, 1963).

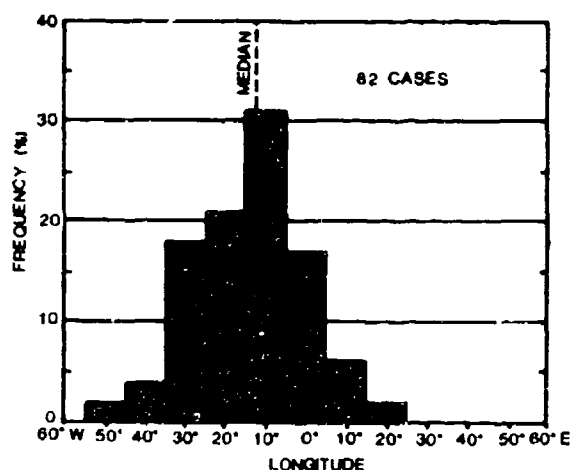


Figure III-D-5. Percent frequency distribution of the appearance of blocking anticyclones at the 500-mb level over the Atlantic at various geographic longitudes (82 cases between 1933 and 1940, 1945 and 1949) (from Reiter, 1963).

Blocking ridges in the European region may, at times, be quite persistent. Of 82 cases investigated by Rex, the most frequent value of persistence was 14 days, the mean value of persistence was 16.6 days, and the longest case in this sample was 34 days. The severe drought conditions in Europe during 1959 were due to a blocking pattern that developed over central Europe during the last days of January and persisted with only short interruptions into the fall season.

From the charts presented in Appendix E it can be seen that many of the typical blocking patterns, especially those with a blocking high over Central Europe, are accompanied by cyclonic activity in the Mediterranean region. The intrusions of cold air along the east side of the block keep the weather unsettled over most of the Mediterranean basin. Figures III-D-6 and III-D-7 (Rex, 1950b) show precipitation and temperature anomalies associated with a typical blocking pattern.

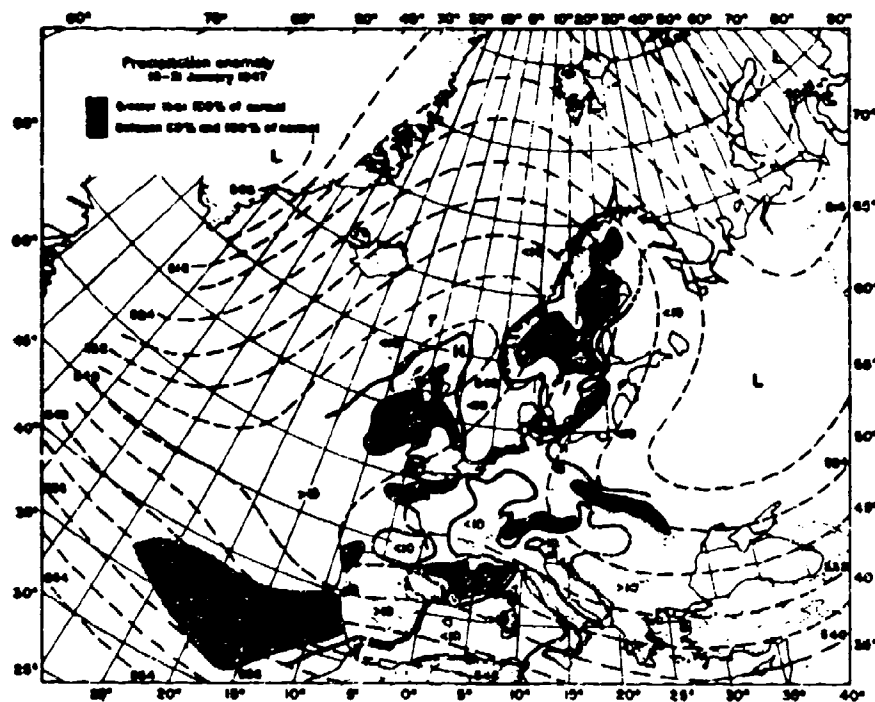


Figure III-D-6. Isanomals of precipitation over the Atlantic-European area during a wintertime case of strong Atlantic blocking action (16-31 January 1947). Isanomalous lines are given for 10, 50, 100, and 150% of normal and are shown as thin solid lines, except in areas of uncertain analysis where they are shown as thin short-dashed lines. Areas recording precipitation amounts greater than 50% of, but less than normal, are indicated by the shading. The mean contour pattern at the 500-mb level is shown by the thin long-dashed lines; contour heights given in dynamic decameters (from Rex, 1969).

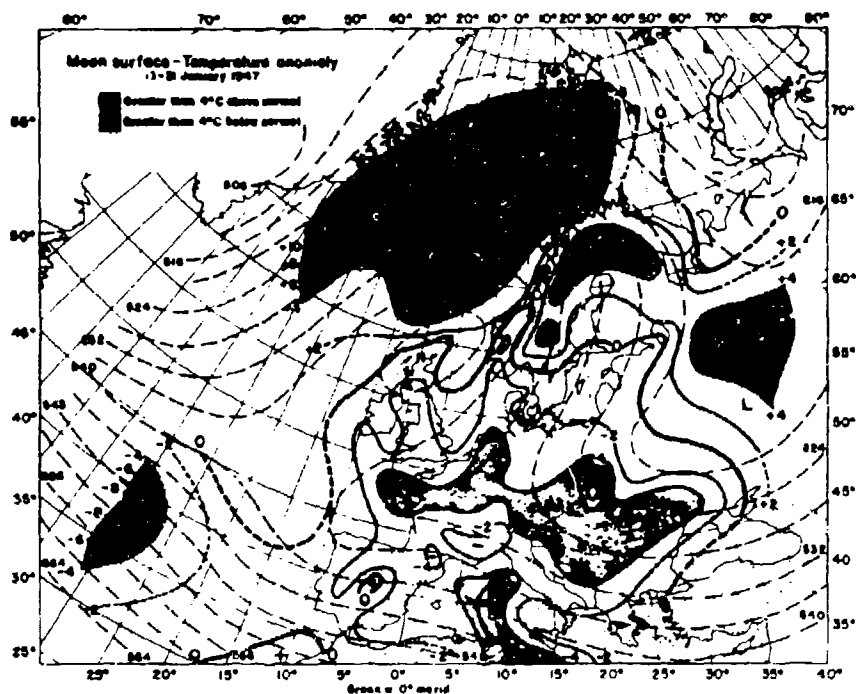


Figure III-D-7. Isanomals of mean surface-temperature over the Atlantic-European area during a wintertime case of strong Atlantic blocking action (16-31 January, 1947). Isanomalous lines are given for each 2°C above and below normal and are shown as thin solid lines, except in areas of uncertain analysis where they are shown as thin short-dashed lines; the zero anomaly line is shown as a heavy solid (or dashed) line. Areas recording mean temperatures more than 4°C above normal are indicated by the dark shading. The mean contour pattern at the 500-mb level is shown by the thin long-dashed lines; contour heights given in dynamic decameters (from Rex , 1969).

E. SIGNIFICANT CYCLONE OCCURRENCES

A composite of typical storm tracks in the Mediterranean region is shown in Figure III-E-1. Of the tracks shown, the so-called Va and Vb ("five-a" and "five-b") cyclone tracks described by Van Bebber (Black, 1969) are of special interest. Vida (1967) distinguishes three groups of cyclones following the Vb track northeastward into northern Yugoslavia. All three groups have associated heavy rainfall, leading to local flooding conditions in Yugoslavia, Hungary, Bulgaria and Rumania. They are:

Group 1: A cold outbreak over the east Atlantic forms into a cut-off low over Central Europe that moves slowly eastward (Figure III-E-2). Heavy precipitation in the southwesterly flow over Yugoslavia, supported by orographic uplifting, may yield in excess of 100 mm in 12 hours.

Group 2: A cyclone forms over the Gulf of Genoa and becomes stationary, coinciding with a planetary long-wave trough under "low-index" (i.e., strongly meridional) hemispheric flow conditions in the belt of mid-latitude westerlies. Short-wave disturbances travel around this stationary cyclone in the southwesterly flow over Italy and the Balkan Peninsula (Figure III-E-3). Heavy precipitation, again, is enhanced by orographic effects.

Group 3: A cyclone forms over northwest Africa and travels northeastward (Figure III-E-4). Orographic effects again enhance the precipitation over Yugoslavia.

The remainder of this section addresses the two most important cyclone occurrences in the Mediterranean basin -- the Genoa and North African depressions. Frequencies of occurrence of these cyclones are shown in figures III-B-24 and III-B-25; their tracks are depicted in Figure III-E-1.

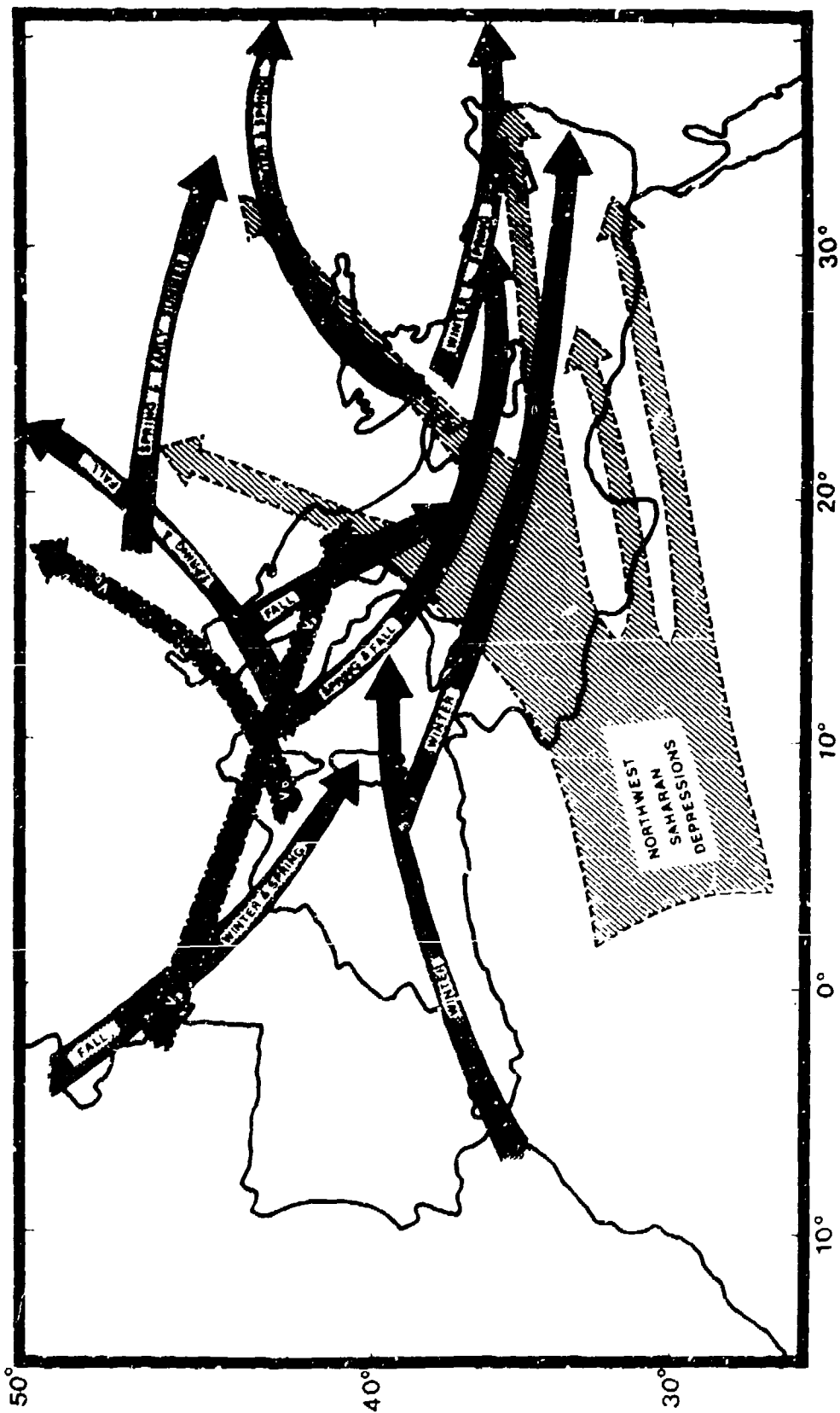


Figure III-E-1. Major cyclone tracks in the Mediterranean region (after Black, 1969; Reiter, 1971, and Fitzpatrick, 1970). Tracks Va and Vb are according to classification by van Bebber.

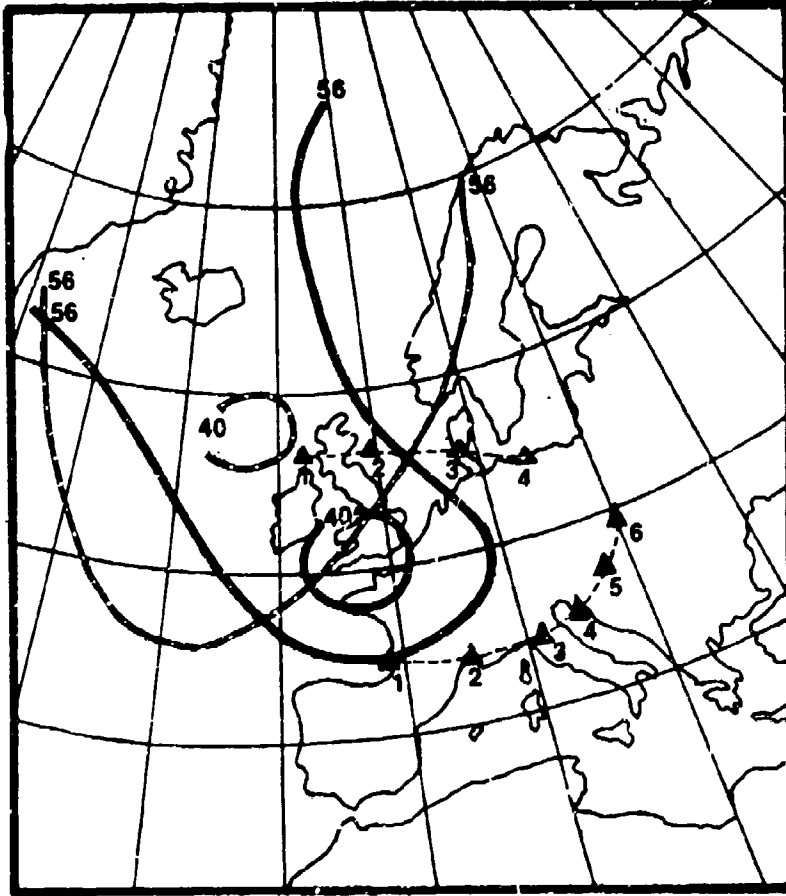


Figure III-E-2. Typical cyclone tracks (Group (1)) and associated 500-mb patterns. Dashed lines are 500-mb contours (geopotential decameters) on 26 June 1958, and solid lines are 500-mb contours on 27 June 1958. Cyclone positions are given at 6-hourly intervals, starting with position "1" at 1900 GMT, 26 June 1958 (after Vida, 1967).

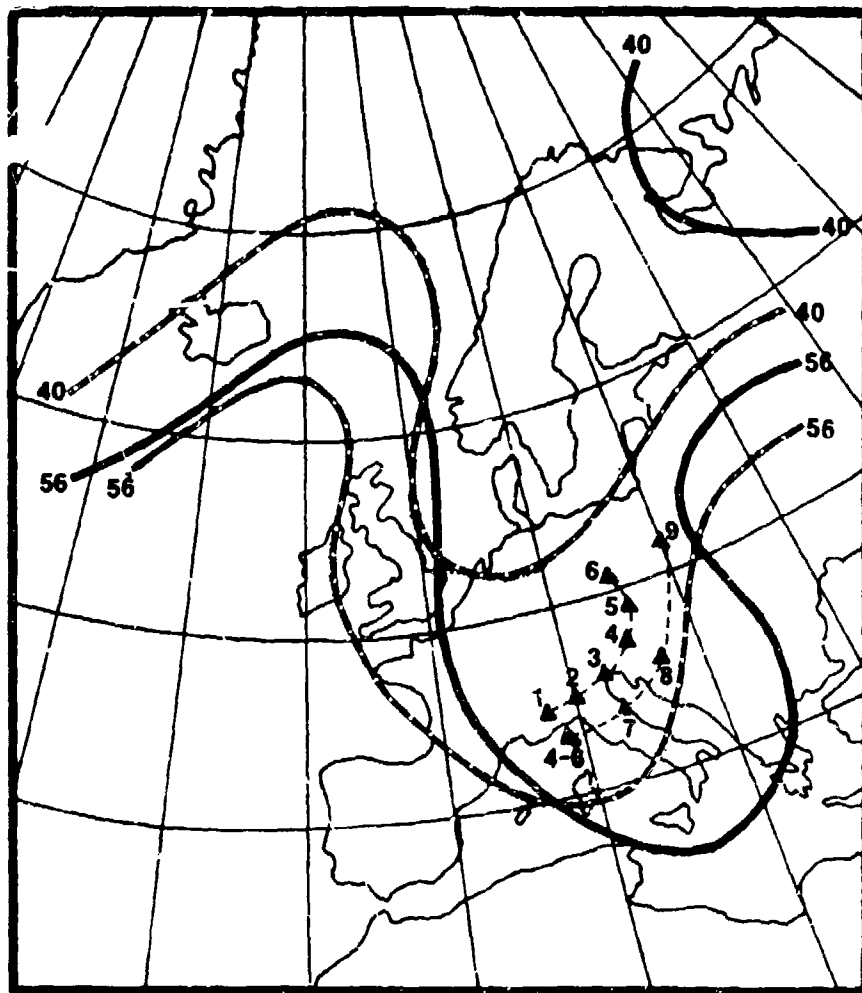


Figure III-E-3. Typical cyclone tracks (Group (2)) and associated 500-mb patterns. Dashed lines are 500-mb contours (geopotential decameters) on 26 October 1956 and solid lines are 500-mb contours on 27 October 1956. Cyclone positions are given at 6-hourly intervals, starting with position "1" at 0700 GMT, 26 October 1956 (after Vida, 1967).

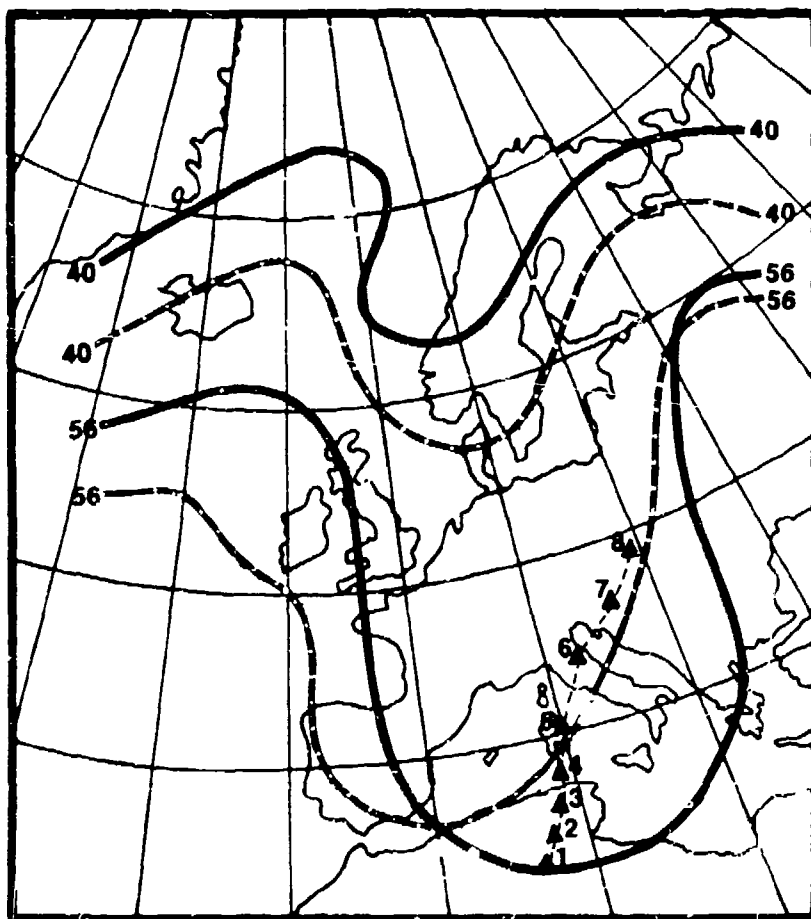


Figure III-E-4. Typical cyclone track (Group (3)) and associated 500-mb patterns. Dashed lines are 500-mb contours (geopotential decameters) on 29 April 1956 and solid lines are 500-mb contours on 30 April 1956. Cyclone positions are given at 6-hourly intervals, starting with position "1" at 1900 GMT, 28 April 1956 (after Vida, 1967).

1. Genoa Depressions (Reiter, 1971)

Genoa depressions are low-pressure systems which form in the Gulf of Genoa and in the Ligurian Sea. Depressions in the upper Po Valley are often included in this consideration. In a broader sense, one may also include lee cyclogenesis south of the Alps and associated depressions over the northern Adriatic Sea.

Outbreaks of cold air over France are frequently associated with Genoa cyclogenesis. The several factors listed below, which are discussed more fully in other sections of this handbook, seem to play an important role in the development of these depressions:

(1) The thermal contrast between land and sea, which has an effect on the surface pressure pattern and its development (see Section V-D).

(2) Jet stream interaction between the PFJ and STJ, which occurs frequently in this region (see Section III-B, para. 5).

(3) Effect of northerly flow over the Alps enhancing cyclogenetic activity along the southern slopes (see Section III-C, para. 1).

(4) Effect of concave terrain features on cyclone formation (see Section III-C, para. 2).

(5) Blocking of cold fronts along the northern rim of the Alps (see Section, III-C, para. 3).

Tracks of Genoa depressions are shown in Figure III-E-1. Although many Genoa depressions remain stationary throughout their life history, the remainder take two main tracks. The first track, associated with strong south-westerly flow aloft, is away from the Gulf of Genoa in a northeasterly to north-northeasterly direction. The second track, with strong surface high pressure over the Balkans, Turkey or the Black Sea, is in a southeasterly direction along the northern border of the Mediterranean.

2. North African Depressions (Reiter, 1971)

North African lows and Sahara depressions, sometimes also referred to as Atlas lee depressions, usually form to the south of the Atlas Mountains. Poor observational data often inhibits detection of the incipient states. Figure III-E-1 shows the most frequent tracks of these cyclones. They often give rise to severe dust storms and sometimes produce intensive rainfall over otherwise arid regions. An associated phenomenon is the sirocco which will be discussed in Section III-F, para. 5.

It appears that the name "Atlas lee depression" for North African lows is a misnomer. The precipitation observed on occasion over northwest Africa with such depressions, and their tendency to migrate out over the Mediterranean, speak against a lee effect. However, with upper-level northwesterly flow, a lee trough often may be discerned, particularly over southern Tunisia.

The most reliable criterion for the development of a low to the south of the Atlas range is the presence of an upper trough lying over Spain with its axis oriented approximately NE-SW, producing a deep southwesterly flow over northwest Africa (Figures III-E-5 and III-E-6). Such a trough may be mobile and, for example, associated with a depression moving eastward across Europe and a cold front advancing southeastward towards the Atlas Mountains. Alternatively, the upper trough may be nearly stationary. This may be the case when a ridge extends across France from the Atlantic anticyclone.

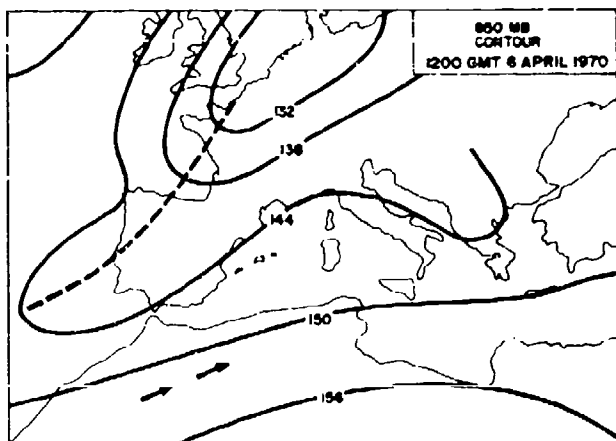


Figure III-E-5. 850-mb analysis, 1200 GMT, 6 April 1970, typical for the development of northwest Saharan depressions (from Reiter, 1971).

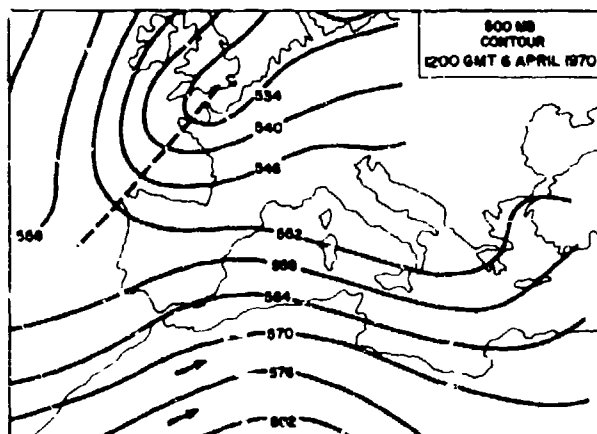


Figure III-E-6. 500-mb analysis, 1200 CMT, 6 April 1970, typical for the development of northwest Saharan depressions (from Reiter, 1971).

The presence of a cold front is apparently immaterial for the development of a depression and in many cases no front is detectable on the surface chart. When a cold front is present, development of the low usually occurs before the front reaches the Atlas range. The surface flow over the Mediterranean appears to be insignificant, having little bearing on whether or not development occurs in the lee of the Atlas Mountains.

Cyclogenesis is most satisfactorily explained by a combination of potential instability in the southwesterly air stream coupled with vorticity advection along the leading flank of the upper trough. Also, as with the case of Genoa cyclogenesis, it appears likely that jet stream interaction plays an important role in cases of strong cyclone development over North Africa (see Section III-B, paras. 4 and 5).

F. LARGE SCALE WIND REGIMES

1. The Mistral (Reiter, 1971)

According to Huschke (1959), the mistral is "a north wind which blows down the Rhone Valley south of Valence and into the Gulf of Lion. It is strong, squally, cold and dry; it is the combined result of the basic circulation, a fall wind, and a jet-effect wind. It blows from the north or northwest in the Rhone Delta, where it is strongest; from the northwest in Provence; and from the northeast in the valley of the Durance below Sisteron." Figure III-F-1 is a locator map for use in the discussion of the mistral. All geographical features referred to in this section will be found in either this figure or Figure 1-A-2 in Section I.

Again according to Huschke (1959): "The mistral has a variety of local names: mangofango in Provence; sécaire, maistrau, maistre or magistral in the Cevennes; dramundán in Perpignan (sta. no. 07747); cierzó in Spain; cers in the Pyrenees, etc. South of Mont Ventoux (sta. no. 07585) a similar wind is named bise. A local west wind of mistral type which descends from Mt. Canigou to the plains of Roussillon is called canigonenc."

A general mistral is characterized by offshore winds along part, or all, of the coast of the Gulf of Lion. Wind speeds often exceed 60 knots and may reach 85 knots in the lower Rhone valley. Even higher velocities are encountered at sea where the braking effect of surface friction in the planetary boundary layer is greatly reduced. At times gale force winds may extend across the Mediterranean all the way to Malta and the Algerian coast.

Strong offshore winds, whose direction is modified by surface friction, require a pressure gradient from west to east. Strong winds along the coast of the Gulf of Lion will be enhanced by a component of the pressure gradient directed toward the Mediterranean and parallel to one or all of the major valleys of the Garonne, the Rhone, and the Durance. Maximum winds occur when the surface isobars are at an angle of 30° to these valleys. Such pressure gradients can be caused by the development of Genoa depressions (see Section III-E, para. 1). Anticyclones over Spain, northern France and/or Central Europe may enhance the required surface pressure gradient. Changes in the gradient may bring about lulls and surges in the mistral.

The sheltering effects of the Pyrenees and the Alps may lead to the formation of sharp shear lines between high and low wind-speed regimes. These shear lines may extend far out over the sea. On occasion, but by no means always, cloud formations have been observed along these shear lines (observation by USS FORRESTAL). In general, however, the mistral is a katabatic wind, associated with low-level divergent flow of cold air. Mass continuity requires a sinking motion and hence cloud-free conditions would be expected.

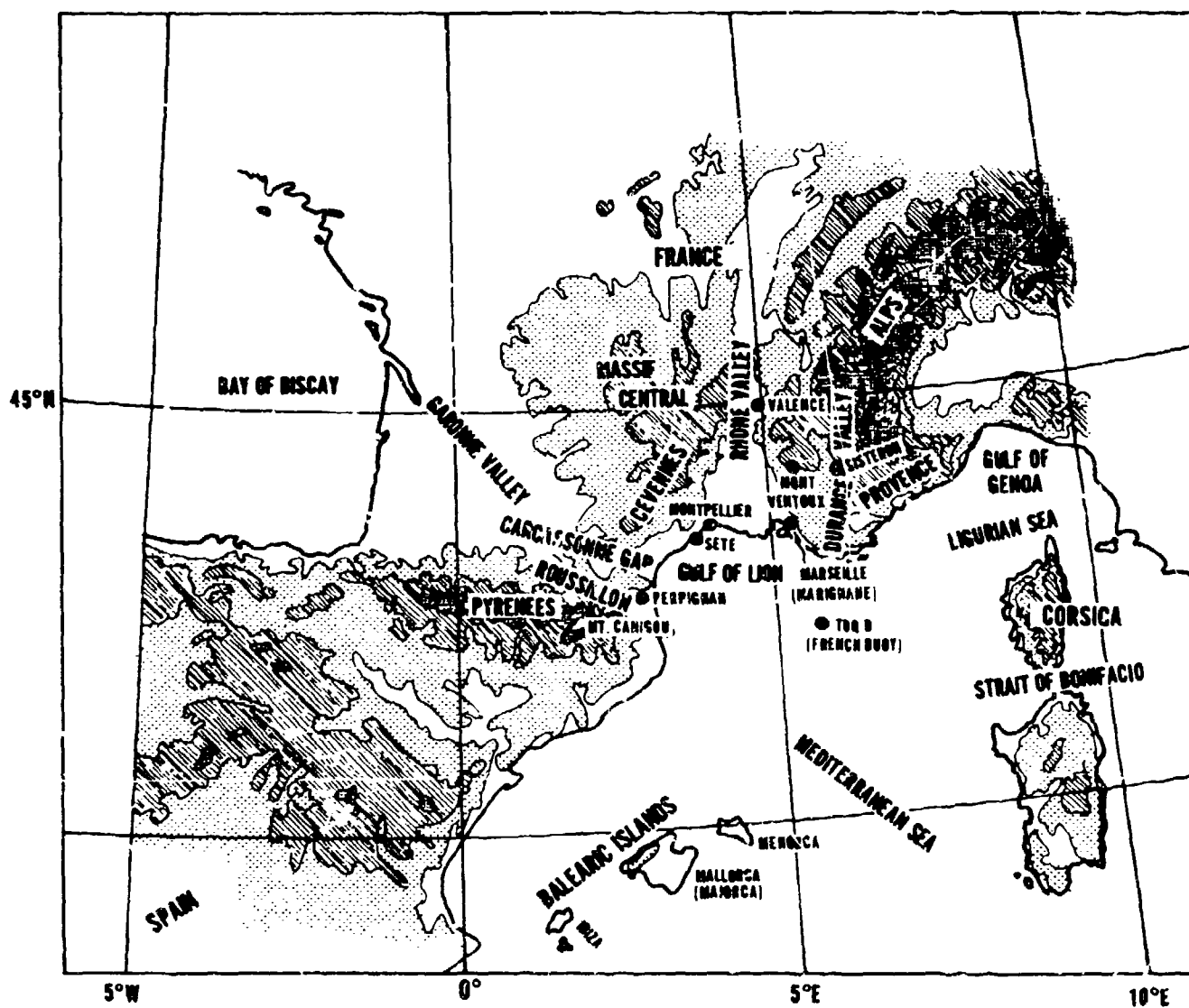


Figure III-F-1. Locator map for the mistral.

The mistral wind regime usually extends to a height of about 2 to 3 km, and is intimately associated with the jet stream regime in the upper troposphere and with the baroclinic waves embedded in the upper flow.

According to Rex (1950a, 1950b), blocking anticyclones have a preferred tendency to occur both near the Greenwich meridian and during the early months of the year (see Section III-D-2, para. 2). Since these highs may persist for many days, they may give rise to prolonged mistral episodes, especially if the northerly-to-northwesterly jet stream assumes a favorable position with respect to the orographic gap between the Pyrenees and the Alps. Wave disturbances and cold outbreaks embedded in the northerly flow over France may lead to individual surges within an extended mistral period.

For practical purposes, the mistral winds are defined as having a direction between 280° and 360° . Figure III-F-2 gives the wind rose for the French buoy TOQD (positioned in the Gulf of Lion at $42^{\circ}13'N$ and $05^{\circ}34'E$) from 1 June 1968 to 31 March 1970. According to this diagram, mistral winds are encountered most frequently from the northwest (320° to 340°). This direction also has the highest incidence of strong 50-knot winds. The wind statistics for TOQD conform rather closely to those computed for Marignane (sta. no. 07650), with the exception that wind speeds tend to be considerably higher over the open ocean than at coastal stations.

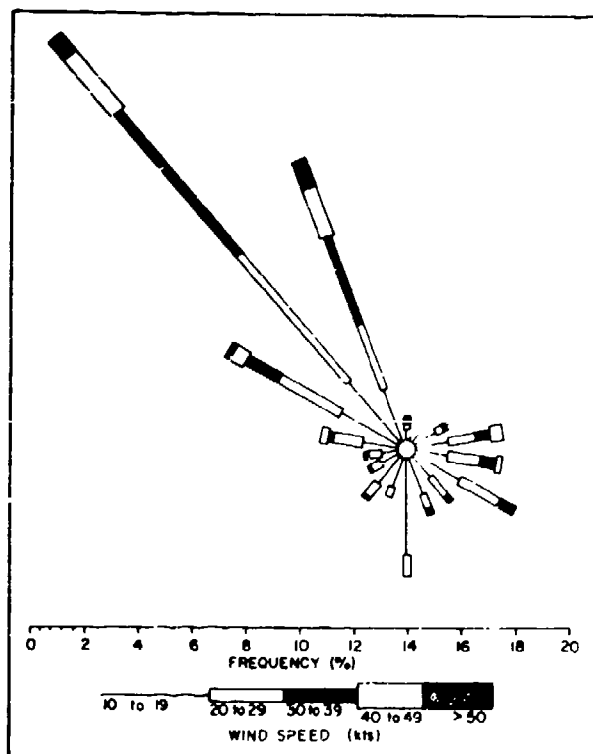


Figure III-F-2. Wind rose for the French buoy TOQD at $42^{\circ}13'N$ and $05^{\circ}34'E$ from 1 June 1968 to 31 March 1970 (from Reiter, 1971).

[illegible]

III-78

In spite of these shortcomings, several interesting conclusions may be reached. Figures III-F-4 and III-F-5, giving the mean wind speeds during mistral conditions (defined by coastal stations) and the frequency of gale force winds (>33 kt), show that the most severe conditions are encountered off the French coast southwest of Montpellier. The sheltering effects of the Pyrenees and of the mountains in Provence are clearly evident. Horizontal wind shears produced by this sheltering effect may be very strong indeed.

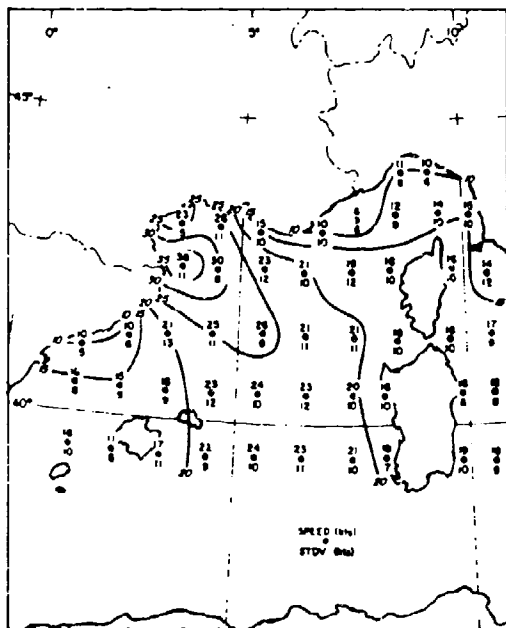


Figure III-F-4. Mean wind speed during mistral as defined in Figure III-F-3 (from Reiter, 1971).

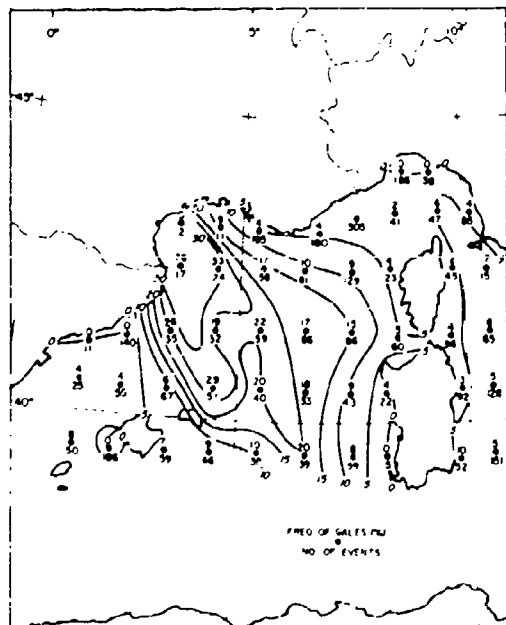


Figure III-F-5. Relative frequency distribution of gale force winds (>33 kt) for mistral situations as defined in Figure III-F-3 (from Reiter, 1971).

USS FORRESTAL reported during her 1965-1966 deployment:

"A definite shear line was found to exist during all mistrals. It was oriented from the northeast tip of Spain southeast to Menorca. FORRESTAL passed through the shear line in the vicinity of 41°N., 03°E. during the first mistral encountered. Winds to the west of the shear line were northerly 8 to 16 knots, and the seas were 3 to 5 feet. In the shear line, winds and seas increased markedly; to the east of the shear line, winds were 35 to 45 knots and the seas were 14 to 20 feet. The width of the line varied. Based on many aircraft observations taken during the four different mistrals, the shear line at times was as narrow as 2 to 3 miles, or as wide as 20 miles. On some occasions it was marked by clouds; on others it was perfectly clear and could only be observed by the different effects of the wind on the surface of the sea. In several instances the surface effects were markedly distinctive and pilots were able to report its location with ease, even from high altitudes. When the line was marked by clouds, the shear usually seemed to be very sharp. Carrier flight operations were easily conducted on the vast or calm side, although the amount of cloud cover near the line caused some concern. Attempts to find clearer skies by penetration of the line to the east resulted in an immediate clearing, and an extremely rapid increase of winds and seas, often to the extent that flight operations were no longer safely feasible. Under these circumstances, flight operations in pleasant conditions were possible just 20 or 30 miles west of the line. Since the line was observed by aircraft to move from east to west, especially at the southern end, operations should be conducted at some distance from it. This movement may displace the line from Menorca as far as Majorca and back again several times during a 24-hour period."

Even though the mistral is a katabatic wind, characterized by the sinking and spreading of cold air (evident from the minima in cloudiness shown in Figure III-F-6), FORRESTAL's report quoted above indicates the possibility of low-level convergence and rising motions at the edges of the mistral regions.

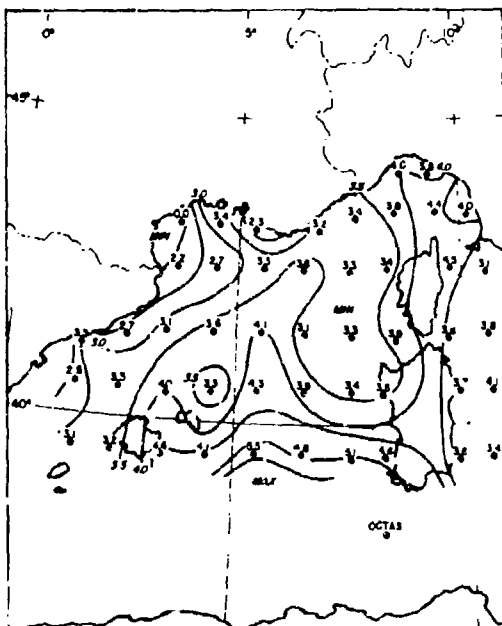


Figure III-F-6. Amount of low clouds in $1^{\circ} \times 1^{\circ}$ squares when mistral is observed at one coastal station or more (from Reiter, 1971).

2. The Bora

It was shown in the preceding section that the mistral depends quite critically on the surface pressure distribution which has to allow a rapid incursion of cold air into the Mediterranean basin. The bora along the Yugoslavian coast, on the other hand, is not as sensitive to the surface pressure distribution. Both mistral and bora have frequently been classified as similar phenomena produced by katabatic flow of cold air down the pressure gradient. It appears, however, that only the bora should be considered as a truly katabatic phenomenon. The kinetic energy of its gusts is derived entirely from the potential energy of cold air that spills over the coastal mountain ranges of Yugoslavia and "falls" down their steep slopes. Much of the mistral's energy is derived from the pressure gradient in the lower troposphere and from the jet effect of the local topography.

A prerequisite for the bora is the accumulation of cold air over the Balkan Peninsula, especially over Yugoslavia. The depth of this cold air reservoir has to reach at least up to the mountain passes which lead through the coastal mountain ranges. Not much air movement needs to be present inland from the coastal mountain ranges, or even at the crest of these mountain ranges, during bora conditions.

The relatively short distance of descent of the cold air masses along the mountain slopes does not suffice to warm the air above, or close to, the normal temperatures of the coastal plains. The bora, therefore, is felt as a cold wind. (The "foehn" or "chinook," on the other hand, arrives in the valleys or at the lee side of a mountain range as a warm katabatic wind (see Section III-F, para. 3)).

According to Hann-Süring (1939) the mean temperature in January on the mountain ridge above Trieste at 350 m above sea level is 1.5°C ; at sea level it is 5.0°C . This gives a monthly mean temperature lapse rate of $0.94^{\circ}\text{C}/100\text{ m}$, which is very close to adiabatic. The mean temperature difference in January between the Bay of Cattaro and Cetinje (672 m) is 8.9°C , or $1.3^{\circ}/100\text{ m}$. This demonstrates the frequent accumulation of cold air in the shallow bowl in which Cetinje is located, and the adiabatic descent of cold air that spills over the edge of this bowl and "falls" along the mountain slopes down to sea level.

The unstable stratification in the adiabatic descent of the bora makes the winds very gusty ("refoli" on the Adriatic Sea); strong winds are confined to the region close to shore, however, and gusts of $50\text{-}60\text{ m sec}^{-1}$ (ca. 105-125 kt) have been measured in Trieste. These gusts blow the spray off the wave crests, causing poor visibility similar to fog ("fumarea").

Anticyclonic bora is characterized by a strong high-pressure system over Central Europe, but no well-developed low to the south. A strong bora can develop, but the wind is usually considerably weaker 10 miles offshore. On the Italian coast the wind may be northwesterly. Skies are clear with the exception, perhaps, of a cloud bank ("foehn" or "chinook" wall) over the coastal mountain range of Yugoslavia. Surface pressure fluctuations of up to 5 mb at coastal stations are caused by the varying vertical extent of the descending cold air.

Cyclonic bora is tied to a depression in the southern Adriatic Sea. Along its southeastern side warm sirocco air is flowing aloft in a southerly to southwesterly air current (see Section III-F, para. 5). Thus the bora in the lowest layers of the troposphere is overrun by warm, moist sirocco air aloft. Skies are usually cloudy with altostratus ("bora scura"), with occasional rain or snow. Winds are strong but less gusty and cover the whole width of the Adriatic Sea.

The bora also shows a certain diurnal variability. On the island of Losinj the frequency maximum occurs between 0600 and 0700 and the intensity maximum between 0700 and 0800. It is in the early morning hours that the supply of cold air over the mountains should be most abundant. The bora is weakest around midnight. The frequency minimum was found near 1400 (Hann-Süring, 1939).

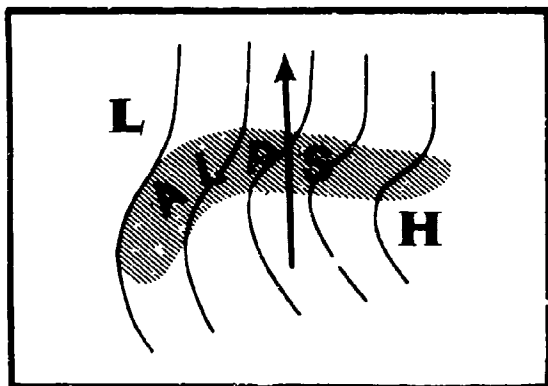


Figure III-F-7. Typical pressure distribution at gradient wind level over Alps during foehn (chinook) flow.

3. The Foehn

The anticyclonic conditions which tend to develop over the Alps under southerly flow aid in the development of foehn or chinook winds (Figure III-F-7). Frictionally induced flow along the pressure gradient moves air rapidly down the leeward slopes. In this descending motion the air is compressed nearly adiabatically (Figure III-F-8), whereas on the windward side the ascending motion is most often accompanied by cloud formation, and hence follows a moist-adiabatic trajectory (Figure III-F-9). Gravity waves (lee waves) often develop, and in their crests lenticular clouds (Moazagotl clouds) may form (Figure III-F-10). The latent heat of condensation is added to the airstream in its ascent up the windward slope. This heat benefits the air during its dry adiabatic descent along the leeward slopes. Therefore, temperatures in the valleys on the lee side of the mountain range may be several degrees higher than the temperature of the air before it started its ascent on the windward side.

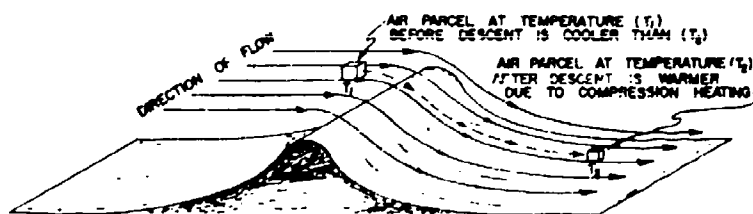


Figure III-F-8. Cross section through ridge showing descent of air parcel on leeward side. Temperature of air parcel at T_2 is greater than temperature of air parcel at T_1 due to compression heating caused by the descent (from Seran, 1967).

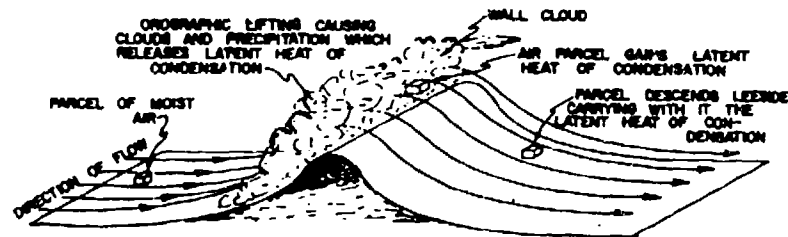


Figure III-F-9. Cross section through ridge showing moist air being lifted on windward side. This lifting causes condensation and the release of latent heat. The air parcel then descends the leeward side and heat gained from the condensation process is realized as warming at stations on the leeward slope (from Beran, 1967).

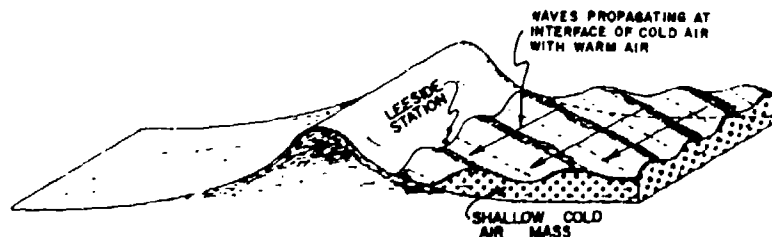


Figure III-F-10. Cross section through ridge with cold arctic or polar air banked against the side of the ridge. Waves are shown forming at top of cold air and periodically submerging stations located near the interface of cold and warm air. This action has been known to cause drastic temperature changes at lee-side stations (from Beran, 1967).

This rise in temperature of an air column that extends from the surface to the tropopause and is located to the lee of mountains brings about a decrease of mass in this column, and hence leads to surface pressure falls (see Figure III-F-7). Typical foehn conditions, therefore, can be recognized easily from surface pressure maps: high pressure over the windward side and over the crest of the mountains, and a relatively narrow tongue of low pressure that extends on the lee side of the mountain range parallel to its crest. The horizontal pressure gradients in this configuration can, at times, become very strong, but do not necessarily correlate with the strength of the foehn winds. Part of this apparent gradient is caused by systematic errors in the reduction of pressure to sea level. The air at mountain stations is rather cold before it starts its adiabatic descent, and using these surface temperatures for the reduction of pressure to sea level usually gives exaggerated high pressure readings. On the other hand, surface temperatures in the valleys on the lee side of the mountain range are high and therefore yield relatively low extrapolated sea-level pressures.

In the upper regions of the leeward slopes the descending air often is rather chilly and can have all the characteristics of a bora. Especially, foehn conditions with northerly winds over the Alps reveal a gusty falling motion of cold air as it spills over the mountain crests and through the passes. This motion is quite clearly revealed if the clouds of the "foehn wall" spill over the crest and dissolve in the violently turbulent motion as the air descends along the lee slopes (Figure III-F-11).

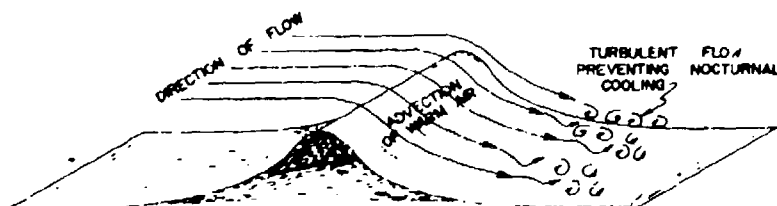
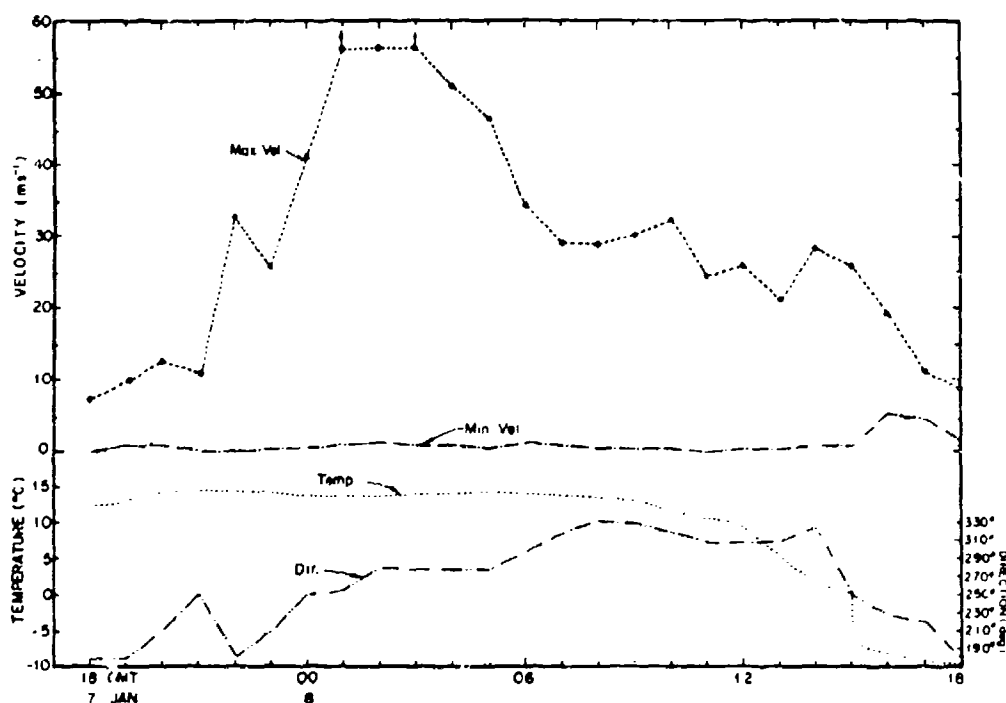


Figure III-F-11. Cross section through ridge showing advection of warm air and turbulence to the leeward side. When this process acts during nighttime, it prevents normal radiation cooling of the surface layer and leeward stations stay relatively warm (from Beran, 1967).

Because of their cascading nature as they move down along the lee slopes, the foehn winds are characterized by rapid speed fluctuations. This is illustrated by the example given in Figure III-F-12 (Lovill, 1969). It shows wind speeds, directions, and temperatures at Boulder, Colorado, during a strong foehn situation. Note that the gusts fluctuate between 0 and more than 55 m sec^{-1} . These strong wind variations may cause extensive damage to structures, parked aircraft, etc.



Figure, III-F-12. Plot of wind and temperature for strong chinook case at Boulder, Colorado, 7 and 8 January 1969 (from Lovill, 1969).

As with the bora, distinction can be made between anticyclonic and cyclonic foehn, depending on the flow characteristics in the upper troposphere (see Section III-F, para. 2). During anticyclonic conditions, cloudiness and precipitation on the windward side is suppressed and the "foehn wall" of clouds may be absent altogether. Under cyclonic conditions, heavy precipitation persists on the windward slopes of the Alps. With southwesterly flow aloft, floods can plague the southern valleys of the Alps if the weather situation holds for several days, as may be the case with a strong depression in the Gulf of Genoa. Persistent northerly foehn situations along the southern slopes of the Alps can dump excessive amounts of snow in the high Alpine regions, especially during wintertime. The danger of avalanches has to be anticipated under these conditions.

If the southerly flow over the Alps comes all the way from North Africa in an extended trough situation, Sahara dust may be carried in this air stream (coinciding with sirocco conditions over the west-central Mediterranean region). If anticyclonic foehn conditions prevail (well to the east of the trough axis) this dust will not be removed by precipitation, but will be carried over the crest of the Alps by the foehn winds, with consequent poor visibility contrasting with the unlimited visibility that usually prevails under foehn conditions.

4. The Etesian (Reiter, 1971)

The etesian is a northerly wind, prevailing during the summer in the Eastern Mediterranean and in the Aegean Sea. "Etesian" in Greek stands for "yearly," indicating the regularity with which these winds appear each summer. The Turkish word for these winds is "meltem." These winds, because of their frequency during the warm season, constitute a major factor in the climate of the Eastern Mediterranean. The prevailing period is May through October-November with maximum frequency and strength occurring in July and August.

Winds are generally northerly along the Greek coast, even during winter, when they may reach speeds exceeding those of the etesian. In May and November the frequency of northerly winds is at a minimum (see Figure III-F-13) and only those northerly winds that occur between May and November are considered as etesian winds, while the remainder form part of the winter season.

The term "etesian" is usually attached to a north wind that exceeds a certain minimum speed. Since the sea breeze in Athens is of a southerly direction and counteracts the etesian, those days for which Athens reports a north wind at noontime and apparently has a general pressure gradient of considerable strength also qualify as "etesian days."

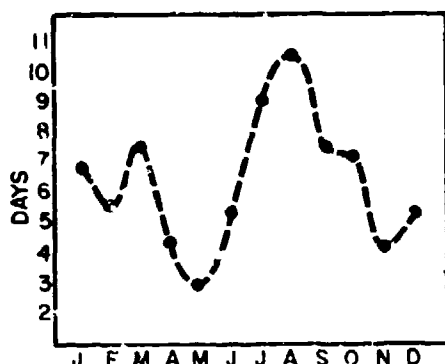


Figure III-F-15. Mean number of days with northwest, north and northeast winds > Beaufort Force 4 (11 kt) at 1400 LT, Hellenikon Airport, Athens (1949-1968) (from Reiter, 1971).

The pressure gradients necessary to drive the etesian winds are provided by a low pressure region along the southern coast of Turkey and a high pressure region over the Balkans. This is evident from the mean sea-level pressure charts for summer and winter (Figures III-F-14 and III-F-15). With such a characteristic pressure pattern, the cause of the etesian winds must be sought partly in the monsoonal character of the circulation between the warm land masses of Asia Minor and the cool Mediterranean, and partly in synoptic disturbances that lead to anticyclogenesis over the Balkans.

The strong winds in an etesian situation may be enhanced by channeling effects between islands (see Section IV-A). Such effects also render wind reports from certain locations unrepresentative.

It was previously stated that the etesian winds are a typical summer phenomenon. Based on the definition of an etesian day from the sea-breeze behavior at Athens, the mean number of etesian days were computed from records between 1893 and 1952 (Table III-F-1). The mean number of days with north or northeast winds at the National Observatory (sta. no. 16714, 5 km (3 n mi) inland), at Nea Philadelphia (sta. no. 16701, 10 km (6 n mi) inland), and at Hellenikon Airport (sta. no. 16716 on the south coast near Athens) is shown in Table III-F-2. Some of this variability is expressed in Table III-F-3. Table III-F-4 shows the mean number of continuous etesian days for each month (May to October) and the number of cases in a 60-year period where the etesian lasted five days or more, and 10 days or more. It will be noted that etesian periods of five days or more are not uncommon and occur on the average about once per month in July and August.

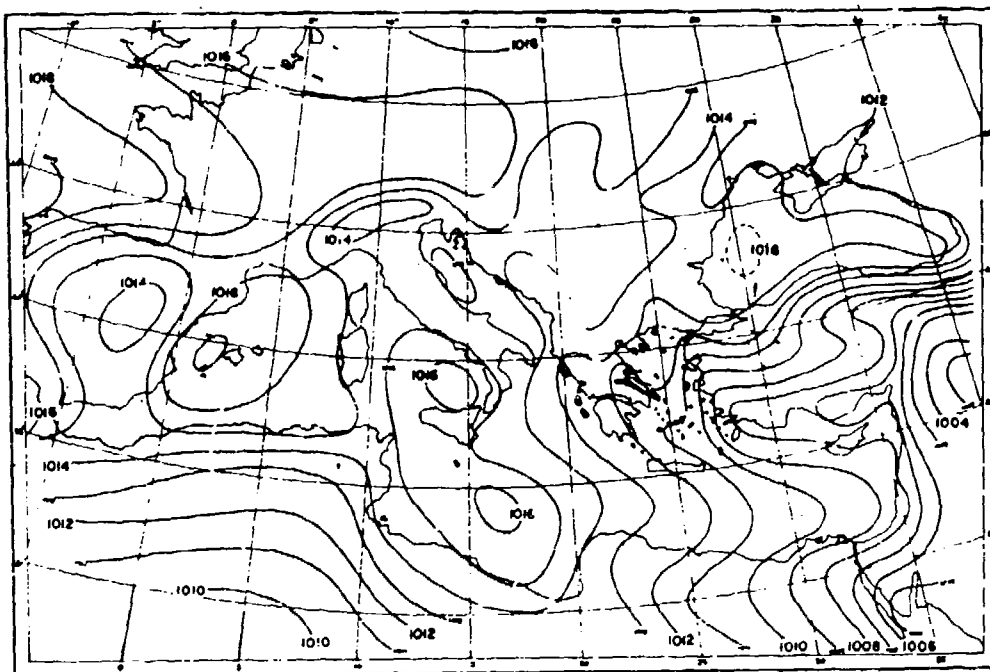


Figure III-F-14. Mean sea-level pressure (mb) during summer (from Reiter, 1971).

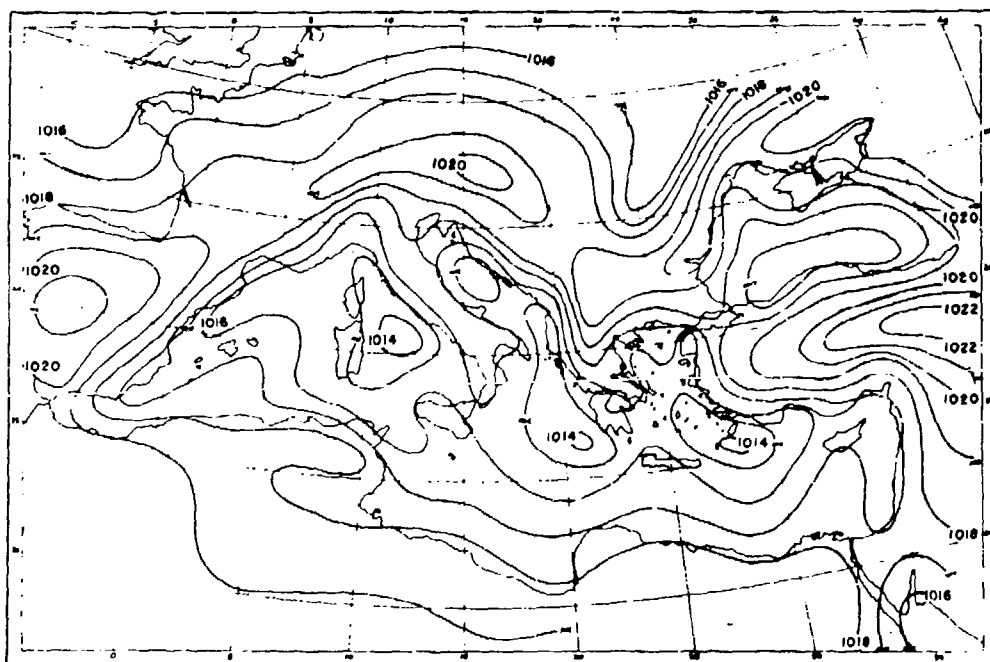


Figure III-F-15. Mean sea-level pressure (mb) during winter (from Reiter, 1971).

Table III-F-1. Mean number of etesian days during the period 1893-1952 at Athens (from Reiter, 1971).

May	Jun	Jul	Aug	Sep	Oct
4.3	6.0	13.0	13.6	11.1	5.7

Table III-F-2. Number of days with north or northeast winds ≥ 1 Beaufort Force (≥ 1 kt) and ≥ 4 Beaufort (≥ 11 kt) (from Reiter, 1971).

Station	Beaufort	May	Jun	Jul	Aug	Sep	Oct
Nea Philadelphia	≥ 1	6.8	9.5	16.1	16.0	13.6	12.5
	≥ 4	3.2	4.0	9.0	8.7	5.8	6.6
Athens Nat. Observatory	≥ 1	5.3	7.5	13.3	14.0	12.3	11.6
	≥ 4	2.3	4.0	8.4	9.1	7.1	6.5
Hellenikon Airport	≥ 1	4.1	6.6	11.1	12.9	11.1	11.1
	≥ 4	2.8	4.7	8.9	10.2	7.4	7.2

Table III-F-3. Maximum and minimum number of etesian days occurring monthly and yearly during period 1947-1969 at Hellenikon Airport (from Reiter, 1971).

No. & Year	May	Jun	Jul	Aug	Sep	Oct	Year (Jun-Sep)
Maximum No. Year	13 1950	15 1957	23 1967	23 1949	18 1964	24 1969	60 1961
Minimum No. Year	0 1959	0 1948	6 1966	2 1968	5 1952	1 1960	27 1968

Table III-F-4. Monthly mean number of continuous etesian days and the number of cases where duration of etesian was ≥ 5 days and ≥ 10 days (60-year period) (from Reiter, 1971).

Number.	May	Jun	Jul	Aug	Sep	Oct
Mean No. of Continuous Days	2.2	2.2	3.7	3.6	3.1	2.4
No. of cases ≥ 5 days	10	18	63	66	46	18
No. of cases ≥ 10 days	1	2	16	13	10	1

Table III-F-5. Variation between the maximum and the minimum wind speed expressed as a percentage of the mean at Rhodes Airport (1955-1964) (from Reiter, 1971).

May	Jun	Jul	Aug	Sep	Oct
92	95	117	104	96	75

A thorough statistical treatment of wind observations (taken at 0800, 1400 and 2000 local time) of 40 island and coastal stations is provided. The streamlines for winds and the frequency of such winds are given in Figure III-F-16. It appears that the Cyclades Islands, which include Naxos (sta. no. 16732) bear the brunt of the etesian throughout the season. In an interpretation of Figure III-F-16, allowance should be made for a bias in the wind measurements used in this analysis due to the channeling effects by islands (see Section IV-A). Even though it appears from Figure III-F-16 that the island of Crete lies outside the main reach of the etesian, strong or gale force winds are frequent along the south coast of this island during the etesian season. This is also observed elsewhere where mountains are oriented perpendicular to the etesian. Katabatic flow on the "lee side" of these mountains generates gusty wind conditions similar to the foehn of the Alps and the chinook of the Rocky Mountains. In the case of Crete, gaps in the island mountain range exercise an additional channeling effect that tends to increase wind speeds locally.

The large diurnal variation in the intensity of the etesian is caused mainly by the differential heating of land and sea (see Section IV-B). This differential heating would normally supply the pressure gradients that drive the land- and sea-breeze system. An additional influence upon the diurnal variation of the etesian is the turbulent mixing in an adiabatic to super-adiabatic planetary boundary layer that extends to a height of approximately 1000 m over land and provides increased momentum transport towards the ground during daytime hours.

Along the west coast of Turkey the sea breeze supports the etesian, as may be seen from Figure III-F-16. Therefore, the maximum wind force along this coast appears near 1700 local time, and the minimum near 0500. The percentage variation between maximum and minimum (expressed as a percentage of the mean wind) is large, due to the superimposed land and sea breeze effect of Asia Minor. Table III-F-5 gives this percentage variation for the airport at Rhodes (or Rhodes, sta. no. 16749).

In Athens, on the other hand, the sea breeze opposes the etesian. Hence the frequency of northerly winds has a minimum near noon because there are days when the sea breeze is stronger than the etesian. An examination of only the days at Athens when the wind at 1400 local time is greater than Force 4 still reveals strongest winds during the daytime. The summer months have a tendency for a secondary minimum in the early afternoon when the opposing effect of the sea breeze is strongest. This secondary minimum is not present during the winter (Figure III-F-17). The percent variation between maximum and minimum winds at Athens is also largest during the etesian season (Figure III-F-18).

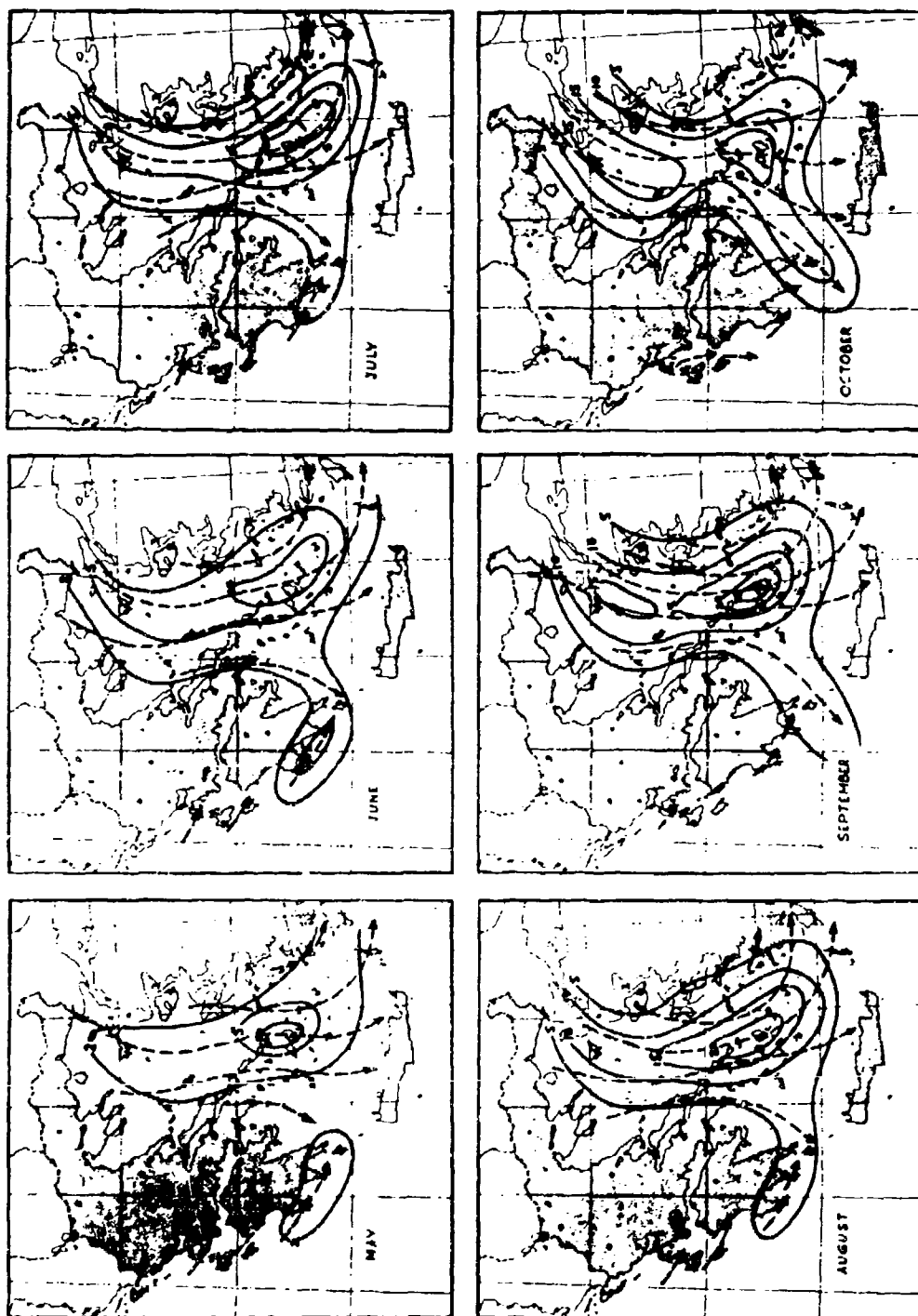


Figure III-F-16. Streamlines (dashed) for winds > Beaufort Force 6 (22 kt) and frequency (solid lines, %) during the etesian season for months as indicated (from Reiter, 1971).

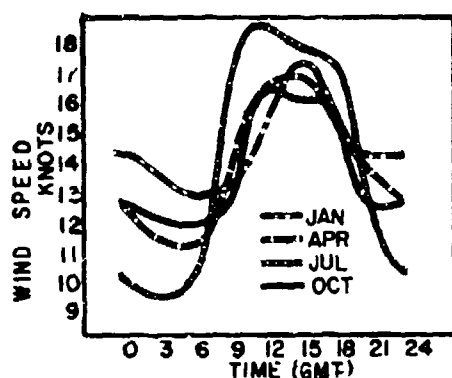


Figure III-F-17. Diurnal variation of mean wind speed (kt) at Athens for those days on which the wind at 1400 LT is > Beaufort Force 4 (11 kt) (from Reiter, 1971).

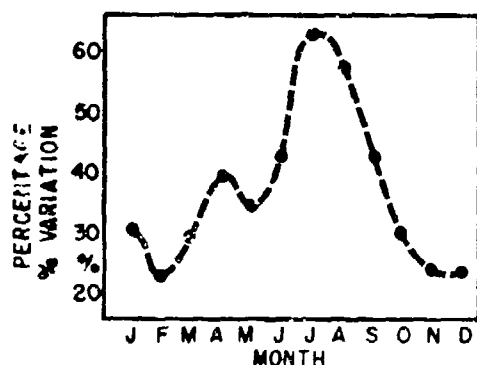


Figure III-F-18. Percentage variation between maximum and minimum winds at Athens (from Reiter, 1971).

An examination of the diurnal variation of winds greater than Force 4 at Limnos (or Lemnos, sta. no. 16651) in the northern part of the Aegean Sea and at Naxos in the southern part has also been made. At Limnos the wind maximum occurs before 1400, whereas at Naxos it is found between 1400 and 1700. At Limnos the mean wind force at 1600 is even less than that at 0500. The variability between maximum and minimum at Naxos is about one half of that at Hellenikon Airport. At Limnos it is still less.

From the foregoing it would appear that the low pressure trough shown along the south coast of Turkey undergoes diurnal pulsations of intensity, so that the etesians are reinforced by the sea-breeze effect in the southern Aegean. In the northern Aegean and near the Macedonian and the Thracian coasts this reinforcement by the sea breeze is absent. The heating of the land during the daytime and its influence upon the pressure gradient even opposes the etesian regime.

The surface flow in the etesian seems to be generally divergent (Figure III-F-16). This agrees with the traditional concept that etesian weather is dry with clear skies. However, it has been reported that the months of May-June and October-November show maxima of instability over Greece, and consequently a maximum of thunderstorm days. Thunderstorms and lightning

frequently occur on the day preceding the outbreak of the etesian, as well as on the first day of the etesian. This is especially true for May-June and September-October, but less so for July and August. In the Aegean Sea during July and August, scattered clouds, mostly altocumulus, herald the establishment of an etesian-wind period for the following day, a fact well known to local fishermen. Orographic clouds may form on some islands during the etesian, especially if winds are strong.

5. The Sirocco (Reiter, 1971)

One of the most important wind regimes of the Mediterranean is the sirocco. According to Huschke (1959), the sirocco is a warm south or southeast wind in advance of North African depressions (see Section III-E, para. 2). The air is dry and dusty, but in crossing the Mediterranean it picks up much moisture. Some of the local names of the sirocco are soteno, khamsin, ghibli, chili, simoon, leveche and morin. The localities which use these names are shown in Table I-C-2 and Figure I-C-2.

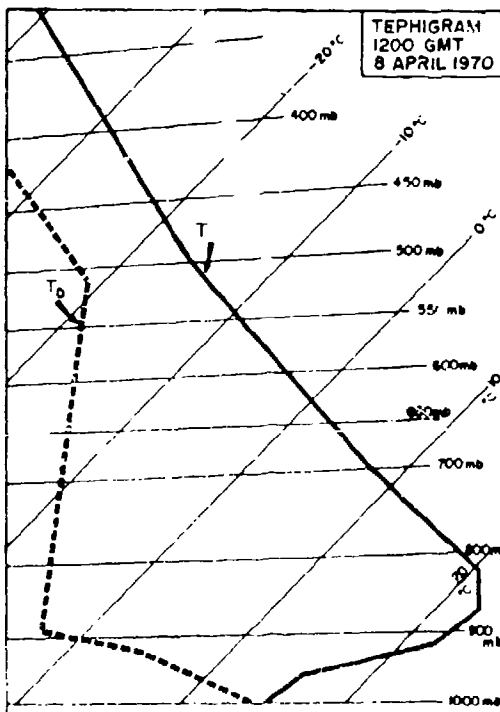


Figure III-F-19. Typical sounding in southwesterly sirocco flow, Malta, 1200 GMT, 8 April 1970 (from Reiter, 1971).

Air-sea interactions described in Section V-C play an important role in the sirocco. In spring, the sea is cool and as the hot sirocco air moves northward in advance of a depression, a substantial inversion -- which may be as great as 15° to 18°C in extreme cases -- is created between the surface and approximately 3000 ft (Figure III-F-19). A time section of sirocco conditions preceding a typical spring depression system moving across Malta is shown in Figure III-F-20.

When sirocco winds are light, low stratus clouds form in amounts which increase with the length of sea track; drizzle and sea fog are to be expected in the Ionian and Adriatic Seas. When the sirocco is strong, vast quantities of dust are trapped beneath the inversion and produce a thick haze that can reduce visibility to a few hundred yards at Malta and farther north (see Section III-K). The dust, raised mainly over the desert during the day, is carried northwards and is often thickest in the Malta area in the late afternoon or evening.

During all seasons, the operation of aircraft, particularly from carriers, is seriously affected by the sirocco. Dense belts of altocumulus castellanus that approach from the southwest and are probably associated with weak troughs in the upper flow should be treated with caution as they often are associated with radical and sudden changes in surface wind speed and direction.

The dust not only reduces visibility, but also causes radar clutter and penetrates everywhere; thick deposits in aircraft cockpits have been observed. Turbulence above the inversion is severe, particularly if castellanus is present (see Section V-A), and pilots report that aircraft may be difficult to control. An indication of the turbulence may be deduced from barograph traces which commonly show violent "pumping" underneath regions with serious turbulence conditions.

The surface inversion produced in spring gives extremely anomalous radar and radio propagation in the dust-laden atmosphere below the inversion (see Section V-E). Helicopters are liable to be out of radio contact at a range of a mile or two.

When the sirocco blows over islands with hilly terrain, turbulence may mix the inversion layer on the down-wind side and ships running for shelter in the lee of the island can experience a sudden uncomfortable rise in air temperature.

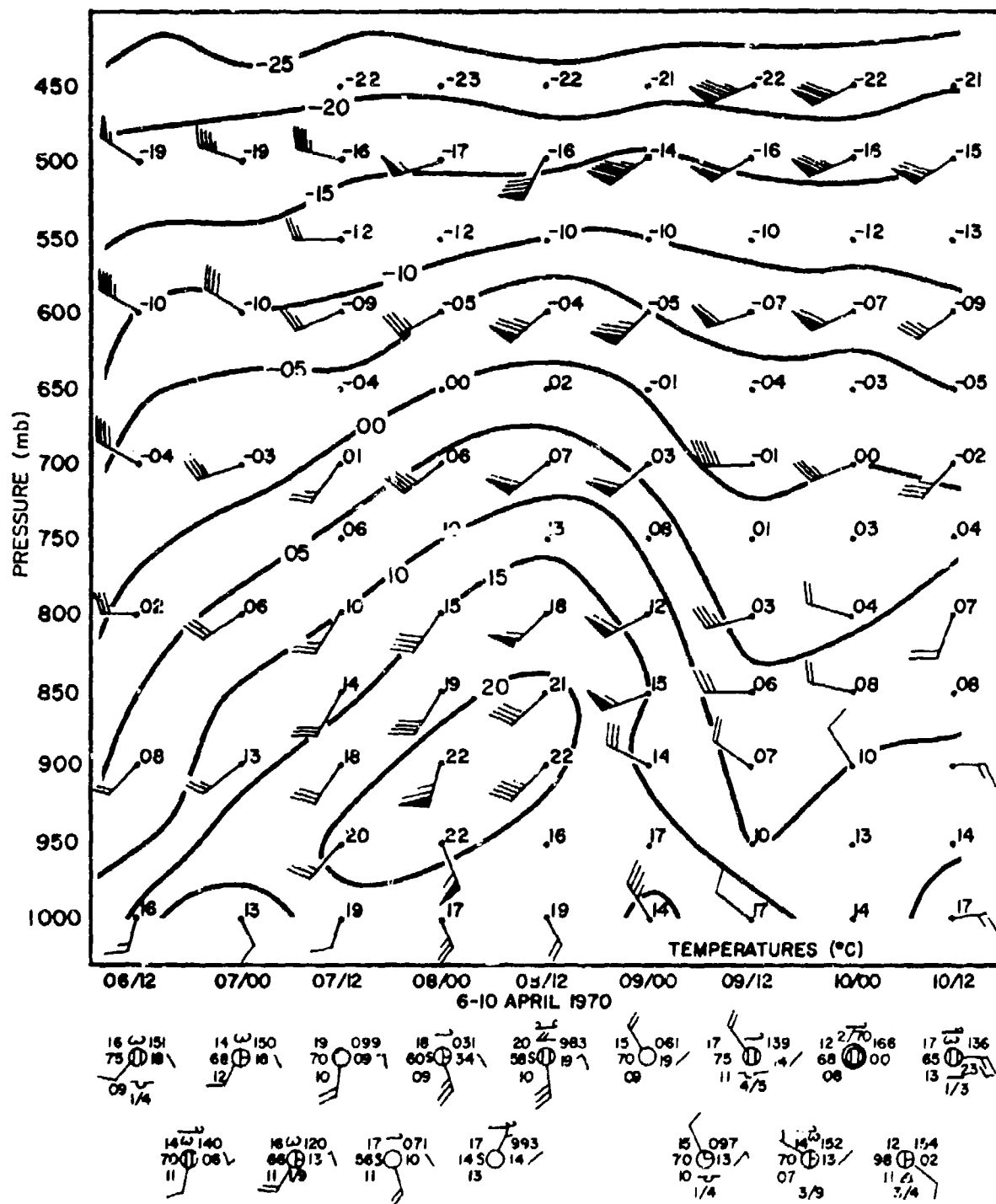


Figure III-F-20. Vertical time cross section of temperature, wind and surface weather conditions at Malta, 6 to 10 April 1970, including a typical sirocco period (from Reiter, 1971).

6. The Levante

This NNE to ENE wind blows in the Western Mediterranean against the coast of Spain. It has a relatively long fetch and, consequently, may lead to rough seas, especially if the driving pressure system -- high over Central Europe and the Iberian Peninsula, low over the Western Mediterranean near the Balearics -- changes only slowly. Frontal troughs moving in a northwesterly upper-air current across the Iberian Peninsula into the Balearic region may cause short spells of the levante. With a well-developed low south of the Balearic Islands, strong NE gales may develop with heavy and continuous rains along the Spanish coast.

G. ANNUAL TEMPERATURE VARIATION

The annual variation of temperature in the Mediterranean region is governed by the fact that large water bodies have a greater conductive capacity, given by

$$\sqrt{\rho \frac{c}{K}},$$

where ρ is the density, c is the heat capacity per unit of mass, and K is the heat conductivity coefficient. Furthermore, unlike the conditions over solid land, solar radiation penetrates to some depth in the ocean, thus providing heat by radiation absorption to a relatively deep layer. In soil, the warming of lower strata occurs entirely by heat conduction (ignoring the effects of percolating ground water). In the ocean, heat is transported mainly by much more efficient convective processes. All this adds up to a slow warming of the ocean from winter to summer, whereas the continental land masses heat up rapidly. In autumn and winter, on the other hand, ocean areas lose their heat much more gradually than the rapidly cooling continents.

The measurement of air temperature is the responsibility of the meteorologist, whereas the determination of sea-surface temperature is the oceanographer's task. Unfortunately, little has been done to date to reconcile these two different data sources into unified maps. However, since rather sharp discontinuities of air temperature measured close to the ground would appear along the coastlines, it may be just as well to represent continental air temperatures and sea-surface temperatures on separate charts.

Figures III-G-1 through III-G-4 show mean monthly air temperatures and sea-surface temperatures of the Mediterranean for the months of January, April, July and October (Royal Netherlands Meteorological Institute, 1957). The following features of interest are noted:

(1) A strong meridional temperature gradient exists in the Black Sea during winter (not shown in these diagrams). This gradient is caused by the frequent intrusions of cold air coming from the interior of Russia (see also Figure III-G-5).

(2) The Adriatic Sea shows a meridional gradient during winter which seems to be typical for a land-locked sea over which cold continental air masses are advected. The gradient vanishes in the northern part of the Adriatic Sea during spring and summer. Here the shallow waters experience a very rapid warming.

(3) In the Western Mediterranean basin the meridional temperature gradient shows quite strongly during spring and summer. Obviously the winds blowing through the Carcassonne Gap and the Rhone Valley -- not necessarily of mistral strength -- are pushing the warm surface waters of the Mediterranean toward the North African coast. Evaporative cooling also has an effect on surface water temperatures.

(4) Warm surface waters also accumulate in the Gulf of Iskenderun from spring until autumn, aided by the etesian winds that prevail during summer.

(5) Cool waters in the Aegean during summer are associated with the etesian.

Figures III-G-5 and III-G-6 show mean January and July air temperatures measured at land stations (Wallen, 1970). The high summer temperatures in the interior of Spain match those of North Africa. During winter the sharp temperature gradients between the Balkan Peninsula and the Adriatic Sea are noteworthy. The cold bora winds descending along the coastal mountain ranges in this region, especially during the winter season, draw their energy from this temperature gradient.

Figures III-G-1 through III-G-4 permit a comparison of seasonal air and sea-surface temperatures from ship observations. Sutcliffe (1960b) provided analyses of these temperature differences for January and July (Figure III-G-7). These temperature differences give an indication of average stability conditions in the air layers close to the water surface. In winter, considerable instability (ca. 2°C) exists in the Gulf of Lion. Similar values appear over the Adriatic Sea, and even larger temperature differences are encountered over the Aegean Sea. The temperature differences diminish toward spring and are reversed during summer, indicating generally stable conditions (warm air overlying cooler water). In autumn, air and sea-surface temperatures again approach each other.

Monthly mean maximum and minimum temperatures for the months of February, May, August and November are shown in Figures III-G-8 through III-G-11. The largest spread between these temperatures occurs over land, as is to be expected. The diurnal range of temperatures is relatively small along the eastern shores of the Mediterranean during February. The diurnal spread increases during spring and summer (Frank and Elliott, 1953)

In Appendix F are listed stations for which mean monthly minimum, maximum, absolute minimum and absolute maximum temperatures are available from the World-Wide Airfield Summaries recently published by the U.S. Naval Weather Service. From this data it is found that, for "continental" stations, July tends to be the warmest month. "Oceanic" stations, due to the slower warming rate of water as compared to land, are warmest during August.

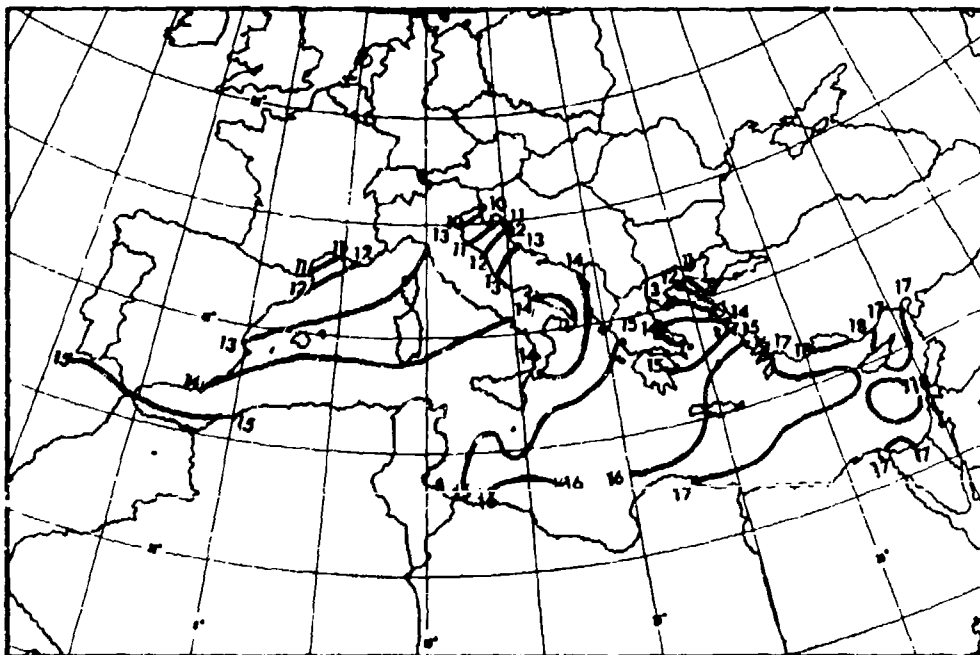
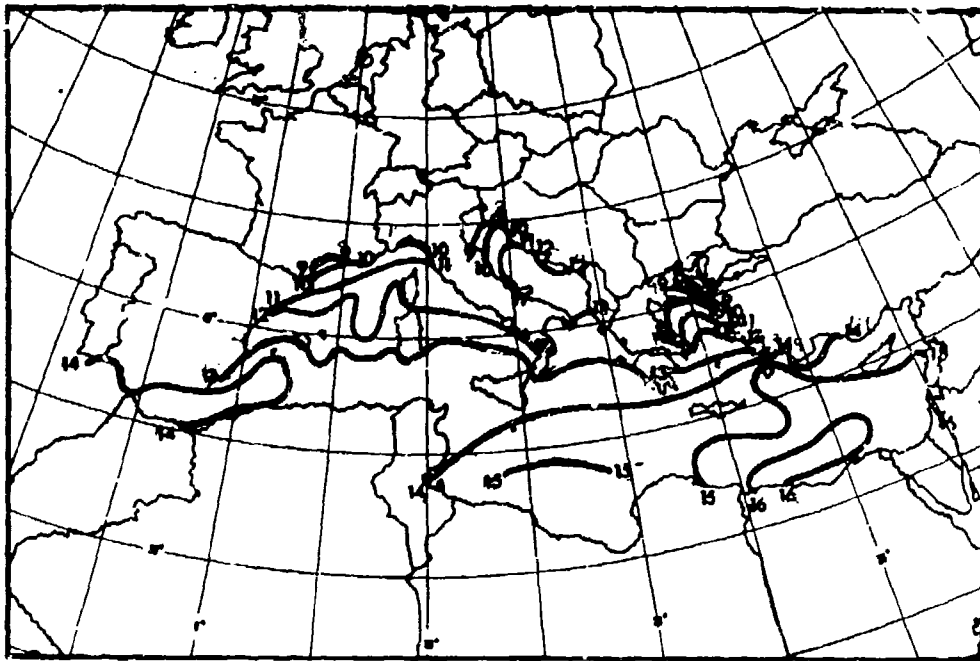


Figure III-G-1. Mean sea-surface temperatures ($^{\circ}\text{C}$) (top) and air temperatures ($^{\circ}\text{C}$) for the Mediterranean area for January (bottom) (after Royal Netherlands Meteorological Institute, 1957).

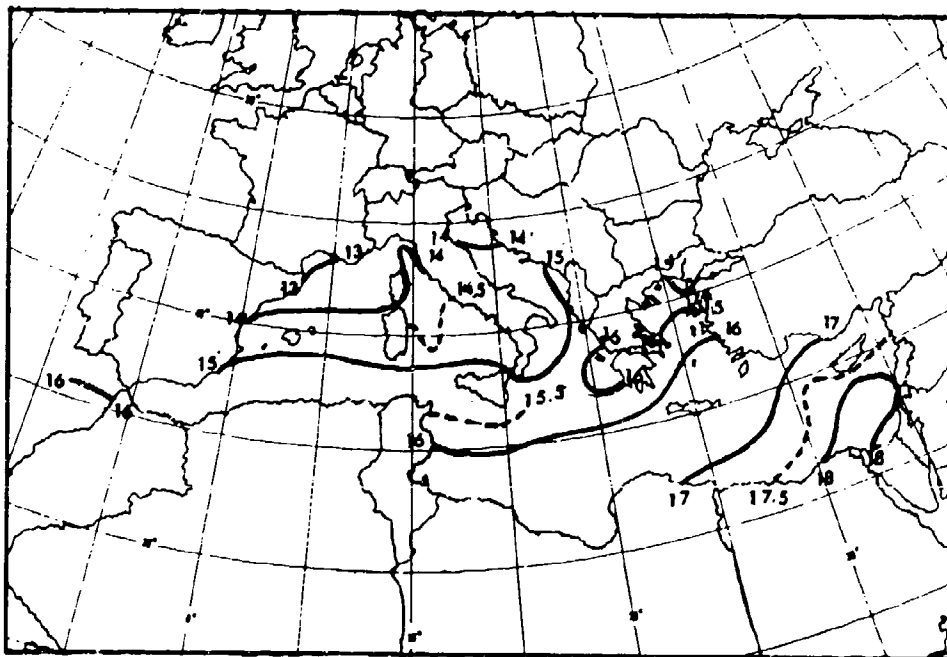
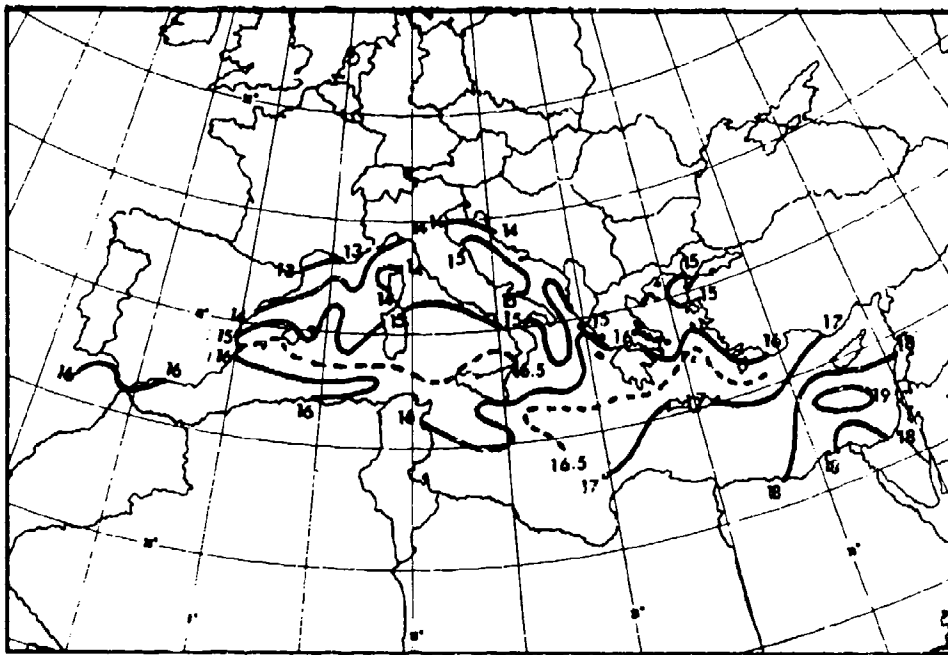


Figure III-G-2. Mean sea-surface temperatures ($^{\circ}\text{C}$) (top) and air temperatures ($^{\circ}\text{C}$) for the Mediterranean area for April (bottom) (after Royal Netherlands Meteorological Institute, 1957).

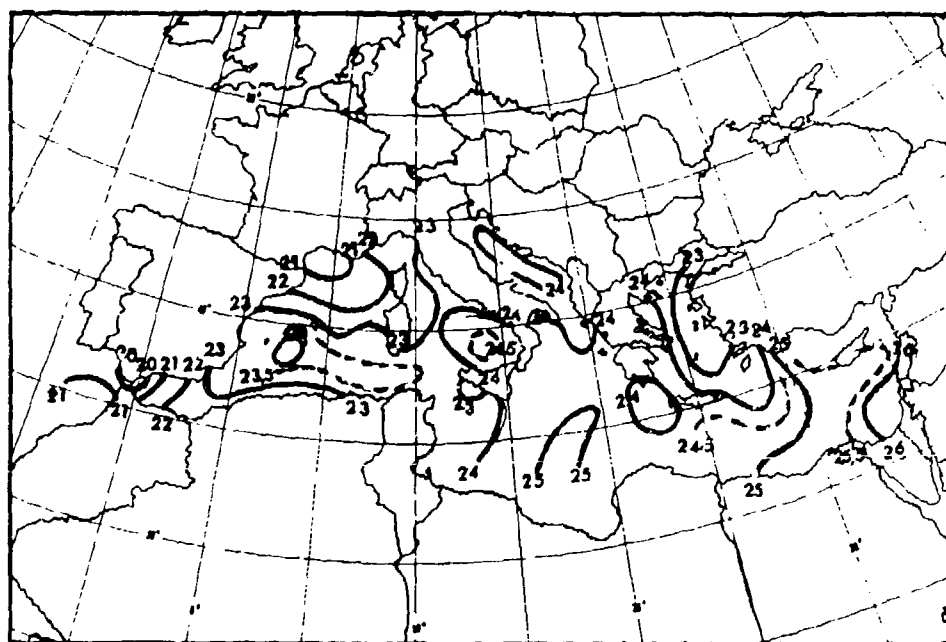
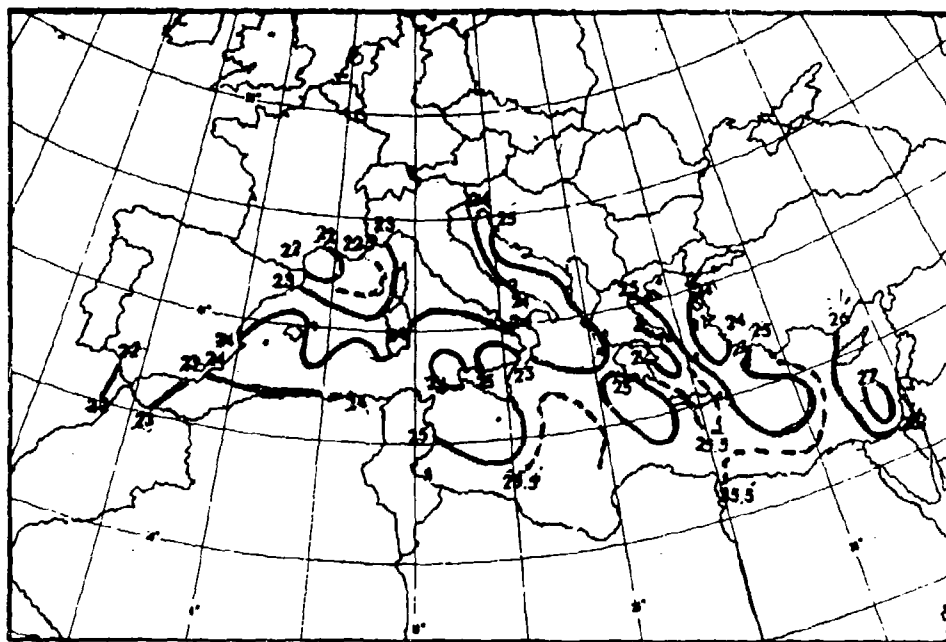


Figure III-G-3. Mean sea-surface temperatures ($^{\circ}\text{C}$) (top) and air temperatures ($^{\circ}\text{C}$) for the Mediterranean area for July (bottom) (after Royal Netherlands Meteorological Institute, 1957).

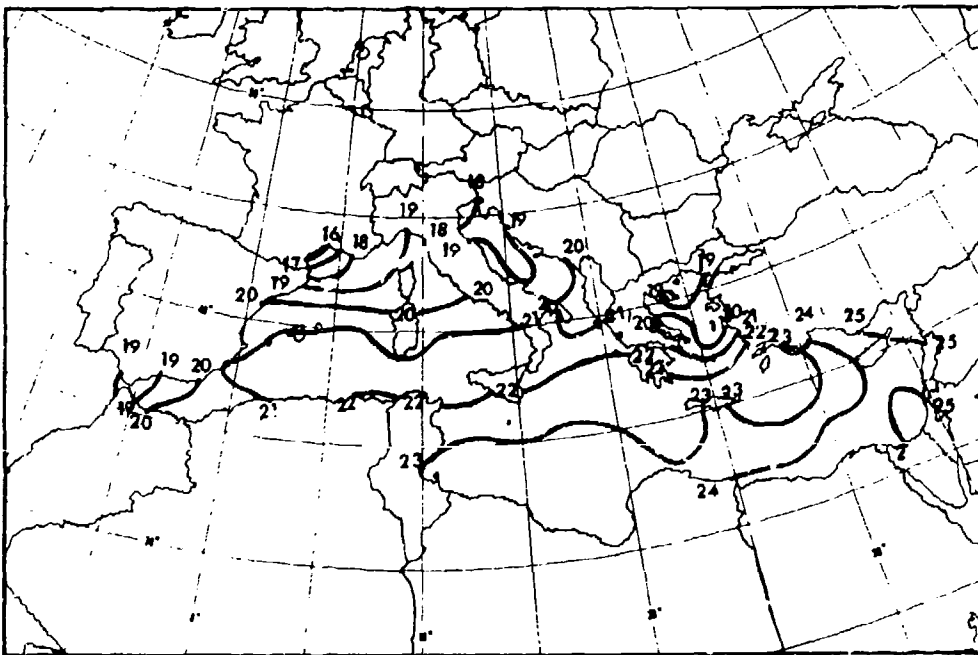
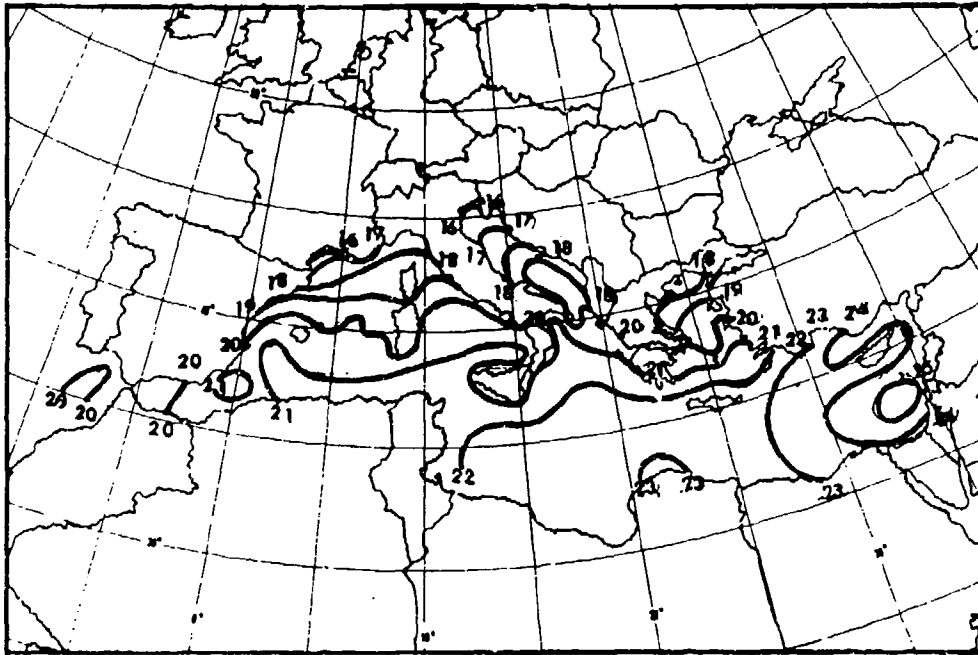


Figure III-G-4. Mean sea-surface temperatures ($^{\circ}\text{C}$) (top) and air temperatures ($^{\circ}\text{C}$) for the Mediterranean area for October (bottom) (after Royal Netherlands Meteorological Institute, 1957).



Figure III-G-5. Mean air temperature at station level, January (°C) (from Wallen, 1970).

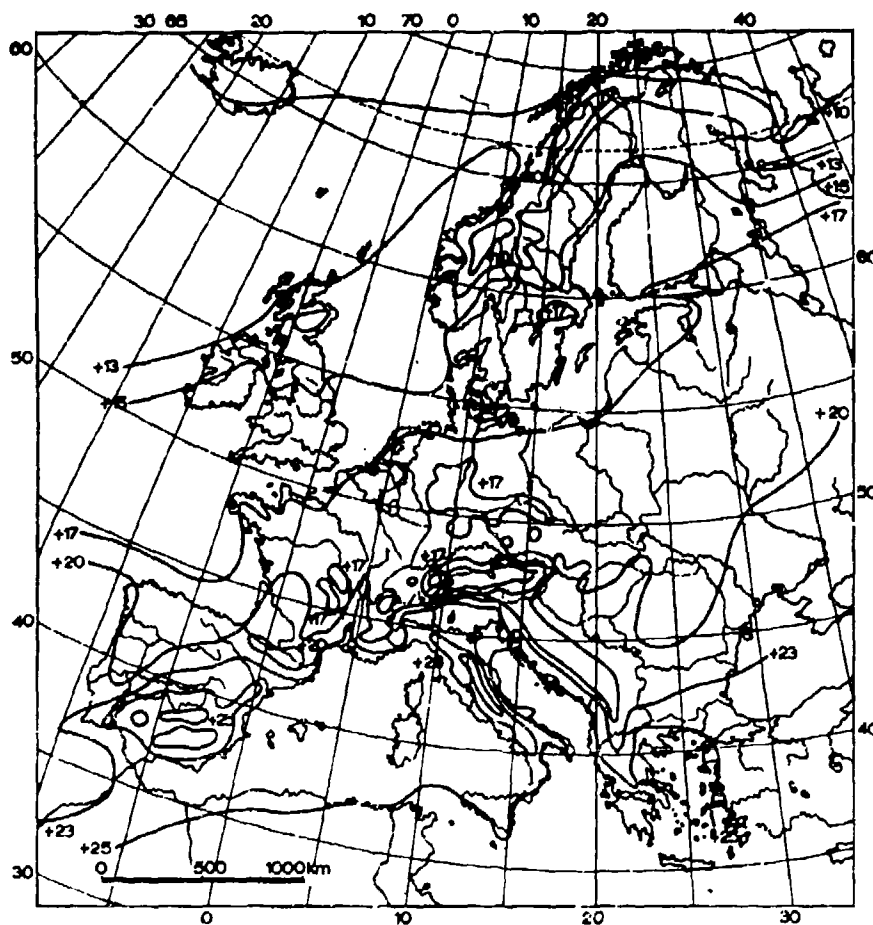
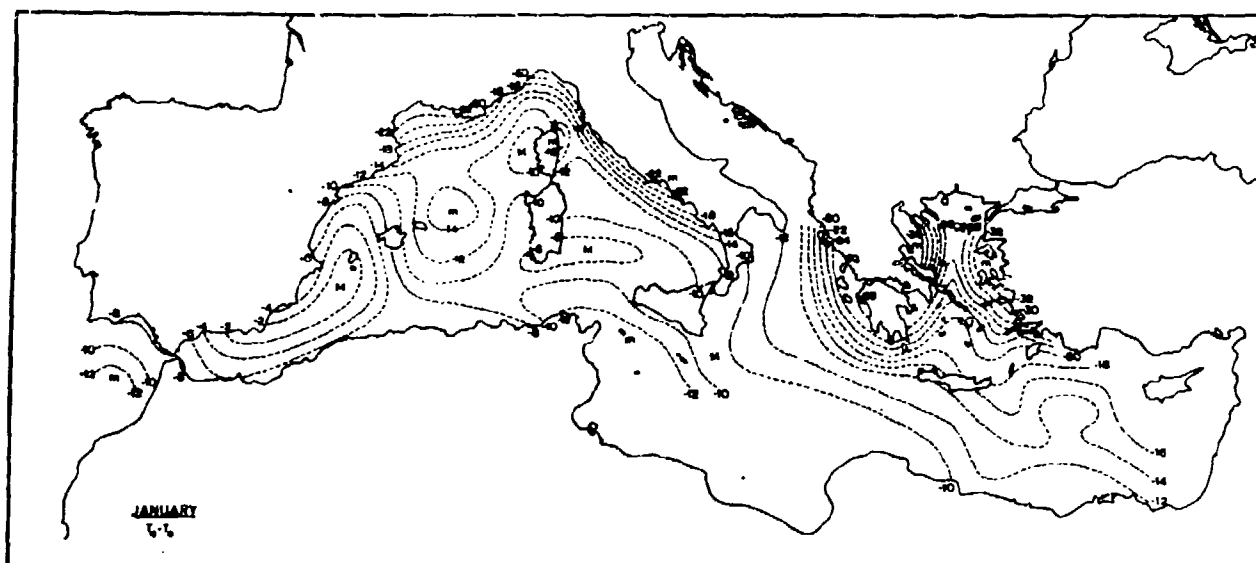
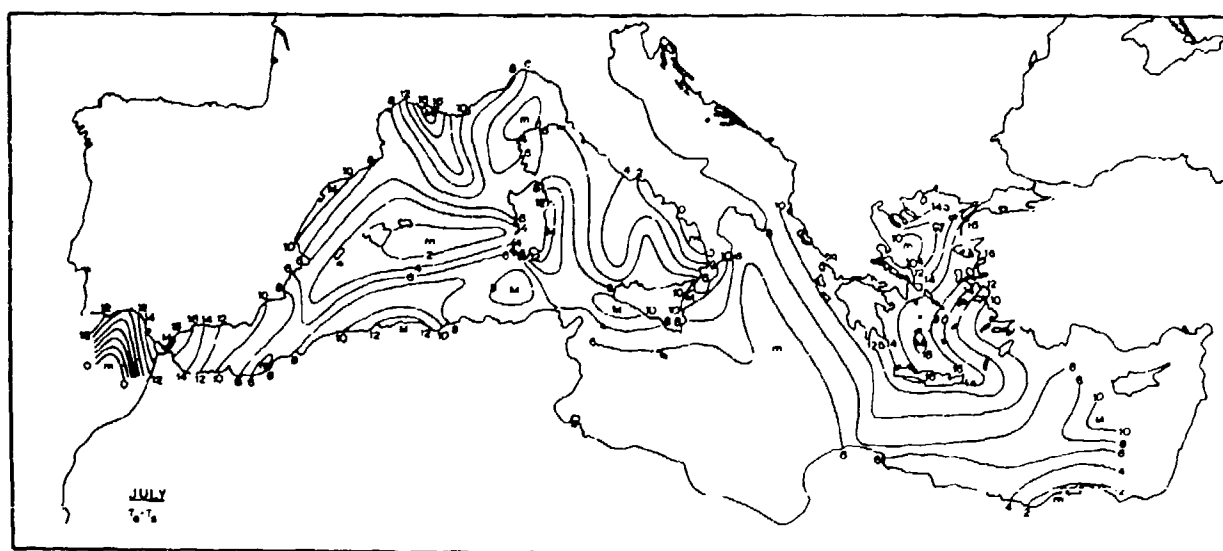


Figure III-G-6. Mean air temperature at station level,
July (°C) (from Wallen, 1970).



a



b

Figure III-G-7. Distribution of the difference between air temperature (T_a) and sea-surface temperature (T_s) in tenths of degrees Celsius for (a) January and (b) July. Relative maxima are denoted by "M" and relative minima are denoted by "m" (from Sutcliffe, 1960b).

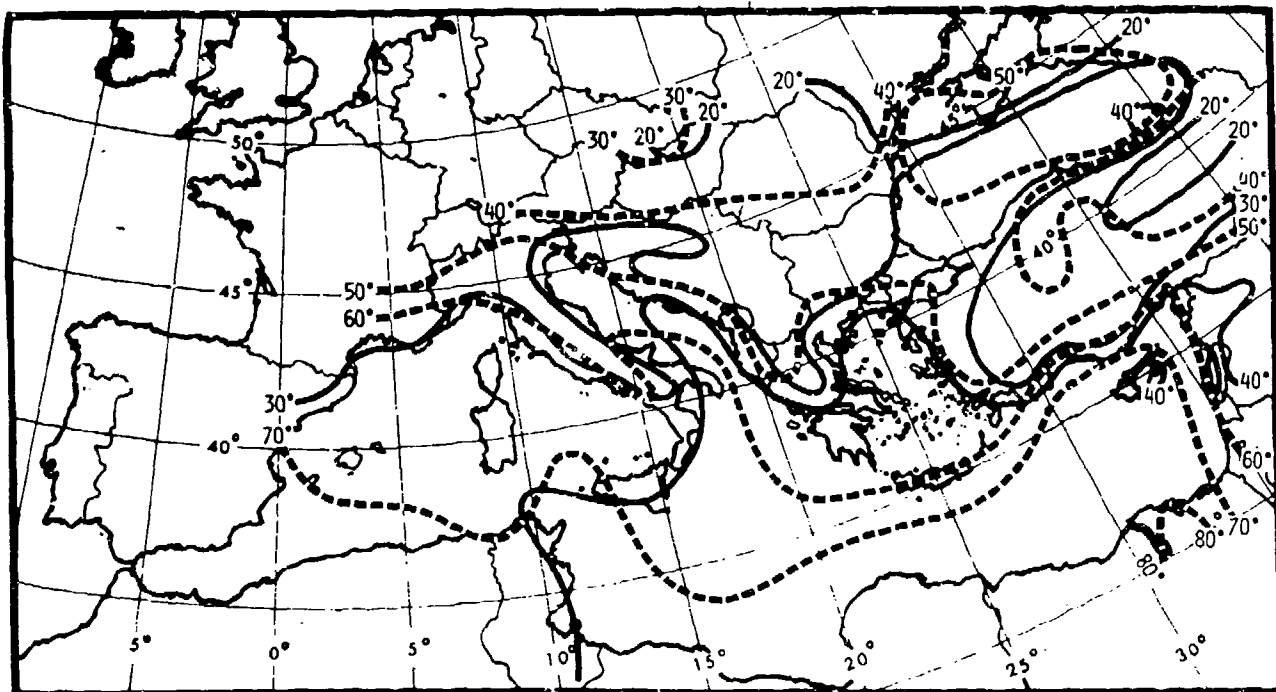


Figure III-G-8. Mean maximum (dashed lines) and mean minimum (solid lines) temperatures ($^{\circ}\text{F}$) for February (from Frank and Elliott, 1953).

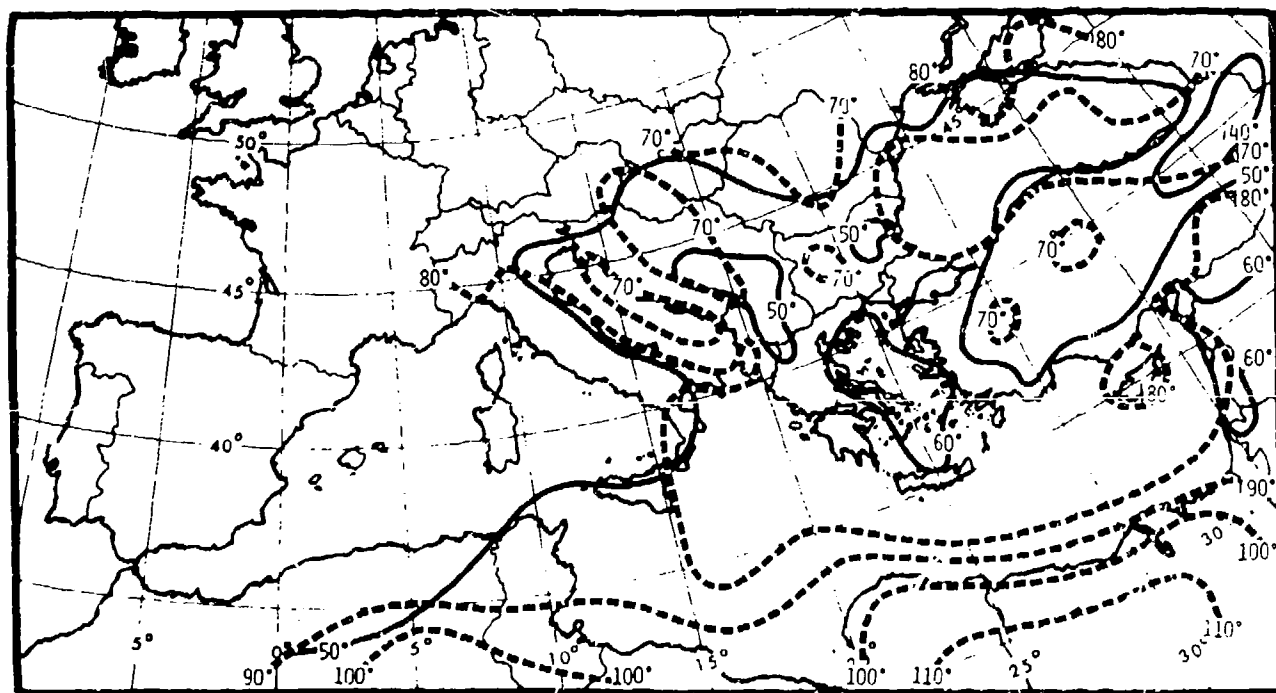


Figure III-G-9. Mean maximum (dashed lines) and mean minimum (solid lines) temperatures ($^{\circ}\text{F}$) for May (from Frank and Elliott, 1953).

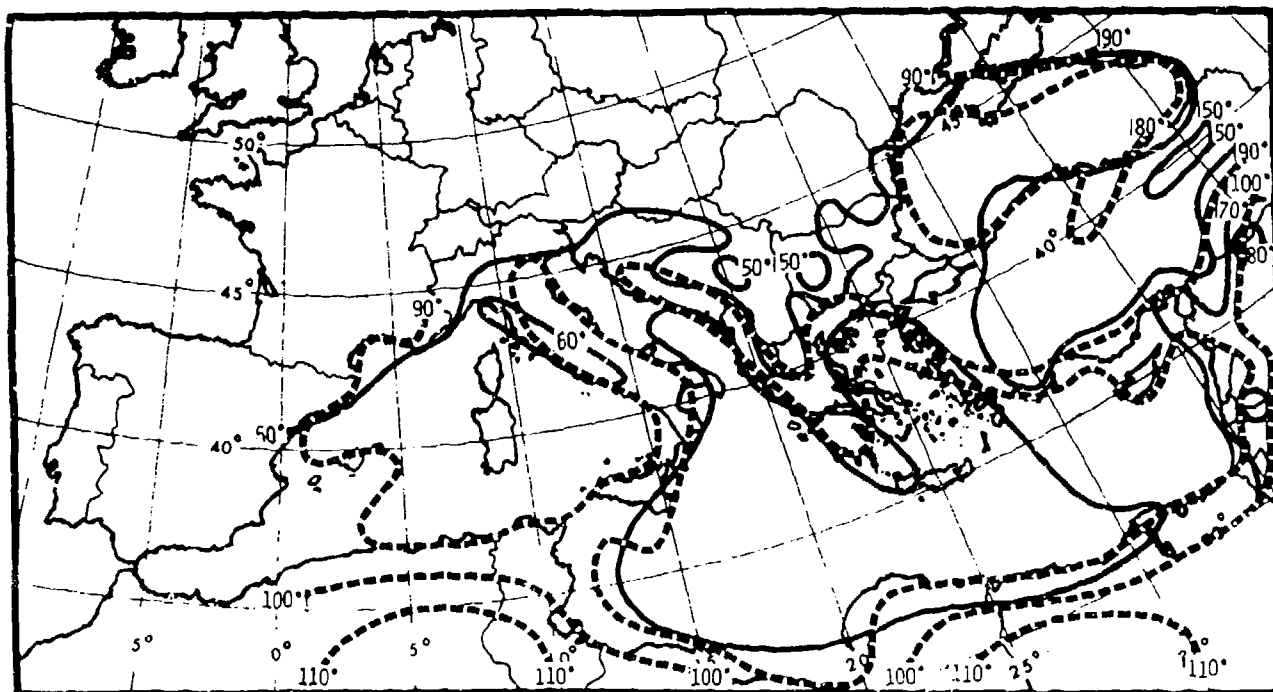


Figure III-G-10. Mean maximum (dashed lines) and mean minimum (solid lines) temperatures ($^{\circ}\text{F}$) for August (from Frank and Elliott, 1953).

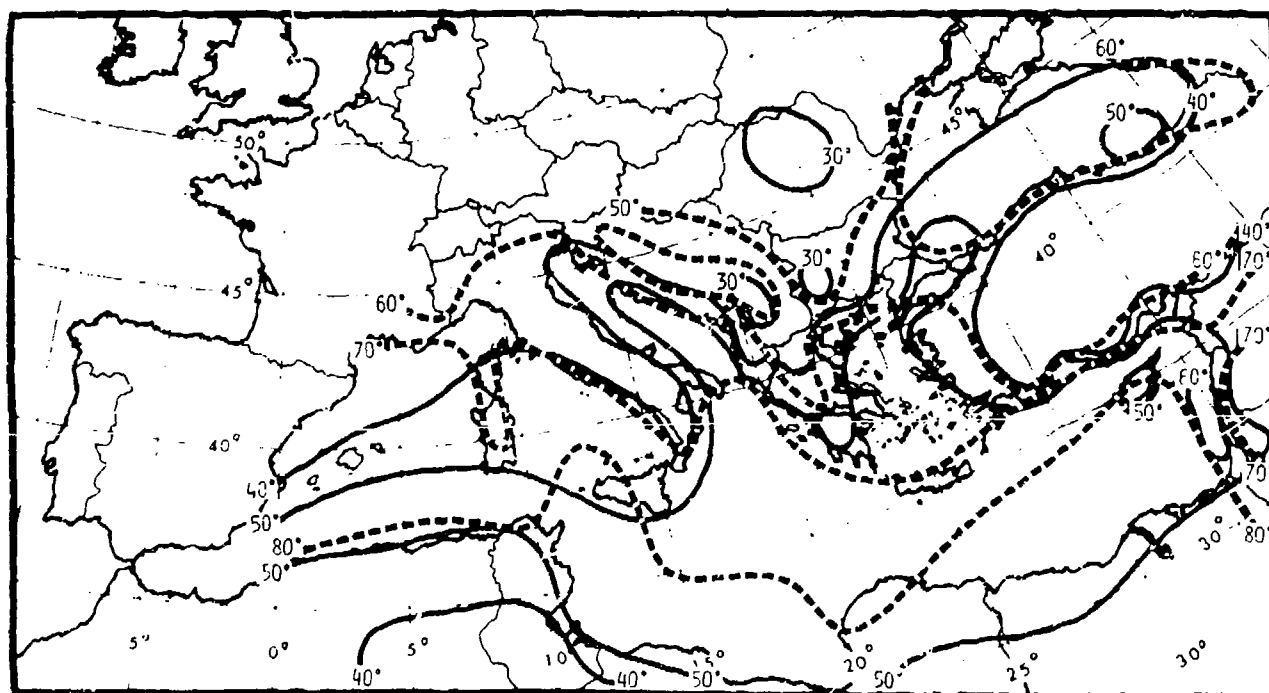


Figure III-G-11. Mean maximum (dashed lines) and mean minimum (solid lines) temperatures ($^{\circ}\text{F}$) for November (from Frank and Elliott, 1953).

H. ANNUAL PRESSURE VARIATION

1. Upper Air

A comparison of Figures II-B-15 and III-B-34 indicates that the height distribution near tropopause level undergoes marked seasonal changes over the Mediterranean region. Contour heights of the 200-mb surface increase by about 500 m (1500 ft) from winter to summer. The prevalence of cyclonic weather regimes during winter is replaced by predominately anticyclonic conditions during summer.

This is also reflected in the monthly mean contour patterns at 500 mb (Figure III-H-1) (Black, 1969). During winter and spring, a trough in the mean contours is located over the Western Mediterranean basin. Frequent cold outbreaks through the Carcassonne Gap and the Rhone Valley, concurrent with mistral episodes off the coast of southern France, occur during this season. Genoa cyclogenesis is also most frequent during winter and spring.

During the summer, anticyclonic flow prevails over the Western Mediterranean and a weak trough is indicated over the eastern basin. This shift in the trough position towards the east coincides with the season of etesian winds in the Aegean Sea. In autumn, the trough shifts back into the Western Mediterranean.

Figure III-H-1 shows that the mean contour height variations between winter and summer at the 500-mb surface are close to 1000 ft.

2. Surface

The sea-surface pressure distributions are given in Figures III-H-2 through III-H-5. During the cold season (November and February mean charts), the low pressure center is located over the Tyrrhenian Sea, signaling a high frequency of occurrence of Genoa cyclones. A high pressure region is centered over the interior of Russia, caused by the cold continental air masses in this region. The low over the Tyrrhenian Sea bisects the high-pressure bridge between the East Atlantic (Azores) high and Russia.

During summer (August) a ridge extends from the Azores into Central Europe. A low pressure region is located over Syria. The relatively strong pressure gradient over the Aegean Sea produces the prevalent etesian winds from the north.

The transition season (May) indicates a rather diffuse pattern with low pressure prevailing over the Balkan Peninsula.

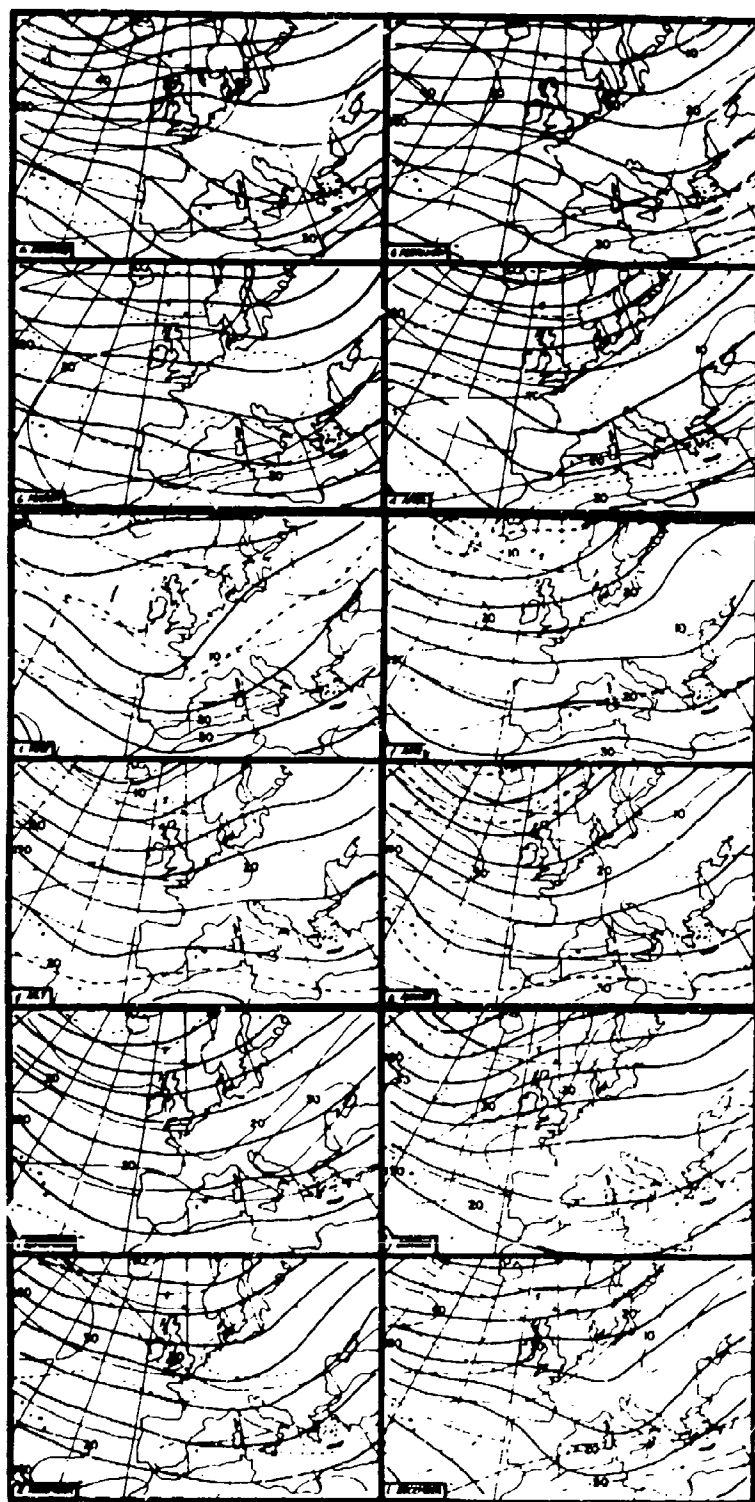


Figure III-H-1. Mean 500-mb circulation over Europe by month. Heavier lines are contours at 200-ft intervals; 180 is 18,000 ft. Isotachs are lighter lines at 10-kt intervals. Intermediate isotachs are dashed (from Black, 1969).

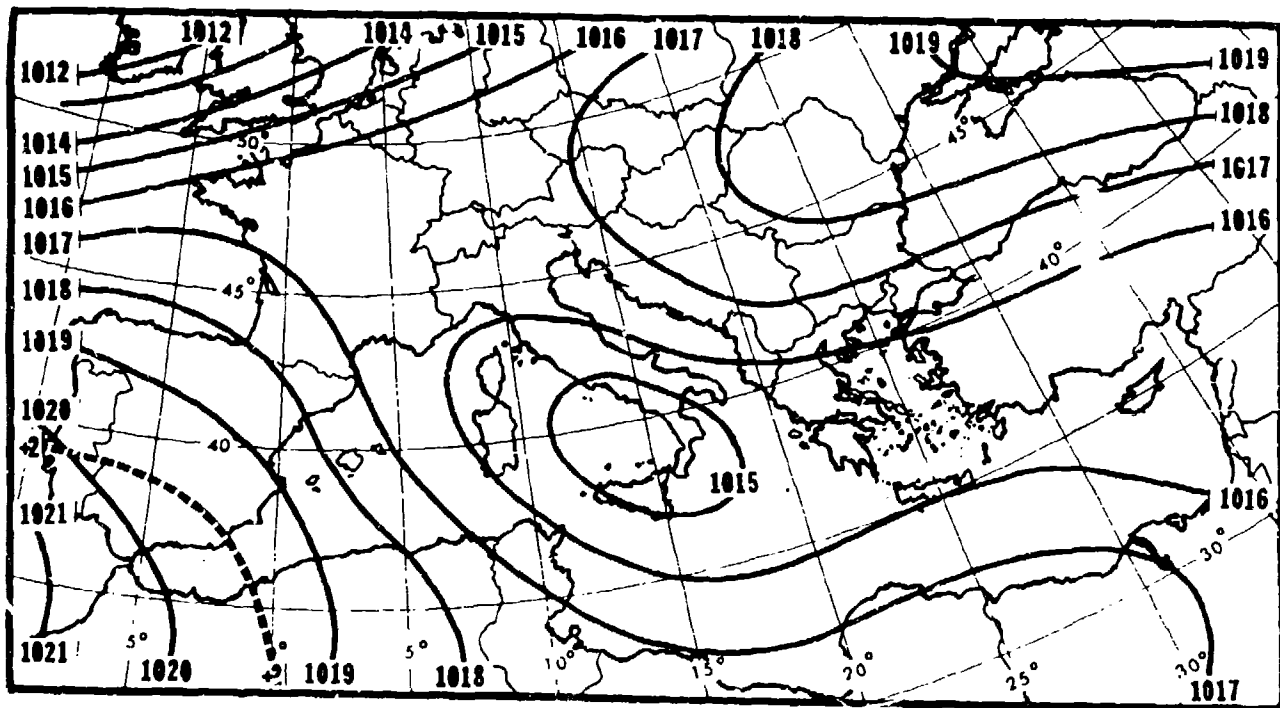


Figure III-H-2. Mean sea-level pressure (mb, solid lines) and three-monthly mean pressure changes (mb, dashed lines) for February (from Frank and Elliott, 1953).

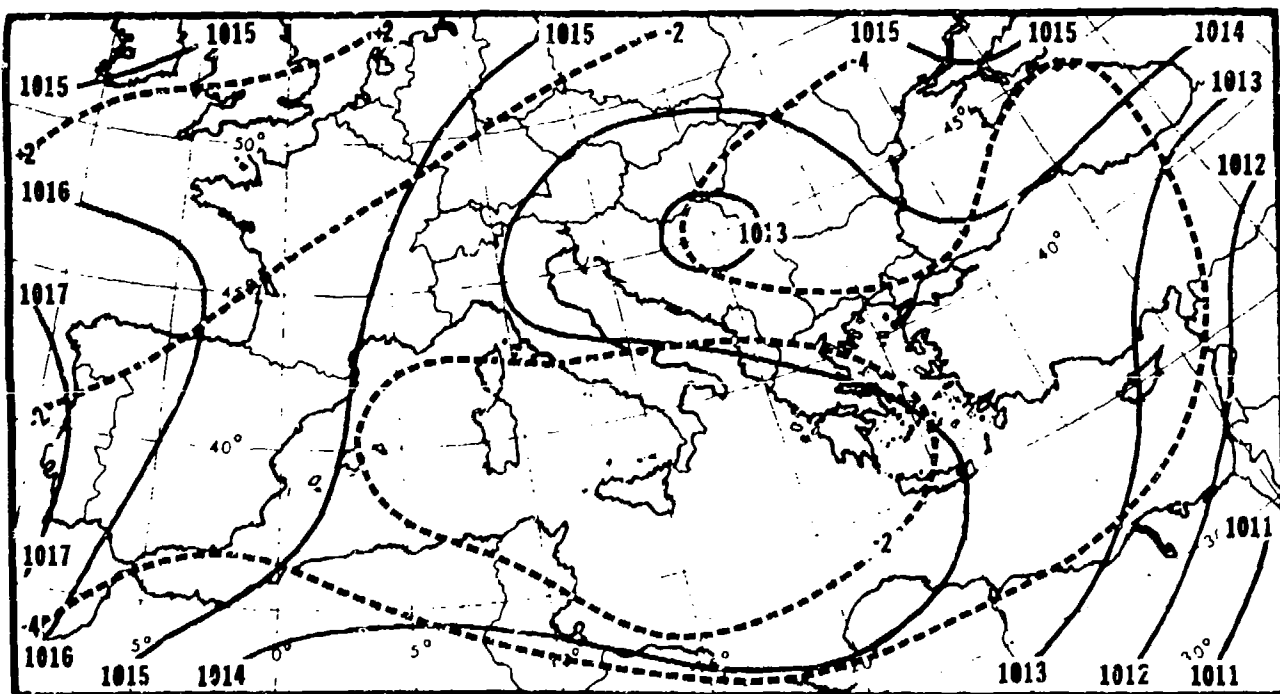


Figure III-H-3. Mean sea-level pressure (mb, solid lines) and three-monthly mean pressure changes (mb, dashed lines) for May (from Frank and Elliott, 1953).

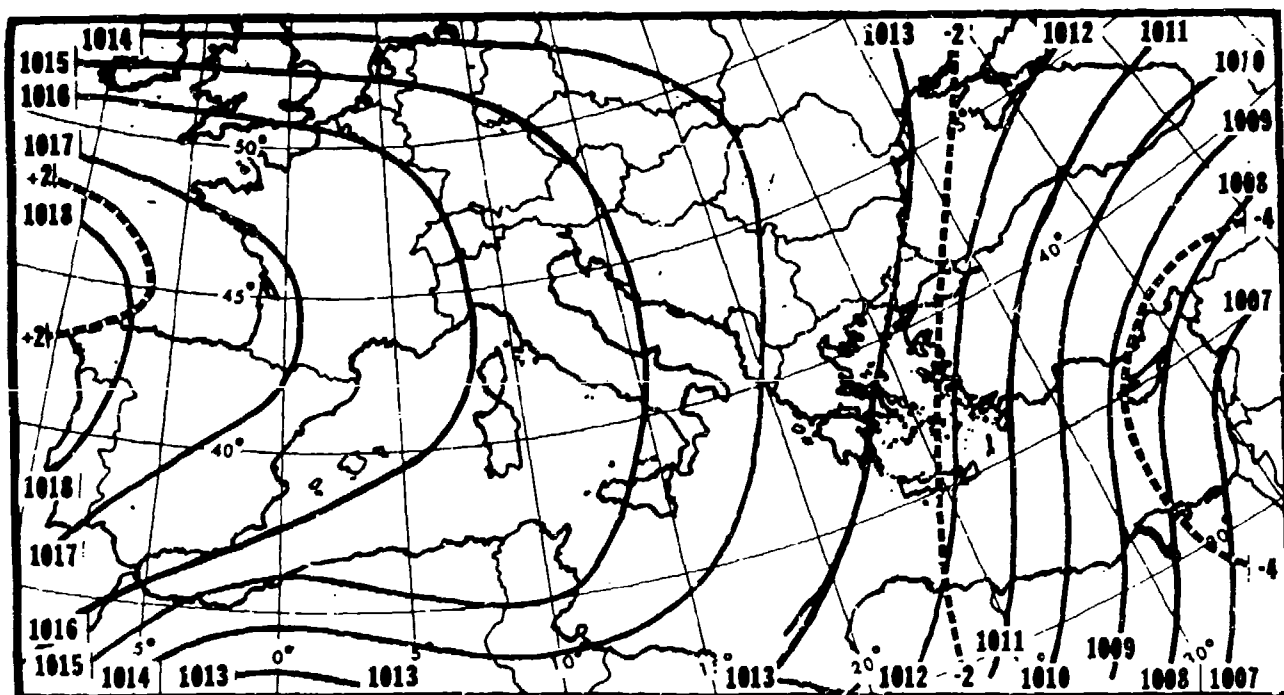


Figure III-H-4. Mean sea-level pressure (mb, solid lines) and three-monthly mean pressure changes (mb, dashed lines) for August (from Frank and Elliott, 1953).

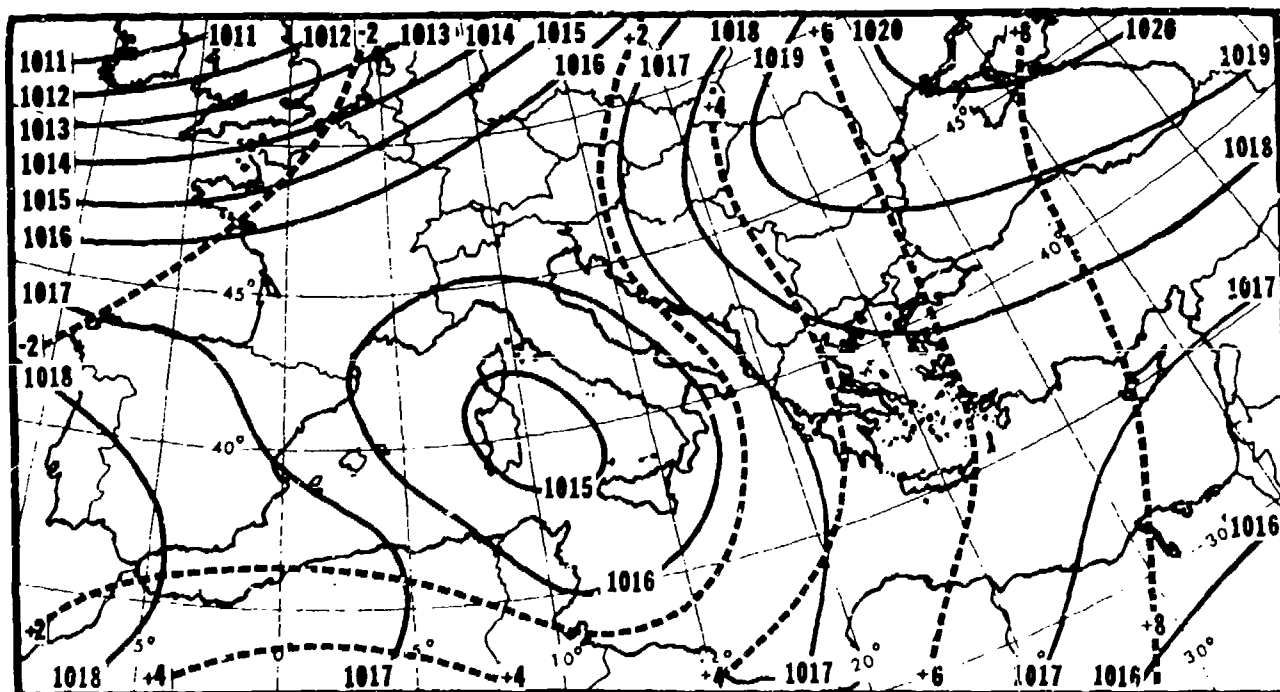


Figure III-H-5. Mean sea-level pressure (mb, solid lines) and three-monthly mean pressure changes (mb, dashed lines) for November (from Frank and Elliott, 1953).

I. PRECIPITATION

The annual pattern of precipitation in the Mediterranean generally follows the seasonal behavior of cyclonic disturbances. In both the western and the eastern basins, cyclonic activity peaks during the winter months (see Figures III-B-18 and III-B-22). Consequently the rainy season also occurs during winter with the passage of frontal disturbances. The thermal instability for January (shown, for instance, in Figure III-G-7) produced by cold air sweeping from the continents over warm ocean water, favors the development of convective cloud systems and shower and thunderstorm activity.

Figure III-I-1 shows mean monthly precipitation values for Malta, indicating the rainy season of winter (Sutcliffe, 1960b). The correlation between thermal instability (positive differences between T_{sea} and T_{air}) and precipitation amounts suggests the prevalence of shower-type rain systems. This conclusion is confirmed by Figure III-I-2 which shows frequency distributions of thunderstorm activity over Milan, Rome, and Malta (Air Ministry, 1962). Milan reveals typical continental conditions with a frequency maximum of thunderstorms during summer when insolation produces superadiabatic lapse rates near the overheated ground. Malta, on the other hand, derives its winter maximum of thunderstorms from instabilities associated with cold-air cutbreaks. Rome shows weak continental characteristics, not nearly as marked as at Milan.

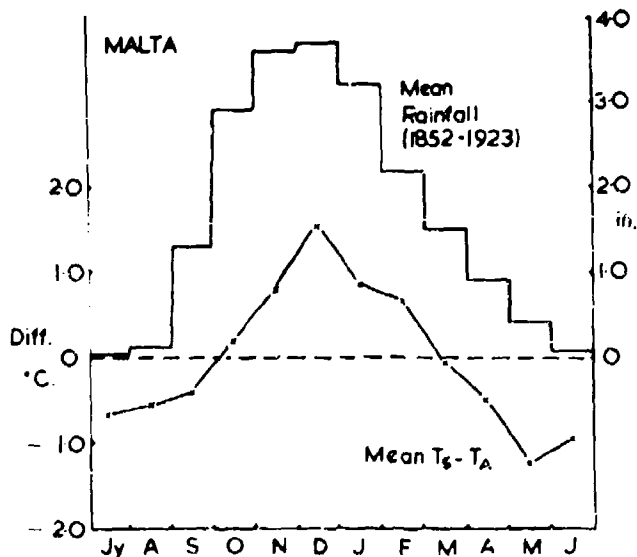
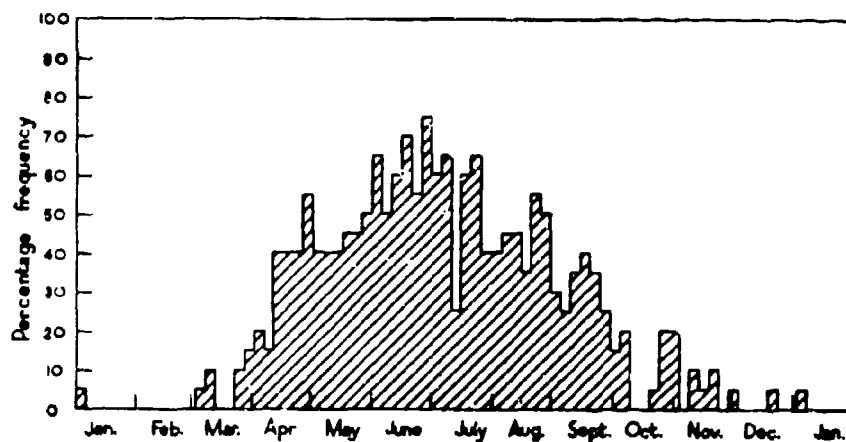
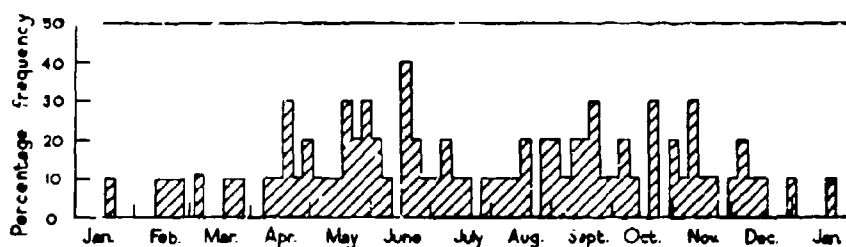


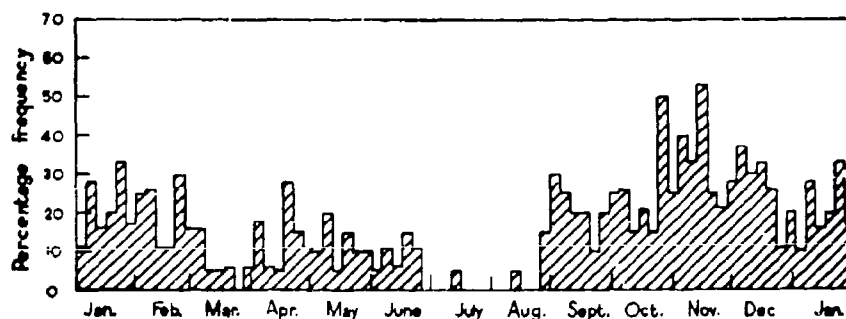
Figure III-I-1. Annual variation of the rainfall in Malta and the difference between sea-surface temperature and air temperature at Malta (from Sutcliffe, 1960b)



a



b



c

Figure III-I-2. Percentage frequency of years in which at least one thunderstorm occurred in the five-day period represented by the columns of the histogram. (a) Milan, 1919-1938, (b) Rome 1929-1938, (c) Malta 1919-1938 (from Air Ministry, 1962).

Another example of continental thunderstorm activity is available from Torrejon Air Base, Spain (Clark, 1971). Table III-I-1 gives the frequency of thunderstorm days by months during the period 1957-1964. June shows the highest frequency of occurrence, and a secondary maximum of nearly the same frequency is found in September.

Table III-I-2 (Clark, 1971) shows the percentage frequency distribution at Torrejon as a function of season and the time of day. At this location thunderstorms occur preferentially between 1500 local time and midnight local time.

Even under sirocco conditions, thunderstorms occur when the air stream is subjected to orographic lifting along the northern coastlines of the Mediterranean and along the Alps. The warm desert air, having traveled across the Mediterranean waters, has picked up enough moisture to become convectively unstable. This instability is released as soon as the low-tropospheric stable stratification is overcome in orographically forced ascending motions (NOAA, Mediterranean Planning Guide).

In the Eastern Mediterranean, Beirut shows a winter maximum for thunderstorms, while Ankara and Zonguldak (Black Sea coast of Turkey) reveal a continental regime with summer thunderstorm activity (Figure III-I-3). The distribution of thunderstorm activity in the Eastern Mediterranean for the various seasons is shown in Figure III-I-4; the annual frequency is shown in Figure III-I-5. Spring and fall favor thunderstorm activity slightly inland from the coast.

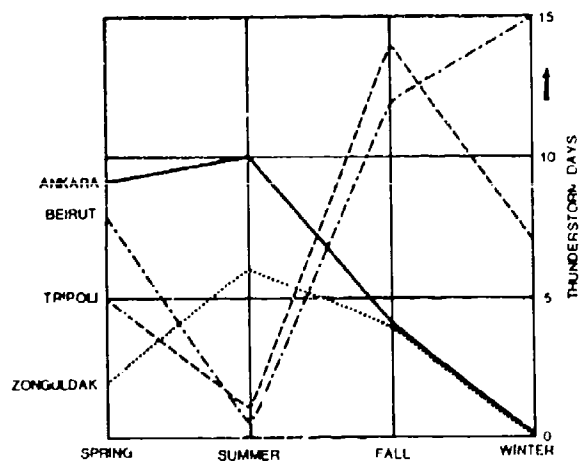


Figure III-I-3. Frequency distribution of thunderstorm days in the Eastern Mediterranean (from Ag. 1968).

Table III-I-1. Frequency of thunderstorm days by month
at Torrejon Air Base, Spain (Clark, 1971).

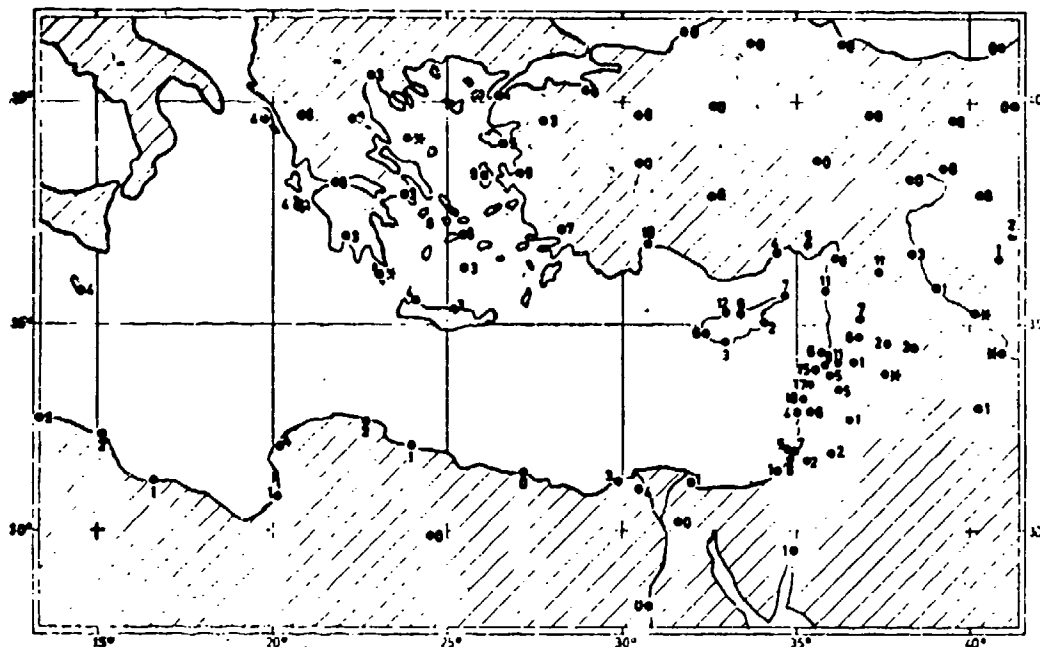
Month	% Days w/TSTM	No. Obs.	Total TSTM Days	Mean Days Per Year
Jan	0.5	217	1	*
Feb	0.5	198	1	*
Mar	1.8	217	4	1
Apr	5.7	210	12	1
May	12.9	217	28	3.5
Jun	21.9	210	46	5.8
Jul	13.4	217	29	3.6
Aug	9.2	217	20	2.5
Sep	21.1	180	38	5.6
Oct	4.4	217	9	1.1
Nov	0.5	210	1	1
Dec	0.5	217	1	1

* < 0.5

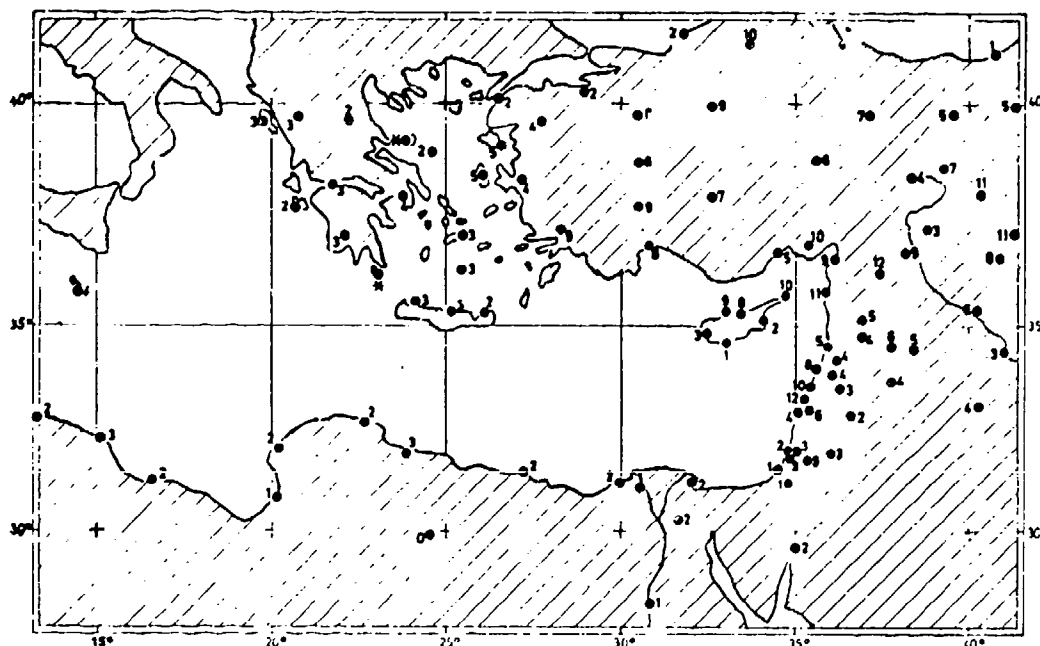
Table III-I-2. Percent frequency of thunderstorm occurrence at Torrejon
Air Base, Spain, during the day (from hourly observations 1958-1969)
(Clark, 1971).

LST	J	F	M	A	M	J	J	A	S	O	N	D	Mean
00-02					0.2	1.0	0.9	0.5	1.6				0.4
03-05					0.2	0.3	1.1	0.5	1.1				0.3
06-08							0.3	0.8	1.1				0.2
09-11					0.2	0.3	0.5	0.5	0.8	0.4			0.2
12-14				0.4	1.4	1.1	0.5	0.2	0.8	0.4			0.4
15-17				0.8	1.5	2.7	0.9	1.1	2.2	0.3			0.8
18-20			0.1	0.6	2.2	3.0	2.3	0.8	1.6	0.4			0.9
21-23					0.8	2.2	3.2	1.2	2.4			0.1	0.8
Mean			*	0.2	0.8	1.3	1.2	0.7	1.4	0.2		*	0.5

* < 0.1



a



b

Figure 11I-I-4. Mean number of days with thunderstorms for (a) winter (b) spring, (c) summer, and (d) fall (asterisk - less than 1/2 day) (from Agi, 1968).

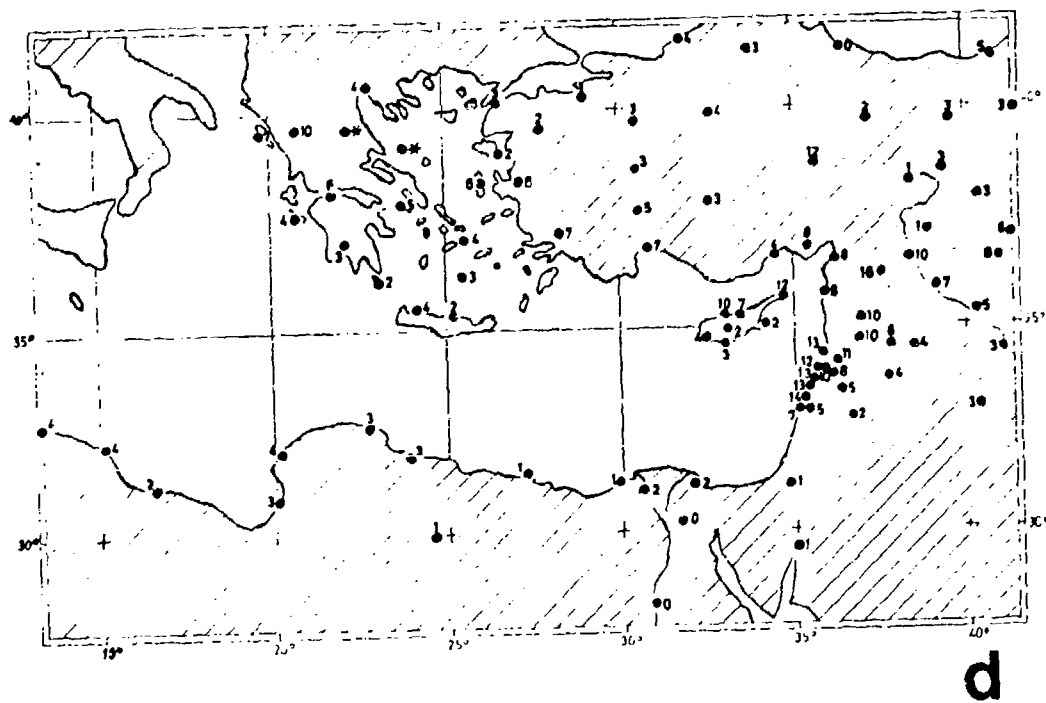
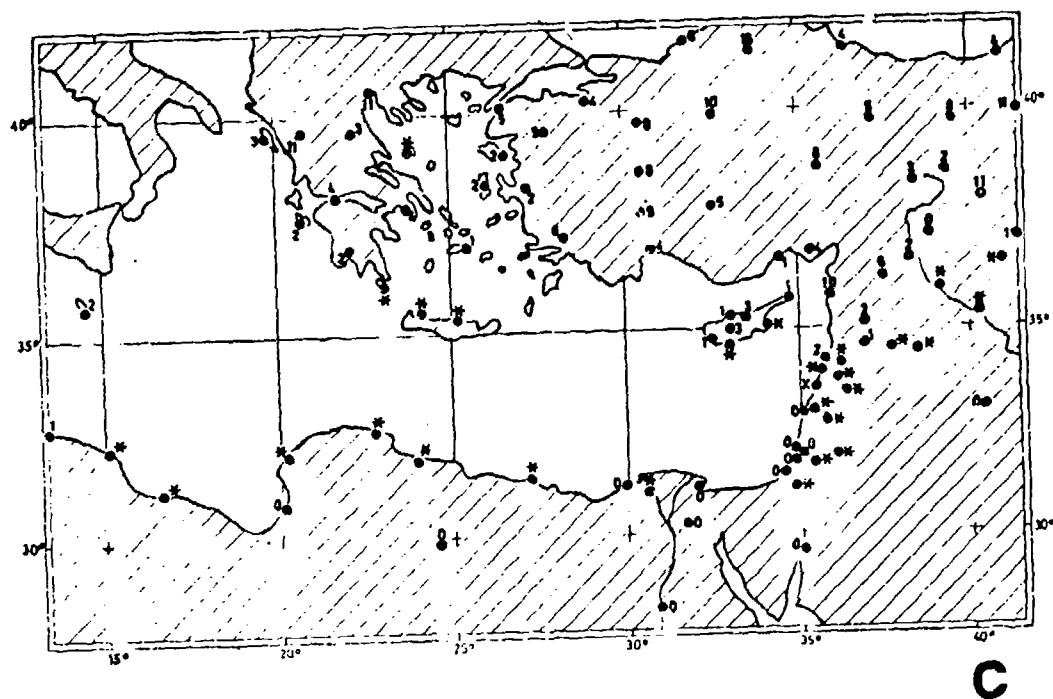


Figure III-I-4 (continued)

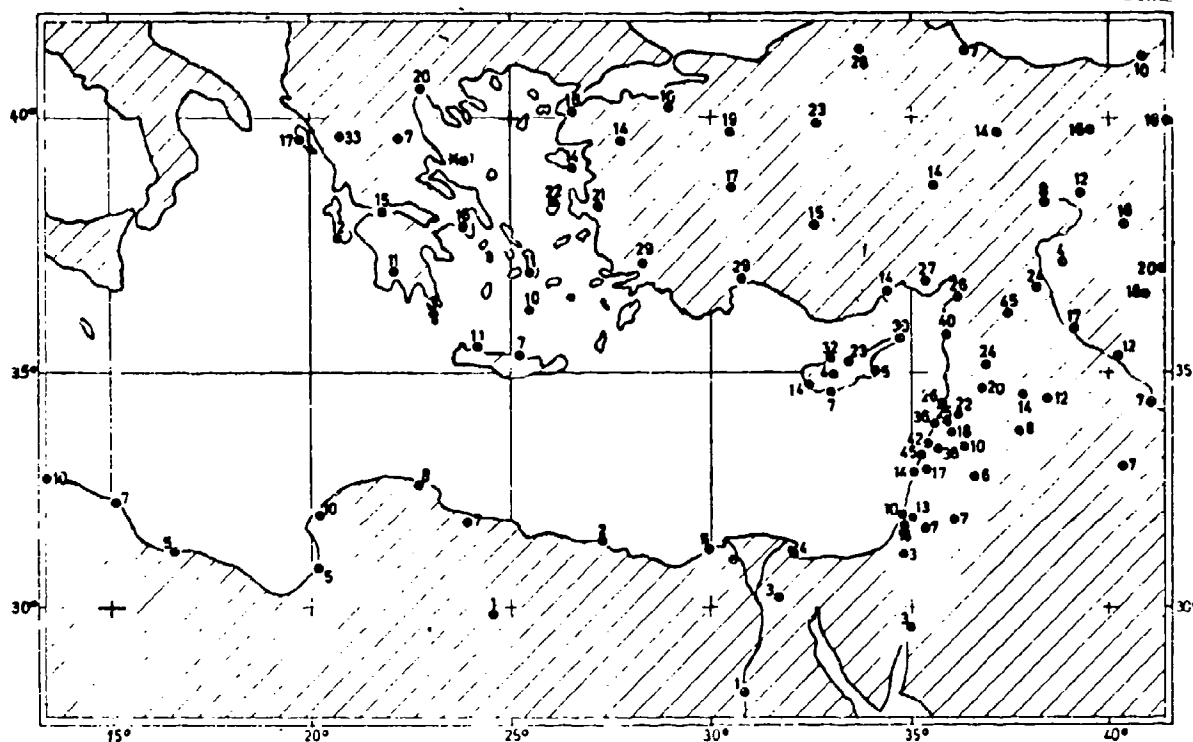


Figure III-I-5. Mean annual number of days with thunderstorms (asterisk - less than 1/2 day) (from Agi, 1968).

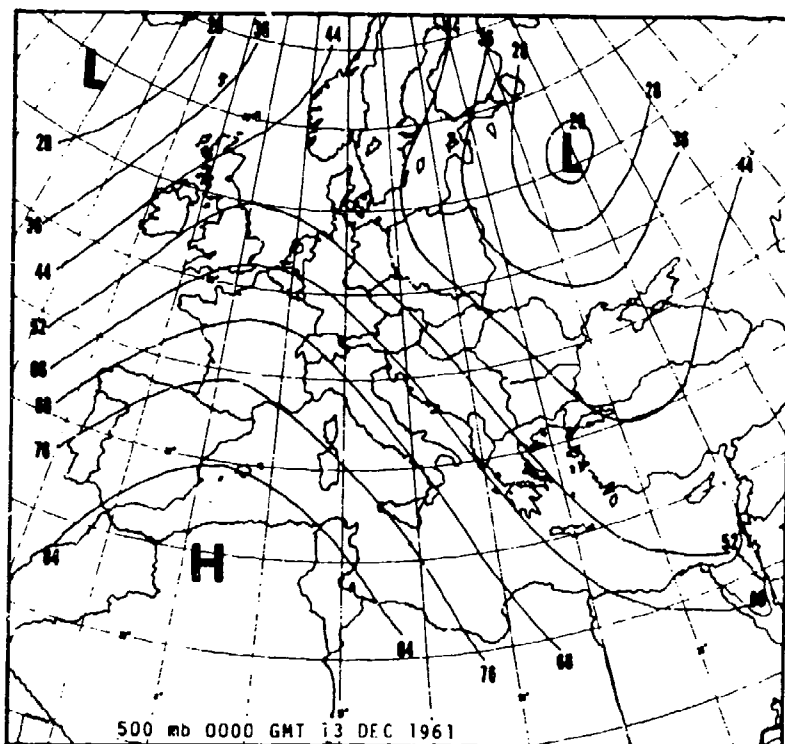
In general, thunderstorm activity in the Mediterranean is weak, with the exception of the head of the Adriatic Sea, the coastal mountain ranges of Yugoslavia, the western and northern mountains of Bulgaria, and the northeastern coast of the Black Sea. The African coast from Libya to Egypt shows a minimum of thunderstorm activity. Appendix F lists stations for which frequencies of thunderstorm activity are available from World-Wide Airfield Summaries.

The dry regime of summer is evident from tabulations of days with precipitation (see list of stations in Appendix F for which precipitation climatology is available). The heartlands of the Balkan Peninsula offer an exception with June appearing as the wettest month of the year.

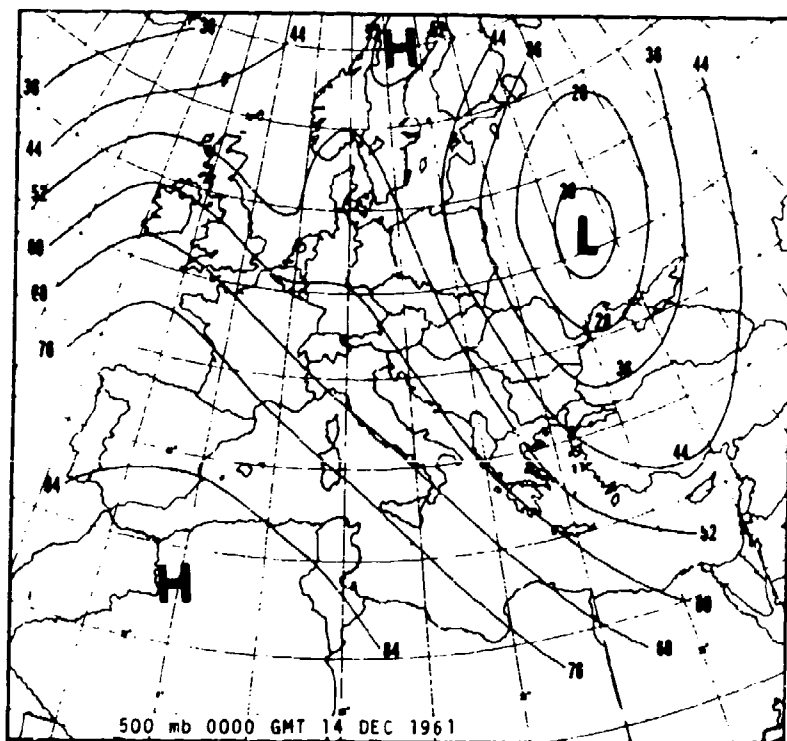
The heaviest precipitation in the Mediterranean region can be expected in the mountain ranges of Yugoslavia, whereas the southeastern coastline of the Mediterranean basin is extremely dry.

Even though most of the wintertime precipitation in the Mediterranean falls in the form of rain, there are occasions of snowfall even at coastal stations; the frequency increases with elevation and with distance from the sea. Snowfalls over Italy are typically associated with cold outbreaks from northeastern Europe, such as may develop with a blocking high formation extending from Spain into Scandinavia. An example is presented in Figure III-I-6.

Hail may occur in the northern Mediterranean anytime during the year, but is more frequent during the season of heaviest precipitation. It is mainly associated with cold fronts and with instability showers and thunderstorms in cold air masses (NOAA, Mediterranean Planning Guide).

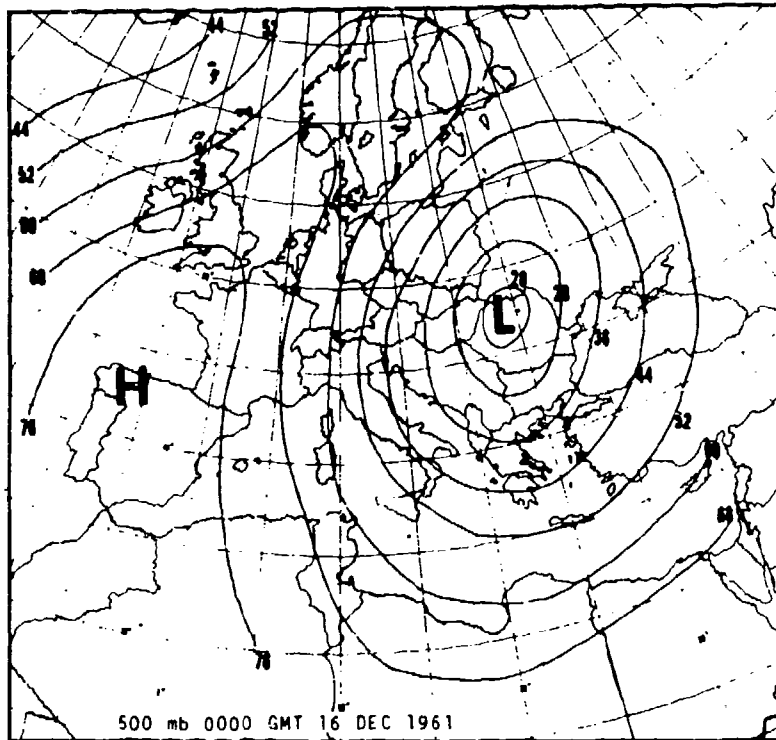


a

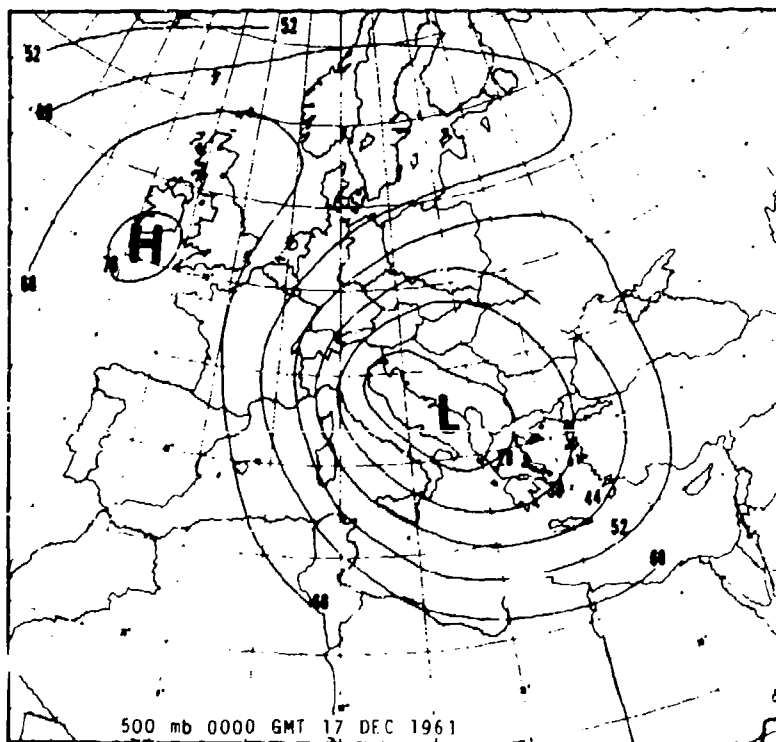


b

Figure III-I-6. 500-mb patterns (geopotential decameters) between 13 and 17 December 1961 (a-d, and surface pressure patterns (mb) on 17 and 18 December 1961 (e,f) over Europe typical for snowfall situation in Italy (after Meschini, 1968).

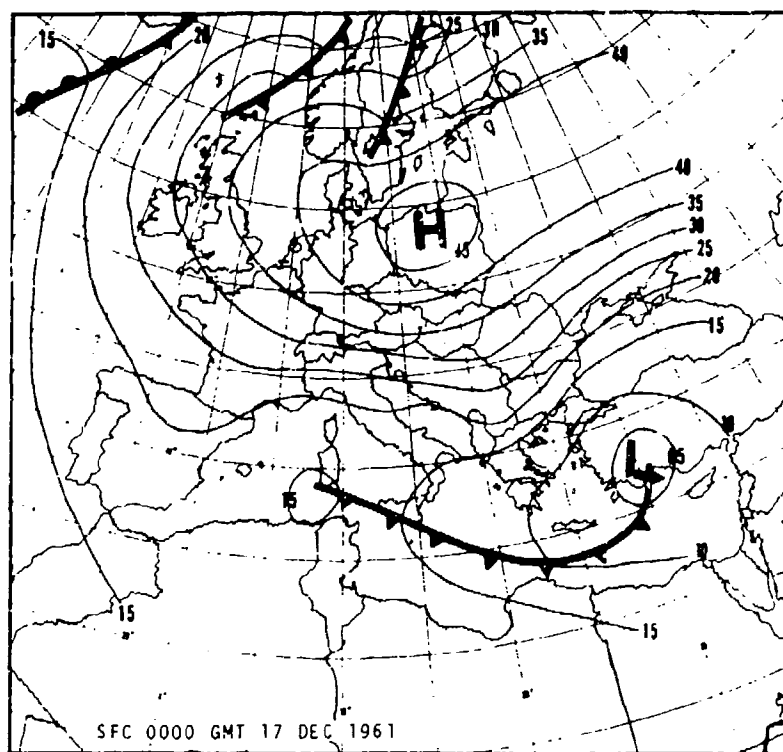


c

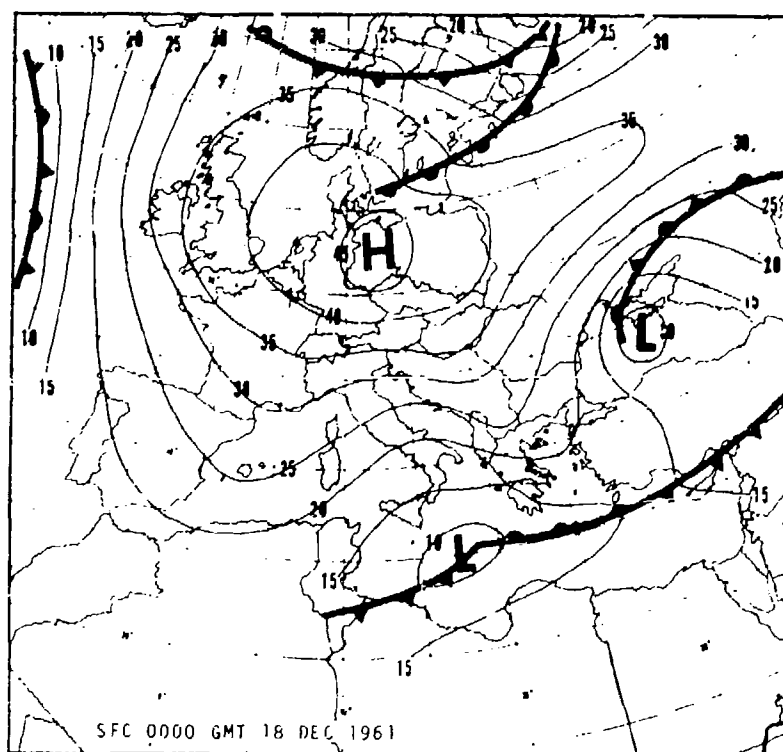


d

Figure III-I-6 (continued)



e



f

Figure III-I-6 (continued)

J. CLOUDINESS

The seasonal trend of cloudiness corresponds closely to that of precipitation (Figures III-J-1 and III-J-2) with a maximum in winter and a minimum in summer. As a whole, however, the Mediterranean area shows relatively little cloudiness even during the cool season when compared to the rest of Europe and to the Atlantic region.

A diurnal variation of cloudiness can be expected in a belt extending 10-15 miles offshore. Low stratus that tends to develop here during winter normally dissipates after sunrise. A second maximum of cloudiness in the afternoon is due to convective activity. The clearest time of the day usually is evening. Under light wind and subsidence conditions, the late morning hours -- after the fog or mist has cleared and before the onset of cumulus development -- also show a minimum of cloudiness (NOAA, Mediterranean Planning Guide).

A significant percentage of cloud cover over North Africa is in the form of high and middle clouds associated with the subtropical jet stream of winter and spring. These clouds frequently occur in elongated bands on the anti-cyclonic side of the jet axis. They are visible from satellite photographs and sometimes extend in a southwesterly current all the way from the equatorial Atlantic into the Sahara (Figure III-B-5). The movement of characteristic features in these cloud bands (traced, for instance, from ATS photographs) conforms well to wind velocities in the middle and upper troposphere (Figure III-B-4, see also Reiter (1972a)).

The distribution of clouds with bases below 1000 feet is similar to the distribution of fog. In winter, such clouds are frequently associated with old stagnant polar air on the north and northwestern shores of the Adriatic, and with a lesser frequency along the north shore of the Mediterranean. In summer they are often found at night and in the early morning associated with the levante in the Strait of Gibraltar and in the Alboran Channel. Low clouds in summer also occur inland from the shores of North Africa, especially over the Nile delta (Air Ministry, 1962).

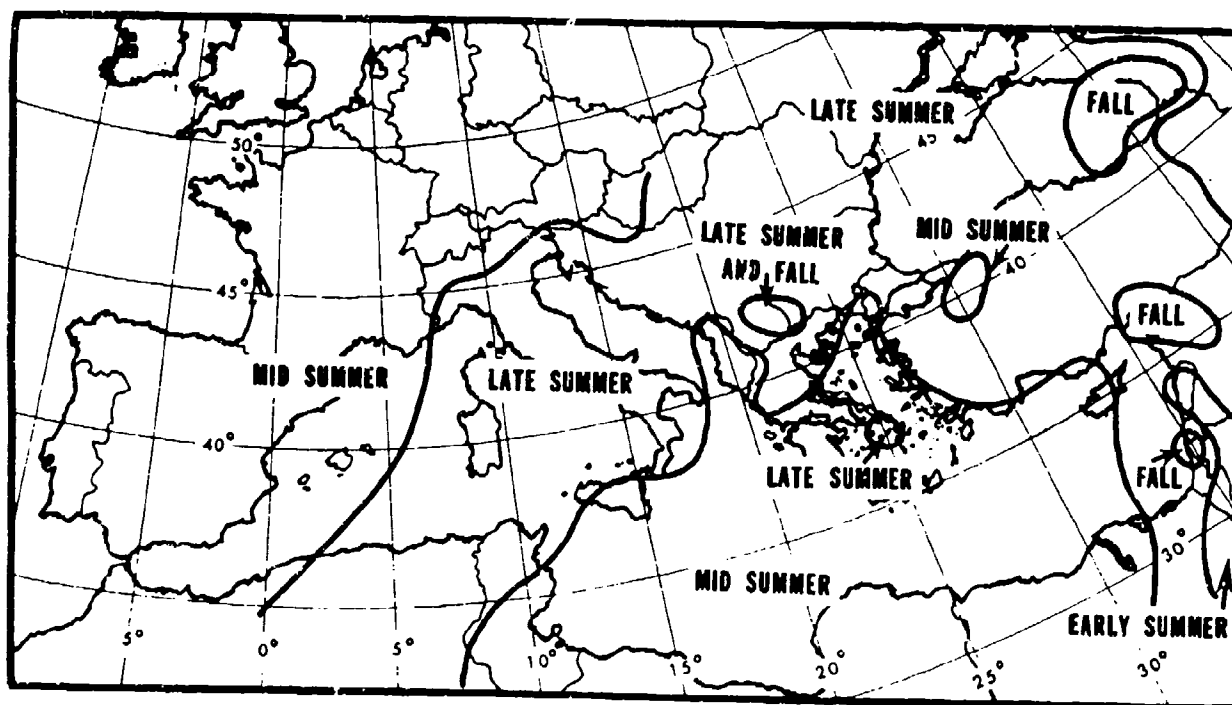


Figure III-J-1. Seasons, denoted by solid lines, of minimum mean cloudiness in the Mediterranean region (from Frank and Elliott, 1953).

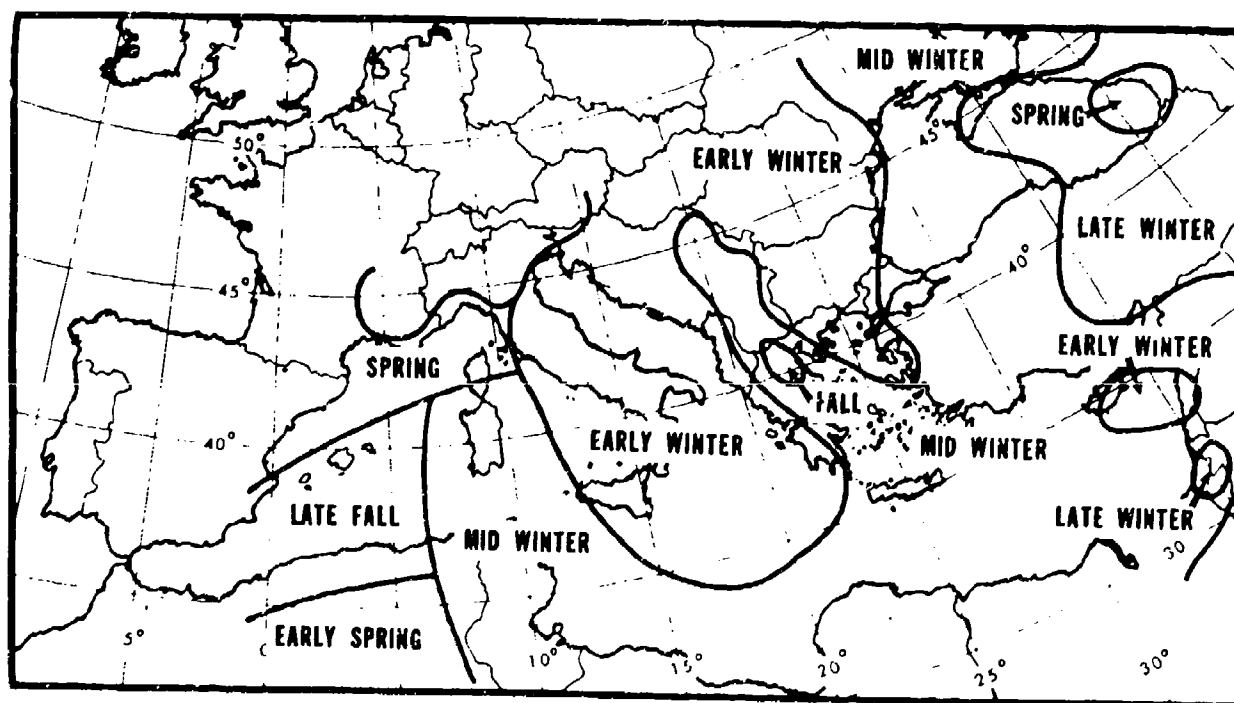


Figure III-J-2. Seasons, denoted by solid lines, of maximum mean cloudiness in the Mediterranean region (from Frank and Elliott, 1953).

K. FOG, HAZE AND VISIBILITY

Visibility, in general, is good in the Mediterranean region because the warm waters inhibit the frequent formation of dense sea fogs. Visibility of less than one-half mile is therefore encountered infrequently.

During winter, the major cause for visibility restriction is precipitation. Maximum frequencies of visibilities less than five miles are found in the Strait of Gibraltar, between Sardinia and the coast of Spain, in the Gulf of Lion, and in the Gulf of Genoa. Visibilities of less than one-half mile occur more than one percent of the time in February only off the southeast coast of Spain and in the southeast corner of the Eastern Mediterranean. In the warm waters south of the northern gulfs, sea fogs are a rare phenomenon.

Along the coast, radiation fog sometimes develops in the early morning when winds are light. It usually dissipates after sunrise. In lower Egypt, for instance, low stratus occurs on about 10 to 15 days in each of the months of July and August, when moist air originating from Mesopotamia or Asia Minor is subjected to radiational cooling. Cyprus and the coasts of Israel show similar effects during spring and summer (see, e.g., Table III-K-1 for Tel Aviv); inland stations show a preponderance of wintertime fog conditions due to radiational cooling. Fog duration, according to Table III-K-2, is usually short in this region, and outbreaks of polar air clear off these fog and low stratus conditions. Where coastal hills and mountains are present, such as near Benghazi, katabatic downslope winds develop at night and prevent the formation of fog and low stratus (Air Ministry, 1962).

The major occurrences of fog and poor visibility in the Mediterranean are generally associated with sirocco conditions. When the sirocco has been associated with sand storms in the North African desert regions, a dense haze severely limits visibility. The dust is raised in the desert mainly during the hot hours of the day and during cold-front passages, is then carried northward, and is often thickest in the Malta area in the later afternoon and evening. Sahara dust has even been observed on many occasions in Central Europe under southerly upper-flow conditions, where it has caused intensive haze.

The dust may be carried to a height of 15,000 to 20,000 feet. Even though the heavier particles settle out quickly, and rain also removes the smaller particles quite effectively, in the absence of such removal mechanisms haze may persist over large areas for several days. A haze layer up to 12,000 feet thick seems to be quite common in the Mediterranean during summer. It adversely affects slant visibility, especially when the observer is flying above the layer and looking downward against the reflecting sun.

Table III-K-1. Average number of foggy nights (1951-1960) for several stations in Israel. Station locations shown in Appendix F (Levi, 1967).

Regions and Stations							
Hills		Hula Valley	Northern Negev	Emeq Yizreel	Coastal Plain		Month
Jerusalem	Har Kenaan	Kefar Blum (1956-1965)	Be'er Sheva (1958-1965)	Ramat David	Lod Airport	Tel Aviv Airport	
3.1	9.7	4.8	1.9	5.7	0.7	0.5	January
4.2	6.9	1.5	2.4	6.7	1.2	1.7	February
2.1	5.9	1.2	2.1	7.1	1.1	1.4	March
2.0	3.7	0.7	1.6	7.9	2.5	2.2	April
0.8	1.6	0.1	3.4	5.4	2.6	3.0	May
1.0	0.6	-	4.8	4.6	2.3	2.3	June
1.8	0.8	-	5.9	3.8	1.4	1.3	July
2.4	0.7	-	7.6	2.5	0.9	0.9	August
2.0	0.8	-	3.0	1.2	0.2	0.4	September
0.5	1.2	0.6	4.8	2.2	1.5	1.4	October
2.3	3.8	0.8	3.6	3.1	0.5	0.2	November
3.8	8.3	3.2	1.2	3.7	0.5	0.4	December

Table III-K-2. Average fog duration (hours, visibility > 1000 m) for several stations in Israel. Station locations shown in Appendix F (Levi, 1967).

Station and Period	Month												Year	Extreme (date)
	J	F	M	A	M	J	J	A	S	O	N	D		
Be'er Sheva 1958-1965	2.00	2.75	2.00	1.50	2.50	2.00	2.75	1.75	2.25	3.00	3.25	2.50	2.25	13.00 (14 Jan 1958)
Ramat David 1957-1965	4.00	2.25	2.25	3.00	3.00	2.50	2.50	2.25	-	2.50	1.75	3.00	2.50	12.00 (18 Jan 1961)
Lod Airport 1956-1965	2.00	3.50	3.25	2.00	3.00	2.50	2.25	1.50	0.25	2.50	2.00	1.00	2.00	10.25 (21 Feb 1957)

Visibility under sandstorm conditions may drop below 50 yards. Visibilities of less than 1000 yards may be quite widespread along the African coastline near an approaching cold front. Even at Malta the visibility under such conditions may drop below two miles.

Rainfall amounts during sirocco situations usually are small but very muddy (Reiter, 1971). As the warm sirocco air picks up moisture from the sea surface and subsequently moves over colder water, fog may form. Thick sirocco fogs have been observed in the northern Adriatic north of Pelagosa, along the west coast of Italy, in the Gulf of Genoa and in the Gulf of Lion, and especially near Sardinia where a sirocco from the southeast has a long fetch across open water. The sirocco frequently brings overcast skies, drizzle and visibility poor enough to obscure the coast. Fog at Venice has been known to continue for as long as five days (Air Ministry, 1962). Figure III-K-1 shows fog occurrence along the Yugoslavian coast on an average annual basis. Tables III-K-3 and III-K-4 provide a detailed seasonal breakdown.

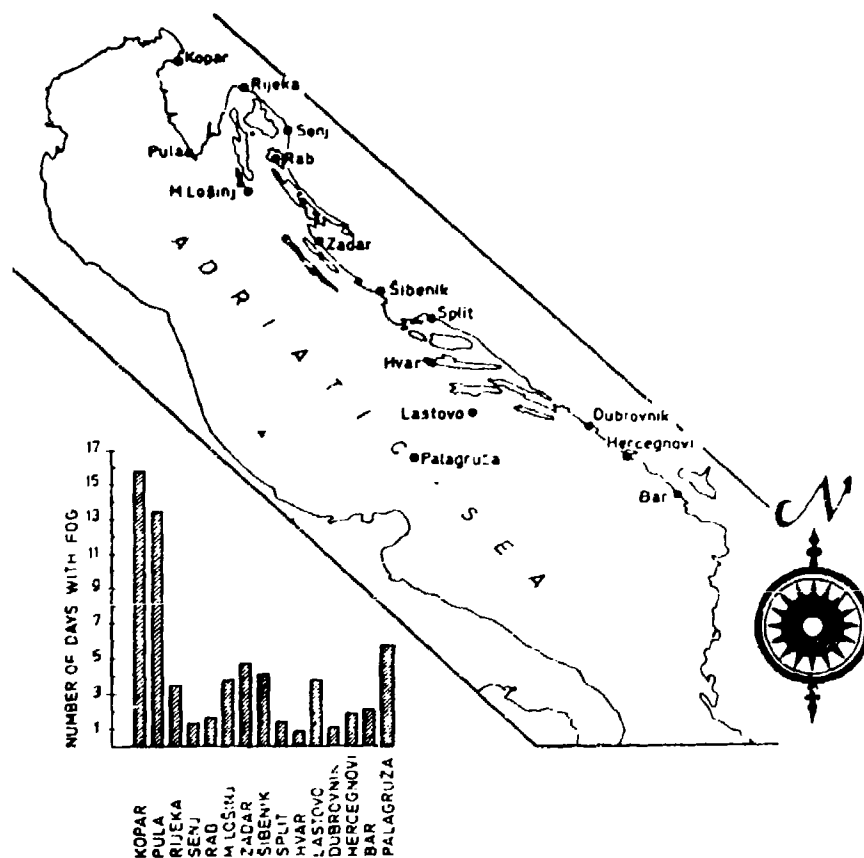


Figure III-K-1. Average number of days with fog for Yugoslavian coastal stations whose locations are indicated on map (from Stipaničić, 1961).

Table III-K-3. Monthly and annual average number of days with fog (1949-1958) for Yugoslavian coastal stations shown in Table F-2 and Figure F-6 of Appendix F (Stipaničić, 1961).

Place	J	F	M	A	M	J	J	A	S	O	N	D	YR
Kopar	3.3	4.4	1.8	0.3	-	-	-	-	0.1	0.9	1.3	3.6	15.7
Pula	1.7	3.5	1.8	0.9	0.2	0.1	-	-	0.4	1.0	1.1	2.7	13.4
Rijeka	0.6	0.9	0.8	0.2	0.1	-	-	-	-	0.1	0.2	0.5	3.4
Senj	0.1	0.4	0.5	-	-	-	-	-	-	-	-	0.3	1.3
Rab	-	0.6	0.5	0.1	-	-	-	-	-	0.3	-	0.2	1.7
M. Lošinj	-	1.0	1.2	0.6	0.2	0.1	-	0.1	0.1	-	0.5	-	3.8
Zadar	0.3	0.9	0.8	-	0.1	-	-	0.1	1.0	0.5	0.4	0.6	4.7
Šibenik	0.3	0.9	0.7	-	0.1	-	-	-	0.1	0.4	0.5	1.1	4.1
Split	-	0.2	0.4	0.2	-	-	-	0.1	0.2	0.2	-	-	1.3
Hvar	-	0.2	0.2	0.2	0.1	-	-	-	0.1	-	-	-	0.8
Lastovo	-	0.1	0.5	0.7	0.3	-	-	0.5	0.3	0.1	-	0.2	3.7
Dubrovnik	-	-	0.4	0.2	0.3	-	-	-	-	0.1	-	-	1.0
Hercegnovi	-	-	0.7	-	0.6	-	-	-	0.1	0.1	0.3	0.1	1.9
Bar	-	-	0.4	0.2	0.6	-	0.1	0.3	0.5	-	-	-	2.1
Palagruža	0.3	0.5	0.8	0.9	1.1	0.3	0.2	-	0.8	0.3	0.3	0.2	5.7

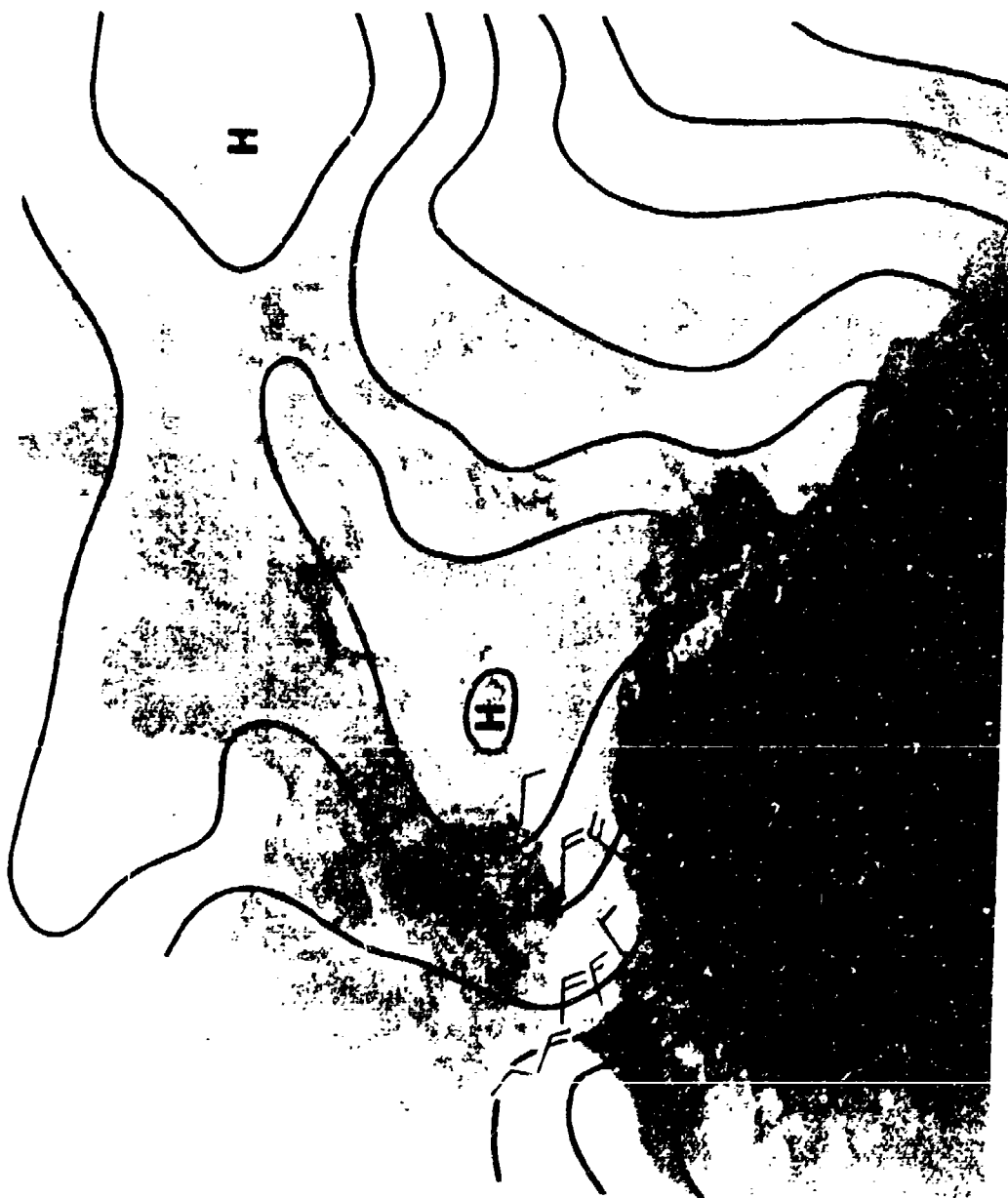
Table III-K-4. Monthly and annual duration, D, of fog in hours for Yugoslavian coastal stations (maximum values are underlined). These data were computed using the formula $D=pN$, where p = the absolute probability of fog and N = the number of monthly or yearly hours. Station locations can be found in Table F-2 and Figure F-6 of Appendix F (Stipaničić, 1961).

Place	J	F	M	A	M	J	J	A	S	O	N	D	YR
Kopar	26.0	<u>57.3</u>	14.1	1.4	-	-	-	-	0.7	6.0	13.0	45.4	166.5
Pula	14.9	<u>34.9</u>	19.3	8.6	0.7	0.7	-	-	4.3	6.7	11.5	23.1	122.7
Rijeka	8.9	<u>11.4</u>	8.9	1.4	0.7	-	-	-	-	0.7	1.4	3.7	35.0
Zadar	2.9	<u>12.0</u>	9.7	-	0.7	-	-	0.7	7.9	3.5	2.9	6.7	43.8
Split	-	4.0	0.7	1.4	-	-	-	0.7	1.4	1.5	-	-	8.8
Lastovo	-	0.6	<u>11.1</u>	7.9	2.2	-	-	5.9	2.2	0.7	-	1.5	35.0
Bar	-	-	<u>3.7</u>	0.7	1.5	-	-	-	2.2	-	-	-	8.8
Palagruža	2.2	2.7	6.7	<u>7.2</u>	5.9	2.2	1.5	-	6.5	2.9	4.3	1.5	35.0

Poor visibility, together with strong winds, low clouds and precipitation, occurs in the Ionian Sea with gregale, and in the Western Mediterranean and the Strait of Gibraltar with vendaval (Air Ministry, 1962).

The warm levanter (local name for "levante" in the Gibraltar area -- see Table I-C-2) winds of late spring and summer also cause fog, low stratus and poor visibility in the Alboran Channel and in the Strait of Gibraltar, as the moist air carried by this wind system moves over cooler waters (see Figure III-K-2 and Table III-K-5). The levanter easterlies also move warm surface water into the Strait of Gibraltar, causing the eastern edge of the fog area to recede slowly westward. A fresh polar outbreak with west winds in its wake signals the end of the levanter and the fog condition, but the upwelling of cold water east of the straits sets the stage for new fog occurrence with the next levanter situation. Levanter fog has a tendency to break up or become patchy during the daytime.

A study of fog formation in the area of Thessaloniki (Greece) (Angouridakis, 1973) shows that warm and humid air masses from the Aegean Sea, sometimes in connection with an approaching warm front, may give rise to fog formation. Table III-K-6 indicates that the cool season is most likely to produce such fog conditions. The weather type shown in Figure III-K-3 has a probability of 33% of producing fog, and the weather type shown in Figure III-K-4 has a probability of 39% of producing fog if they occur during the months of December, January, or February. During the rest of the year probabilities for fog formation are lower. All other weather patterns also show reduced fog formation probabilities.



a

Figure III-K-2. Low clouds and fog associated with levanter winds in the Alboran Channel and Strait of Gibraltar, 1200 GMT, 13 May 1973. Solid lines are isobars from FIB/SLP-MED analysis plotted on: (a) DMSR high-resolution visual for 1121 GMT and (b) DMSR IR for 1121 GMT.



b

Figure III-K-2 (continued)

Table III-K-5. Average number of days with fog (May-November)
in the Strait of Gibraltar (Air Ministry, 1962).

May	June	July	Aug	Sept	Oct	Nov
2	5	11	8	4	3	3

Table III-K-6 (a). Number of cases with fog at 0600 and 1200 GMT during the
period 1952-1969 in the area of Thessaloniki, Greece (Angouridakis, 1973).

GMT	J	F	M	A	M	J	J	A	S	O	N	D	YR
0600	104	81	44	12	-	-	-	-	3	9	43	121	417
1200	38	14	5	-	-	-	-	-	-	-	13	29	99

Table III-K-6 (b). Mean number of cases with fog at 0600 GMT and standard
deviation in the area of Thessaloniki, Greece (Angouridakis, 1973).

Mean; S.D.	J	F	M	A	M	J	J	A	S	O	N	D	YR
Mean	5.8	4.5	2.4	0.7	-	-	-	-	0.2	0.5	2.4	6.7	23.2
S.D.	3.15	3.02	1.89	0.94	-	-	-	-	0.30	0.96	1.54	3.51	8.58

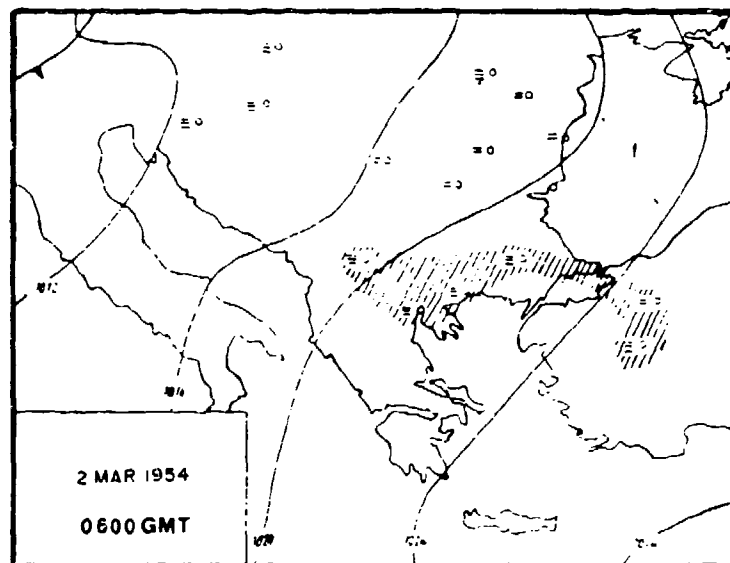


Figure III-K-3. Surface weather pattern of 0600 GMT, 2 March 1954, typical for fog formation in northern Greece (from Angomidakis, 1973).

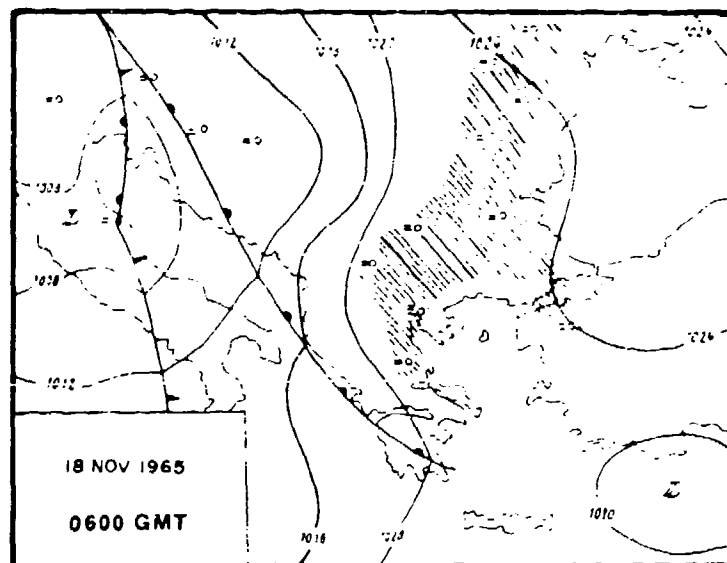


Figure III-K-4. Surface weather pattern of 0600 GMT, 18 November 1965, typical for fog formation in northern Greece (from Angomidakis, 1973).

IV. MESOSCALE WEATHER PHENOMENA

A. CHANNELING AND CORNER EFFECTS

The preceding sections have dealt with the synoptic scale phenomena of lee cyclogenesis and chinook winds. Orographic features, however, also exercise their influence on the atmosphere on smaller scales which cannot be detected from the regular radiosonde network. Channeling and corner effects are among the orographically controlled flow phenomena which are of mesoscale dimensions of the order of 10^1 to 10^2 km.

Some channeling effects have been mentioned in context with the mistral and the etesian. The mountain barrier of the Pyrenees on the one side and the plateau region of central France on the other side contribute to the strong winds that come out of the Carcassonne Gap under north-of-west wind conditions. The Rhone Valley is another gap between the mountains of central France (the Cevennes) and the Alps, through which strong mistral winds are channeled into the Gulf of Lion. These winds occur so frequently that trees in the Rhone Valley are bent in the direction of the airflow down the valley.

The channeling effect of the Rhone Valley should not be confused with the diurnal variation of valley and mountain breezes produced by the daily cycle of insolation and radiational cooling (see Section IV-B, para. 1). In these diurnal wind systems, the valley breeze (directed from the plains towards the mountains) usually exceeds the mountain breeze (from the mountains towards the plains) in strength. The strong mistral winds emerging from the Rhone Valley are generated by a synoptic scale pressure gradient which fosters outflow of air into the Mediterranean basin. The valley and mountain breeze system acts only as a second order disturbance or modulator upon this channeled air flow.

The Straits of Gibraltar, Bonifacio and Messina offer other typical examples of increased wind speeds due to channeling effects under the proper directions of the surface pressure gradient. The many islands in the Aegean Sea also lead to local anomalies in wind speed and direction that are well known to local seafarers.

The relatively small obstacles of islands also bring about corner effects of airflow which are below the resolution of our synoptic observation system. This is especially true when the lower levels of the troposphere are stably stratified and the airstream tends to deviate quasi-horizontally around the island, rather than going over it as the synoptic-scale pressure gradient might

suggest. Consequently, surface wind observations on shore might not be representative of the synoptic flow pattern. Stations on the windward and leeward sides of an island might experience lower wind speeds than stations on the two sides of the island around which the airflow is diverted. The venturi effect of this airflow can be expected to cause systematic mesoscale disturbances in the surface pressure distribution, with lower pressure likely to prevail on the high-wind-speed sides of the island.

The disturbance of the air stream caused by islands blocking the flow of a stably stratified air current may sometimes be observed far downstream of the barrier. Chopra and Hubert (1965) described cloud vortex patterns that extended over 540 km downstream of the island of Madeira off the coast of West Africa (Figure IV-A-1).

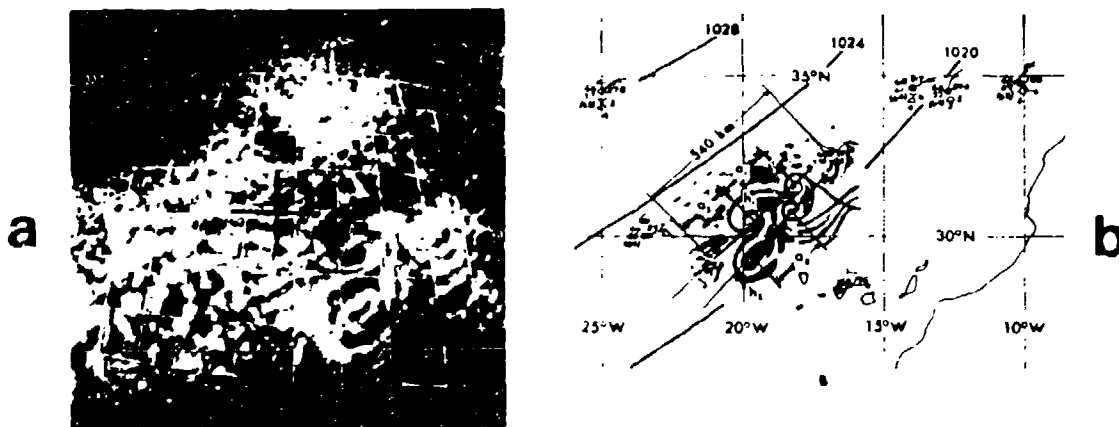


Figure IV-A-1. (a) TIROS VI picture of eddy pattern, pass 3547/3546, taken 1133 GMT, 19 May 1963 (from Chopra and Hubert, 1965). (b) Eddy pattern of (a) superimposed on surface analysis for 1200 GMT, 19 May 1963 (from Chopra and Hubert, 1965).

B. DIURNAL EFFECT.

To avoid semantic confusion, the established custom of naming winds in accordance with the direction from which they are blowing will be strictly observed here. Thus, for example, a valley wind means a wind that blows from the valley towards the mountains, just as a westwind is a wind that blows from the west, and a sea breeze blows from the sea towards land.

Diurnal wind systems are caused by the 24-hour cycle of insolation, giving rise to a similar cycle in the temperature of the earth's surface. If there are horizontal differences in the heating rates of the atmosphere, produced by

differences in the underlying terrain, the 24-hour insolation and nocturnal cooling cycle will produce horizontal temperature gradients. These, in turn, will set up horizontal pressure gradients which drive the observed diurnal wind systems.

Because of their dependence on insolation and nocturnal cooling, these wind systems will respond strongly to the amplitudes of the diurnal radiation fluxes in the atmosphere. Cloudy days will witness strongly reduced circulation systems as compared to clear days. Moisture in the air will also damp the range of diurnal temperature variations. The passage of synoptic-scale disturbances may, at times, completely mask the diurnal circulation systems. Persistent synoptic-scale flow patterns may be modulated by superimposed diurnal temperature and circulation variations.

1. Mountain and Valley Winds

Air layers close to the earth's surface will heat and cool more strongly during a 24-hour cycle, mainly because of heat exchange with the earth's surface and turbulent heat fluxes, than layers in the "free atmosphere" at some distance from the ground. A horizontal surface which intersects sloping terrain will show greater diurnal temperature variations at the point of intersection with the ground than at a point where this horizontal surface lies some distance above the sloping terrain. Therefore, horizontal temperature gradients will develop along the same horizontal surface during the course of the day (higher temperatures at the point of intersection than at a point some distance away). These temperature gradients will reverse their signs as diurnal heating of the ground gives way to nocturnal cooling.

The solenoids between the quasi-horizontal isobaric surfaces and the isothermal surfaces will set a circulation system into motion that may be referred to as "slope winds" (Figure IV-B-1). Wind and temperature profiles along a slope during the warming phase of the diurnal cycle are illustrated in Figure IV-B-2. The resulting pattern of potential temperatures, in arbitrary units, is shown in Figure IV-B-3.

A typical valley not only consists of the slopes on either side (which, incidentally, have different exposure to the sun during the course of a day, and hence have differently developed slope-wind systems), but also has a gentle slope to the bottom of the valley from the crest of the mountains out into the plains. As a consequence, a superposition of slope-wind systems on the sides of the valley should be expected with a true mountain and valley wind system. This is illustrated schematically in Figure IV-B-4.

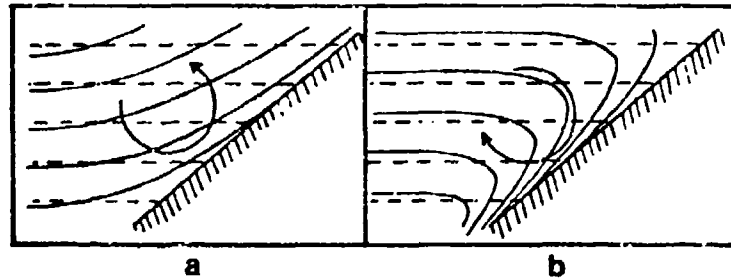


Figure IV-B-1. Isobars (dashed lines) and isotherms (solid lines) along mountain slopes (a) during the day (b) during the night. Arrows indicate direction in which the circulation accelerates (from Hann-Süring, 1939).

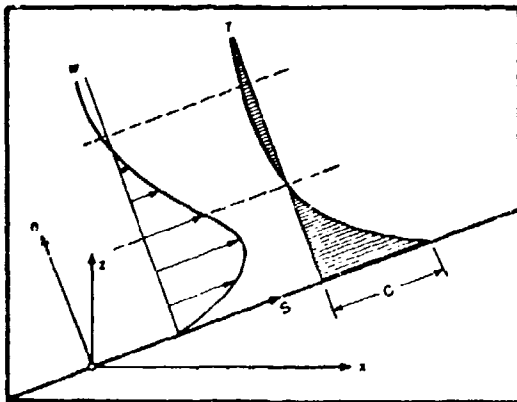
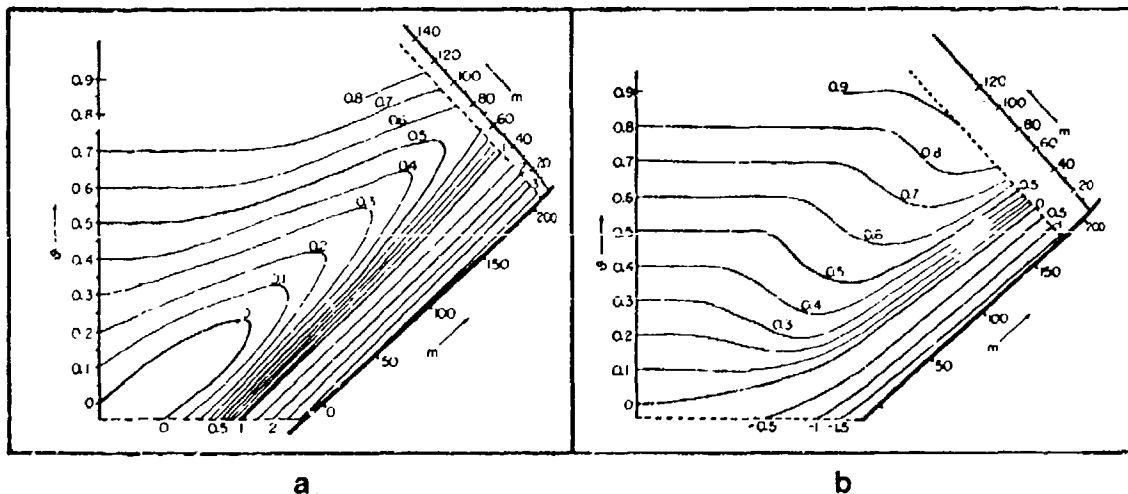


Figure IV-B-2. Schematic profiles of wind (W) and temperature (T) along a slope (S) over western United States during the warming phase of the diurnal cycle. C is the temperature increase at the surface of the slope, n is the direction normal to S (from Defant, 1951).



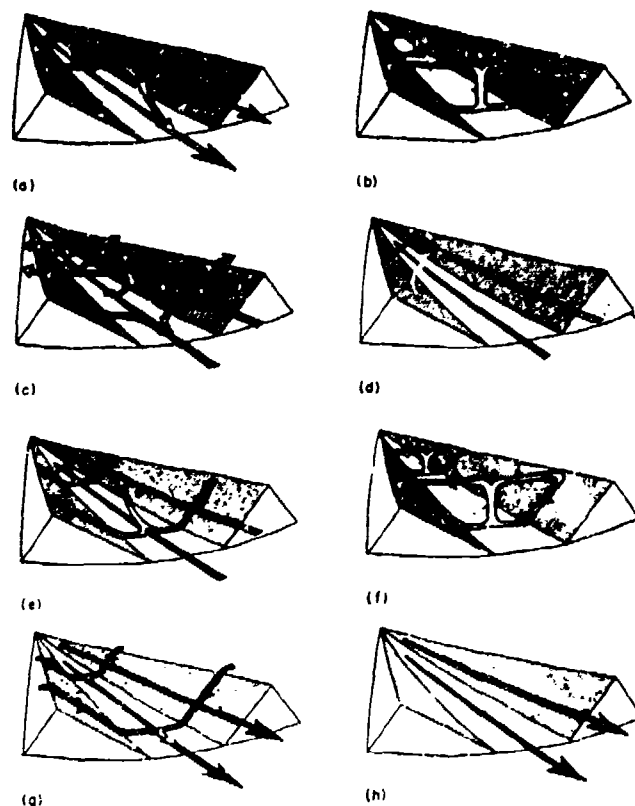


Figure IV-B-4. Schematic illustration of the normal diurnal variations of the air currents in a valley (from Defant, 1951).

(a) Sunrise; onset of upslope winds (white arrows), continuation of mountain wind (black arrows). Valley cold, plains warm.

(b) Forenoon (about 0900); strong slope winds, transition from mountain wind to valley wind. Valley temperature same as plains.

(c) Noon and early afternoon; diminishing slope winds, fully developed valley wind. Valley warmer than plains.

(d) Late afternoon; slope winds have ceased, valley wind continues. Valley continues warmer than plains.

(e) Evening; onset of downslope winds, diminishing valley wind. Valley only slightly warmer than plains.

(f) Early night; well-developed downslope winds, transition from valley wind to mountain wind. Valley and plains at same temperature.

(g) Middle of night; downslope winds continue, mountain wind fully developed. Valley colder than plains.

(h) Late night to morning; downslope winds have ceased, mountain wind fills valley. Valley colder than plains.

An example of the diurnal wind system in Innsbruck (Austria) is shown in Figure IV-B-5. Buettner (1967) gives an example for a valley station in the Mount Rainier area of Washington State (Figures IV-B-6 and IV-B-7). From these diagrams it appears that the valley winds usually exceed the mountain winds in strength. Also, there appears to be a reversal of wind direction with height, suggesting the existence of a counter-circulation at some distance above the valley bottom. Pilot balloons entering this counter-current may actually return to a position above their original release point.

Mountain breezes often are less steady than valley breezes. The cold air which forms along the slopes during the nocturnal cooling cycle tends to build up "avalanches" which roll down the slopes and produce quasi-periodic wind variations.

2. Sea Breeze Regimes

Since water has a greater conductive capacity than (dry) soil, it warms more slowly under insolation and cools more slowly at night. The differential heating between land and sea produces temperature gradients which change their sign during the course of a day. The resulting pressure gradients produce the well-observed phenomenon of land and sea breezes. If the synoptic scale pressure gradients are weak, a "closed" circulation system may result, with winds at the surface and at about 2000 m height blowing in nearly opposite directions. A classical example of this is shown in Figure IV-B-8.

A theoretical model of the land and sea breeze which agrees well with observations, has been published by Estoque (1952). Figures IV-B-10 through IV-B-21 show computer-simulated flow patterns which develop under different gradient wind conditions (Figure IV-B-9 shows the coordinate system used in these figures). Special attention should be drawn to the case of slight gradient winds directed offshore. The sea breeze, in this case, overcomes the gradient winds and moves inland with almost a front-like character. The inland penetration of the sea breeze is reduced, and its arrival time is retarded, in comparison to other wind conditions.

The ascending motions at the edge of the "sea-breeze front" can trigger convective cloud developments and thunderstorms. The interaction of the sea breeze in Athens with the etesian wind regime has been described in Section III-F, para. 4.

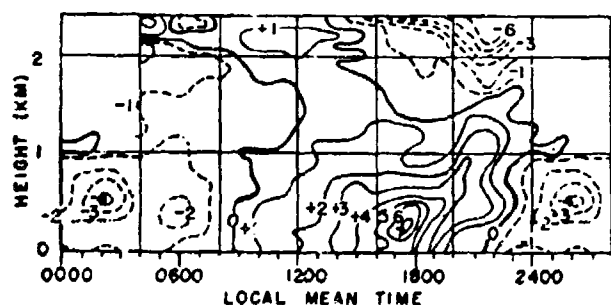


Figure IV-B-5. Mean velocity isopleths of the mountain and valley winds at Innsbruck (numbers are wind speed components (m sec^{-1}) in the direction of the valley; + upvalley, - downvalley) (from Defant, 1951).

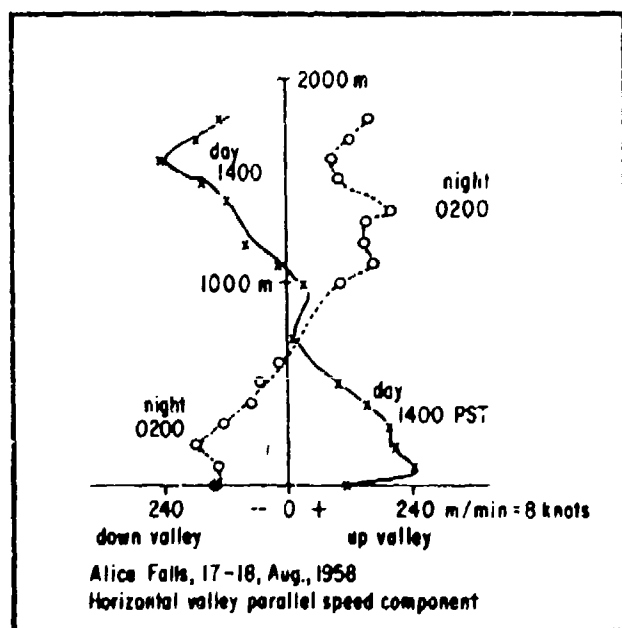


Figure IV-B-6. Typical mountain and valley wind diagram for Alice Falls, Washington (from Buettner, 1967).

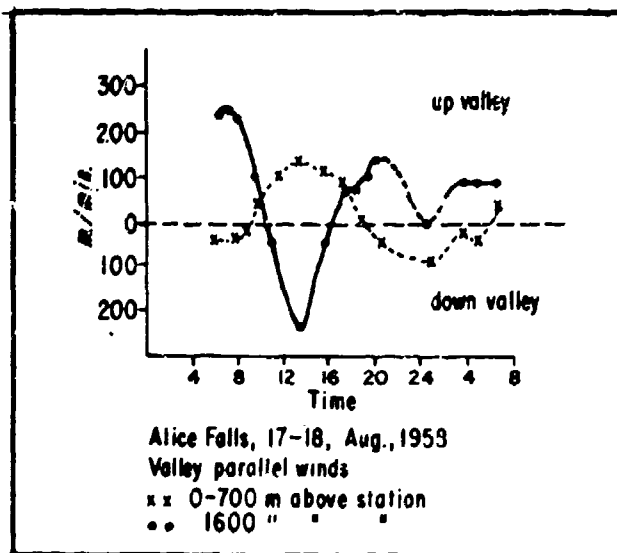


Figure IV-B-7. Daily variation of valley and anti-valley system, Alice Falls, Washington (from Buettner, 1967).

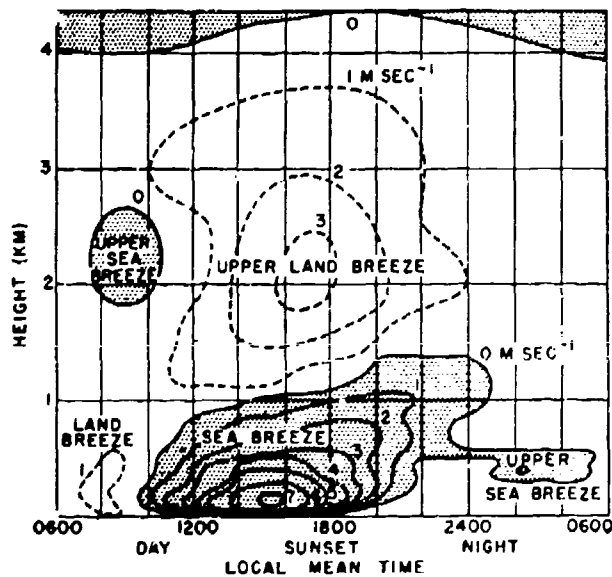


Figure IV-B-8. Velocity isopleths for the land and sea breeze in Batavia (from Defant, 1951).

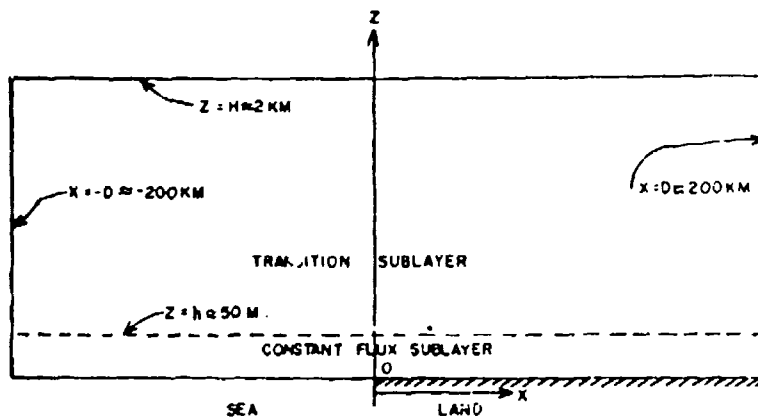


Figure IV-B-9. Coordinate system used in Figures IV-B-10 through IV-B-21 (from Estoque, 1962).

NOTE: Figure IV-B-9 (above) shows the coordinate system used in Figures IV-B-10 through IV-B-21 (see following pages). A discussion of "Diurnal Temperature and Pressure Variations" concludes Section IV and is presented following these figures.

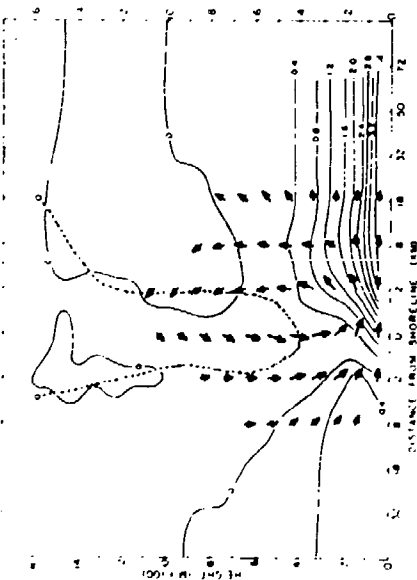


Figure IV-B-10. Case for zero gradient wind at 1100 local time.*

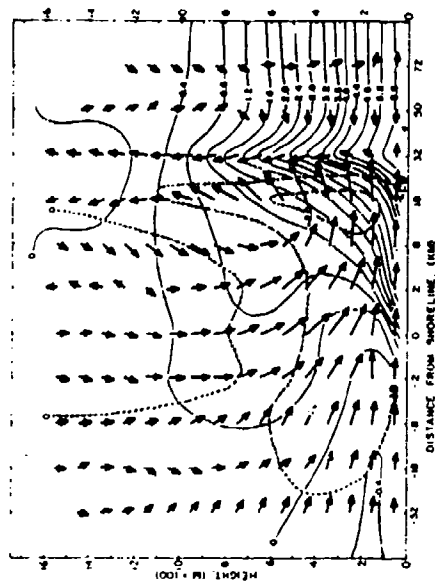


Figure IV-B-11. Case for zero gradient wind at 1700 local time.*

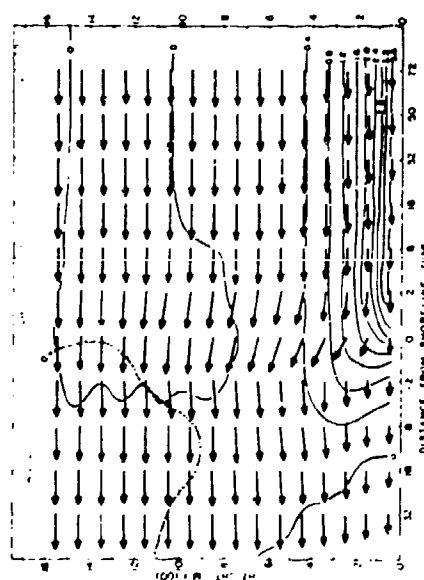


Figure IV-B-12. Case for 5 m sec⁻¹ offshore wind at 1100 local time.*

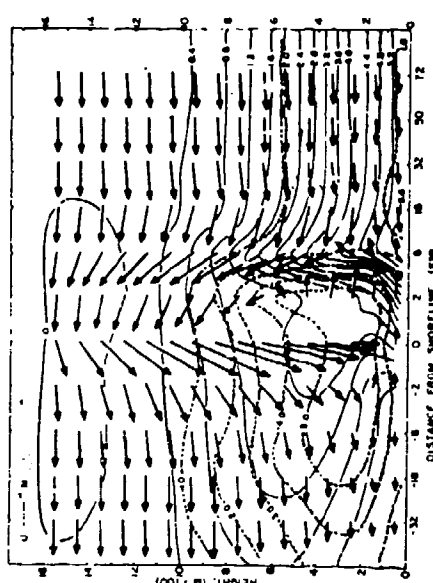


Figure IV-B-13. Case for 5 m sec⁻¹ offshore wind at 1700 local time.*

*Landward and vertical circulation (indicated by length and direction of arrows) and temperature change (solid lines) from 0800. Dashed lines indicate wind velocity component (m sec⁻¹) into the figure (from Estoque, 1962).

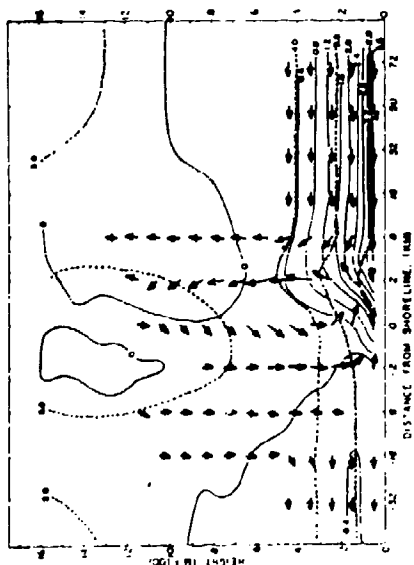


Figure IV-B-14. Case for 5 m sec^{-1} wind into figure at 1100 local time.*

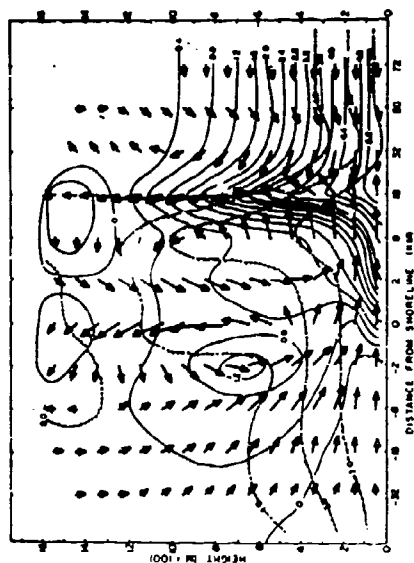


Figure IV-B-15. Case for 5 m sec^{-1} wind into figure at 1700 local time.*

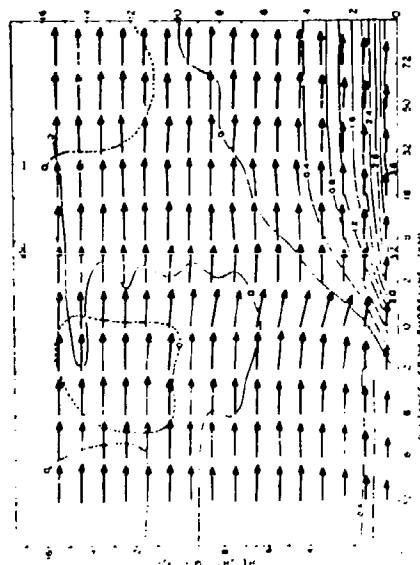


Figure IV-B-16. Case for 5 m sec^{-1} onshore wind at 1100 local time.*

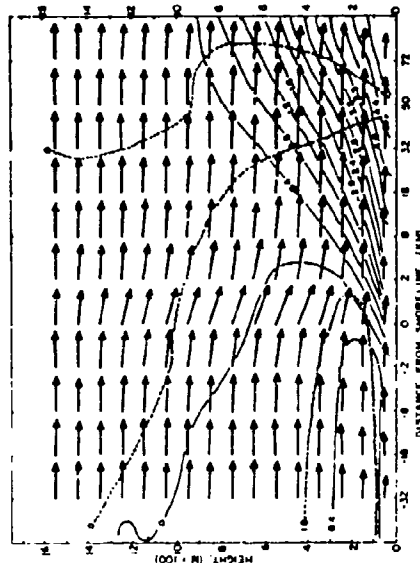


Figure IV-B-17. Case for 5 m sec^{-1} onshore wind at 1700 local time.*

*Landward and vertical circulation (indicated by length and direction of arrows) and temperature change (solid lines) from 0800. Dashed lines indicate wind velocity component (m sec^{-1}) into the figure (from Estoque, 1962).

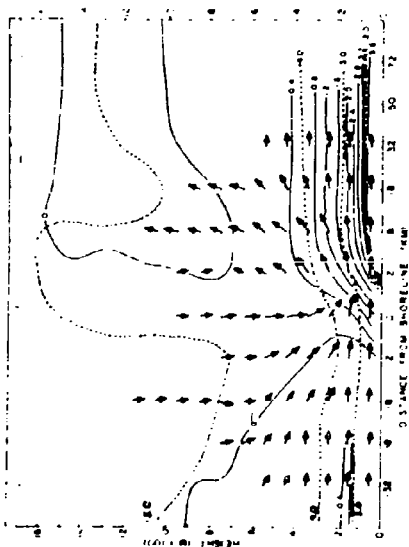


Figure IV-B-18. Case for 5 m sec^{-1} wind out of figure at 1100 local time.*

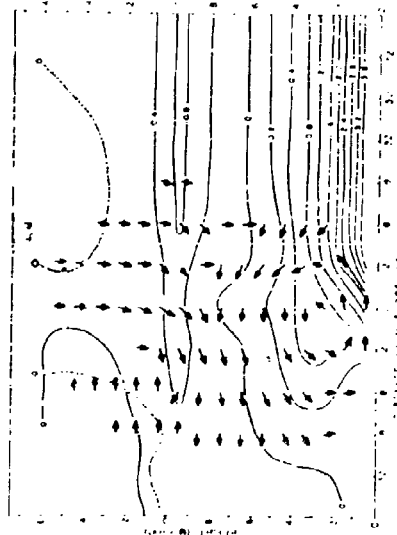


Figure IV-B-20. Case for zero wind isothermal surface layer at 1100 local time.*

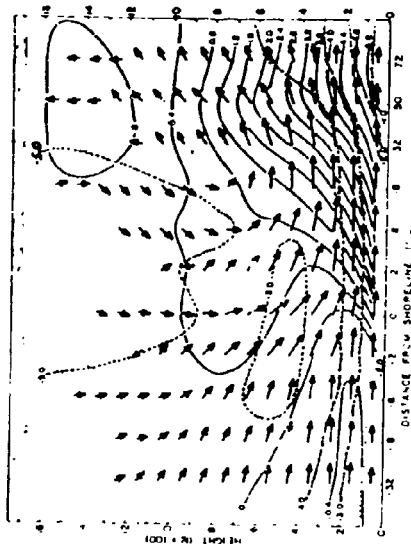


Figure IV-B-19. Case for 5 m sec^{-1} wind out of figure at 1700 local time.*

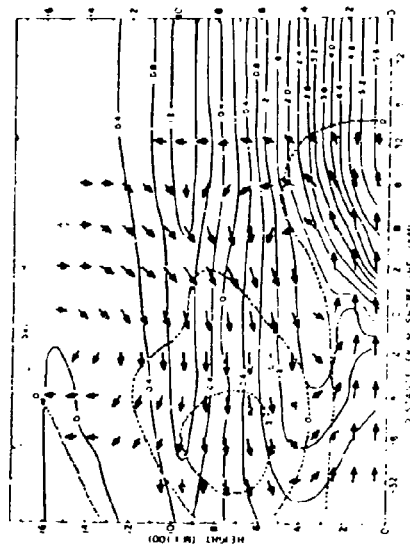


Figure IV-B-21. Case for zero wind isothermal surface layer at 1700 local time.*

*Landward and vertical circulation (indicated by length and direction of arrows) and temperature change (solid lines) from 0800. Dashed lines indicate wind velocity component (m sec^{-1}) into the figure (from Estoque, 1962).

3. Diurnal Temperature and Pressure Variations

The diurnal temperature variation in the lowest layers of the atmosphere essentially depends on:

- (1) The radiation budget at the earth's surface
- (2) The conductive capacity of the underlying surface
- (3) The intensity of turbulent heat exchange in the lower atmosphere

Aside from the solar elevation angle, cloudiness exercises a drastic influence upon the radiation budget. The amplitude of the diurnal temperature variation is cut down appreciably during overcast days as compared to clear days. Persistent aerosol concentrations, as may occur during sirocco conditions, also influence the radiation budget by decreasing the intensity of direct solar radiation. If aerosol concentrations are only moderate and if particle sizes are small (in the micron to submicron range), this loss in direct radiation may be offset by an almost equivalent gain in scattered radiation.

Under heavy aerosol concentrations the incoming solar radiation is most strongly affected at low solar elevation angles, when the sun's rays have to penetrate a thick layer of the atmosphere. This will be the case during the early morning and late afternoon hours. A significant modification of the diurnal temperature variation should be felt under such conditions. However, since such haze conditions are usually coupled with high moisture concentrations in the lower atmosphere, the blocking off of direct solar radiation is compensated for by an enhanced "greenhouse effect" which can keep temperatures uncomfortably high even after sunset. High temperatures, combined with high relative humidities, contribute to human discomfort during sirocco conditions, even at night.

The conductive capacity of the underlying surface causes the diurnal temperature variation to be much larger over land than over the ocean. Within the domain of the sea-breeze regime, maximum temperatures are reached in the morning before the sea breeze develops, or in the afternoon when the land breeze returns.

The effects of turbulent heat exchange tend to keep the range of the diurnal temperature variation lower under windy conditions than under calm conditions. Daytime temperatures also are kept relatively low if an inversion is already dissolved in the early morning hours and the heat from the lowest layers of the atmosphere is distributed by turbulent mixing over a deep layer of the troposphere.

The local effects on the diurnal heating cycle will generate horizontal temperature gradients which, in turn, will produce horizontal pressure gradients. These will give rise to well-organized circulation systems, like the land and sea breezes, and mountain and valley winds. Details of the diurnal pressure variations are provided in Appendix G.

V. SMALL SCALE PHENOMENA OF INTEREST TO THE MEDITERRANEAN FORECASTER

A. CLEAR AIR TURBULENCE (CAT) - A GENERAL REVIEW

In Figures III-B-9, III-B-12 and III-B-13, observations of moderate and severe turbulence have been entered. These diagrams corroborate the fact that CAT in the jet stream region is associated with strong vertical (directional) wind shear. Two types of turbulence may be distinguished:

- (1) Turbulence caused by convective motions in a thermally unstable atmosphere.
- (2) Turbulence under generally stable thermal stratification, but with vertical wind shear.

The bumpiness normally encountered by an aircraft in the planetary boundary layer or friction layer of the lower troposphere is caused by either thermal convection ("thermals") or by mechanical turbulence when air moves over rough terrain, or by a combination of both effects. The vertical wind shear within the friction layer, and the turning of wind with height, help to generate bumpy flight conditions. Since this type of turbulence is expected by the seasoned pilot, it is not included in the category of clear air turbulence. Neither is the turbulence that is found in the close vicinity of cumulus or cumulonimbus clouds.

The weather forecaster should be aware that flight conditions in the planetary boundary layer under strong low-level winds may be hazardous. The strong vertical wind shears which prevail close to the ground (e.g., in the mistral over coastal airports) may lead to a misjudgment in the rate of descent during approach to the runway. Since, under constant airspeed, the headwind lessens rapidly close to the ground, an approaching airplane may find itself descending more rapidly than anticipated because of a loss of lift in the lower part of the friction layer. Accidents have been reported in which aircraft landed short of the runway because vertical wind shears were not fully considered. Turbulence under strong low-level winds aggravates the difficulty of the approach maneuver.

High-level turbulence in the vicinity of cumulonimbus clouds may be extremely violent. Figure V-A-1 shows schematically the range of scatter of presently available turbulence data in the form of spectra. The hatched area pertains to thunderstorm turbulence. Both coordinate scales in this diagram are logarithmic, meaning that over each unit interval along the coordinate the quantity changes by an order of magnitude. The abscissa contains the frequency of turbulent gusts or eddies, as it would be observed by a stationary anemometer at, say, the 10 km level in the upper troposphere. Units are in cycles per day. The abscissa is also labeled in terms of eddy periods (seconds, minutes, etc.). The abscissa labeling on top of the diagram translates the time scale into a space scale, giving turbulent eddy dimensions in meters rather than gust duration in seconds. This permits the use of diagrams to estimate gust effects on aircraft.

An airplane flying at $400 \text{ kt} \approx 200 \text{ m sec}^{-1}$ true airspeed will experience one bump per second from eddies which are 200 m long (see labeling on top of Figure V-A-1). Shorter eddies will produce higher-frequency vibrations in the same aircraft. Thus, in order to interpret Figure V-A-1 for an aircraft with 200 m sec^{-1} true airspeed, the time and frequency scales on the abscissa must be moved towards the left until the "1-sec" mark is underneath the mark for 200 m.

The ordinate contains the kinetic energy of turbulent eddies per unit of frequency (in $\text{km}^2 \text{ hr}^{-2} \text{ day}$). It can be estimated that the thunderstorm turbulence indicated by the shaded area is approximately one order of magnitude stronger than the line (upper curve) that is given for moderate clear air turbulence. This is at least one good reason why aircraft should stay out of the severe up- and down-draft regions of a thunderstorm.

The energy of eddies, $S(k)$, in the atmosphere increases with eddy size (or with decreasing frequency, k), roughly according to

$$S(k) \propto k^{-2/3} \quad \text{V-A(1)}$$

where a is a constant close to unity, and ϵ is the so-called rate of dissipation of energy. This means that severe turbulence dissipates its energy more rapidly than moderate or light turbulence. As an example, intense wing-tip vortices are eroded or dissipated faster with stronger and gustier winds than with light and quasi-laminar flow.

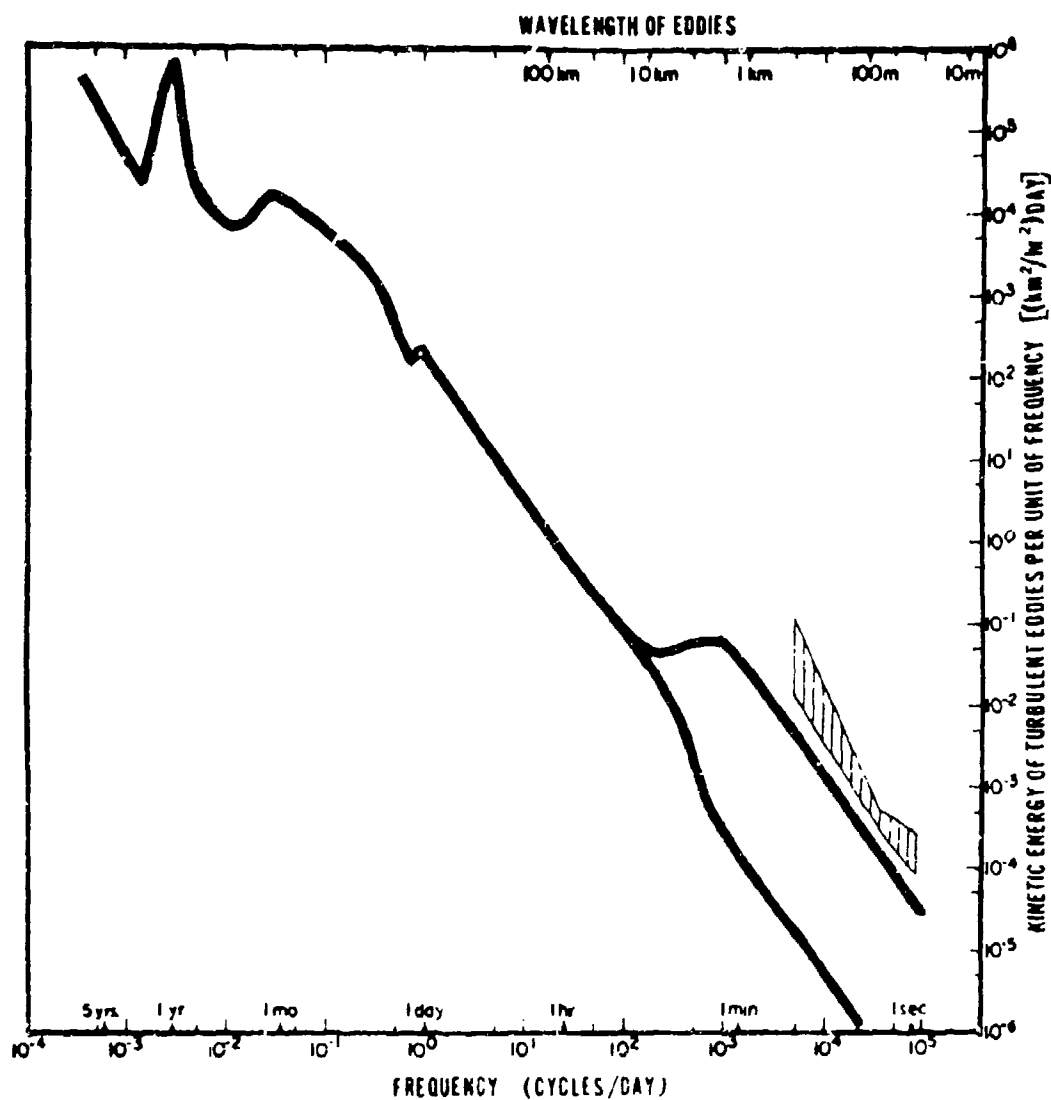


Figure V-A-1. Average spectra for E-W wind component in the free atmosphere. Lower spectrum curve is representative for smooth air without turbulence, upper spectra moderate CAT. Shaded area represents severe turbulence in thunderstorms (from Reiter, 1972b).

Even though the eddy kinetic energy increases with eddy size, as shown in Figure V-A-1, an aircraft will not respond in terms of CAT vibrations to eddies beyond a few hundred meters in dimension. (Supersonic aircraft, of course, are subject to stronger accelerations from large eddies than are slower aircraft.) Nevertheless, these larger eddies must be watched carefully, especially when they occur in the form of waves rather than random turbulence. Waves sometimes reveal a tendency to break down into violent turbulence, thus losing their laminar flow characteristics. This is schematically indicated in Figure V-A-2. Figure V-A-3 shows a photograph of such a breaking "Kelvin-Helmholtz wave" revealed by the shape of a rapidly changing cloud bank formation.

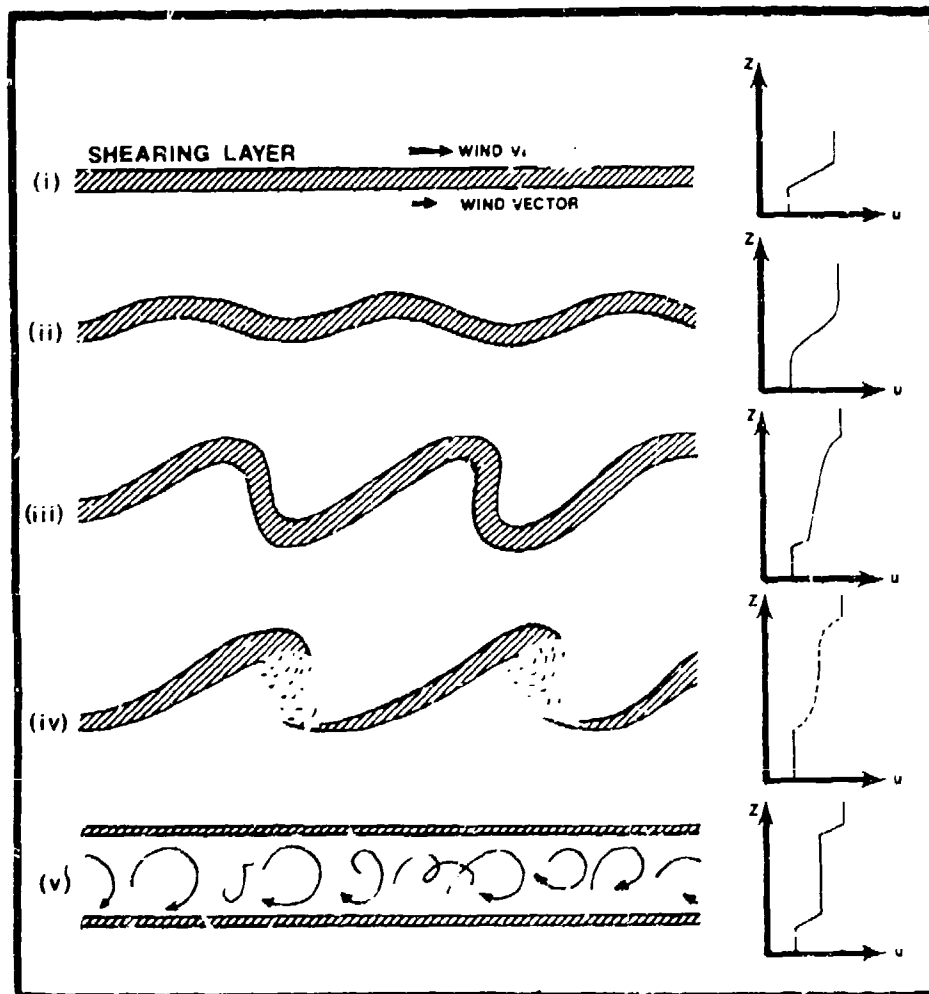


Figure V-A-2 Breakdown of shearing layer with schematic wind profiles.



Figure V-A-3. Photograph of Kelvin-Helmholtz wave clouds
(photograph courtesy of James E. Lovill).

Waves which have a tendency to break up into CAT frequently occur over mountain ranges. These mountains need not be large; even coastlines, hills or island chains may occasionally produce significant CAT in the upper troposphere and stratosphere. Figure V-A-4 shows an aircraft traverse over the Rocky Mountains near Boulder, Colorado, on 20 February 1968. The potential isotherm pattern in this diagram clearly depicts the lee-wave structure, especially the strong downdraft over and immediately to the east of the Continental Divide. This downdraft constitutes the foehn or chinook winds (see Section III-F, para. 3). In the case presented here, the whole depth of the troposphere is occupied by the subsidence characteristics of foehn conditions.

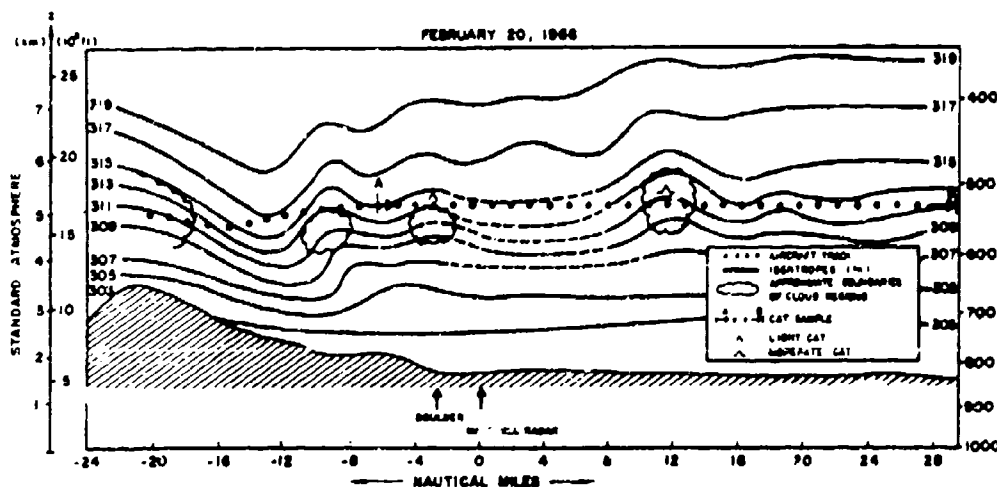


Figure V-A-4. Vertical cross section along aircraft track in the Boulder, Colorado area (from Reiter, 1972b).

Two regions of CAT were encountered during this flight, each associated with a well-structured lee wave. The longitudinal wind-component record (headwind component) also reveals the wave structure. The upper part of Figure V-A-5 contains a smoothed wind record which shows quite clearly the mesoscale waves. The lower part gives the small-scale wind disturbances which were superimposed upon the smoothed record shown in the upper part of the diagram. The two turbulent regions, one centered at about 53 minutes and another at 56 minutes flight time, are quite evident. The first region consisted of two major up- and down-drafts. The second patch resembled four or five relatively regular short waves, reminiscent of the Kelvin-Helmholtz waves shown in Figures V-A-2 and V-A-3.

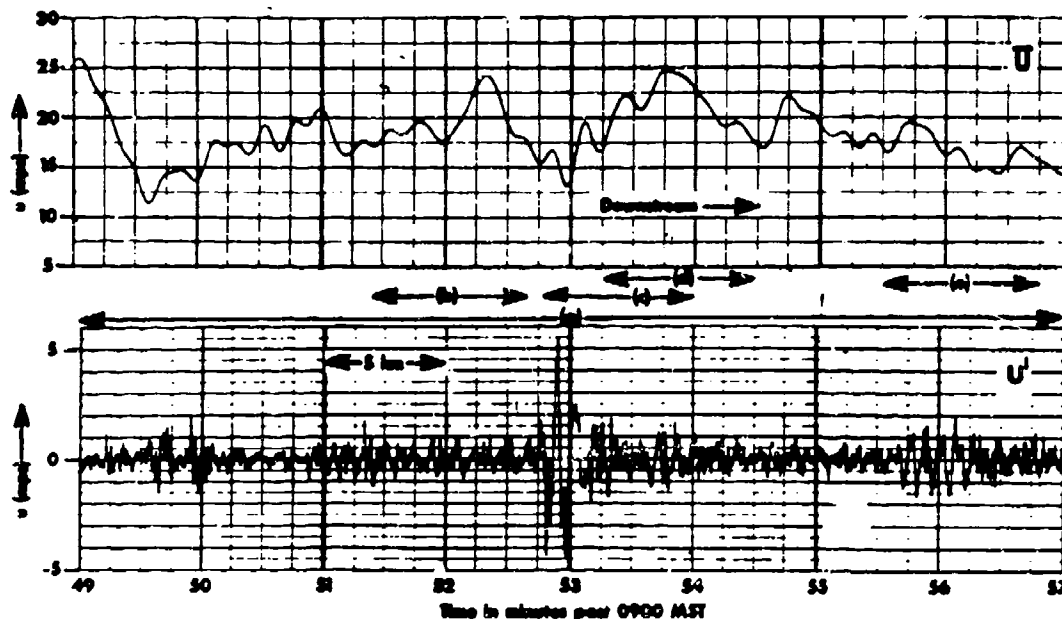


Figure V-A-5. Top: Smoothed velocity component along aircraft track shown in Figure V-A-4 after removing the small-scale wind disturbance. Bottom: Velocity component along aircraft track showing the small-scale disturbances (from Reiter, 1972b).

The patchiness of severe CAT shown in Figure V-A-5 is typical of this phenomenon. For this reason it is impossible to forecast the more bothersome cases of CAT accurately. Only general guidelines can be given to support an assessment of regions in the atmosphere where CAT is more likely to occur than in others.

The formation of lee waves, their forecasting aspects, and CAT associated with them will be discussed in more detail in Section V-B; here, mainly CAT and jet streams are discussed.

The main ingredient of CAT near jet streams is a strong vertical wind shear, produced by a change of either wind speed, or wind direction, or both, with height. Such shears are usually associated with a thermally stable layer such as the "jet stream front" (i.e., the baroclinic zone below the jet core) or the baroclinic region above the jet core. These regions are shown schematically in Figure V-A-6.

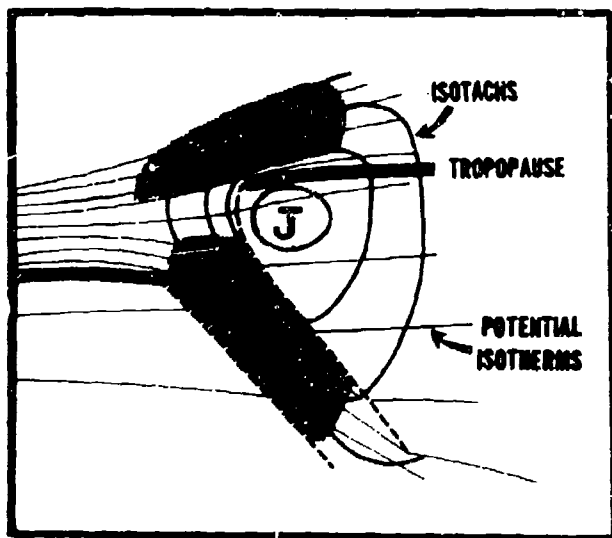


Figure V-A-6. Schematic cross section through jet stream showing isotachs, potential isotherms, and tropopause locations. Baroclinic regions are indicated by shading. Boundary of frontal zone is shown by dashed line.

The readiness of atmospheric flow to break down into random turbulence is expressed by the Richardson number

$$Ri = \frac{\frac{g}{\theta} \frac{\partial \theta}{\partial z}}{\left(\frac{\partial u}{\partial z}\right)^2 + \left(\frac{\partial v}{\partial z}\right)^2} = \frac{\frac{g}{T} \left(\frac{\partial T}{\partial z} + r\right)}{\left(\frac{\partial u}{\partial z}\right)^2 + \left(\frac{\partial v}{\partial z}\right)^2} \quad V-A(2)$$

where θ is the potential temperature and T the actual temperature in degrees Kelvin, r is the dry-adiabatic lapse rate ($r \approx 1^\circ\text{C}/100 \text{ m}$), and u and v are the zonal and meridional wind components, respectively. Hydrodynamic theory predicts that laminar flow should break down into turbulent flow if $Ri \leq 0.25$. In the real atmosphere, even layers with Ri slightly larger than 1 have to be suspected of being turbulent.

The presence of turbulence, once started, will destroy the original structure of the atmosphere. Turbulent transport of heat tends to make an adiabatic layer out of the originally stable layer. At the same time, vertical momentum transport will destroy the wind shear. The vertical distributions of humidity and of chemical admixtures also will be equalized by the action of CAT. This is illustrated schematically in Figure V-A-7. Therefore, the following sequence of events may be postulated:

- (1) A stable layer with vertical wind shear deforms into gravity waves.
- (2) These waves, under critical shear conditions (given, e.g., by the Richardson number) tend to break down and degenerate into turbulence (see Figures V-A-2 and V-A-3).
- (3) Turbulence destroys the original stratification. An adiabatic layer is formed, bounded by a stable and shearing layer on its top and bottom. These two stable layers may be subject to the same processes (1) and (2). Thereby the depths of the adiabatic layer will grow until there is not enough wind shear left over a relatively deep layer to sustain turbulence.

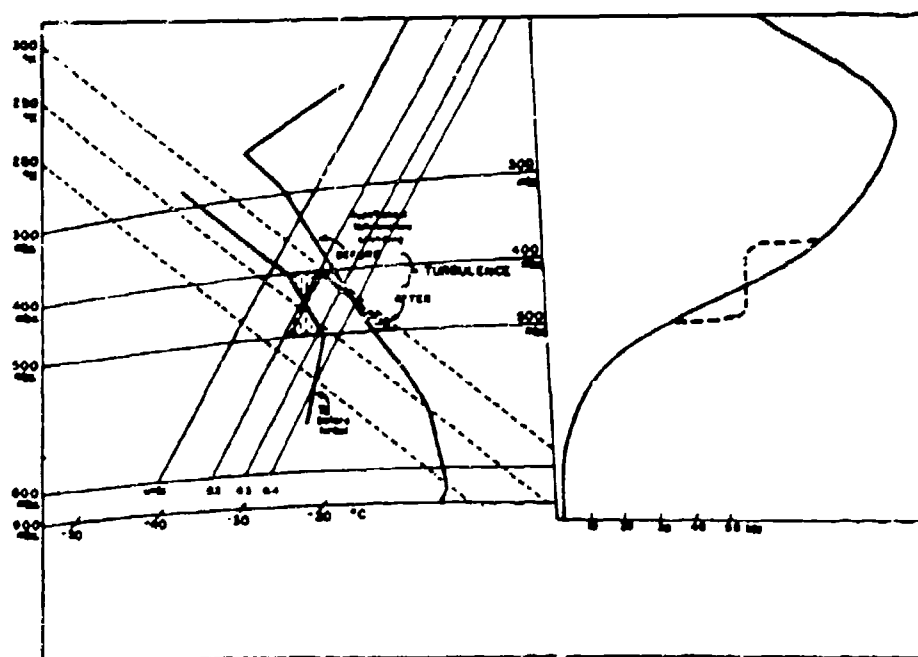


Figure V-A-7. Schematic view of effects of turbulence on vertical wind, temperature and humidity profiles. Solid lines indicate conditions before the onset of turbulence, dashed lines after the establishment of a turbulent layer (from Reiter and Hayman, 1962).

Figure V-A-6 illustrates the fact that stability and shear conditions conducive to the development of CAT through steps (1), (2) and (3) are present in the vicinity of jet streams. In the stratosphere, systematic wind variations with height over layers that are 2 to 3 km deep (Figure V-A-8) are frequently found. These variations are caused by the superposition of gravity inertia waves and may, at times, give rise to CAT. The peculiar mesoscale temperature structure in the stratosphere which is often observed as a sequence of adiabatic and stable layers (Figure V-A-9) may be viewed at times as a consequence of such turbulence. The layers appearing in this diagram need no longer be turbulent; they may have been caused by turbulence far upstream.

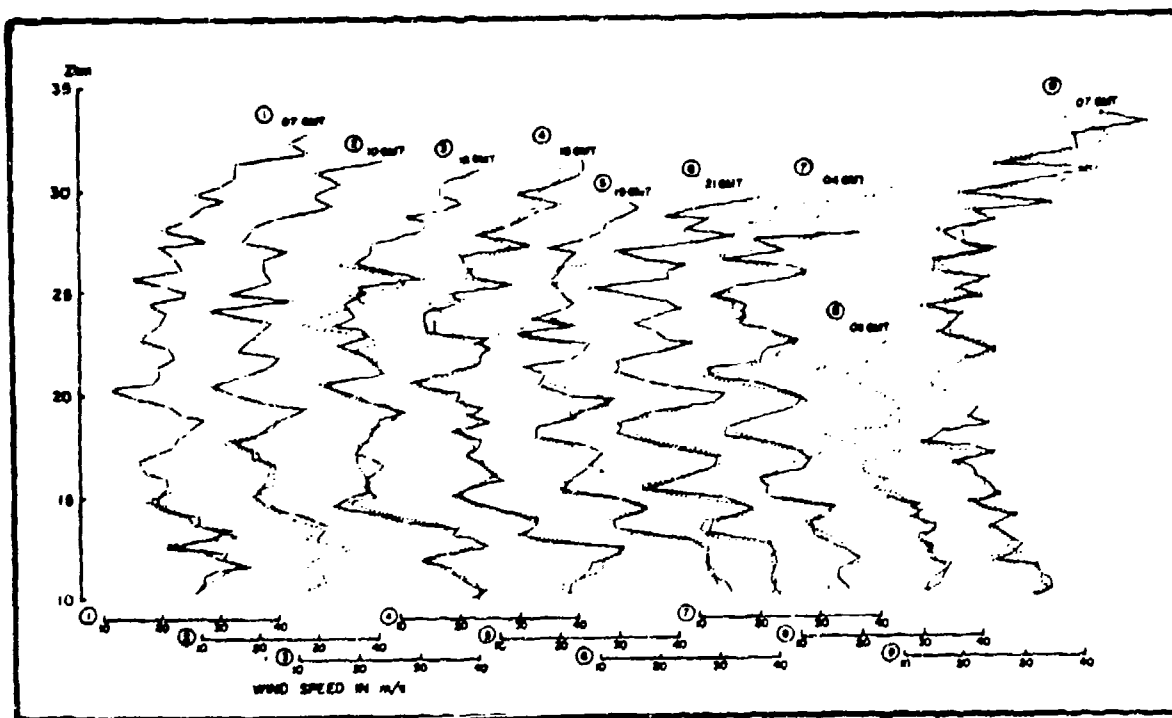


Figure V-A-8. Vertical wind profiles (m sec^{-1}) at Magny-les-Hameaux, France, 12-21 March, 1968 (from Reiter, 1972b).

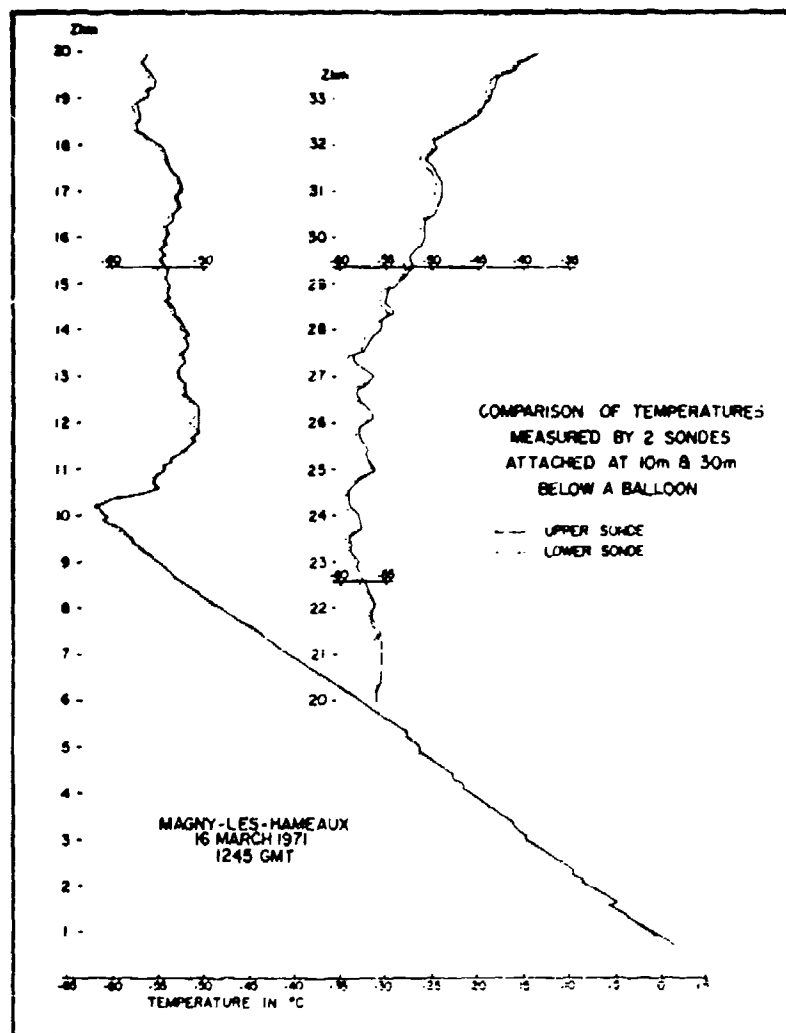


Figure V-A-9. Vertical temperature profiles measured by two sondes at 10 m and 30 m distance from the same balloon, at 1245 GMT, 16 March 1971, Magny-les-Hameaux, France (from Reiter, 1972b).

The presence of strongly shearing layers in the atmosphere may be hazardous to aviation in two ways: by the possible generation of CAT as discussed above, and by a sudden loss in headwind component, hence in lift, acting on an aircraft that passes through such a layer. The latter effect is particularly worrisome with heavy aircraft whose bulk possesses considerable inertia. If the aircraft passes from a strong into a weak headwind or even into a tailwind, for instance, the sudden loss in lift may upset the aircraft. Since under this loss the aircraft loses altitude rapidly, there may be a tendency for the pilot (or autopilot) to compensate with a climbing attitude. This may further reduce the airspeed and thus compound the problem. The actual turbulence usually associated with such shearing layers will make the situation even worse.

From the foregoing discussion it becomes quite obvious that forecasts of the location of strongly shearing layers, and of the magnitude and the direction of the wind shear vector (Figure V-A-10) are of great benefit to the pilot. Not only will such forecasts help him to locate and avoid CAT regions, but they will also help him to plan remedial action once the aircraft is exposed to CAT.

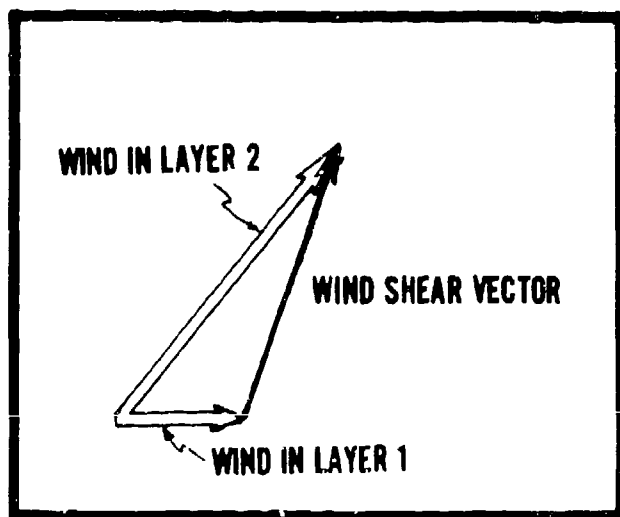


Figure V-A-10. Definition of wind shear vector.

B. MOUNTAIN WAVES AND CAT

Studies by Clodman, et al. (1961), Colson (1963) and Foltz (1967) indicate that clear air turbulence is more frequently found over mountainous or hilly terrain than over plains or oceans. Obviously, air flow over corrugated terrain features generates disturbances of finite amplitude which may cause an air current with vertical wind shear to become distorted into waves (notably Kelvin-Helmholtz waves of several hundred meters wavelength). Under suitable conditions these waves become unstable and break down into eddies of various sizes which are experienced as CAT by an aircraft flying through them.

The most obvious waves generated in a stably stratified flow over a mountain range are the so-called lee waves with typical wavelengths of several kilometers. Lenticular or "Moazagoti" clouds are often associated with such wave patterns. If these waves have relatively small amplitudes, the airflow through the wave pattern is more or less laminar and little, if any, CAT will be experienced. Quite often, however, such waves reach considerable amplitudes and the flow becomes strongly turbulent, giving rise to severe CAT. Under extreme conditions the energy contained in the lee-wave system may actually be passed on to, and distributed over, the array of smaller eddies felt as CAT. Reiter and Foltz (1967) made estimates of such an extreme effect of mountain waves on the occurrence of CAT.

It should be pointed out that not only large mountain ranges, but also relatively low hills -- even coast lines -- may give rise to lee-wave formation.

Turbulence theory predicts that the kinetic mean energy of turbulent eddies of a certain size is proportional to the -5/3 power of the eddy diameter, expressed by a "wavelength" or "wave number" (see Eq. V-A(1)). This power law holds within the so-called "inertial subrange" of turbulence which, for all practical purposes, also encompasses the range of eddy sizes which are felt as CAT. The kinetic energy of such eddies can be expressed by

$$\overline{KE} = \frac{1}{2} \overline{w^2} = \frac{1}{2\lambda} \int_0^\lambda w_0^2 \sin^2 2\pi \frac{x}{\lambda} dx, \quad V-B(1)$$

where w is the vertical velocity in a sinusoidal wave pattern of wavelength λ and of amplitude w_0 . Integration of Eq. V-B(1) yields

$$\overline{KE} = \frac{w_0^2}{4}, \quad V-B(2)$$

i.e., the kinetic energy associated with a wave pattern in a vertical plane is proportional to the squared amplitude of the vertical velocity pattern. (Horizontal components of eddy velocity and of wave amplitudes may be ignored since aircraft respond much more readily to vertical than to horizontal gusts.)

Figure V-B-1 shows idealized spectra of light-to-severe turbulence and their relationship to vertical velocities of lee waves of 1, 6, and 20 km horizontal wavelengths. The assumption is made that the total kinetic energy of these waves is made available to CAT eddies in a "cascading" process of energy, by which large eddies break up into smaller ones and redistribute their energy without losing any of it to buoyant or viscous forces. In accordance with such cascading conditions, a slope of $-5/3$ has been assigned to these spectra.

Figure V-B-1 shows that short lee waves need much smaller vertical motions to produce a certain level of CAT than do long lee waves.

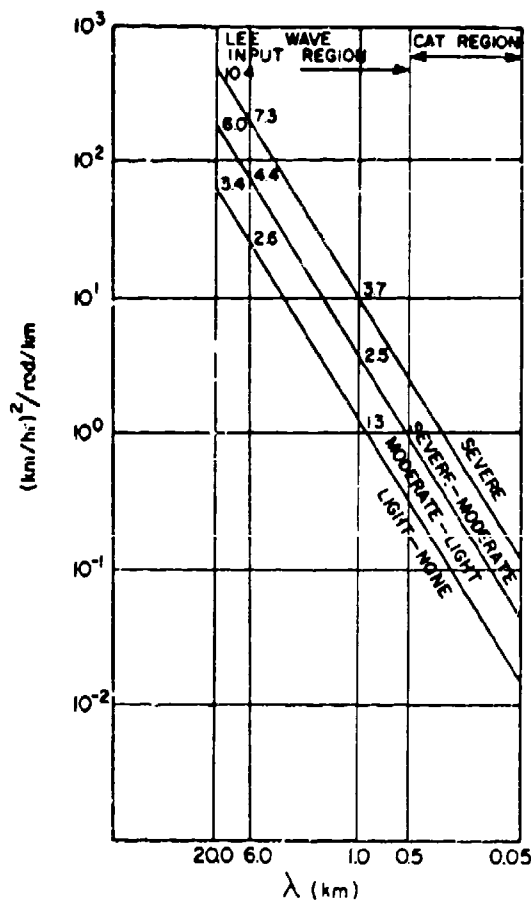


Figure V-B-1. Spectra for various intensity levels of CAT, extrapolated with " $-5/3$ slope" to lee wavelengths. Numerical values entered along the spectrum lines are maximum vertical velocities w_0 required to yield the necessary spectral densities at the appropriate wavelengths (from Reiter and Foltz, 1967).

It appears that if estimates can be made of the occurrence of lee waves, their wavelengths, and their maximum vertical velocities, w_0 , the maximum intensity of CAT that could be encountered downstream of these waves could be predicted (Note: The waves will have to break down into turbulence before CAT can be felt. This requires some time from the initiation of the wave pattern, and therefore CAT is more likely to be felt not directly over the mountain range that causes the disturbance of the flow pattern, but rather at a distance of tens of kilometers downstream (see Figure V-B-2)). Areas of severe CAT are located closer to the generating mountain range than areas of light CAT.



Figure V-B-2. Areas of most frequent occurrence of severe, moderate, and light to moderate CAT in the Western United States. Isopleths are given in terms of number of occurrences per 18 month, per 3600 (nm)^2 area (from Reiter and Foltz, 1967).

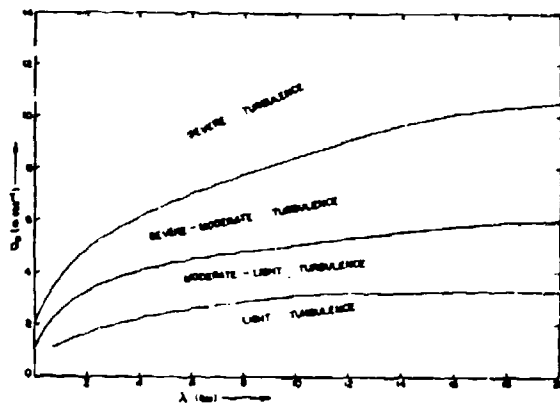


Figure V-B-3. Estimate of intensity level of CAT from maximum vertical velocity w_0 in lee waves of wavelength λ (from Reiter and Foltz, 1967).

Figure V-B-3 can be used to estimate the intensity of CAT if the lee-wave length, λ , and the maximum vertical velocity encountered in the inflection points of the waves are known (Foltz, 1967). λ can be estimated from satellite data, if lenticular cloud patterns are visible. Using lee-wave theory, λ could also be calculated from radiosonde data. Because of the shortcomings of the theory, however, and because of inaccuracies in measurements, this is usually a cumbersome and less reliable procedure (see Foltz, 1967, and Reiter and Foltz, 1967).

w_0 can be obtained from the approximate expression:

$$w_0 = 2-hbe^{-kb} k^2 U_1, \quad \text{V-B(3)}$$

where h is the height of the mountain range above the surrounding terrain, and b is its half width, given by:

$$z = \frac{hb^2}{b^2 + x^2}, \quad \text{V-B(4)}$$

where z is the height of the terrain at distance x from the crest of the mountain ridge. Typical values for h and b (in km) for some U.S. mountain ranges are given in Table V-B-1. Values for European and North African ranges, as well as for larger Mediterranean islands, remain to be calculated. U_1 is the wind component normal to the mountain range at gradient wind level. k is the horizontal lee-wave number ($k = \frac{1}{\lambda}$) and λ is the lee-wave length (in km).

Example:

$b = 2.5 \text{ km}$ Equivalent to Sangre de Cristo Mountains
 $h = 1.1 \text{ km}$ in Colorado
 $\lambda = 10 \text{ km}$
 $k = \frac{1}{10} \text{ km}^{-1}$
 $U_1 = 20 \text{ m sec}^{-1}$
 $w_0 = 2.7 \text{ m sec}^{-1}$

According to Figure V-B-3, one could expect light to moderate CAT under these conditions.

Table V-B-1. The height and half-width (km) of important United States mountain ranges (Reiter and Foltz, 1967).

Mountain Range	Height (h) (km)	Half-Width (b) (km)
Sangre de Cristo	1.1	2.5
Colorado Rockies	0.9	2.5
Southern Wasatch	0.3	2.2
Southern Sierras	1.1	8.0
Ruby Hills	0.8	2.0
Northern Sierras	0.5	2.5
Northern Wasatch (SLC DEN)	0.6	4.0
Montana Rockies	0.8	3.0
Big Horn Mountains	0.6	2.0
Black Hills	0.3	4.0
Wind River Range	1.0	2.0

C. AIR-SEA INTERACTIONS

The sea absorbs much of the solar energy that passes through the atmosphere, with only about 8% of it being reflected by the sea surface. In turn, the sea gives the energy back to the atmosphere partly as longwave radiation and partly as sensible heat exchange, but mainly as latent heat exchange through the evaporation of water. The latter accounts for the greatest part of the energy exchange and affects mostly the atmosphere above and for some distance down wind from the intake region.

The quantitative aspect of the exchange of the sensible and latent heat between the ocean and the atmosphere depends greatly on the difference between the temperatures of the sea surface and the air, the saturation vapor pressure of the sea surface, and finally the water vapor pressure of the air above it. Over-water air temperatures and dew points are measured and reported by ship observers, but the synoptic analysis of these parameters is not satisfactory, due partly to errors in taking these measurements and partly to the effect of the presence of the ship, as well as to the sparseness of the observation network. Using those measurements, the heat exchanges are presently best computed with formulas devised and tested by Norwegian workers in the 1940's. As is wave analysis/forecasting, sea-air interaction analysis/forecasting is a separate branch of oceanography, and a detailed presentation of its principles in this monograph is not appropriate.

The rate of evaporation and distribution of moisture in near-surface layers of the atmosphere have profound effects on the index of refraction (see Section V-E), and consequently on radar and radio propagation. Its detailed forecasting at present is still difficult and uncertain.

It should be mentioned that the properties of the surface air adjust relatively rapidly to the properties of the sea surface. In general, after a five-hour travel of an air mass paralleling the isotherms over the sea surface, equilibrium conditions will have been established. However, the surface wind seldom blows parallel to the sea-surface isotherms, and consequently the surface-air properties are seldom identical to the sea-surface properties.

The most intensive air-sea interactions take place in coastal regions where air masses with properties differing greatly from those of the sea surface move over the sea. In these areas some immediate effects of the energy feedback to the atmosphere can be noticed; in the Mediterranean these areas experience rapid cyclogenesis (see Section V-D).

D. SEA-SURFACE TEMPERATURE EFFECTS ON CYCLOGENESIS

During the cold season the waters of the Mediterranean are significantly warmer than the continental land surfaces, especially those of Europe and Asia Minor. This temperature contrast tends to produce an effect, albeit slight, of a "heat low" over the Mediterranean basin, similar to the much stronger heat low observed over the Iberian Peninsula during summer. The low-pressure effect caused by the underlying warm ocean surface is confined to the lowest layers of the troposphere over which the convective heating processes are distributing sensible and latent heat.

From the expression for geostrophic relative vorticity,

$$\zeta_g = \frac{g}{f} \nabla^2 Z + u \frac{\partial f}{\partial y}, \quad \text{V-D(1)}$$

we find that the Laplacian of the contour field, Z ,

$$\nabla^2 Z = \frac{\partial^2 Z}{\partial x^2} + \frac{\partial^2 Z}{\partial y^2} \quad \text{V-D(2)}$$

contributes positively towards the magnitude of cyclonic vorticity in the lower troposphere, if the contours are shaped as indicated schematically in Figure V-D-1. The term u in Eq. V-D(1) is the zonal wind speed, g is the acceleration of gravity, f is the Coriolis parameter, and $\beta = \frac{\partial f}{\partial y}$.

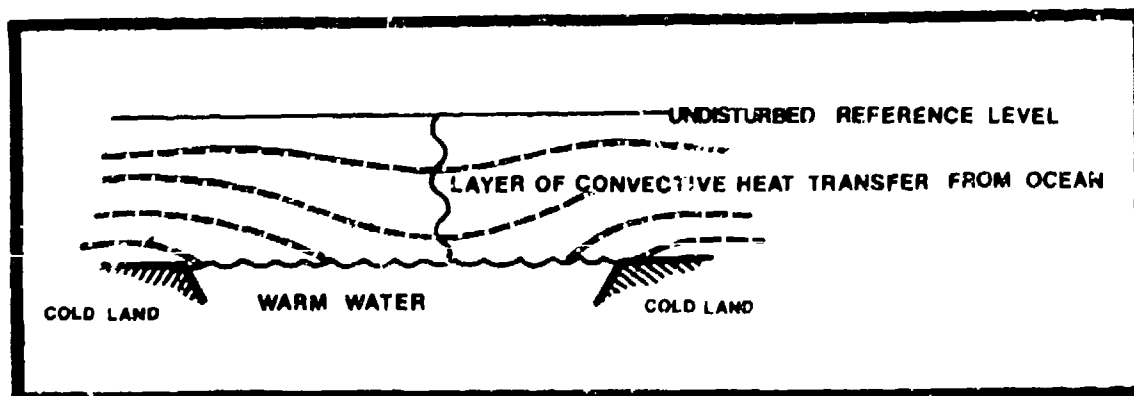


Figure V-D-1. Schematic of low-pressure effect caused by underlying warm ocean surface.

The movement of cold air masses, such as occurs during mistral situations in winter over relatively warm water (e.g., in the Gulf of Genoa), will produce a positive vorticity contribution in the lower troposphere through the Laplacian term in Eq. V-D(2), as sketched in Figure V-D-1. This contribution will be superimposed upon the vorticity patterns in the upper troposphere which are controlled by the jet stream systems (see Section III-B, para. 5). It is of interest to note that during winter the sea-surface temperature effects on cyclogenesis in the Gulf of Genoa, postulated in Eq. V-D(1) and Figure V-D-1, work in unison with the orographic effects described in Section III-C. This is perhaps the reason for cyclogenesis in this region to be so dominant during the cold season. In summer, the thermal effects of a relatively cool ocean are in opposition to the orographic effects. Consequently, cyclonic activity in the Gulf of Genoa is greatly diminished (Figure III-B-25). Of course, the summer jet stream systems are also much weaker and are located farther to the north than during winter.

E. REFRACTIVE INDEX PROBLEMS

1. Electromagnetic Refraction

The electromagnetic refractive index, n , is the ratio of the phase velocity, c , of a plane electromagnetic wave in a vacuum to its phase velocity, v , in a dielectric medium, such as the atmosphere, or:

$$n = \frac{c}{v} \quad \text{V-E(1)}$$

In a non-magnetic medium, the refractive index is given by

$$n = \sqrt{K}, \quad \text{V-E(2)}$$

where K is the relative dielectric constant (see Straiton, 1964).

Since n is a small quantity for the atmosphere, refractivity is usually defined as

$$N = (n-1) \times 10^6 \quad \text{V-E(3)}$$

For frequencies up to 70,000 MHz, refractivity is given by (see Straiton, 1964):

$$N = 77.6 \frac{P}{T} + \frac{3.73 \times 10^5 e}{T^2} \quad \text{V-E(4)}$$

where P is the atmospheric pressure in mb, T is the absolute temperature in degrees Kelvin, and e is the partial pressure of water vapor in mb. In the presence of strong vertical humidity gradients, which are often associated with inversions in the lower troposphere, the second term on the right side of Eq. V-E(4) assumes major importance.

From detailed vertical temperature and humidity soundings, one should be able, at least theoretically, to obtain vertical profiles of N . In reality, however, the atmospheric temperature and humidity stratification is of a much greater level of detail than can be measured by standard radiosonde ascents. Consequently, vertical N -profiles computed from radiosonde data should be taken only as a first approximation of actual conditions. Examples of detailed N -profiles are given in Figure V-E-1 (Straiton, 1964) and in Figure V-E-2 (Bean, 1964). These profiles were obtained from direct measurements of the radio refractivity by refractometers carried on an aircraft.

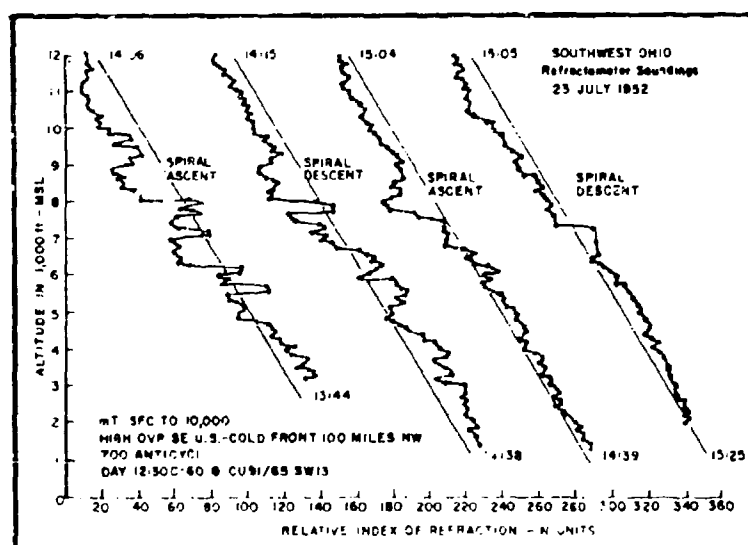


Figure V-E-1. A series of aircraft soundings made with the Crain refractometer in an area over central Ohio over a period of one hour illustrating the rapidity with which the shape of the profiles may vary due to topographic and convective effects (from Straiton, 1964).

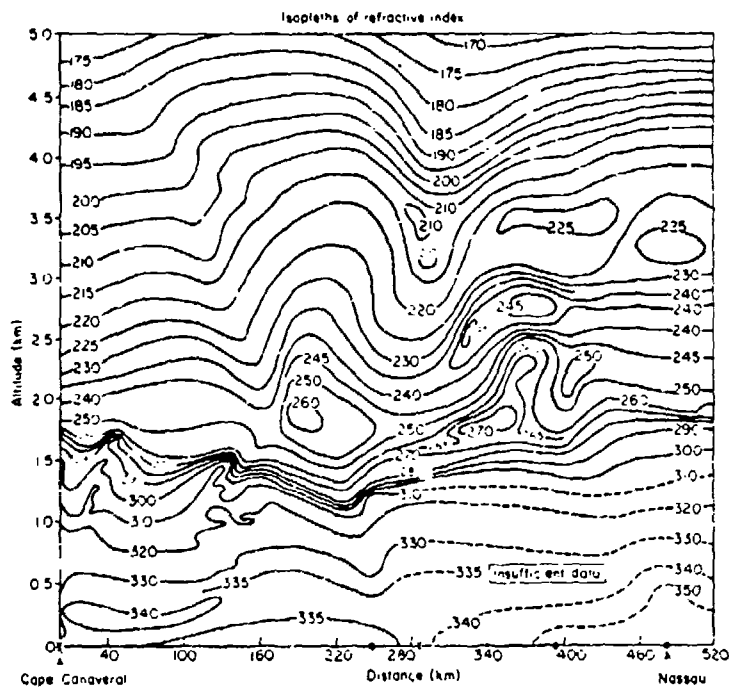
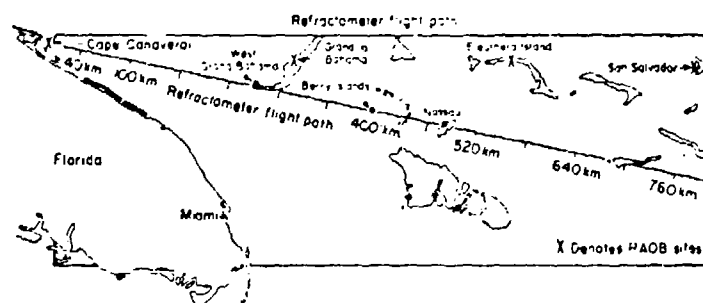


Figure V-E-2. Isopleths of refractive index and map of refractometer flight for 7 May 1957, Cape Canaveral to Nassau (from Bean, 1964).



If an electromagnetic wave travels in free space, its path follows a straight line. Due to the presence of variations in refractive index along the path of the wave, this path becomes curved -- increasingly so, the stronger the refractive index gradient. "Trapping" of a ray can occur when a layer exists in which the vertical decrease of N is greater than 157 N-units per kilometer or 48 N-units per 1000 feet. Values much greater than this are not at all unusual in some areas of the world, the Mediterranean being one of them. Figure V-E-3 illustrates schematically an elevated layer with a greater than usual decrease of N with height. The bottom of this layer is located at a height h_B and the top is at h_T .

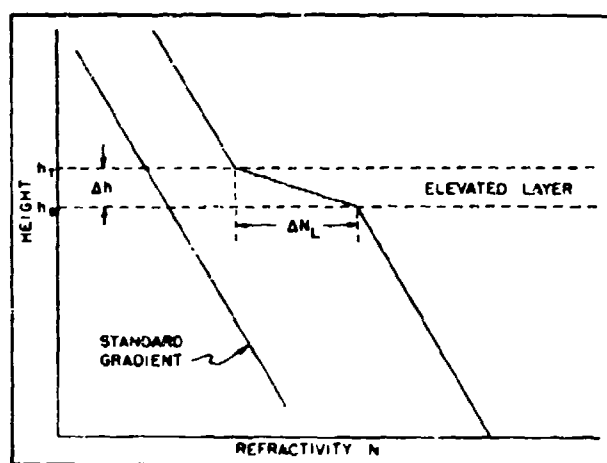


Figure V-E-3. Schematic diagram of decrease of N with height showing an elevated trapping layer with strong decrease of ΔN (from U.S. Navy Weather Research Facility, 1960).

If the radar or radio transmitter/receiver is located well below such a trapping layer, the electromagnetic wave beams will be refracted by the layer, but will still be able to penetrate the layer. This is shown in Figure V-E-4. If the angle α between the ray and the top surface of the trapping layer becomes smaller than a certain critical value ($\sim 1^\circ$), the beam will not penetrate this surface but will curve back into the layer towards the earth (Figure V-E-5). At $\Delta N/\Delta Z = -48$ N-units/1000 ft, the curvature of this ray with this critical angle of incidence equals the curvature of the earth. If N decreases with height by more than 48 N-units/1000 ft, the curvature of the ray will be proportionately larger, and will exceed the curvature of the earth. Under such

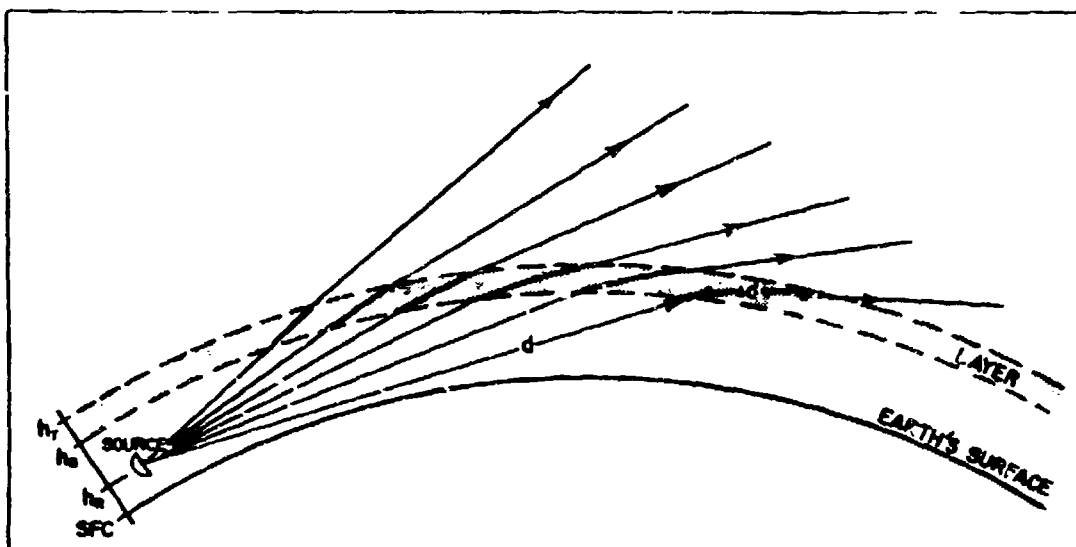


Figure V-E-4. Ray refraction by an elevated layer -- radar well below layer (from U.S. Navy Weather Research Facility, 1960).

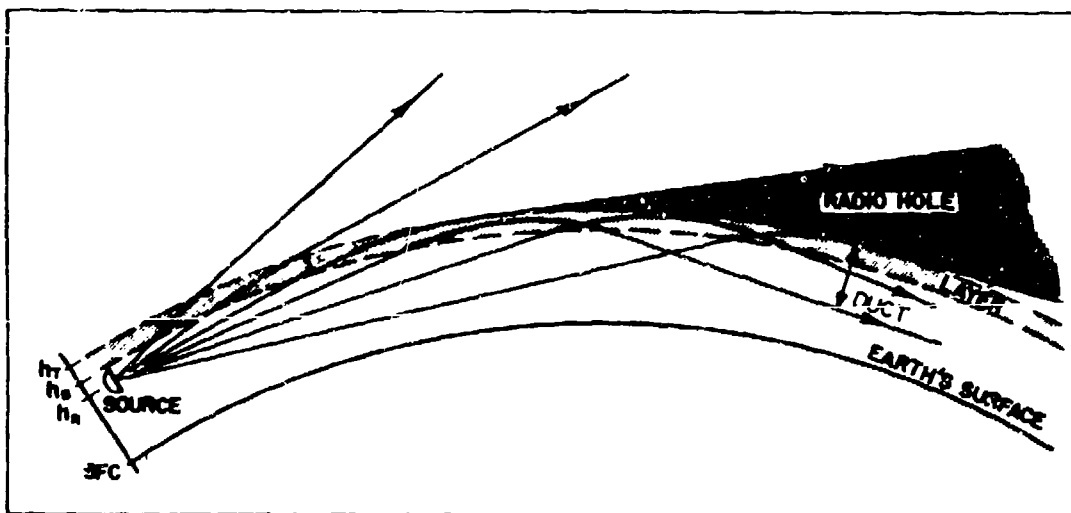


Figure V-E-5. Ray refraction by an elevated layer -- radar just below layer (from U.S. Navy Weather Research Facility, 1960).

conditions the ray will leave the bottom of the trapping layer and enter the non-trapping atmospheric layer below. One of two things might now happen -- the ray might strike the earth's surface and be reflected, or the ray will gradually recurve back into the trapping layer because of the unusual decrease of N with height in the atmosphere below the trapping layer. In both cases a "duct" is formed. A duct is defined as the layer between the top of the trapping layer and the lowest level to which the rays penetrate below this trapping layer (Figure V-E-5). The ray-trace diagram of Figure V-E-6 illustrates the frequently occurring conditions in which the duct varies in depth with range and also "leaks" energy through its top surface.

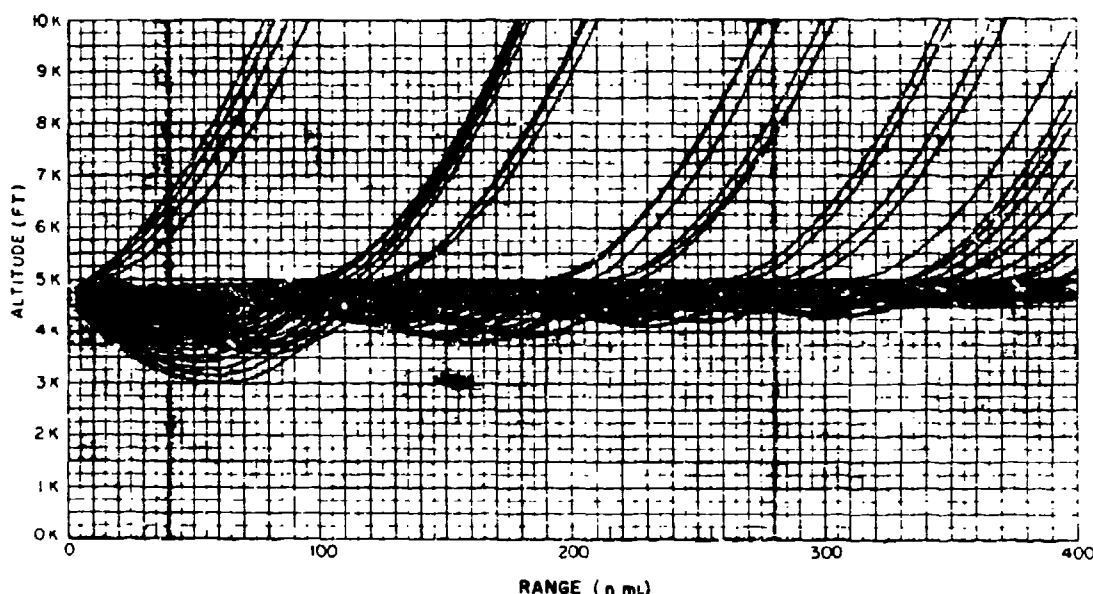


Figure V-E-6. A leaky duct layer. Family of ray paths calculated for a 500-ft thick horizontal interface, a gradient in the interface that changes linearly from 0.2 N units per foot at zero range to 0.05 N units per foot at 400 n mi, and a gradient above and below the interface of 0.01 N units per foot (from Purves, 1974).

Weather conditions in the Mediterranean quite frequently lead to ducting conditions that are adverse to radio communication and radar tracking. Under sirocco conditions, with warm moist air close to the ocean surface and dry air above an inversion, severe ducting conditions should be expected.

It should be pointed out that ducting layers, while inhibiting detection of targets and communication with aircraft flying above these layers at low angles of elevation, will cause extended ranges even beyond the visible horizon to objects located below the ducting layer. Radar transmissions within the ducting layer may, for instance, be bounced back from shore lines and other objects located beyond the visible horizon and which, under normal conditions, would not be displayed on the radar screen.

Discontinuities in electromagnetic refractivity along the path of an electromagnetic wave may also cause a certain amount of backscatter of the signal. In the lower troposphere such backscatter is mainly due to inhomogeneities in the water vapor distribution. In the upper troposphere, where water vapor is a rather sparse constituent of the atmosphere, backscatter should be expected mainly from temperature inhomogeneities, in accordance with Eq. V-E(4) (see Ottersten, 1969). Such backscatter makes turbulent regions and thermal convection in the atmosphere visible on the radar screen (especially on 10-cm radar) as certain types of "angels." Insects and sand carried by the wind constitute more obvious targets for radar backscatter. Again, sirocco conditions, with winds blowing off the Sahara and carrying sand, adversely affect the usefulness of radar because of the backscatter cluttering the radar screen. This is especially true close to the African coast, where the atmosphere under such wind conditions still contains relatively large sand particles.

2. Optical Refraction

The contribution of water vapor to refractivity at optical wavelengths is very small. Only at radio or radar wavelengths is there an enhanced field interaction with the water vapor molecule (Straiton, 1964). In the spectrum region of optical wavelengths, the water vapor contribution may be taken into account by considering virtual instead of actual temperatures. The water vapor effect increases sharply in the far-infrared and submillimeter portion of the spectrum and then remains essentially constant throughout the entire radio/radar region of the spectrum.

The curvature, K , of a light ray is given by

$$K = (n_\lambda - 1) \frac{P}{T_v} \frac{273}{1013.3} (r' - r), \quad \text{V-E(5)}$$

where n_λ is the refractive index (wavelength dependent), P is the barometric pressure in mb of mercury, T_v is the virtual temperature in °K, Γ' is the autoconvective lapse rate (equal to 3.42°C/100 m), and Γ is the actual lapse rate (counted negative in case of an inversion) (after Neuberger, 1951). According to List (1958), n_λ is close to 1.00028 for most wavelengths. Hence:

$$K = (75.4 \times 10^{-6}) \frac{P}{T_v^2} (3.42 - \Gamma) \quad \text{V-E(6)}$$

where P is measured in mb, T_v in °K, and Γ in °C/100 m.

In a homogeneous atmosphere $\Gamma = \Gamma'$, and hence the light rays are straight lines. For large lapse rates, convective activity produces inhomogeneities which cause scintillation. With strong inversions ($\Gamma < 0$), the curvature of the light rays approaches that of the earth's surface (which usually is several times larger) and total reflection (mirages) may occur. If the viewer is located below the inversion, he may see objects below the horizon whose images are reflected at the inversion. If the viewer is located at the top of a warm layer (perhaps with a superadiabatic lapse rate), objects above this layer will be reflected.

3. Acoustic Refraction

The velocity of sound, c , in a perfect gas is given by:

$$c = \sqrt{\frac{C_p}{C_v} \frac{RT}{M}} \approx 330 \text{ m sec}^{-1} \text{ at } 0^\circ\text{C}, \quad \text{V-E(7)}$$

where C_p and C_v are the specific heats at constant pressure and constant volume respectively, R is the universal gas constant, M is the molecular weight, and T is absolute temperature in °K (List, 1958). Thus, the velocity of sound depends mainly on temperature. Moisture effects enter through an adjustment of the molecular weight.

Inversions lead to a bending of the sound rays and, if critical incidence angles are exceeded, to a total reflection of sound. Wind and wind shear have a significant influence on the spreading of sound since it is added as a vector to the sound velocity, and wind and wind shear effects often outweigh the temperature effects. Peculiar focusing effects of sound waves may result at some distance from the source.

The dependence of the speed of sound on temperature is utilized by the acoustical radar. An intermittent sound signal is transmitted upward into the atmosphere and bounced back from an inversion. Measurements of the round trip travel time of the signal allow an accurate and continuous monitoring of the inversion height. It has been mentioned earlier that inversion conditions, especially with moist air below and dry air above, may seriously disturb radio and radar contact. It would appear that acoustic radar equipment would offer a convenient tool to monitor such adverse conditions.

REFERENCES

- Aerospace Science Div., 1968: Catalogue of European large-scale weather types. Revised by HQ 2nd Weather Wing, Aerospace Sci. Div., 68 pp.
- Agi, M., 1968: Wetter und Klimat im östlichen Mittelmeergebiet unter besonderer Berücksichtigung des zyperntiefs. Meteorologische Abhandlungen, Band LXXV, Heft 4, Institut für Meteorologie und Geophysik der Freien Universität Berlin.
- Air Ministry, Meteorological Office, 1962: Weather in the Mediterranean, general meteorology. Vol. 1 London: Her Majesty's Stationery Office, 372 pp.
- Angouridakis, V.E., 1973: Fog and weather types in the area of Thessaloniki, Zeitschr. f. Meteorologie 23(7/8), 237-241.
- Bean, B.R., 1964: Tropospheric refraction. Advances in Radio Research, Vol. 1, New York, Academic Press, 53-120.
- Baran, D.W., 1967: Large amplitude lee waves and chinook winds. J. Appl. Meteor., 6, No. 5, 865-877.
- Black, R.E., 1969: Cyclones and anticyclones in Europe. 2nd Weather Wing, USAF, AWS, 68 pp.
- Buettner, K.J., 1967: Valley wind, sea breeze, and mass fire: Three cases of quasi-stationary airflow. Colorado State University, Atmos. Sci. Paper No. 122.
- Chopra, K.P. and L.F. Hubert, 1965: Mesoscale eddies in wake of islands. J Atmos. Sci., 22, No. 6, 652-657.
- Clark, R.E., 1971: Forecasting the occurrence and onset of thunderstorms at Torrejon Air Base, Spain. 2nd Weather Wing, USAF, AWS.
- Clodman, J., G.M. Morgan, Jr. and J.T. Ball, 1961: High level turbulence, USAF, AWS Tech. Rep. 158, 1961.
- Colson, D., 1963: Analysis of clear air turbulence data for March 1962. Mon. Wea. Rev., 91, No. 2, 73-82.
- Defant, F., 1951: Local winds. Compendium of meteorology, Boston, Amer. Meteor. Soc., 655-672.
- Estoque, M.A., 1962: The sea breeze as a function of the prevailing synoptic situation. J. Atmos. Sci., 19, No. 3, 244-250.
- Fitzpatrick, T G., 1970: Forecasters handbook, Naval Weather Service Environmental Detachment, Naples, Italy, 67 pp.

- Flohn, H., 1964: Investigations on the tropical easterly jet. Bonner Meteorol. Abhand., No. 4.
- Foltz, H.P., 1967: Prediction of clear-air turbulence, Colorado State University Atmos. Sci. Paper No. 106.
- Frank, S.R. and R.D. Elliott, 1953: Operational weather of the Mediterranean area, area 1, AROWA 09-1053-097.
- Godev, H., 1970: On the cyclogenetic nature of the Earth's orographic form. Arch. Meteor. Geophys. Bioklim. Ser. A., 19: 299-310.
- Godev, N., 1971a: The cyclogenetic properties of the Pacific coast: possible source of errors in numerical prediction. J. Atmos. Sci. 28, 968-972.
- Godev, N., 1971b: Anticyclonic activity over South Europe and its relationship to orography. J. Appl. Meteor., 10, 1097-1102.
- Hann-Süring, 1939: Lehrbuch der Meteorologie, Verlag Willibald Keller, Leipzig, 2 Vols.
- Hess, P. and P. Brezowsky, 1969: Catalog of European large scale weather patterns. Deutscher Wetterdienst, Bericht, 15 (113), 56 pp.
- Hinkes, H., 1951: Frontenanalyse mit Hilfe von Bergbenachtungen. Ein Beitrag zur Frage des Voreilens der Kaltluft in der Höhe. Arch. Meteor. Geophys. Bioklim., Ser. A, 4: 238-262.
- Huschke, E.H., 1959: Glossary of meteorology. Boston: American Meteorological Society, 639 pp.
- Johns, D.H., 1964: High-level charts and jet streams. Proc. Joint ICAO/WMO Seminar Cairo-Nicosia, 1961, WMO Tech. Note No. 64, 104-115.
- Klein, W.H., 1957: Principal tracks and frequencies of cyclones and anticyclones in the Northern Hemisphere. U.S. Weather Bur. Res. Paper No. 40.
- Levi, M., 1967: Fog in Israel. Israel J. Earth-Sci., 16, 7-21.
- List, R.J., 1958: Smithsonian Meteorological Tables. Washington: Smithsonian Institution Press, 527 pp.
- Lovill, J.E., 1969: Transport processes in orographically induced gravity waves as indicated by atmospheric ozone. Colorado State University, Atmos. Sci. Paper No. 135, 78 pp.
- Lovill, J.E., 1972: Characteristics of the general circulation of the atmosphere and the global distribution of total ozone as determined by the Nimbus III satellite infrared interferometer spectrometer. Colorado State University, Atmos. Sci. Paper No. 180, 72 pp.
- Martin, F.L., and V.V. Salomonson, 1970: Statistical characteristics of subtropical jet-stream features in terms of MRIR observations from Nimbus II, J. Appl. Meteor., 9, No. 3, 508-520.
- Meschini, A., 1968: Le nevicate in Italia nel periodo 1959-1962 e la situazione di blocco del 14-22 Dicembre 1961. Rivista di Meteor. Aeronautica, 28, No. 3, 17-25.

- Neuberger, H., 1951: General meteorological optics. Compendium of meteorology, Boston, Amer. Meteor. Soc., 61-97.
- NOAA, (no date): Mediterranean planning guide. Environmental Data Service, 20 pp.
- Ottewill, H., 1969: Atmospheric structure and radar backscattering in clear air. Radio Science, 4, No. 12, 1179-1193.
- Petterssen, S., 1956: Weather analysis and forecasting, volume 1, New York: McGraw-Hill Book Co., Inc., 428 pp.
- Purves, C.G., 1974: Geophysical aspects of atmospheric refraction. Aerospace Systems Branch, Space Systems Division, Naval Research Laboratory, NRL Report 7725.
- Reiter, E.R., 1963: Jet-stream meteorology. Chicago: University of Chicago Press, 515 pp.
- Reiter, E.R., 1969: Atmospheric transport processes, part 1: energy transfers and transformations, AEC Critical Review Series, USAEC Report TID-24868.
- Reiter, E.R., 1971: Digest of selected weather problems of the Mediterranean. NAVWEARSCHFAC Tech. Paper No. 9-71.
- Reiter, E.R., 1972a: Atmospheric transport processes, part 3: hydrodynamic tracers, AEC Critical Review Series, USAEC Report TID-25731.
- Reiter, E.R., 1972b: Fundamental problems of atmospheric science: Remote sensing of the troposphere; Boulder, CO, NOAA and University of Colorado, 72091642 (NTIS: COM-72-51061).
- Reiter, E.R. and R.W. Hayman, 1962: On the nature of clear-air turbulence. Colorado State University, Atmos. Sci. Paper No. 28.
- Reiter, E.R. and A. Nania, 1964: Jet-stream structure and clear-air turbulence (CAT). J. Appl. Meteor., 3, No. 3, 247-260.
- Reiter, E.R. and H.P. Foltz, 1967: The prediction of clear-air turbulence over mountainous terrain. J. Appl. Meteor., 6, No. 3, 549-556.
- Rex, D.F., 1950a: Blocking action in the middle troposphere and its effect upon regional climate. I, Aerological study of blocking action. Tellus, 2, No. 3, 196-211.
- Rex, D.F., 1950b: Blocking action in the middle troposphere and its effect upon regional climate. II, The climatology of blocking action. Tellus, 2, No. 4, 275-301.
- Rex, D.F., ed., 1969: Climate of the free atmosphere. New York: Elsevier Publishing Co., 450 pp.
- Royal Netherlands Meteorological Institute, 1957: The Mediterranean; oceanographic and meteorological data.
- Stipaničić, V., 1961: Fogs on the east Adriatic coast. Translated and published for ESSA and NSF as Doc. IT 67-58040, Transactions and Reviews, 260-M8, No. 7 (1968).

- Straiton, A.W., 1964: Measurement of the radio refractive index of the atmosphere. Advances in Radio Research, Vol. 1, New York, Academic Press, 1-52.
- Sutcliffe, R.C., 1960a: The Mediterranean in relation to the general circulation, UNESCO/WMO seminar on Mediterranean synoptic meteorology, Rome, 1958. Meteorologische Abhandlungen, Band IX, Heft 1, Institut für Meteorologie und Geophysik der Freien Universität Berlin, 125-133.
- Sutcliffe, R.C., 1960b: Depressions, fronts and air mass modifications in the Mediterranean. UNESCO/WMO seminar on Mediterranean synoptic meteorology, Rome, 1958. Meteorologische Abhandlungen, Band IX, Heft 1, Institut für Meteorologie und Geophysik der Freien Universität Berlin, 135-143.
- U.S. Navy Weather Research Facility, 1960: Meteorological aspects of radio-radar propagation. NAVWEPS 50-IP-550.
- Vida, M., 1967: Die Witterung in Slowenien (Südostalpengebiet): Vb - Zyklonenzug. Intern. Congress on Alpine Meteor., Switzerland, 1966. Wissenschaftliche Abhandlungen, 230-234.
- Wallen, C.C., ed., 1970: Climates of Northern and Western Europe. New York: Elsevier Publishing Co., 253 pp.

APPENDIX A

A THEORETICAL DESCRIPTION OF THE RELATIONSHIP BETWEEN JET STREAMS AND CYCLONE DEVELOPMENT AND MOVEMENT (REITER, 1972)

Development of surface cyclones depends on the divergence of flow aloft which, in turn, is controlled by the changes in vorticity that an air parcel flowing on an isotropic or isobaric surface undergoes. This can be expressed by the vorticity equation in its simplest form:

$$\frac{dQ}{dt} = - DQ, \quad (1)$$

where the vertical component of the absolute vorticity, Q , is given by

$$Q = \frac{\partial v}{\partial x} - \frac{\partial u}{\partial y} + f. \quad (2)$$

u and v are the westwind and southwind components, and f is the Coriolis parameter, given by

$$f = 2\Omega \sin \phi. \quad (3)$$

Ω is the angular velocity of the earth ($\Omega = 7.292116 \times 10^{-5} \text{ rad sec}^{-1}$), and ϕ is the geographic latitude. The horizontal divergence, D , is given by

$$D = \frac{\partial u}{\partial x} + \frac{\partial v}{\partial y}. \quad (4)$$

$D > 0$ indicates divergence, $D < 0$ indicates convergence. The change of vorticity of an air parcel, $\frac{dQ}{dt}$, may also be written as

$$\frac{dQ}{dt} = \frac{\partial Q}{\partial t} + u \frac{\partial Q}{\partial x} + v \frac{\partial Q}{\partial y} + w \frac{\partial Q}{\partial z}. \quad (5)$$

The first term on the right side is the local change of vorticity. The remaining three terms give the advection of vorticity by horizontal (u, v) and vertical (w) wind components.

The vertical component of the absolute vorticity may also be obtained from

$$Q = \frac{V}{r_s} + \frac{\partial V}{\partial n} + f, \text{ where} \quad (6)$$

$V = \sqrt{u^2 + v^2}$ is the horizontal wind speed, r_s is the streamline radius, and n is the distance normal to the streamline, measured positive towards the left when looking downstream. The first term on the right of Eq. (6) is commonly referred to as the "curvature vorticity," the second term as the "shearing vorticity."

Figure A-1 shows the isotach and streamline configuration around a typical jet maximum. The divergence and convergence distribution, also indicated in this diagram, follows Eq. (1) and fits the change of vorticity along the streamlines. With divergence aloft at the jet stream level, air will be removed from a vertical column. This causes pressure falls at the base of the column, namely at the earth's surface:

$$\left(\frac{\partial p}{\partial t}\right)_0 = - \int_0^\infty \left(u \frac{\partial \rho}{\partial x} + v \frac{\partial \rho}{\partial y}\right) d\phi - \int_0^\infty \left(\rho \frac{\partial u}{\partial x} + \rho \frac{\partial v}{\partial y}\right) d\phi. \quad (7)$$

The first term contains the effect of advection of air masses with different densities. ϕ is the geopotential height. The second term, which usually exceeds the first term by one order of magnitude, gives the effect of velocity divergence. $\left(\frac{\partial p}{\partial t}\right)_0$ is the resulting pressure change at the earth's surface.

Divergence aloft, according to Eq. (7), gives rise to surface pressure falls, hence to cyclogenesis. In Figure A-1 this is indicated by the formation of a frontal wave in the left front quadrant of the jet maximum. Directions are given in terms of an observer looking downstream.

Also of note is the formation of a secondary wave in the right rear quadrant of the jet maximum. This wave will form only if the shearing vorticity effect of Eq. (6) exceeds the curvature vorticity effect, i.e., in relatively straight flow. This is the reason why over the Atlantic, under relatively zonal flow conditions, a whole family of wave disturbances (a "cyclone family") is usually found traveling in the jet stream belt. Over the United States, where cyclogenesis most frequently occurs with deep troughs to the lee of the Rocky Mountains, the curvature term in Eq. (6) usually exceeds the shearing vorticity term, prohibiting an upper divergence field from forming in the right rear quadrant of a jet maximum. Under such conditions usually only one major storm develops, without a tail of smaller "daughter cyclones."

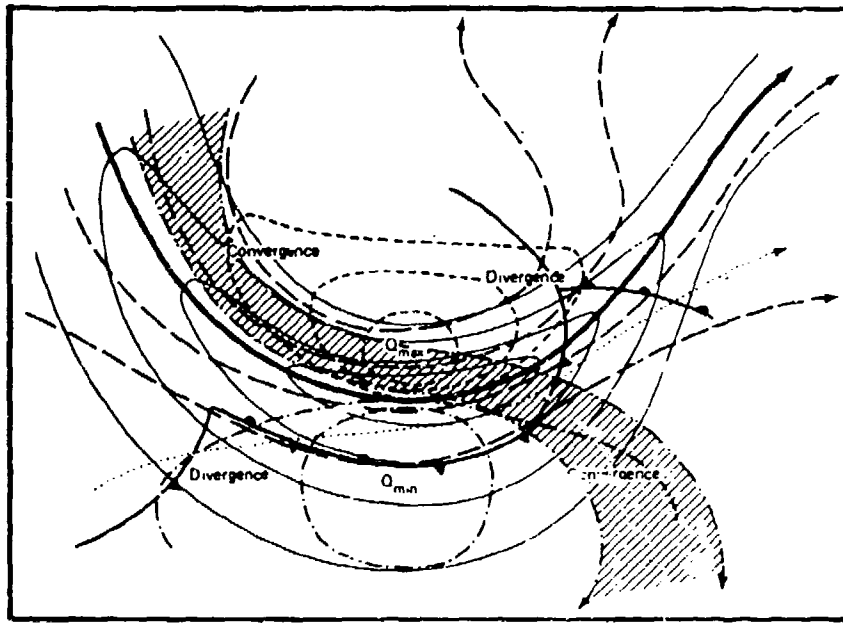


Figure A-1. Schematic diagram of surface fronts and absolute vorticity distribution and of divergence at the 300-mb level in the vicinity of a jet maximum. Isotachs are drawn as solid lines. \frown warm front. \blacktriangle cold front. Streamlines are dashed lines with arrows. Isolines of vorticity (arbitrary units) are short dashed lines on the cyclonic side and dash-dot lines on the anticyclonic side of the jet stream. The shaded band indicates movement of stratospheric air into the troposphere. The dotted line with arrow depicts tropospheric air ascending through the jet stream into the stratosphere.

From the foregoing discussion it is easily seen that the amplitude of the quasi-stationary or slow-moving planetary long waves strongly influences cyclone development patterns. In a large-amplitude, deep, long-wave trough the development of only one major storm should be expected -- something to bear in mind when watching for Genoa cyclogenesis. Under more zonal flow conditions and with poorly developed long-wave amplitudes, a sequence of cyclonic disturbance may develop in the jet stream belt.

REFERENCE

Reiter, E.R., 1972: Atmospheric transport processes, part 3: hydrodynamic tracers, AEC Critical Review Series, USAEC Report TID-25731.

APPENDIX B

BAROCLINICITY AND THERMAL WIND EQUATION

The term "baroclinicity" describes the fact that surfaces of equal density or equal temperature (marked T_1 , T_2 , etc. in Figure B-1(a)) are inclined against constant pressure surfaces (P_1 , P_2 ..., etc.). If both sets of surfaces are parallel to each other, the state of the atmosphere is called "barotropic" (see Figure B-1(b)).

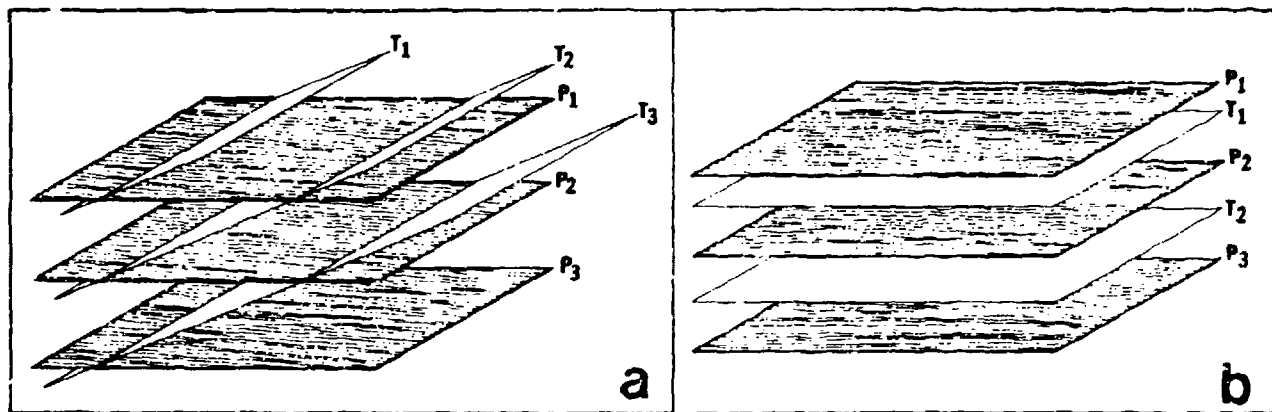


Figure B-1. Relationship between surfaces of equal temperature ($T_1 < T_2 < T_3$) and pressure ($P_1 < P_2 < P_3$) for (a) baroclinic and (b) barotropic atmosphere.

Underneath the core of the jet stream (STJ as well as PFJ) is found a baroclinic region in the atmosphere, the so-called "jet stream front." In Figure V-A-6 this is the region in which the potential isotherms slant strongly downward from left to right. Frontal zones in the lower troposphere are also characterized by baroclinicity.

Above the jet stream core is found a region of "negative baroclinicity," in which the potential isotherms slope in the opposite direction (Figure V-A-6).

According to the thermal wind equation, in a baroclinic atmosphere the geostrophic wind changes with height. The presence of vertical wind shears, therefore, is an indication of the baroclinic structure of the atmosphere. This equation may be written in component form as:

$$\frac{\partial v}{\partial z} = \frac{g}{fT} \frac{\partial T}{\partial x} + \frac{v}{T} \frac{\partial T}{\partial z} \quad \text{and} \quad (1)$$

$$\frac{\partial u}{\partial z} = - \frac{g}{fT} \frac{\partial T}{\partial y} + \frac{u}{T} \frac{\partial T}{\partial z} , \quad (2)$$

where u, v = wind components in the x and y direction respectively; f = Coriolis parameter; g = acceleration of gravity ($g = 9.81 \text{ m sec}^{-2}$); T = temperature in $^{\circ}\text{K}$; z = vertical coordinate.

The last terms on the right side of these two equations are usually insignificantly small. It may be stated, therefore, that the vertical wind shear depends mainly on the magnitude of the horizontal temperature gradient measured normal to the wind direction.

APPENDIX C

CONSERVATION OF ABSOLUTE ANGULAR MOMENTUM (REITER, 1972)

The absolute angular momentum, given by

$$\mathbf{G}_a = r_a^2 \boldsymbol{\Omega}_a \quad (1)$$

is conserved if

$$\frac{d\mathbf{G}_a}{dt} = \frac{\partial \mathbf{G}_a}{\partial t} + \mathbf{v} \cdot \nabla \mathbf{G}_a = 0, \quad (2)$$

where r_a is the magnitude of the position vector from the axis of rotation to the moving point and $\boldsymbol{\Omega}_a$ is the vector of absolute angular velocity, measured in an inertial coordinate system.

Using the following substitutions:

$$\boldsymbol{\Omega}_a = \boldsymbol{\Omega} + \boldsymbol{\Omega}_r$$

$$r_a = a \cos \phi$$

$$f = 2\Omega \sin \phi$$

$$u = \Omega_r a \cos \phi$$

$$\delta y = a \delta \phi,$$

where $\boldsymbol{\Omega}$ = vector of the earth's rotation and Ω is the magnitude of this vector

$\boldsymbol{\Omega}_r$ = rotational vector of the zonal wind velocity u measured relative to the earth's surface, and Ω_r is the magnitude of this vector

ϕ = geographic latitude

a = earth's radius,

we arrive at

$$\frac{\partial G_a}{\partial y} = 0 = \frac{\partial u}{\partial y} - f - \frac{u}{a} \tan \phi, \quad (3)$$

for steady ($\partial G_a / \partial t = 0$) and horizontal [$w(\partial G_a / \partial z) = 0$] motions (v is the vertical wind component). The term G_a is the magnitude of the vector \mathbf{G}_a .

Because of pressure gradients in the atmosphere, which lead to accelerations and decelerations, individual air parcels may not be considered as "closed systems." The absolute angular momentum, therefore, will not be conserved along air trajectories except under special conditions of indifferent hydrodynamic stability. Such conditions are frequently met on the anticyclonic side of well-developed jet maxima where, according to Eq. (3), the lateral wind shear is given by:

$$\frac{\partial u}{\partial y} = f + \frac{u}{a} \tan \phi, \quad (4)$$

Jet streams constitute powerful transport mechanisms by virtue of their great wind velocities and the vertical circulation systems with which they are associated.

The last term in Eqs. (3) and (4) represents the vorticity of a zonal current on a sphere. Under normal conditions of atmospheric flow in middle latitudes (i.e., outside extremely strong jet streams), one finds that $(u/a) \tan \phi \ll f$. Therefore, one may approximate

$$\frac{\partial u}{\partial y} \approx f, \quad (5)$$

for flow conditions under conservation of absolute angular momentum. The same condition may be derived from the equation of motion

$$\frac{\partial u}{\partial t} + u \frac{\partial u}{\partial x} + v \frac{\partial u}{\partial y} + w \frac{\partial u}{\partial z} = -\alpha \frac{\partial p}{\partial x} + fv, \quad (6)$$

under the assumptions of steady-state ($\partial u / \partial t = 0$), zonally symmetric ($\partial u / \partial x = 0$), and horizontal ($w = 0$) motions in the absence of external forces [$\alpha(\partial p / \partial x) = 0$]. If one assumes, furthermore, that v is constant everywhere ($dv/dt = 0$), the second component equation in the frictionless form of the equation of motion reduces to the equation for geostrophic flow, $fu = -\alpha(\partial p / \partial y)$. Annular rings of geostrophic motions thus may fulfill horizontal shear conditions commensurate with conservation of absolute angular momentum. This has been verified by "dishpan" experiments. These geophysical model experiments have demonstrated that the tendency toward conservation of absolute angular momentum plays an important role in the generation and maintenance of certain types of jet streams. Especially, the flow processes associated with the Hadley cell and with the formation of the subtropical jet stream may be considered to follow at least a tendency for conservation of absolute angular momentum. Lateral wind shears in

the tropical easterly jet stream over India during summer revealed a similar tendency. Individual jet maxima associated with the polar front jet stream frequently show broad regions on the anticyclonic side of the jet axis in which $\partial u / \partial y \approx f$, which suggests that absolute angular momentum is conserved in the rising warm air that flows through the jet stream system.

REFERENCE

Reiter, E.R., 1972: Atmospheric transport processes, part 3: hydrodynamic tracers, AEC Critical Review Series, USAEC Report TID-25731.

APPENDIX D

POTENTIAL VORTICITY (REITER, 1972)

For adiabatic motions between two isentropic surfaces separated by the pressure increment Δp , we may write the two-dimensional divergence as

$$D = - \frac{1}{\Delta p} \frac{d(\Delta p)}{dt} \quad (1)$$

The vorticity equation in the form of Eq. (1) in Appendix A then yields

$$\frac{d}{dt} \left(\frac{Q}{\Delta p} \right) = 0, \quad (2)$$

where Q , the vertical component of the absolute vorticity, is defined by Eq. (2) in Appendix A. From Eq. (2) above, the quantity in parentheses, called the potential vorticity, is conserved.

It can be shown that, under conservation of potential vorticity, zonal adiabatic airflow over a large N-S oriented mountain range will deform into Rossby waves with anticyclonic conditions over the mountain ridge and with a trough to the lee of the mountains. As Δp decreases during upslope motion within an isentropic slab of air, the absolute vorticity, Q , and hence the relative vorticity, decreases, which leads to anticyclonic flow. On the lee side, opposite conditions prevail. It has been shown that flow over a dome of cold air behaves in a similar manner. Furthermore, since potential vorticity conditions on the cyclonic side of the jet stream are different from those on the anticyclonic side, the flow under conservation of potential vorticity will be deflected to a different degree on the two sides of a jet maximum. This may lead to a splitting of the jet stream.

A northerly flow over an E-W oriented mountain range, such as the Alps, behaves differently from a westerly flow over the Rocky Mountains; the decrease in Δp during the upslope motion north of the mountain ridge will be, at least partly, compensated by the decrease in f , which causes little, if any, deflection of the current by a change of the relative vorticity. South of the Alps, however, the relative vorticity will not only have to overcome the increase in Δp in the denominator of Eq. (2) but also the decrease of f in the numerator. Consequently strong cyclonic development should be expected. The formation of Genoa cyclones may in part be due to such an effect. It can be

shown that in a northerly air current, baroclinic instability affects wave disturbances with shorter wavelength than it does in a westerly flow. Undoubtedly this effect is also of significance in Genoa cyclogenesis.

Under similar considerations of constant potential vorticity, southerly flow should lead to strongly anticyclonic flow conditions over the southern slopes of the Alps, but to reduced cyclogenetic activity along the northern slopes. The anticyclonic regime south of the mountain crest is expected to induce c inook or foehn conditions in the mountain valleys of the Alps.

REFERENCE

Reiter, E.R., 1972: Atmospheric transport processes, part 3: hydrodynamic tracers, AEC Critical Review Series, USAEC Report TID-25731.

APPENDIX E

INDIVIDUAL LARGE SCALE WEATHER TYPES

WITH EXAMPLES (AEROSPACE SCIENCE DIV., 1968)

1. INTRODUCTION

This appendix describes typical examples -- surface and 500 mb -- of individual European large scale weather types. Discussions of the synoptic features and synopses of the accompanying weather are presented in Paragraphs 2 through 29; the tables on facing pages give the percentage of days per month that the particular feature occurs and the number of consecutive days per month that it occurs. Each example shown is a good representation of the particular large scale weather type.

The surface and 500-mb maps on the following pages are reproduced from the daily weather maps of the German Weather Service, which uses certain analytical symbols that are not generally used by U.S. Navy forecasters or analysts. For convenient reference and interpretation, these symbols are depicted and defined in Figure E-1 below.














	Cold Front:	through all layers
	Cold Front:	surface
	Cold Front:	aloft
	Cold Front:	modified in temperature only (warming at surface)
	Warm Front:	through all layers
	Warm Front:	surface
	Warm Front:	aloft
	Warm Front:	modified in temperature only (cooling at surface)
	Occluded Front:	without temperature change at the surface
	Occluded Front:	with cooling at the surface
	Occluded Front:	with warming at the surface
	Quasi-Stationary Front	
	Line of Convergence or Trough	

Figure E-1. Analytical symbols used on weather maps.

2. CYCLONIC WESTERLY FLOW WITH SLIGHT SOUTHERLY COMPONENT (WS TYPE)

a. Description

Individual disturbances move along a frontal zone (which is shifted relatively far to the south) from the sea southwest of Ireland across the Bay of Biscay and France into east-central Europe, and from there in a northeasterly direction. Sometimes they also affect a low in upper Italy. The center of the central surface low is usually located south of 60N so that the northern North Atlantic and northern Europe are under the influence of high pressure and easterly flow. A wedge of the Azores high cell, which is situated south of the Azores, reaches the northwestern and northern part of Africa. The 1015-mb isobar is usually situated to the south of the Pyrenees Mountains and the Ligurian Sea.

b. Characteristic Weather

Generally the weather is very rainy. It is occasionally warm and humid in the spring. In summer it is cool. Strong cold air advection in winter and spring can bring heavy snowfall to the northern lowland plains. Strong winds are frequent with this synoptic type.

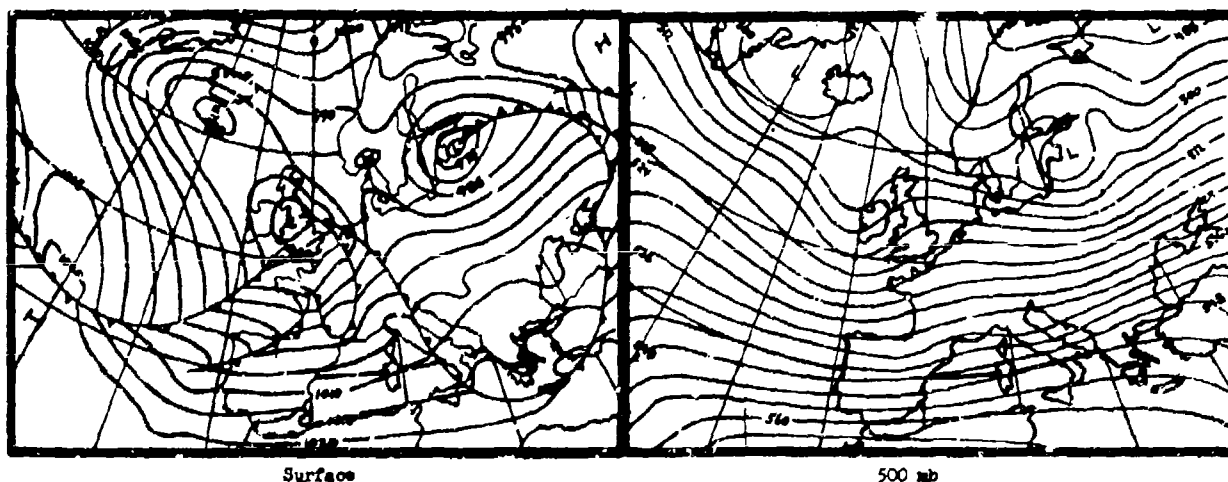


Figure E-2. Typical example of WS type.

TABLE E-1

NUMBER OF DAYS PER MONTH THAT WS WEATHER TYPE OCCURS *

JAN	FEB	MAR	APR	MAY	JUN	JUL	AUG	SEP	OCT	NOV	DEC
1.2	1.5	1.9	0.8	0.3	0.3	0.3	0.4	0.3	0.8	1.0	1.8

TABLE E-2

NUMBER OF CONSECUTIVE DAYS PER
MONTH THAT WS WEATHER TYPE OCCURS *

	1	2	3	4	5	6	7	8	9	10	11	12	≥13
JANUARY		1	3	5	1	1	2	2	4	1			1
FEBRUARY			5	3	1	3	1	1	1			1	2
MARCH		1	10	8	4	3	1	1		1	1	1	
APRIL	1		1	9	2		2						
MAY		1	1	2	1								
JUNE				3	2	1		1					
JULY		1	6			1					1		
AUGUST				1	1	3		1					
SEPTEMBER			2	1	1				1				
OCTOBER			5	5		3	1		1				
NOVEMBER	1		7	2	4	1	1			1			
DECEMBER	2	7	5	4	5	3	1	2	3				1

*The results shown in these and subsequent tables in this appendix were developed from data recorded during an unbroken 86-year period 1881 through 1967. The results shown in the even-numbered tables have not been normalized.

3. ANTICYCLONIC WESTERLY FLOW (WA TYPE)

a. Description

The frontal zone is displaced to about 60N. Individual disturbances travel from the sea west of Scotland across the northern part of the British Isles and southern Scandinavia to northwest Russia. Their fronts affect central Europe slightly and for only a short time. The surface and the upper lows are usually located north of 65N. The Azores high cell is situated north of the islands with a wedge reaching across southern Europe. The 1005-mb isobar generally follows the German coast line.

b. Characteristic Weather

The weather in the northern coastal areas of Europe is more unsettled in winter than in summer. Scattered precipitation in the form of rain is typical. The hilly region of southern Germany has generally fair weather with increasing cloudiness and intermittent light showers. Snow frequently accompanies this system in winter; in summer, thunderstorms are typical. Temperatures are usually mild in the coastal regions in winter but frosty near the Alps. In summer it is cool in the north and warm in the south. Strong winds are frequent in the coastal areas in winter.

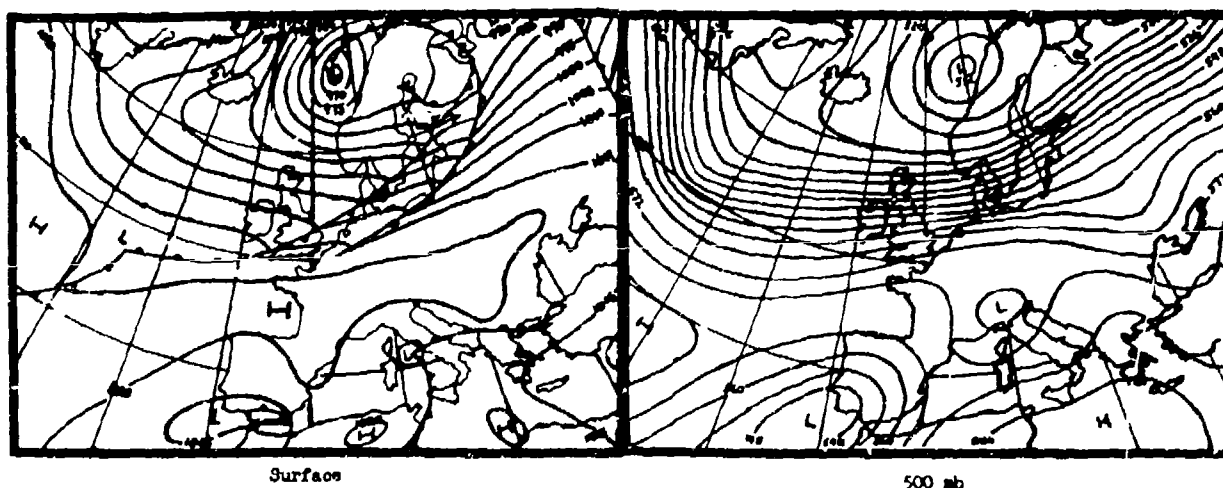


Figure E-3. Typical example of WA type.

TABLE E-3

NUMBER OF DAYS PER MONTH THAT WA WEATHER TYPE OCCURS

JAN	FEB	MAR	APR	MAY	JUN	JUL	AUG	SEP	OCT	NOV	DEC
1.8	1.0	1.1	1.0	1.1	1.2	2.1	2.6	2.2	2.2	1.6	1.2

TABLE E-4

NUMBER OF CONSECUTIVE DAYS PER
MONTH THAT WA WEATHER TYPE OCCURS

	1	2	3	4	5	6	7	8	9	10	11	12	≥13
JANUARY	1	1	15	7	1	2	3	3		1			
FEBRUARY			14	5	1				1				
MARCH	1	2	7	1	2	2	2			1			1
APRIL	2	5	10	4	1							1	
MAY		3	8	5	2	3	3						
JUNE		2	6	3	12	1		2	1	1			
JULY		8	3	12	6	8		3					
AUGUST	2	3	14	10	4	2	6	2			2		1
SEPTEMBER	1	1	10	8	6	3	2	3		2		1	
OCTOBER		5	14	7	5	4	2	1	1	1			
NOVEMBER	2	10	12	5	4	4		1					
DECEMBER	2	11	12		3		1	1					

4. CYCLONIC WESTERLY FLOW (WZ TYPE)

a. Description

Individual disturbances travel between 50N and 60N across the British Isles and North and Baltic Seas to eastern Europe. From here they curve to the northeast. This is considered to be the normal position of the Atlantic frontal zone. The surface low is frequently north of 60N causing a low pressure influence over the northern Atlantic and Norwegian Sea. The Azores high cell, which is situated in its normal position, usually has a wedge toward the southern part of France and, at times, toward the area of the Alps. Northern Italy generally experiences anticyclonic flow.

b. Characteristic Weather

Unsettled weather is characteristic of this type of flow. Precipitation alternates with scattered cloudiness. This condition lasts a half a day or more. Winter precipitation is rain; summer has thundershowers. Temperatures are cool in summer and mild in winter. Strong winds often occur.

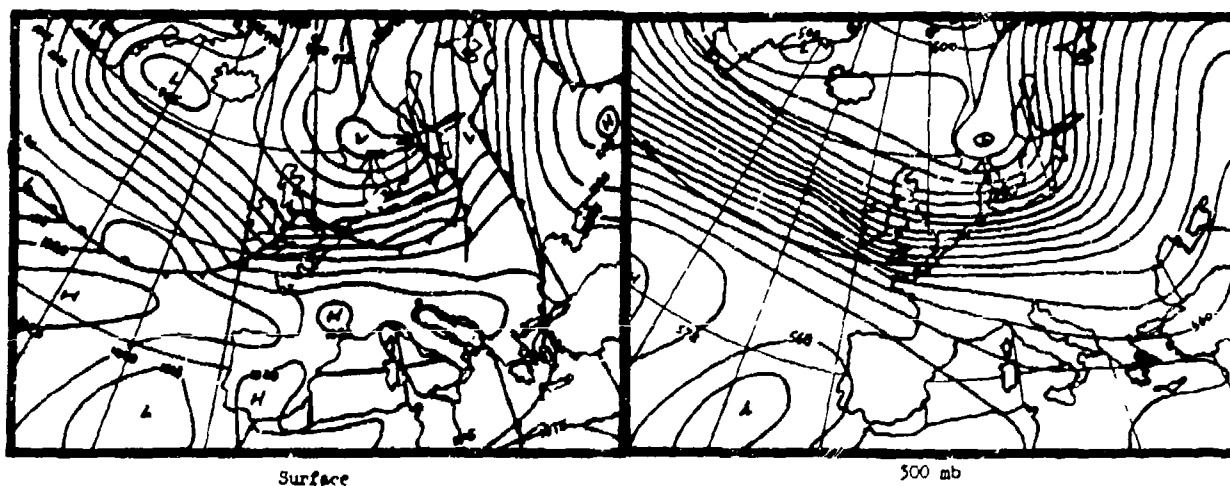


Figure E-4. Typical example of WZ type.

TABLE E-5

NUMBER OF DAYS PER MONTH THAT WZ WEATHER TYPE OCCURS

JAN	FEB	MAR	APR	MAY	JUN	JUL	AUG	SEP	OCT	NOV	DEC
4.0	3.4	3.3	3.6	3.6	4.6	6.4	7.5	4.5	4.6	4.2	5.4

TABLE E-6

NUMBER OF CONSECUTIVE DAYS PER
MONTH THAT WZ WEATHER TYPE OCCURS

	1	2	3	4	5	6	7	8	9	10	11	12	≥13
JANUARY	1		17	9	9	11	4	1	4		2	1	4
FEBRUARY		5	12	9	9	7	5	2	3	3		2	
MARCH		3	20	12	6	6	3	3	1		1		2
APRIL	4	7	15	14	10	8	7	3		1		1	
MAY	1	6	19	17	11	6		6	1	1	1		1
JUNE	6	7	18	13	13	9	3	5	4	1	2		1
JULY	2	11	24	21	11	13	3	11	5	3	1	1	3
AUGUST	6	10	23	15	18	8	5	7	4	3	1	2	6
SEPTEMBER	1	7	17	10	10	6	6	2	5	2			3
OCTOBER	1	4	18	9	11	8	3	5	3		1	2	5
NOVEMBER	4	11	11	12	12	8	6	1	2	3	4		
DECEMBER	4	15	19	14	12	4	5	2	9	3	2	1	3

5. HIGH PRESSURE BRIDGE OVER CENTRAL EUROPE (BM TYPE)

a. Description

A bridge of high pressure connects the Azores high, which is situated north of the Azores, with a high located over eastern Europe or over southern or central Russia. This bridge does not extend beyond 60N. Individual disturbances move along the frontal zone, situated north of 60N, and north of the British Isles across the Norwegian Sea toward northern Russia. The fronts affect the German coastal area only slightly. An upper wedge of the Azores high reaches to central Europe where it temporarily splits off to become an independent cell. The high pressure zone at the surface is at times displaced to 55N, so that large portions of central Europe are under easterly flow. The Mediterranean Sea is an area of low pressure.

b. Characteristic Weather

The weather is generally fair and dry with thunderstorm activity in mid-summer. The cold season is slightly unsettled in the coastal area with drizzle and fog or low stratus occurring infrequently. It is warm in summer. Sharp radiational cooling in winter makes this season cool.

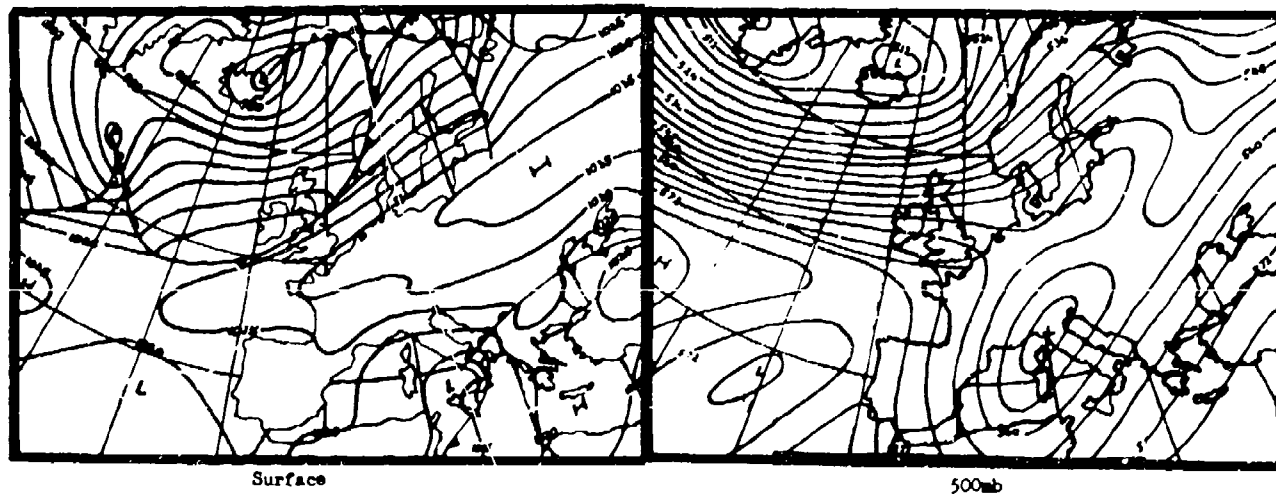


Figure E-5. Typical example of BM type.

TABLE E-7

NUMBER OF DAYS PER MONTH THAT BM WEATHER TYPE OCCURS

JAN	FEB	MAR	APR	MAY	JUN	JUL	AUG	SEP	OCT	NOV	DEC
1.1	1.2	0.9	1.5	1.0	1.2	1.1	1.9	1.9	2.1	2.6	3.0

TABLE E-8

NUMBER OF CONSECUTIVE DAYS PER
MONTH THAT BM WEATHER TYPE OCCURS

	1	2	3	4	5	6	7	8	9	10	11	12	≥13
JANUARY	4	3	9	2	3	1		1	1		1		
FEBRUARY		1	7	3	6	4	1	2					
MARCH		1	9	4	1	1							1
APRIL	1	7	8	6	3	1	1	1	1	1		1	
MAY	1	1	11	3	2	2			1			1	
JUNE	1	6	6	5	2		3	2				1	
JULY	1	7	11	6	2	2	1				1		
AUGUST		4	14	10	5	5	1	1					1
SEPTEMBER	1	4	10	8	5	5	2	2		1		1	1
OCTOBER	2	7	15	7	4	1	5	2	1	1			
NOVEMBER	4	11	17	9	11	1	4	1		1		1	
DECEMBER	7	11	15	12	3	7	6	1	1				

6. WELL-DEFINED CLOSED HIGH OVER CENTRAL EUROPE (HM TYPE)

a. Description

There is an extensive high over central Europe which closes at least temporarily in the upper levels -- a transitory upper wedge is not included here. The Atlantic frontal zone stretches with anticyclonic curvature north of 60N. Low pressure lies to the west and east side of the high. Aloft, significant troughs extend from the centers of low pressure over the northern North Atlantic (mostly Iceland-southern Greenland) and northern Siberia. Usually a trough exists over eastern Russia.

b. Characteristic Weather

In summer it is generally fair and dry with scattered chunderstorm activity. In the cold season ground fog and low stratus occur. In summer it is warm; in winter it is cool.

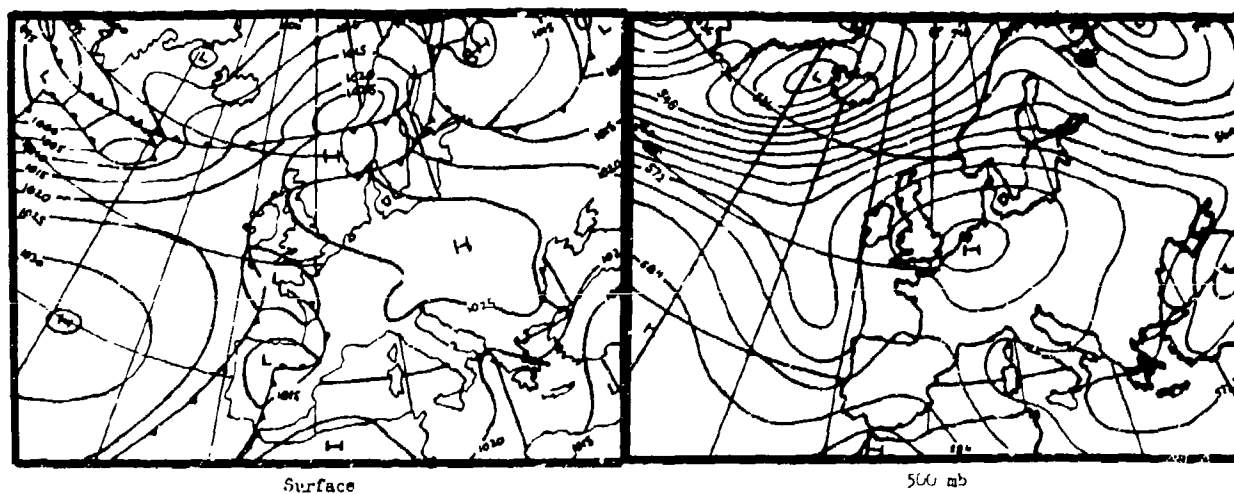


Figure E-6. Typical example of HM type.

TABLE E-9

NUMBER OF DAYS PER MONTH THAT HM WEATHER TYPE OCCURS

JAN	FEB	MAR	APR	MAY	JUN	JUL	AUG	SEP	OCT	NOV	DEC
4.5	3.7	3.3	2.2	2.9	2.9	3.3	3.0	4.5	3.3	2.2	2.0

TABLE E-10

NUMBER OF CONSECUTIVE DAYS PER
MONTH THAT HM WEATHER TYPE OCCURS

	1	2	3	4	5	6	7	8	9	10	11	12	≥13
JANUARY	1	7	17	11	10	8	3	5	2			2	5
FEBRUARY	1	5	17	8	7	3	5	4	1	3	1	2	2
MARCH	3	7	17	13	4	7	3	1	3	2	1		1
APRIL	2	12	12	9	6	1	2	3		1			
MAY	3	7	19	13	1	5	3	4	3				
JUNE	3	12	16	10	7	6	3	2		2	1		
JULY	2	15	29	12	9	4	3	2	1			1	
AUGUST	4	10	26	11	7	3	4		2			1	1
SEPTEMBER	2	4	20	19	12	4	3	6	2	3	1		2
OCTOBER	6	11	13	14	7	4	6		3			1	
NOVEMBER	9	17	9	6	3	2	2	1	1	1		1	1
DECEMBER	6	19	10	13	7	4	1	5		1			

7. ANTICYCLONIC SOUTHWESTERLY FLOW (SWA TYPE)

a. Description

The frontal zone extends from the sea southwest of Iceland in a northeasterly direction towards northwest Russia. It is framed by a high pressure zone over western or central Russia and by a zone of low pressure over the Atlantic and the northern Norwegian Sea. Individual disturbances travel along the frontal zone which follows the Norwegian coast toward the Arctic Sea. There, they are either steered towards the southeast by an upper trough lying over western Russia, or they continue eastward along the north side of another high located east of the Ural Mountains. Very often there is a high pressure area over Greenland and the northern Norwegian Sea so that Iceland, though within the northeasterly flow, is on the cold side of the broad trough.

b. Characteristic Weather

In the hilly terrain of Bavaria, it is mostly fair and dry. The cold season has ground fog and occasional low stratus. It is generally cloudy along the coastal area with intermittent light precipitation. All seasons are warmer than normal. Strong winds occur along the coastal areas in winter.

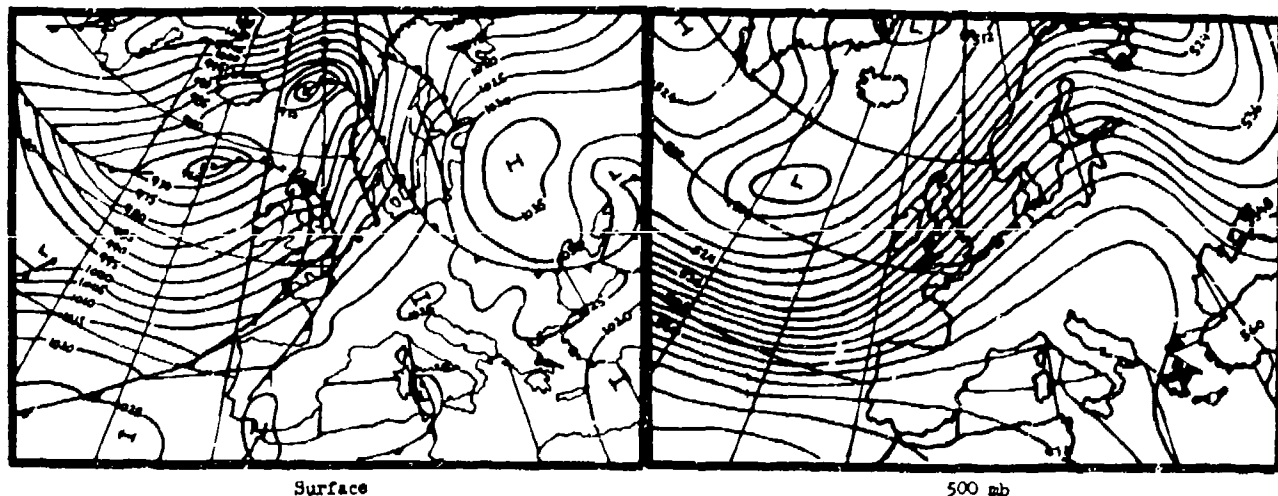


Figure E-7. Typical example of SWA type.

TABLE E-11

NUMBER OF DAYS PER MONTH THAT SWA WEATHER TYPE OCCURS

JAN	FEB	MAR	APR	MAY	JUN	JUL	AUG	SEP	OCT	NOV	DEC
0.8	0.7	0.6	0.5	0.4	0.2	0.3	0.2	0.4	0.7	0.7	0.7

TABLE E-12

NUMBER OF CONSECUTIVE DAYS PER
MONTH THAT SWA WEATHER TYPE OCCURS

	1	2	3	4	5	6	7	8	9	10	11	12	≥13
JANUARY	1	2	6	4	1	3		1					
FEBRUARY	1	2	6	1	2		1	1	1				
MARCH		2	8	4			2						
APRIL		4	3	4	1								
MAY	1	1	1	1	3		1						
JUNE			2	1	1	1							
JULY		1	2	2	1	1							
AUGUST			1	4	3								
SEPTEMBER		1		2	1	1			2				
OCTOBER	1	3	6	5	2	2	1		1				
NOVEMBER	2	4	9	2			1						
DECEMBER	2	4	5	2	3	1	1						

8. CYCLONIC SOUTHWESTERLY FLOW (SWZ TYPE)

a. Description

The frontal zone extends from the sea area north of the Azores across the English Channel in a northeasterly direction towards northern Russia. It is framed by a high centered over south or southwestern Russia with a wedge stretching southwestward across the central Mediterranean to northwest Africa, and by a zone of low pressure located over the North Atlantic, Norwegian Sea and Arctic Ocean. Individual disturbances travel from the area north of the Azores across the British Isles and Scandinavia to the coast of the Arctic Ocean. Their fronts seriously affect all of central Europe. A cold northwesterly flow along the southeast side of the Greenland high covers almost the entire Norwegian Sea and the northwestern part of the North Atlantic.

b. Characteristic Weather

The weather is unsettled (especially in winter) with frequent precipitation. This is mostly rain except in southeastern and central Europe and along the northern edge of the Alps. In summer there is little rain just to the north of the Alps. Summer is only moderately warm, but the remaining seasons are warmer than normal. Strong to gale force winds occur in the northern lowland plains during the cold season.

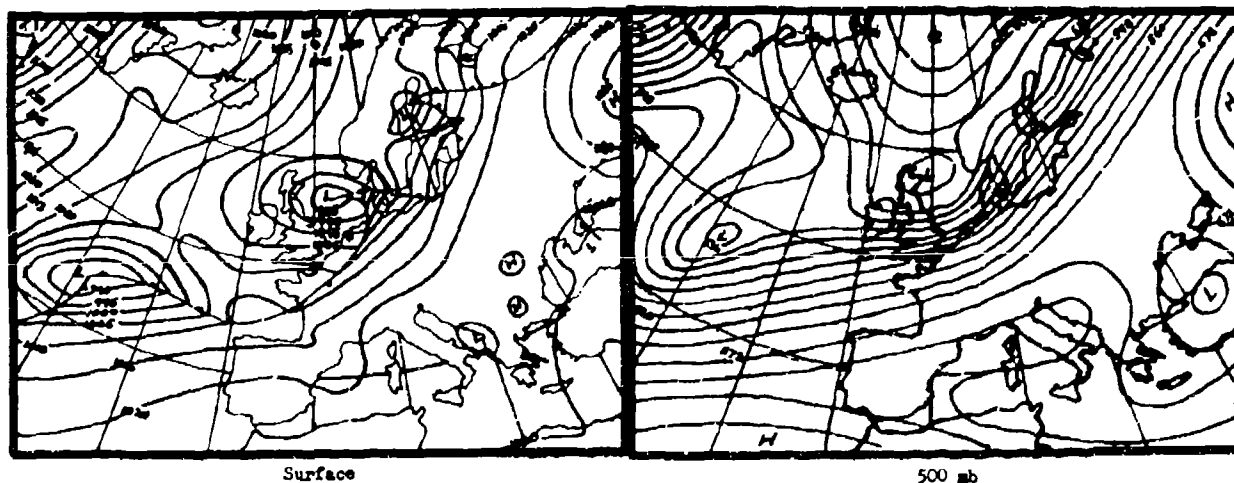


Figure E-8. Typical example of SWZ type.

TABLE E-13

NUMBER OF DAYS PER MONTH THAT SWZ WEATHER TYPE OCCURS

JAN	FEB	MAR	APR	MAY	JUN	JUL	AUG	SEP	OCT	NOV	DEC
1.1	0.5	0.3	0.1	0.3	0.3	0.1	0.2	0.1	0.6	0.7	0.5

TABLE E-14

NUMBER OF CONSECUTIVE DAYS PER
MONTH THAT SWZ WEATHER TYPE OCCURS

	1	2	3	4	5	6	7	8	9	10	11	12	≥13
JANUARY		1	9	6	3	2	1	1	1		1		
FEBRUARY		2	3	2	3		1		1				
MARCH		1	1		2	1							
APRIL		2	1	2	1								
MAY	1	1	1	3	2		1						
JUNE			1	1			1	1					
JULY		1		2									
AUGUST	1	2	1	2	1								
SEPTEMBER		2	2		1								
OCTOBER		1	6	6	3				1				
NOVEMBER		1	3	5	5	2			1	1			
DECEMBER		2	7	2	2								

9. ANTICYCLONIC NORTHWESTERLY FLOW (NWA TYPE)

a. Description

The center of the subtropic high cell lies at the western edge of Europe. It is displaced northeastward from its normal position, but it is not blocking -- usually it is not farther north than 50N. Low pressure exists over the northern North Atlantic and Norwegian Sea with troughs extending to the western Atlantic, western Russia and the eastern Mediterranean. The frontal zone extends in an anticyclonic curve north of the British Isles, thence in a southeasterly direction to western Russia. Individual disturbances pass along the front from the central Atlantic south of Iceland, to Scandinavia and then toward western and southern Russia. Their fronts sometimes affect the eastern part of central Europe.

b. Characteristic Weather

Western central Europe is fair and dry while east-central Europe has slightly unsettled weather with local light precipitation. Precipitation falls partly as rain in winter. The eastern Alpine foothills will be temporarily under upslope effect. Temperatures in the west will be near normal; however, in the east they will be mild in the low levels in winter and cool in the warm season.

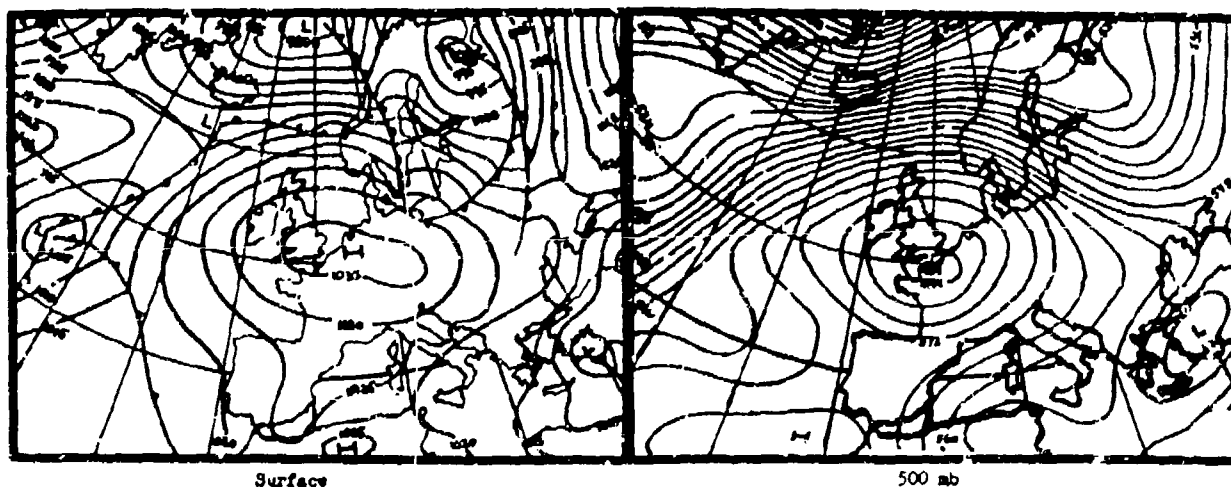


Figure E-9. Typical example of NWA type.

TABLE E-15

NUMBER OF DAYS PER MONTH THAT NWA WEATHER TYPE OCCURS

JAN	FEB	MAR	APR	MAY	JUN	JUL	AUG	SEP	OCT	NOV	DEC
1.1	1.1	1.1	1.0	1.2	2.3	3.1	2.3	1.0	0.8	1.1	0.8

TABLE E-16

NUMBER OF CONSECUTIVE DAYS PER
MONTH THAT NWA WEATHER TYPE OCCURS

	1	2	3	4	5	6	7	8	9	10	11	12	≥13
JANUARY	1	3	1	4	2	2	1		3		1		
FEBRUARY	1	2	6	1	3	3		2	1				
MARCH	1	4	8	2	3	3	2	1	1				
APRIL	2	5	7	5	2	3							
MAY		4	7	5	4	2	1	1					
JUNE	4	14	17	7	1	6	4					1	
JULY	10	17	11	15	9	4	1	3	1		2		
AUGUST	3	8	13	11	6	2	2						
SEPTEMBER	4	7	4	4	3	1	2		1				
OCTOBER	6	6	4	3			2						
NOVEMBER	5	5	12	2	4		1	1					
DECEMBER	5	5	12	1	1		1						

10. CYCLONIC NORTHWESTERLY FLOW (NWZ TYPE)

a. Description

A cell of the subtropical high (not blocking) is displaced north-eastward to the western Bay of Biscay with its center south of 50N. A low pressure area is over the northwestern Atlantic and Scandinavia with troughs extending to eastern Europe and southern Russia -- the troughs have extensions into the central Mediterranean Sea. The frontal zone stretches in an anti-cyclonic curve to the sea west of Scotland, curving over the British Isles in a southeasterly direction toward southeastern Europe. Individual disturbances travel along this zone from the central North Atlantic across England on a southeasterly track to central Europe. From there, they travel along the eastern rim of the Alps and across the northern edge of southeastern Europe, toward the east or northeast. Secondary disturbances form over northern Italy and travel eastward.

b. Characteristic Weather

The weather is generally very unsettled with frequent showery precipitation and heavy precipitation in the warm season. Precipitation occurs in the form of snow during the winter. There is strong upslope effect at the Alps. Temperatures are colder than normal in all seasons; however, there is mitigation of temperatures in the lower levels in winter. Strong winds occur in the east.

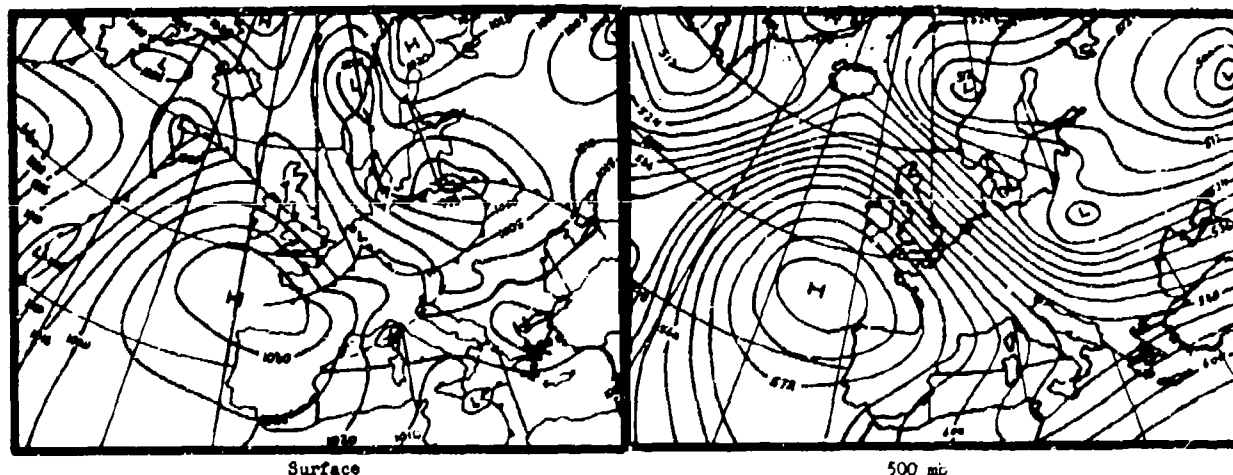


Figure E-10. Typical example of NWZ type.

TABLE E-17

NUMBER OF DAYS PER MONTH THAT NWZ WEATHER TYPE OCCURS

JAN	FEB	MAR	APR	MAY	JUN	JUL	AUG	SEP	OCT	NOV	DEC
1.5	1.1	0.9	1.2	0.8	1.2	2.2	1.5	1.2	1.0	1.2	1.5

TABLE E-18

NUMBER OF CONSECUTIVE DAYS PER
MONTH THAT NWZ WEATHER TYPE OCCURS

	1	2	3	4	5	6	7	8	9	10	11	12	≥13
JANUARY	2	1	3	6	6	3	1	1		1			
FEBRUARY	4	1	13	5	2	1	2				1		
MARCH	4	4	8	5	3	3							
APRIL	2	3	8	11	4	2							
MAY		1	7	6	4	1							
JUNE			7	8	4		2	1	1				
JULY		10	9	17	5	2	3	2					
AUGUST		8	9	7	2	3	1	3					
SEPTEMBER		3	6	7	4	3		1	1				
OCTOBER	1	5	5	4	2	2	3						
NOVEMBER	3	2	7	6	5	1	2						
DECEMBER	1	7	8	5	7	2	2						

11. WELL-DEFINED CLOSED HIGH OVER NORWEGIAN SEA (HNA TYPE)
(ANTICYCLONIC FLOW OVER CENTRAL EUROPE)

a. Description

There is a closed, blocking high over the southern Norwegian Sea. Very often it is connected with the Polar high and has a strong wedge extending in a southeasterly direction as far as central Europe. The Atlantic frontal zone splits over the western Atlantic into two branches: one passes over Greenland to the north, the other extends eastward across the south-central Atlantic. Individual disturbances occasionally travel into the Mediterranean along the latter frontal zone. There are meridional troughs on the sides of the high -- one in the western Atlantic, and one extending from the Arctic Ocean to the Black Sea with a weak extension to the west. This sometimes results in a cut-off upper low over southwestern Europe. There is cyclonic northerly flow over eastern Europe and western Russia, with fronts occasionally affecting eastern Germany. Low pressure extends over the western and central Mediterranean Sea.

b. Characteristic Weather

Weather is often fair in the warm season with increasing cloudiness and thunderstorms towards the east. Winter has mostly radiation weather -- cold to very cold. Spring is usually only moderately warm. Summer is warm, sometimes sultry, but not hot.

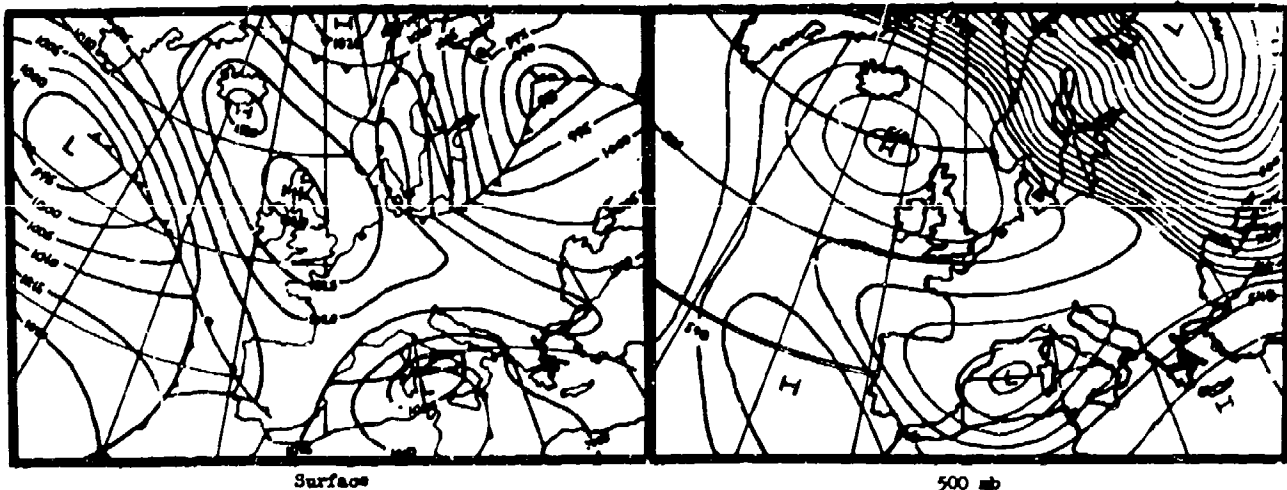


Figure E-11. Typical example of HNA type.

TABLE E-19

NUMBER OF DAYS PER MONTH THAT HNA WEATHER TYPE OCCURS

JAN	FEB	MAR	APR	MAY	JUN	JUL	AUG	SEP	OCT	NOV	DEC
0.4	0.4	0.7	1.5	1.7	2.0	0.8	0.8	0.9	1.0	0.6	0.5

TABLE E-20

NUMBER OF CONSECUTIVE DAYS PER
MONTH THAT HNA WEATHER TYPE OCCURS

	1	2	3	4	5	6	7	8	9	10	11	12	≥13
JANUARY			4	2	2	2							
FEBRUARY	1	1	3	1	1	2	1						
MARCH	1		10	5		1	1		1				
APRIL		7	11	5	4	1	1	2	1				
MAY		2	10	8	7	4	2		1	1			
JUNE		5	11	6	6	4	1		1			1	
JULY		2	4	6	1	2							
AUGUST	1	4	5	1	1	3	2	1					
SEPTEMBER		3	8	4	3	1	1	2					
OCTOBER	3	4	5	2	2	2	2	1					
NOVEMBER	2	3	5	1		2							
DECEMBER	1	2	2	2	3	2		1					

12. WELL-DEFINED CLOSED HIGH OVER NORWEGIAN SEA (HNZ TYPE)
(CYCLONIC FLOW OVER CENTRAL EUROPE)

a. Description

The closed, blocking high over the Norwegian Sea is often connected with the Polar high. It is flanked by meridional troughs. The easterly trough stretches from the low pressure area over northern Russia across Scandinavia to western Europe. It deflects the cold air stream from central Europe. On the eastern side of the upper trough there is advection of milder air from the southwest. In this stage, cut-off lows lie over western and west-central Europe with cyclonic weather. The eastern branch of the cold air stream flows across Russia to the Ural Mountains. The Atlantic frontal zone splits over the west Atlantic into two branches: one follows along the west coast of Greenland, and the other is directed to the south-central Atlantic. Individual disturbances move across the Bay of Biscay into central Europe.

b. Characteristic Weather

The cold season is cloudy with snowfall. In summer there is varying cloudiness with frequent thunderstorm activity toward the south. These are often warm front thunderstorms with considerable amounts of precipitation. Winter is cold. The warm season in the north is cool, but the hilly parts of southern Germany are warm and humid.

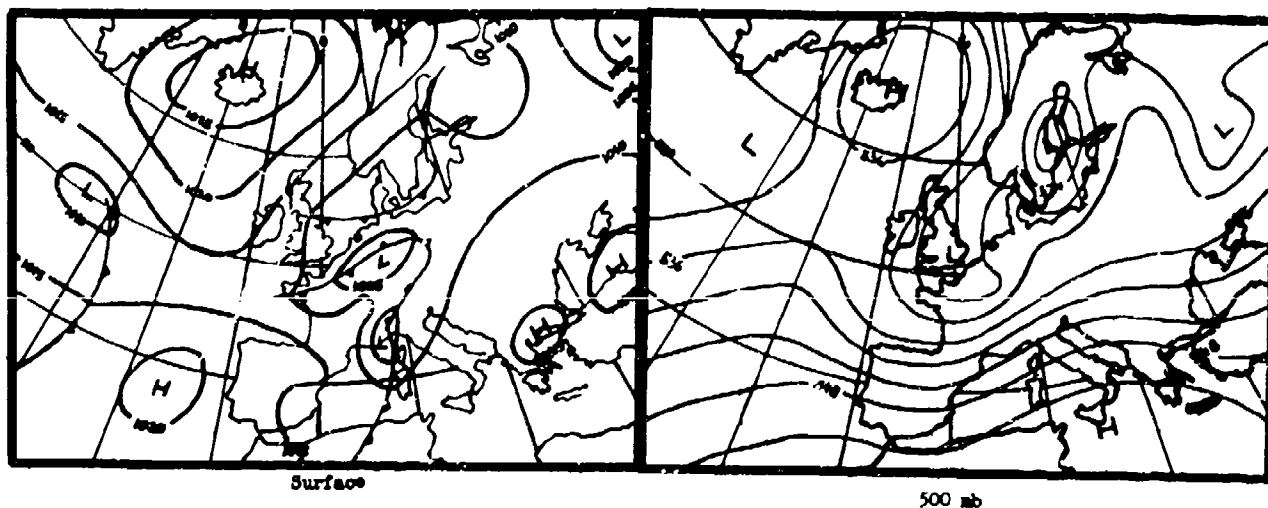


Figure E-12. Typical example of HNZ type.

TABLE E-21

NUMBER OF DAYS PER MONTH THAT HN2 WEATHER TYPE OCCURS

JAN	FEB	MAR	APR	MAY	JUN	JUL	AUG	SEP	OCT	NOV	DEC
0.2	0.2	0.4	0.6	0.6	0.6	0.3	0.3	0.2	0.7	0.3	0.2

TABLE E-22

NUMBER OF CONSECUTIVE DAYS PER
MONTH THAT HN2 WEATHER TYPE OCCURS

	1	2	3	4	5	6	7	8	9	10	11	12	≥13
JANUARY	1	3		2	1	1			1				
FEBRUARY	2	1	2	1		1	1						
MARCH		2	5	2	3		1						
APRIL	1	1	3	4		1	2						
MAY		1	5	3	2					1	1		
JUNE	1	3	8	1	3			1					
JULY		2	4	4									
AUGUST	1	2	3	1									
SEPTEMBER		2	3										
OCTOBER	3	3	5	2	3	1							
NOVEMBER		4	2	1	1	1							
DECEMBER		2	1	1	1	1							

13. WELL-DEFINED CLOSED HIGH OVER BRITISH ISLES (HB TYPE)

a. Description

A closed, blocking high over the British Isles is flanked by two marked meridional troughs. One lies over the western Atlantic, the other one stretches from the Arctic Sea to eastern Europe. The Atlantic frontal zone stretches in a wide anticyclonic curve across Iceland in a southeasterly direction to western Russia. Individual disturbances of usually minor intensity travel along it from the Norwegian Sea to eastern Europe and continue in a northeasterly direction. West-central Europe is little affected by this frontal zone. The southern area is covered by a trough, often of only weak intensity, stretching from the Black Sea to southwestern Europe.

b. Characteristic Weather

The weather is mostly fair and dry with northerly to northeasterly flow into western and central Europe. It is cloudy with infrequent scattered light precipitation in the east. Slight upslope effects occur at times along the eastern Alps. It is moderately warm during most of the year; however, in mid-winter it gets very cold.

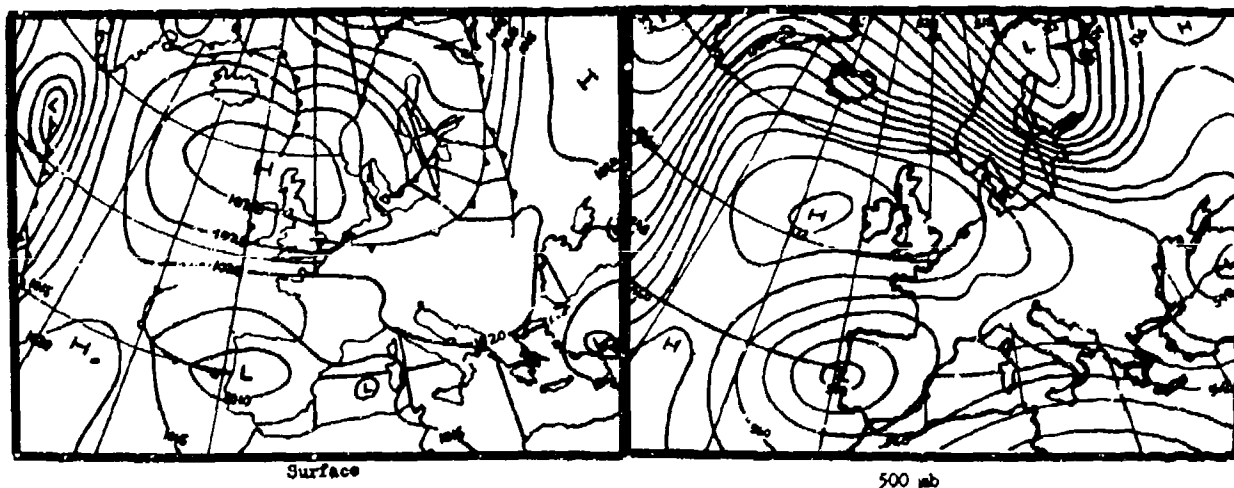


Figure E-13. Typical example of HB type.

TABLE E-23

NUMBER OF DAYS PER MONTH THAT HB WEATHER TYPE OCCURS

JAN	FEB	MAR	APR	MAY	JUN	JUL	AUG	SEP	OCT	NOV	DEC
0.5	0.9	1.0	1.0	1.1	1.1	0.7	0.7	1.2	0.8	0.6	0.6

TABLE E-24

NUMBER OF CONSECUTIVE DAYS PER
MONTH THAT HB WEATHER TYPE OCCURS

	1	2	3	4	5	6	7	8	9	10	11	12	≥13
JANUARY			4	1		3	1	1					
FEBRUARY	1	3	5	6	4		1	1					
MARCH		5	7	3	2	2	1				1		
APRIL			4	3	3	2	1		2				
MAY	2	2	6	8	2		1	2		1			
JUNE	2	4	8	3	4	1	1	1		1			
JULY		2	2	5	1			2					
AUGUST		1	7	3	2				1				
SEPTEMBER		1	7	5	4	1	1	1		1	1		
OCTOBER		3	6	3	2	1	2						
NOVEMBER	4	2	7	2	1	2		1					
DECEMBER	1	1	7	1	2		2	1					

14. ANTICYCLONIC NORTHERLY FLOW (NA TYPE)

a. Description

On the surface there is either a closed high over the eastern British Isles or the North Sea or a high pressure bridge between southwest Europe and the Polar high. Aloft there is a wedge over the eastern half of the British Isles flanked by extensive lows or troughs over the north Atlantic and northwest Russia. The Atlantic frontal zone curves to the north over the eastern Atlantic and generally does not connect with the Russian low center. On the western side of the Russian low, weak wave disturbances travel across eastern Europe to the south or southeast. Their extensions affect east-central Europe.

b. Characteristic Weather

Western and central Europe have scattered cloudiness and, at times, are fair and dry. The weather becomes unsettled toward the east with frequent precipitation of a showery nature. In winter, precipitation is always in the form of snow. It is moderately warm during summer in the west, and unpleasantly cold in the east. The winter often has severe cold weather.

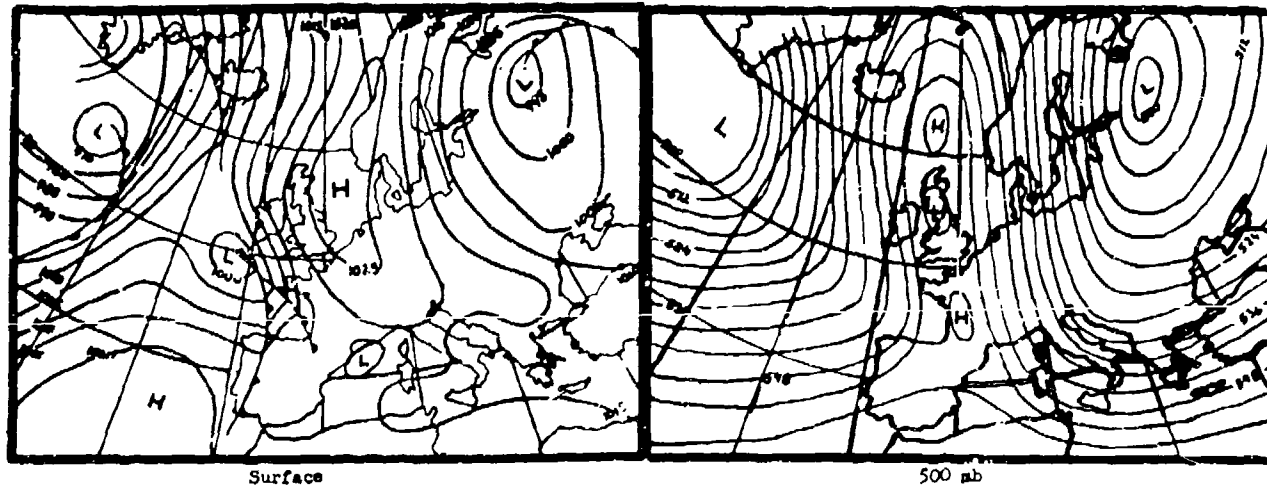


Figure E-14. Typical example of NA type.

TABLE E-25

NUMBER OF DAYS PER MONTH THAT NA WEATHER TYPE OCCURS

JAN	FEB	MAR	APR	MAY	JUN	JUL	AUG	SEP	OCT	NOV	DEC
0.1	0.1	0.4	0.1	0.9	0.7	0.5	0.4	0.3	0.1	0.2	0.2

TABLE E-26

NUMBER OF CONSECUTIVE DAYS PER
MONTH THAT NA WEATHER TYPE OCCURS

	1	2	3	4	5	6	7	8	9	10	11	12	≥13
JANUARY	1	1	2										
FEBRUARY		1	2		1								
MARCH		3	5	2									
APRIL	1	5	1	1									
MAY	1	4	8	5	1	3		1					
JUNE	2	1	3	2	1	1	1						
JULY	1	1	5	3	2							1	
AUGUST		7	4	2	1	1							
SEPTEMBER		4	4	1									
OCTOBER		1	1										
NOVEMBER		1	1	1									
DECEMBER		1	2	1									

15. CYCLONIC NORTHERLY FLOW (NZ TYPE)

a. Description

A closed and blocking high lies over the eastern Atlantic. On the surface there is a temporary bridge to the Polar high which is frequently broken by disturbances. The Atlantic frontal zone passes in an anticyclonic curve across Iceland into the southern Norwegian Sea. From there it runs across the North Sea into the Mediterranean and continues on into Russia. There is another high in the area east of the Ural Mountains. Individual disturbances, frequently stronger than normal, travel from Iceland across the North Sea into central Europe. Cold air penetrates into the Mediterranean Sea often causing the formation of secondary lows in the Gulf of Genoa which move off toward the east and northeast.

b. Characteristic Weather

Gusty northerly winds and unsettled weather with considerable precipitation occur on the northern edges of the mountains. There is a very pronounced upslope effect in the Alps. Winter and spring have snow with heavy shower activity. It is considerably colder than normal in all seasons.



Figure E-15. Typical example of NZ type.

TABLE E-27

NUMBER OF DAYS PER MONTH THAT NZ WEATHER TYPE OCCURS

JAN	FEB	MAR	APR	MAY	JUN	JUL	AUG	SEP	OCT	NOV	DEC
0.7	0.6	1.2	1.2	1.6	1.7	0.8	0.6	0.9	0.6	0.5	0.4

TABLE E-28

NUMBER OF CONSECUTIVE DAYS PER
MONTH THAT NZ WEATHER TYPE OCCURS

	1	2	3	4	5	6	7	8	9	10	11	12	≥13
JANUARY	1	2	8	2	3		1	1					
FEBRUARY		2	7	3	2				2				
MARCH		6	10	6	1	1		1	1				
APRIL	3	8	9	8	2	1		1					
MAY	2	9	16	8	7			1					
JUNE		9	8	7	2	3	1	2	1		1		
JULY	2	1	10	2	1		2						
AUGUST		1	2	3	2				1			1	
SEPTEMBER		4	11	2	1	1	1						
OCTOBER		3	8		3								
NOVEMBER	1		5	1	1	1			1				
DECEMBER		3	6	2		1	1						

16. TROUGH OVER CENTRAL EUROPE (TRM TYPE)

a. Description

A trough over north-central Europe reaches southward to the central Mediterranean. It is flanked by areas of high pressure situated over the northern Atlantic and Russia. Individual disturbances travel in the frontal zone in a southeasterly direction reaching from the northwestern Atlantic to southern France and then from the central Mediterranean across Hungary and Poland to northern Russia. The disturbances often deepen over the Mediterranean. The axis of the upper trough extends from the Norwegian Sea to the western Mediterranean.

b. Characteristic Weather

Typical weather is unsettled with frequent precipitation. In the western parts this is often in showery form -- mostly as snow in the cold season. Trough situations cause very heavy precipitation especially in the south and east. In all seasons it is colder than normal, particularly in the west. During the cold season, temperatures in the east are about normal.

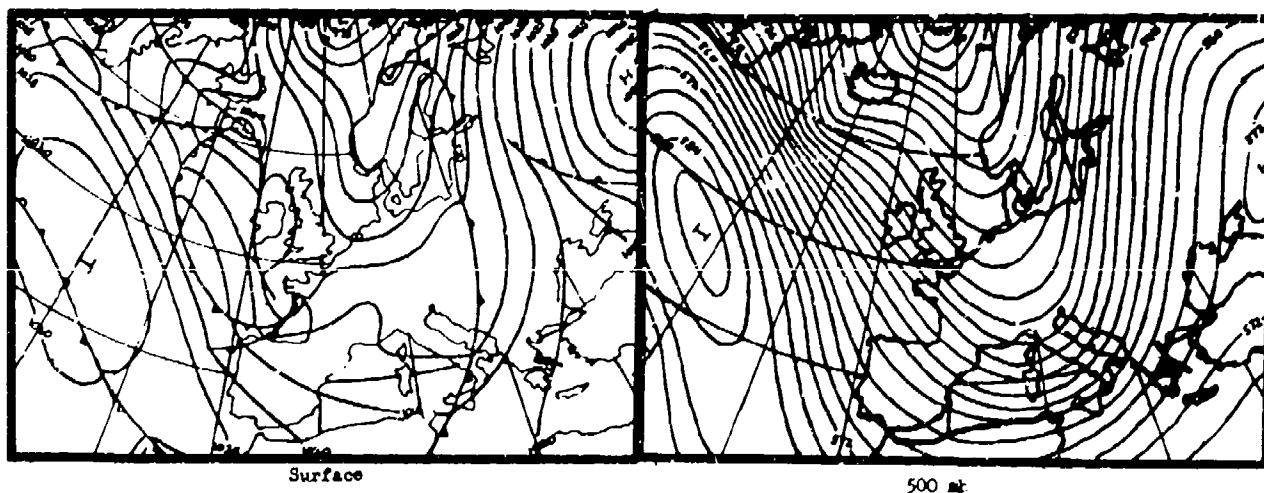


Figure E-16. Typical example of TRM type.

TABLE E-29

NUMBER OF DAYS PER MONTH THAT TRM WEATHER TYPE OCCURS

JAN	FEB	MAR	APR	MAY	JUN	JUL	AUG	SEP	OCT	NOV	DEC
1.2	1.2	1.3	1.6	1.2	0.9	1.2	0.9	1.3	1.1	1.4	0.9

TABLE E-30

NUMBER OF CONSECUTIVE DAYS PER
MONTH THAT TRM WEATHER TYPE OCCURS

	1	2	3	4	5	6	7	8	9	10	11	12	≥13
JANUARY	2	4	10	4	3	3					1		
FEBRUARY	1	3	9	4	5	3	1	1		1			
MARCH		4	9	4	4	1		3					
APRIL	2	10	7	11	3	1	1	1	1				
MAY	5	8	10	6	2	2							
JUNE	2	6	9	5	1	1	1						
JULY	4	7	8	6	1	1		2					
AUGUST	1	7	7	1	2	2	1						
SEPTEMBER	3	3	14	6	3	1	1	1					
OCTOBER	4	7	10	4	2	3	1						
NOVEMBER	3	9	8	10	4	2	1		2				
DECEMBER	6	5	5	4	3	1		1		1			

17. WELL-DEFINED CLOSED LOW OVER BRITISH ISLES (TB TYPE)

a. Description

There is a surface low center located over the British Isles or south or west of them. In contrast to the trough situation, the low is surrounded on all sides by high pressure, especially at its northern side. The Atlantic frontal zone splits off the American east coast into two branches: one goes across eastern Labrador to the north, the other passes across the southern North Atlantic into southwestern Europe. The number of individual disturbances which approach from the west and join the central low, however, are few. Circular steering can be observed and pressure change areas move on a cyclonic course along the north side of the system from east to west.

b. Characteristic Weather

The weather is slightly unsettled in the west but not unpleasant, with intermittent precipitation and frequent thunderstorms with abundant rain in the warm season. Precipitation, even in winter, is mostly rain. It is generally fair toward the east with frequent foehns in the northern Alps. It is warmer than normal in all seasons, especially in the cold season. Summer is often warm and sultry. In winter a thaw period occurs in the west.

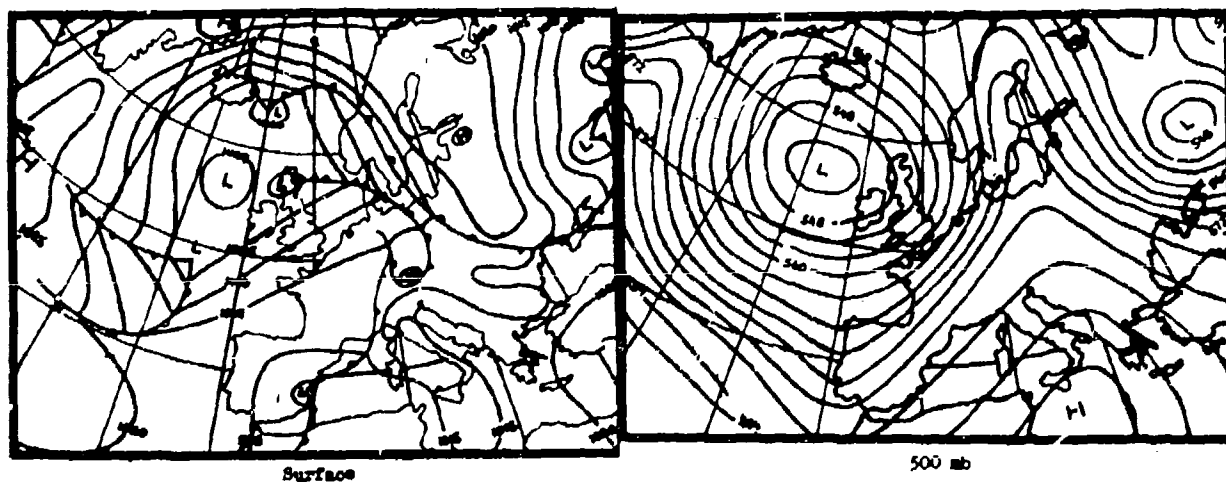


Figure E-17. Typical example of TB type.

TABLE E-31

NUMBER OF DAYS PER MONTH THAT TB WEATHER TYPE OCCURS

JAN	FEB	MAR	APR	MAY	JUN	JUL	AUG	SEP	OCT	NOV	DEC
0.3	0.6	0.4	0.9	1.2	0.6	0.8	1.3	0.4	0.5	0.7	0.7

TABLE E-32

NUMBER OF CONSECUTIVE DAYS PER
MONTH THAT TB WEATHER TYPE OCCURS

	1	2	3	4	5	6	7	8	9	10	11	12	≥13
JANUARY		1	3	2			1						
FEBRUARY		1	7	3	1		1						
MARCH	1	2	6	3		1							
APRIL			6	9		1	1				1		
MAY		2	6	6	4	5		1					
JUNE			4	3	1		2						
JULY		1	10	3	4	2		1					
AUGUST		4	9	6	5	2	2	1					
SEPTEMBER		2	2	3	3	1							
OCTOBER	1	3	4	3	3			1	1				
NOVEMBER	1	2	5	2	3	1		1	1				
DECEMBER	2	1	5	2	1	1	1	1					

18. TROUGH OVER WESTERN EUROPE (TRW TYPE)

a. Description

There is a trough from the Norwegian Sea across the western European coastal area into the western Mediterranean Sea. It is flanked by high pressure over the North Atlantic and western Russia. The Atlantic frontal zone runs from the middle of the North Atlantic to northern Spain, then curves over the western Mediterranean in the direction of the western parts of central and northern Europe. Individual disturbances pass along the frontal zone with their intensity temporarily decreasing over western Europe. Aloft the axis of the trough usually stretches from the western Norwegian Sea across the British Isles to Spain.

b. Characteristic Weather

Characteristic weather is slightly unsettled in the west but not unpleasant. There is intermittent precipitation with frequent thunderstorms and abundant rain in the summer. Precipitation in winter is usually in the form of rain. Toward the east, it is fair at times, with frequent foehns in the northern Alps. It is warmer than normal during all seasons. A thaw period occurs in winter, especially in the west. Summer is often warm and sultry.

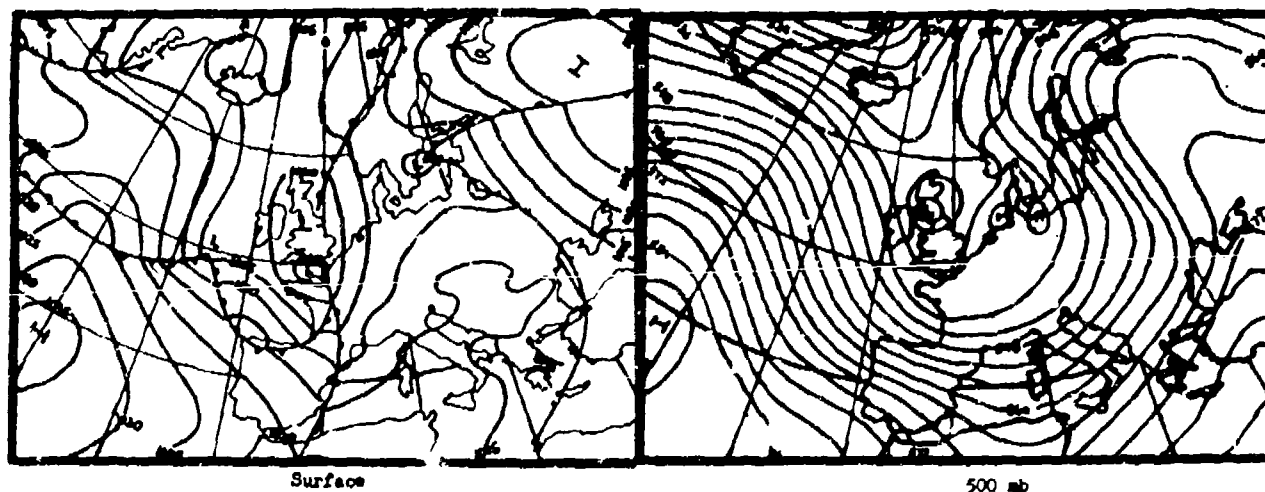


Figure E-18. Typical example of TRW type.

TABLE E-33

NUMBER OF DAYS PER MONTH THAT TRW WEATHER TYPE OCCURS

JAN	FEB	MAR	APR	MAY	JUN	JUL	AUG	SEP	OCT	NOV	DEC
0.3	0.4	0.6	0.8	1.0	0.7	1.0	1.0	0.7	1.0	0.7	0.5

TABLE E-34

NUMBER OF CONSECUTIVE DAYS PER
MONTH THAT TRW WEATHER TYPE OCCURS

	1	2	3	4	5	6	7	8	9	10	11	12	≥13
JANUARY	3	1	2			1			1				
FEBRUARY	2	2	1	1	1	1	1						
MARCH		1	5	5	3	1							
APRIL	2	4	4	9	1	1	1						
MAY	2	5	7	4	2	2							
JUNE	1	4	10	4	1	1		1					
JULY	3	8	14	6	1	2							
AUGUST	1	5	8	5	10	1	1						
SEPTEMBER	2	6	11	1	1	3							
OCTOBER	6	6	6	3		1	1	1	1		1		
NOVEMBER	5	5	11	5	1	1							
DECEMBER	2	10	5		1	1							

19. ANTICYCLONIC SOUTHERLY FLOW (SA TYPE)

a. Description

A blocking high at the surface with a strong wedge aloft reaches from eastern Europe to western Russia into northeastern Europe or northern Russia. The Atlantic frontal zone is located to the west of the high and extends from the sea area north of the Azores to the European west coast, there turning northward. Individual disturbances pass along the front and affect only the coastal areas from Spain to Norway. The low center is located in the area southwest or south of Iceland. East of the high there is a trough over the interior of Russia.

b. Characteristic Weather

In the west there is variable cloudiness, but it is dry. Fog occurs in the mornings with low stratus in the cold season. Toward the east it is fair with morning fog. Strong foehns occur along the northern Alps. In autumn, and occasionally in winter, there is frequent radiational cooling. In fall, during the day, and in the remainder of the seasons it is warmer than normal. Summer is often hot, but seldom sultry.

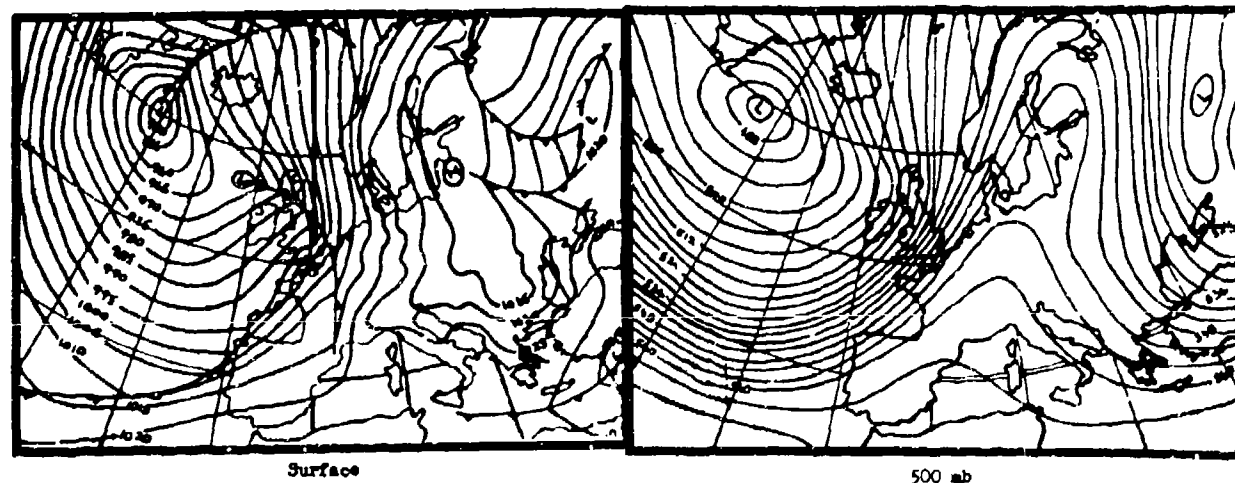


Figure E-19. Typical example of SA type.

TABLE E-35

NUMBER OF DAYS PER MONTH THAT SA WEATHER TYPE OCCURS

JAN	FEB	MAR	APR	MAY	JUN	JUL	AUG	SEP	OCT	NOV	DEC
1.2	0.5	0.9	0.4	0.3			0.1	0.9	0.9	1.6	0.8

TABLE E-36

NUMBER OF CONSECUTIVE DAYS FOR
MONTH THAT SA WEATHER TYPE OCCURS

	1	2	3	4	5	6	7	8	9	10	11	12	≥13
JANUARY	1	2	11	7	2			1			1		
FEBRUARY		3	4	2		2							
MARCH		5	10	5	2	1							
APRIL		4	5	3		1							
MAY	1	1	4	2									
JUNE			1										
JULY		1	1										
AUGUST		1	1	1									
SEPTEMBER		2	9	2	3	1		1					1
OCTOBER		7	11	2	4	1	1						
NOVEMBER		2	8	4	2	2	4	1	2	1			
DECEMBER	3	3	7		1	1	1	1		1			

20. CYCLONIC SOUTHERLY FLOW (SZ TYPE)

a. Description

There is a blocking high at the surface with a strong wedge aloft from west or central Russia to the Arctic Sea. The frontal zone along the western side of this blocking high runs from the Azores to western Europe. Individual, mostly weak disturbances travel from the western Mediterranean across the western Alps into northern Europe. The center of the low lies south or southeast of Iceland. East of the high there is a trough over western Siberia.

b. Characteristic Weather

It is cloudy at times with only light precipitation in winter. This is in the form of rain or drizzle. It is frequently gloomy with fog or low stratus in the cold season. Only the area north of the Alps is temporarily fair due to the foehns. Warm frontal thunderstorms with abundant precipitation may occur in summer. It is warmer than normal in all seasons, especially in summer. Exceptions to this are individual winter situations with low stratus. Summer is often sultry. Strong winds occur in coastal areas.

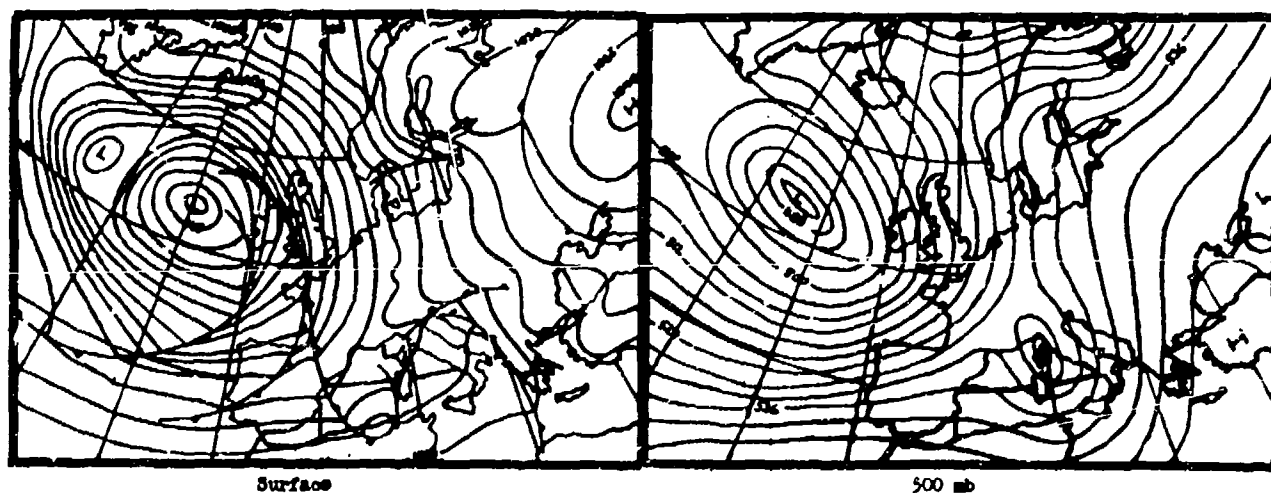


Figure E-20. Typical example of SZ type.

TABLE E-37

NUMBER OF DAYS PER MONTH THAT SZ WEATHER TYPE OCCURS

JAN	FEB	MAR	APR	MAY	JUN	JUL	AUG	SEP	OCT	NOV	DEC
0.2	0.5	0.3	0.2					0.1	0.2	0.4	0.5

TABLE E-38

NUMBER OF CONSECUTIVE DAYS PER
MONTH THAT SZ WEATHER TYPE OCCURS

	1	2	3	4	5	6	7	8	9	10	11	12	≥13
JANUARY		1	1	1	2								
FEBRUARY		1	4	1	3		1		1				
MARCH	1	2	3	3									
APRIL	1	1		2	1								
MAY	1												
JUNE													
JULY													
AUGUST													
SEPTEMBER		1	2										
OCTOBER	1	3	3		2	1							
NOVEMBER	2		2	2	1	1	1						
DECEMBER	1	3	4	3	3	1		1					

21. ANTICYCLONIC SOUTHEASTERLY FLOW (SEA TYPE)

a. Description

The blocking high is orientated from southeastern Europe or southern Russia towards the northwest with its center over southern Scandinavia or as a bridge reaching across the Norwegian Sea to Greenland. Low pressure lies over the central North Atlantic with a pronounced extension reaching to the Mediterranean area. Weak fronts occasionally touch west-central Europe. The Atlantic frontal zone runs from the southern North Atlantic to southwestern Europe; there it turns to the northwest across the British Isles. On the eastern side of the high there is a trough reaching from the Arctic Ocean to eastern Russia.

b. Characteristic Weather

Variable cloudiness occurs in the south and west with mostly clear skies elsewhere. There is often morning fog in the cold season. Foehn occur in the northern Alps. It is warmer than normal in spring, hot in summer, and colder than normal in winter. Below-freezing temperatures occur in the north and east.

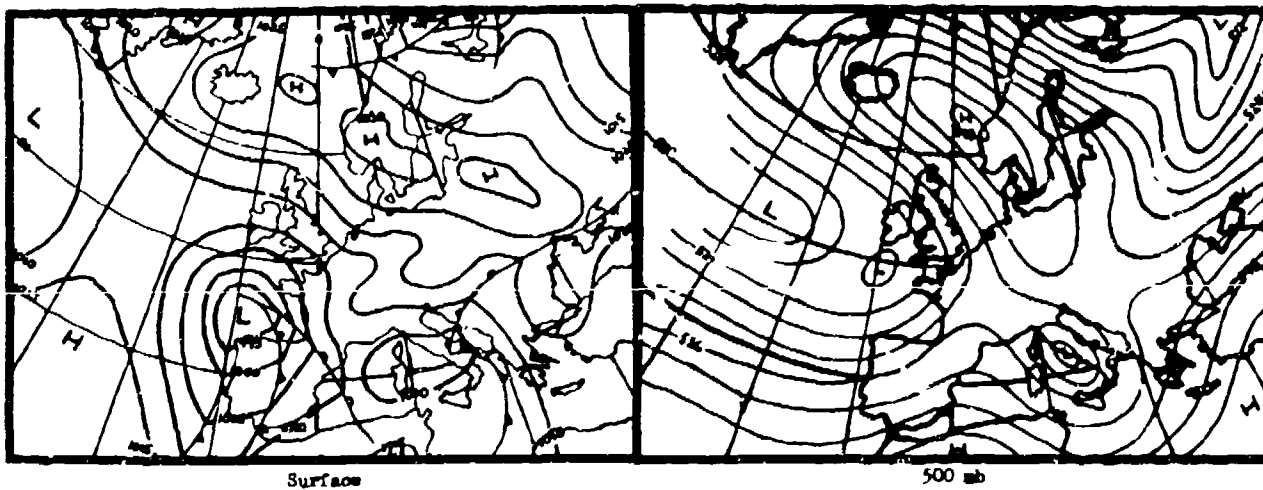


Figure E-21. Typical example of SEA type.

TABLE E-39

NUMBER OF DAYS PER MONTH THAT SEA WEATHER TYPE OCCURS

JAN	FEB	MAR	APR	MAY	JUN	JUL	AUG	SEP	OCT	NOV	DEC
0.5	0.4	1.1	0.8	0.7	0.2			0.7	1.1	0.8	0.9

TABLE E-40

NUMBER OF CONSECUTIVE DAYS PER
MONTH THAT SEA WEATHER TYPE OCCURS

	1	2	3	4	5	6	7	8	9	10	11	12	≥13
JANUARY		1	4	2		2	1						
FEBRUARY	1	2	2	2		1							
MARCH		3	7	7	3	2	1	1	1				
APRIL		5	6	2			1		2	1			
MAY	1	2	4	6						1			
JUNE		1	1	2		1							
JULY													
AUGUST			1										
SEPTEMBER	1	3	6	4	2		1						
OCTOBER	1	6	8	5	2	1	2	1	1				
NOVEMBER	1	2	9	5	2	1							
DECEMBER		4	7	2	1	4	1						

22. CYCLONIC SOUTHEASTERLY FLOW (SEZ TYPE)

a. Description

There is an extensive blocking high with its center over eastern Russia with a wedge in a northwesterly direction to the Polar region. On the west side a low pressure area extends from the Atlantic across western Europe to the western Mediterranean Sea. This often occurs with a cut-off low aloft. The Atlantic frontal zone runs from the central North Atlantic across central Europe towards the Norwegian Sea.

b. Characteristic Weather

Weather is unsettled with intermittent precipitation which occurs in the form of rain in winter. It is generally dry in the northeast. It is often humid in the warm season. Warm frontal thunderstorm activity causes abundant rain. Light foehns occur near the Alps. It is warmer than normal in the west and colder than normal in the east in winter.

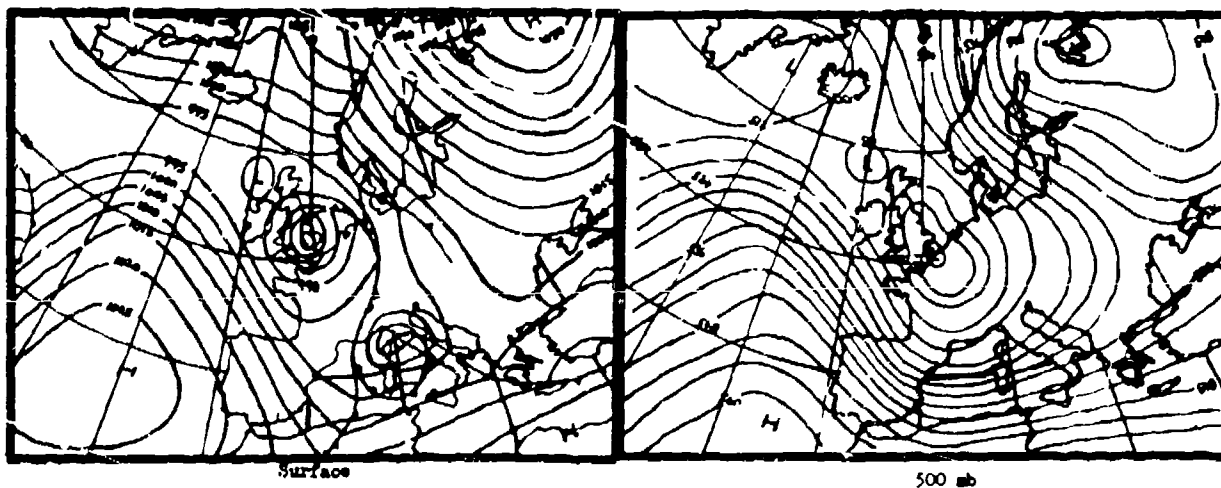


Figure E-22. Typical example of SEZ type.

TABLE E-41

NUMBER OF DAYS PER MONTH THAT SEZ WEATHER TYPE OCCURS

JAN	FEB	MAR	APR	MAY	JUN	JUL	AUG	SEP	OCT	NOV	DEC
1.1	0.8	0.8	0.8	0.3				0.2	0.4	0.5	0.5

TABLE E-42

NUMBER OF CONSECUTIVE DAYS PER
MONTH THAT SEZ WEATHER TYPE OCCURS

	1	2	3	4	5	6	7	8	9	10	11	12	≥13
JANUARY	1	1	5	2	4	1	4	2					
FEBRUARY		1	4	1	2		1	1		1			
MARCH		2	7	6		2			1				
APRIL		4	3	1	2	1	2	1					
MAY	1	1	3	1	1								
JUNE													
JULY													
AUGUST		1											
SEPTEMBER			4	2									
OCTOBER	1	2	3		3	2			1				
NOVEMBER		1	3	1		3							
DECEMBER		1	3	2	1	2	1						

23. WELL-DEFINED CLOSED HIGH OVER FENNOSCANDIA (HFA TYPE)
(ANTICYCLONIC FLOW OVER CENTRAL EUROPE)

a. Description

There is a closed blocking high with its center over Fennoscandia or the Baltic Sea. On its south side there is easterly flow, usually from western Russia across central Europe to the North Sea. The Atlantic frontal zone extends in a meridional direction to the Arctic Sea, there curving into southern Russia (trough over eastern Russia). There is no strong upper low over central Europe or the Mediterranean area.

b. Characteristic Weather

Characteristic weather is mostly fair and dry. Severe cold spells often occur in winter. In the transitional seasons it is colder than normal at times, but in the warm season it is hot with considerable thunderstorm activity.

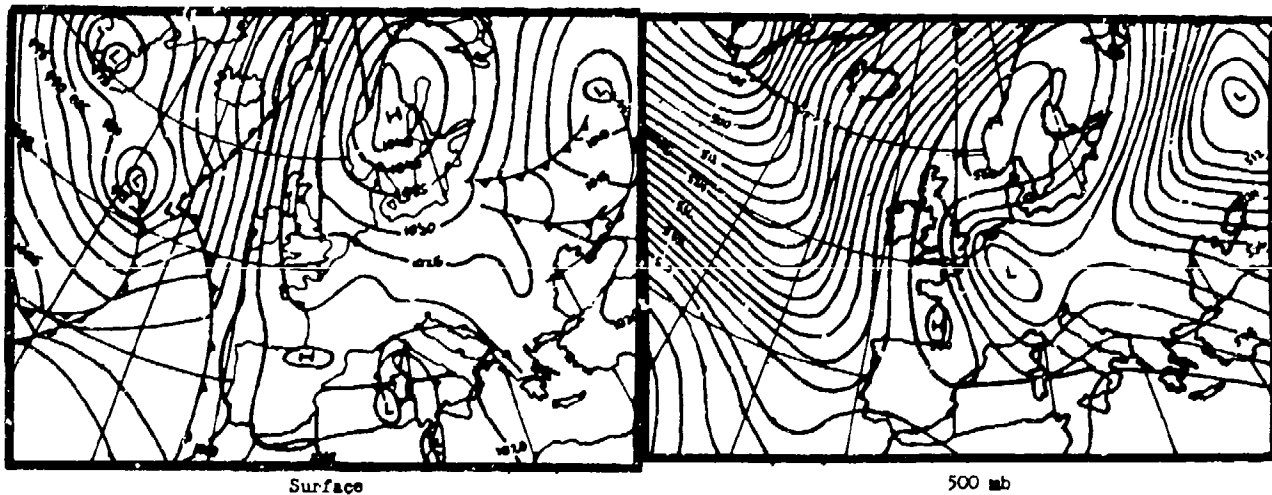


Figure E-23. Typical example of HFA type.

TABLE E-43

NUMBER OF DAYS PER MONTH THAT HFA WEATHER TYPE OCCURS

JAN	FEB	MAR	APR	MAY	JUN	JUL	AUG	SEP	OCT	NOV	DEC
1.9	1.5	1.2	1.5	1.1	0.4	0.5	0.7	1.1	1.4	0.7	1.2

TABLE E-44

NUMBER OF CONSECUTIVE DAYS PER
MONTH THAT HFA WEATHER TYPE OCCURS

	1	2	3	4	5	6	7	8	9	10	11	12	≥13
JANUARY	1	2	6	9	3	4	3	1	1	1			
FEBRUARY		1	9	6	2	2	1	2	1				
MARCH	1		15	6	2		1	2					
APRIL		3	7	7	2	3		1	1	1			
MAY	1	3	11	6	2	2			1				
JUNE		2	8	2		1							
JULY		3	3	2	1	1		1					
AUGUST	2	2	2	2		2	2		1				
SEPTEMBER		3	6	5	2	1	1		1				1
OCTOBER		6	7	4	3	1			1				1
NOVEMBER	2	1	8	2	1	3							
DECEMBER	2	4	8	3	5	2	1						1

24. WELL-DEFINED CLOSED HIGH OVER FENNOSCANDIA (HFZ TYPE)
(CYCLONIC FLOW OVER CENTRAL EUROPE)

a. Description

There is a closed blocking high over central or northern Fennoscandia and an extensive upper low over the central and southern parts of central Europe which results in easterly flow at the surface. The flow is from western Russia, across north-central Europe to the North Sea. Disturbances usually come from an easterly direction only during the winter and then only as isolated cold air pockets which split off from the Siberian cold air reservoir. They travel slowly across central Europe to the Norwegian Sea. Large-scale over-running is caused by moist, warm air which moves in from the low to the south. The Atlantic frontal zone splits into two branches over the eastern Atlantic. One branch passes in the direction of eastern Greenland, then across the Arctic Ocean into eastern Russia; the other goes across the Bay of Biscay and the Mediterranean into southern Russia.

b. Characteristic Weather

The weather is unsettled with precipitation -- in winter as snow and in the warm season as rain with frequent thunderstorms. In the east, rainfall is sometimes very abundant. In the cold season, below-freezing temperatures occur. In the warm season it is more often humid and warm than hot.

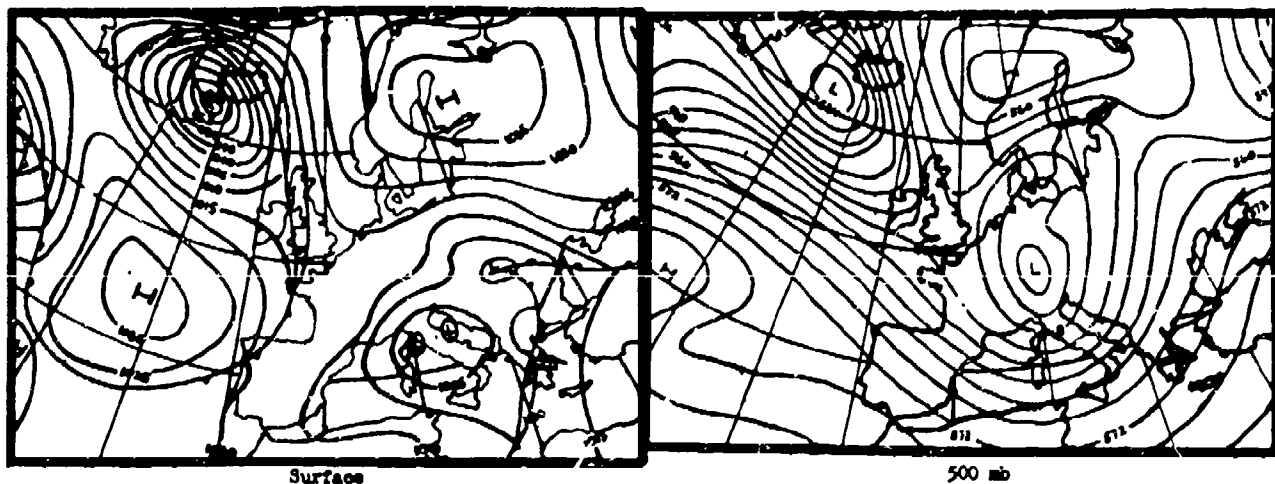


Figure E-24. Typical example of HFZ type.

TABLE E-45

NUMBER OF DAYS PER MONTH THAT HFZ WEATHER TYPE OCCURS

JAN	FEB	MAR	APR	MAY	JUN	JUL	AUG	SEP	OCT	NOV	DEC
0.3	0.2	0.3	0.2	0.1	0.1	0.1	0.1	0.1	0.2	0.3	0.3

TABLE E-46

NUMBER OF CONSECUTIVE DAYS PER
MONTH THAT HFZ WEATHER TYPE OCCURS

	1	2	3	4	5	6	7	8	9	10	11	12	≥13
JANUARY		1	3	2		1							
FEBRUARY		1	2	3									
MARCH			5	2	1								
APRIL			1	2	2								
MAY			2	1	1	1							
JUNE		1	2				2						
JULY		1	2	1									
AUGUST	1			2									
SEPTEMBER			1	2			1						
OCTOBER	1	1	1	1	1								
NOVEMBER			3	3	2			1					
DECEMBER	1	1	5	2	1	1							

25. WELL-DEFINED CLOSED HIGH OVER NORWEGIAN SEA AND FENNOSCANDIA
(HNFA TYPE) (ANTICYCLONIC FLOW OVER CENTRAL EUROPE)

a. Description

There is a blocking high pressure zone, often a high pressure bridge, extending from Russia, Fennoscandia or the Baltic Sea to the Norwegian Sea or to Greenland. Along the southern side there is easterly flow, often from the interior of Russia to the northern North Atlantic, occasionally even to the south of Greenland. In the south, there is a weak Atlantic low pressure system with a trough of low pressure extending eastward. The low center is located near the Bay of Biscay, but the frontal zone is not pronounced. North of the high pressure zone there is westerly flow from northern Greenland over the Arctic Ocean to northern Russia.

b. Characteristic Weather

It is often fair in the north and east with variable cloudiness towards the south and west. Scattered precipitation falls as snow in winter. It is hot in summer and severely cold in winter. The north and east have the greatest annual temperature extremes.

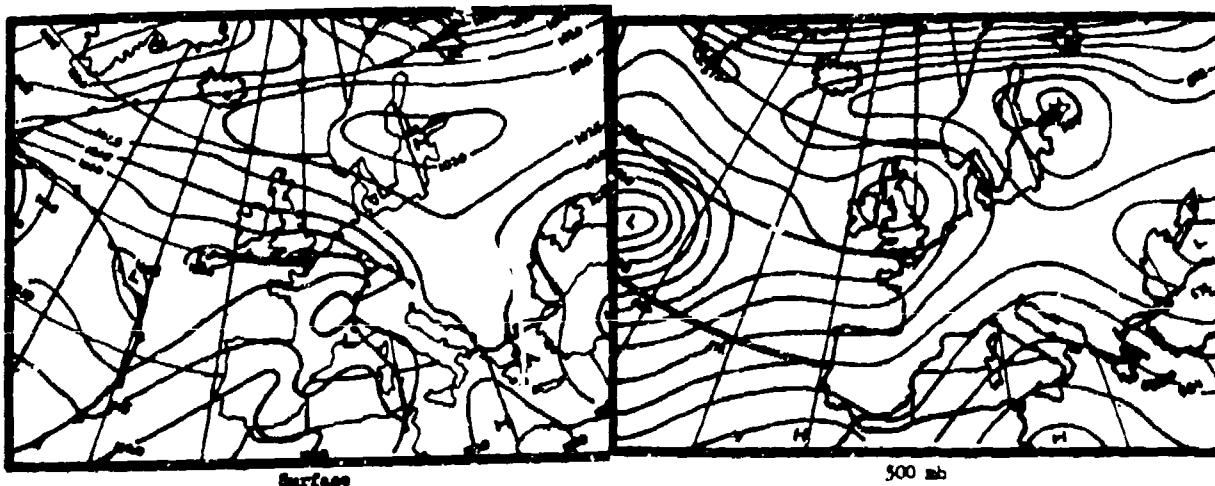


Figure E-25. Typical example of HNFA type.

TABLE E-47

NUMBER OF DAYS PER MONTH THAT HNFA WEATHER TYPE OCCURS

JAN	FEB	MAR	APR	MAY	JUN	JUL	AUG	SEP	OCT	NOV	DEC
0.3	0.5	0.2	0.5	1.4	0.6	0.1		0.3	0.2	0.1	0.1

TABLE E-48

NUMBER OF CONSECUTIVE DAYS PER
MONTH THAT HNFA WEATHER TYPE OCCURS

	1	2	3	4	5	6	7	8	9	10	11	12	≥13
JANUARY			3	1		1	1						
FEBRUARY		1	4	3	1		1	1					
MARCH			1				1		1				
APRIL			4	3			1	1					1
MAY		3	9	5	3	2	1	2	1				
JUNE		1	3	4	1	1	1						
JULY			1	1									
AUGUST													
SEPTEMBER			2	1		1	1						
OCTOBER		4	2										
NOVEMBER			1	2									
DECEMBER					3								

26. WELL-DEFINED CLOSED HIGH OVER NORWEGIAN SEA AND FENNOSCANDIA
(HNFZ TYPE) (CYCLONIC FLOW OVER CENTRAL EUROPE)

a. Description

At the surface there is a blocking high pressure zone extending from northern Russia across Fennoscandia to the Norwegian Sea, often as a bridge to Greenland. Aloft there is a weak bridge between a high over Russia and a high over the northern Atlantic or Greenland. Sometimes there is also a trough-like connection between the low pressure over the northern regions and an upper low located over central or south-central Europe (similar to HFA). Frequently there are large-scale overrunning processes occurring within the range of this low. At the surface, central Europe experiences general easterly flow; the Atlantic frontal zone does not extend to the east very markedly. A low pressure region is located south of the zone of high pressure with its main centers over the Atlantic and over central or western Europe.

b. Characteristic Weather

It is mostly cloudy with frequent and abundant precipitation -- in winter as snow, in the warm season as frequent thunderstorms. In winter severe cold occurs, especially in the north, and in the warm season it is rather warm and humid.

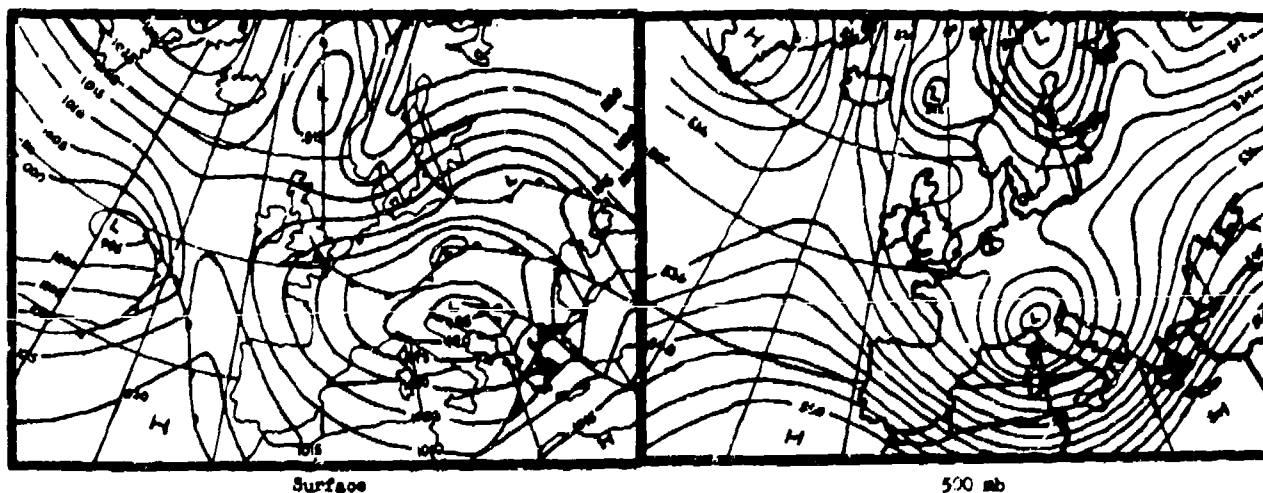


Figure E-26. Typical example of HNFZ type.

TABLE E-49

NUMBER OF DAYS PER MONTH THAT HNFZ WEATHER TYPE OCCURS

JAN	FEB	MAR	APR	MAY	JUN	JUL	AUG	SEP	OCT	NOV	DEC
0.1	0.5	1.2	0.3	1.0	0.2	0.2	0.1	0.2	0.2	0.3	0.2

TABLE E-50

NUMBER OF CONSECUTIVE DAYS PER
MONTH THAT HNFZ WEATHER TYPE OCCURS

	1	2	3	4	5	6	7	8	9	10	11	12	≥13
JANUARY	1		1	1	1		2						
FEBRUARY	1	2	1	3	1			1					1
MARCH			7	2	3	3		2					1
APRIL			8	1	2			1					
MAY			5		2								
JUNE	2	1	1		2								
JULY			3				1						
AUGUST	1		2	1	1								
SEPTEMBER			2	2									
OCTOBER			2	1	1								
NOVEMBER			7	2									
DECEMBER		1	1				1						

27. NORTHEASTERLY FLOW (NE TYPE)

a. Description

There is a high pressure bridge from the Azores across the British Isles to Fennoscandia or sometimes from southwestern Europe across France and the Baltic Sea to northern Russia. In the latter case the high pressure bridge is weak. At its southeastern flank there is also a low pressure system aloft with its center over central Europe, especially in winter. Along the northeast flank of the high, the Atlantic frontal zone stretches from the western Atlantic to the northeast often causing southwesterly flow over the Atlantic. Near the center of the bridge of high pressure over the British Isles or the North Sea, there is a danger of a temporary break-through of Atlantic disturbances in a southeasterly direction to the Mediterranean area or to south-central Europe. Often this break is recurrent, followed by a reestablishment of the high pressure bridge.

b. Characteristic Weather

In the cold season, especially towards the southeast, it is cloudy with precipitation in the form of snow, which is at times abundant and long-lasting. The warm season is pleasant and fair with only widely scattered thunderstorms. Winter is colder than normal and during temporary clearing sometimes severely cold.

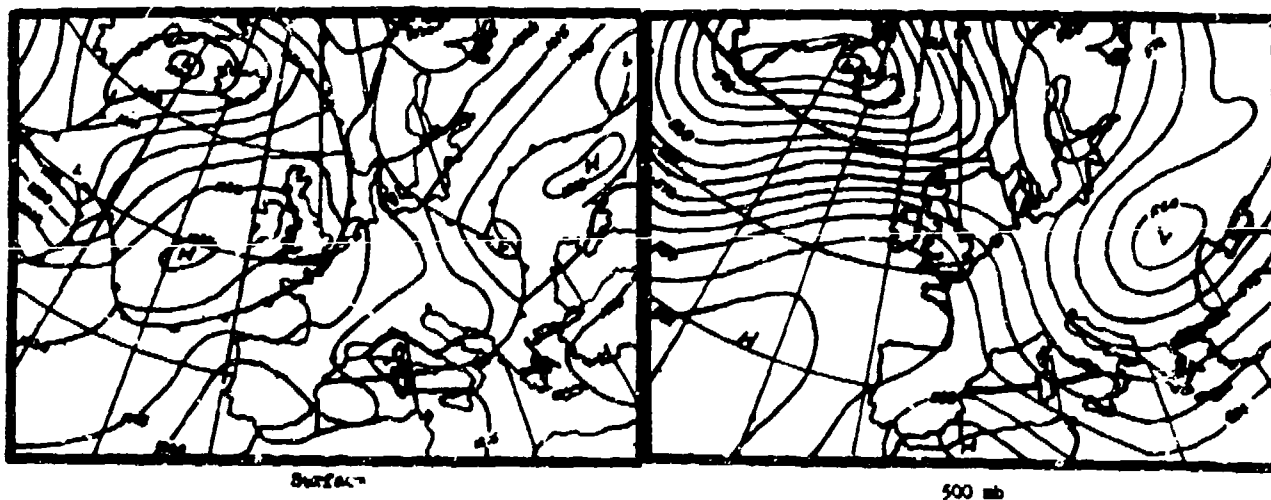


Figure E-27. Typical example of NE type.

TABLE E-51

NUMBER OF DAYS PER MONTH THAT NE WEATHER TYPE OCCURS

JAN	FEB	MAR	APR	MAY	JUN	JUL	AUG	SEP	OCT	NOV	DEC
1.1	1.3	1.8	2.2	2.6	0.2	0.2	0.1	0.4	0.8	0.5	0.7

TABLE E-52

NUMBER OF CONSECUTIVE DAYS PER
MONTH THAT NE WEATHER TYPE OCCURS

	1	2	3	4	5	6	7	8	9	10	11	12	≥13
JANUARY	1	2	8	4	4	2				2			
FEBRUARY	3	3	10	6	1	1	1	1		1			
MARCH	5	4	12	2	5	3		2	1	1			1
APRIL	2	5	18	12	6	3	1			2			
MAY	1	8	20	11	5	3	3	1					1
JUNE		2	1	1	2				1				
JULY		1	2	1			1				1		
AUGUST			2			2							
SEPTEMBER		1		2		1		1		1			
OCTOBER	3	4	4	5	5								
NOVEMBER	2	3	5	2									
DECEMBER	9	10	7					1					

28. WELL-DEFINED CLOSED LOW OVER CENTRAL EUROPE (TM TYPE)

a. Description

In contrast to the trough situation, the central surface low over central or west-central Europe and the low aloft over the western portions of continental Europe are surrounded on almost all sides by high pressure. The Atlantic frontal zone often splits over the western Atlantic into two branches: one passes over western Greenland to the northeast; the other, often very weak, passes across the North Atlantic into southwestern Europe. A marked circular steering pattern over central Europe can be observed frequently. Pressure change areas move on the northern side of the system from east to west. The more western areas are affected more by Gulf of Genoa developments than by the trough situations.

b. Characteristic Weather

Frequent, often very heavy, precipitation occurs in the cold season. Often this is snow, especially in the western areas. In summer the weather is usually warm and humid with thunderstorm activity.

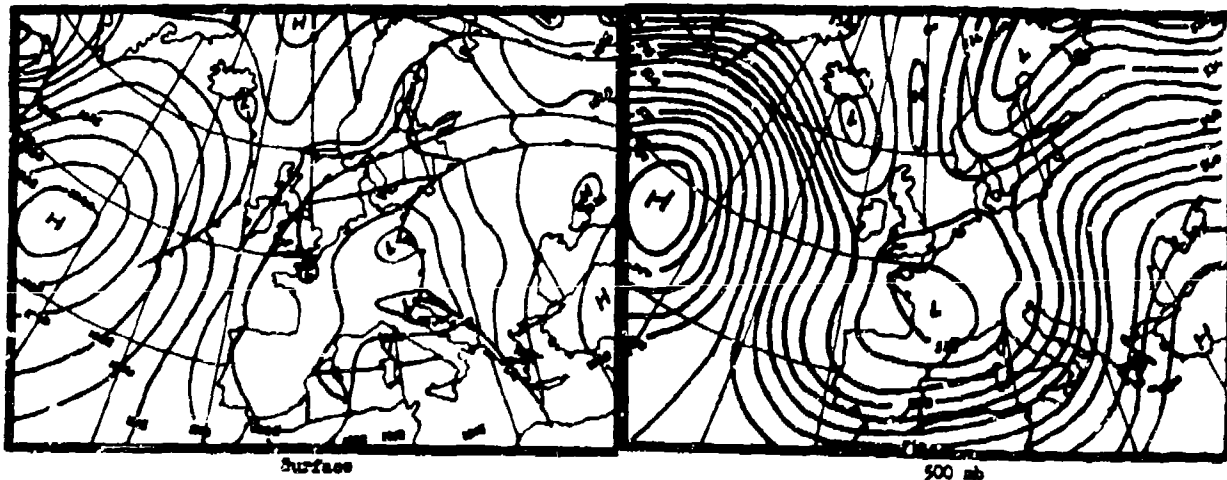


Figure E-28. Typical example of TM type.

TABLE E-53

NUMBER OF DAYS PER MONTH THAT TM WEATHER TYPE OCCURS

JAN	FEB	MAR	APR	MAY	JUN	JUL	AUG	SEP	OCT	NOV	DEC
1.1	0.8	1.1	1.2	1.2	0.7	0.9	0.4	0.6	0.7	0.9	0.5

TABLE E-54

NUMBER OF CONSECUTIVE DAYS PER
MONTH THAT TM WEATHER TYPE OCCURS

	1	2	3	4	5	6	7	8	9	10	11	12	≥13
JANUARY	1		3	2	2	4		2		2			
FEBRUARY			6	1	4	2	1	1					
MARCH		1	9	7	3	1							
APRIL	1		4	4	7	3	2	2				1	
MAY		9	3	5	1	3	1	1					
JUNE		4	4	3	3	1							
JULY		3	5	6	2	2	1						
AUGUST		2	5	2					1				
SEPTEMBER	1	1	5	2	1	1	1						
OCTOBER		4	7	3	1	2							
NOVEMBER	4	4	10	5	1	1							
DECEMBER		2	5	1	1			1					

29. NORTHWESTERLY SLOPED TROUGH (WW TYPE)

a. Description

There is a very marked Atlantic frontal zone lying usually between 50N and 55N and a blocking high with its center over western Russia. On the western side of the high the frontal zone turns sharply to the north towards western Scandinavia so that the associated bad weather areas become stationary in a meridional zone west of the Elbe River.

b. Characteristic Weather

The western and northwestern portions of the region experience frequent, and often abundant, snowfalls during the winter. The northeast and southeast sections are frequently free of precipitation. Winters are generally mild except in the east where it is colder than normal. Summers are generally cool. Strong winds occur in the west and northwest in winter.

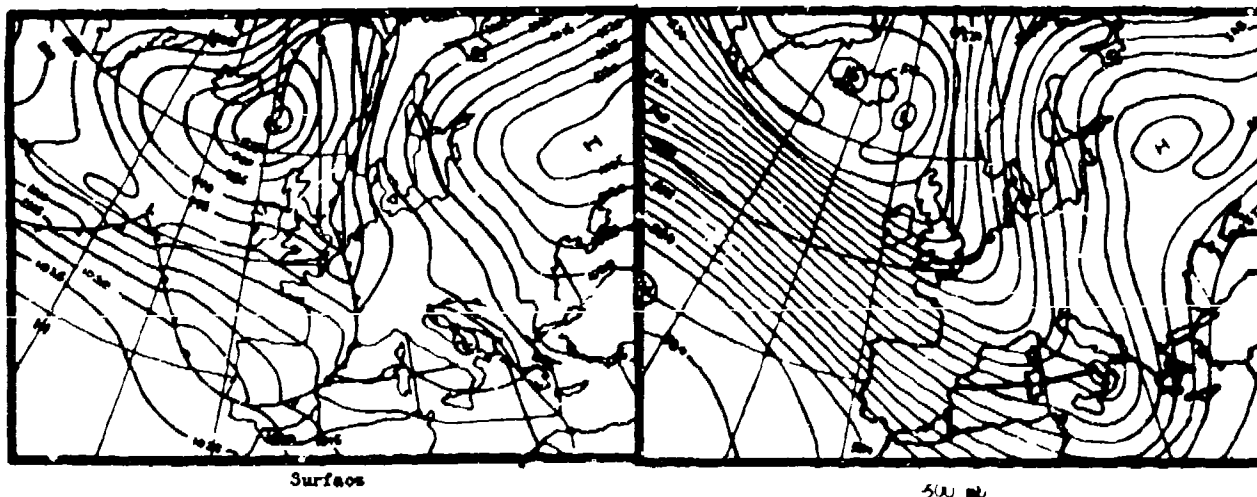


Figure L-29. Typical example of Ww type.

TABLE E-55

NUMBER OF DAYS PER MONTH THAT WW WEATHER TYPE OCCURS

JAN	FEB	MAR	APR	MAY	JUN	JUL	AUG	SEP	OCT	NOV	DEC
1.1	0.4	0.9	0.4	0.2	0.6	0.4	0.8	0.5	0.6	1.4	1.5

TABLE E-56

NUMBER OF CONSECUTIVE DAYS PER
MONTH THAT WW WEATHER TYPE OCCURS

	1	2	3	4	5	6	7	8	9	10	11	12	≥13
JANUARY		3	8	6	1	1		1			1		
FEBRUARY		4	7		1	1							
MARCH		5	10	3	3	1	1						
APRIL			4	3	2			1					
MAY			2	2		1							
JUNE		1	5	2	4		1						
JULY		2	5	2		1	1						
AUGUST	1	3	3	4	3	2	1						
SEPTEMBER	1	4	5	5			1						
OCTOBER	2	4	3		1	1	2						
NOVEMBER	5	5	13	6		3	1	1	1	1	1		
DECEMBER	5	11	7	4	4	4		1					

REFERENCE

Aerospace Science Div., 1968: Catalogue of European large-scale weather types.
Revised by HQ 2nd Weather Wing, Aerospace Sci. Div., 68 pp.

APPENDIX F

LIST OF STATIONS FOR WHICH CLIMATOLOGICAL DATA ARE AVAILABLE FROM WORLD-WIDE AIRFIELD SUMMARIES

The U.S. Naval Weather Service has recently published a series of climatological summaries for selected airfields which is world-wide in scope. Since copies of these reports can be obtained from the National Technical Information Service (NTIS), Springfield, Virginia 22151, it was felt that it was unnecessary to duplicate them here. However, to aid the reader in using these World-Wide Airfield Summaries for the region surrounding the Mediterranean, a listing of climatological parameters along with available stations from these reports is compiled in this appendix.

Table F-1 is a listing of parameters found in the World-Wide Airfield Summaries for both airfields and climatic areas that have been selected as being nearly homogeneous climatologically. It should be mentioned that snowfall information is not available in the Mediterranean region. A listing of countries (in alphabetical order) is found in Table F-2. This table also lists stations, by increasing WMO Station Index Numbers, for which climatological data are available. These stations, arranged according to numbered climatic areas, are given an arbitrary station number (indicated by /) where WMO Index Numbers are not assigned. References to Figures F-1 through F-20, which include the station locations and boundaries of climatic areas, are also listed in Table F-2.

Table F-1. Data available from World-Wide Airfield Summaries

AIRFIELD DATA AND AIRFIELD AREA DATA

Climatological data applicable only to a specified airfield. The data consist of statistical parameters based on actual weather observations made at the airfield. If actual weather observations are not available the data consist of estimates of the statistical parameters, prepared by a climatologist, based on actual meteorological data from surrounding weather stations.

Table F-1 (continued)

CLIMATIC AREA DATA

Climatological data representative of a nearly homogeneous climatic area. The data are average (or representative) values based on a sample of climatological data available from weather stations within the area. The area data do not imply that the specific condition simultaneously exists at all locations within a country or large climatic area. In rolling and mountainous terrain there may be considerable variation in the data from one location to another within the climatic area.

LOCAL STANDARD TIME

Standard time applicable to a 15° meridional zone. (Zones proceed east and west from the zone centered on the prime meridian and extending from 00730E to 00730W.) No consideration is given to local deviations from the 15° zone boundaries.

AIRFIELD PARAMETERS

Absolute Maximum (Minimum) Temperature-Degrees F.

The highest (lowest) temperature observed in the specified month during the whole period for which observations are available.

Mean Daily Maximum (Minimum) Temperature-Degrees F.

The average of all the daily maximum (minimum) temperatures observed in the specified month.

Mean No. Days With Maximum Temperature Greater Than Or Equal To 90°F.

The average of the number of days in the specified month on which the maximum temperature was observed to be equal to or greater than 90°F.

Mean No. Days With Minimum Temperature Less Than Or Equal To 32°F (0°F).

The average of the number of days in the specified month on which the minimum temperature was observed to be equal to or less than 32°F (0°F).

Mean Dew Point Temperature-Degrees F.

The average of all hourly dew point temperatures observed in the specified month.

Mean Relative Humidity-Percent

The average of all hourly relative humidity values observed in a specified month.

Mean Pressure Altitude-Feet

The average station pressure observed at the airfield in the specified month converted to an altitude by using the U.S. Standard Atmosphere.

Table F-1 (continued)

Mean Monthly Precipitation-Inches

The average of the monthly total amount of all forms of precipitation, reduced to its liquid equivalent, observed in the specified month.

Mean Monthly Snowfall-Inches

The average of the monthly total amount of snowfall observed in the specified month.

Mean No. Days With Precipitation Greater Than Or Equal to 0.1 Inch
(Snowfall Greater Than or Equal To 1.5 Inches)

The average of the number of days in the specified month on which the daily amount of precipitation (snowfall) was observed to be equal to or greater than 0.1 inch (1.5 inches).

Mean No. Days With An Occurrence of Visibility Less Than 0.5 Mile

The average of the number of days in the specified month on which there was at least one observation of visibility less than 0.5 mile.

Mean No. Days With Thunderstorms

The average of the number of days in the specified month on which the weather observer heard thunder.

Percent Frequency Surface Wind Speed Greater Than 16 Knots
(Greater Than 27 Knots)

The frequency, expressed as a percent of the total number of hourly weather observations considered, during the specified month, in which the surface wind speed was observed to be greater than 16 knots (27 knots).

Percent Frequency Ceiling Less Than 5,000 Feet And/Or Visibility
Less Than 5 Miles

The frequency, expressed as a percent of the total number of hourly weather observations considered, during the specified month, in which the ceiling was observed to be less than 5,000 feet and/or the visibility was observed to be less than 5 miles.

Percent Frequency Ceiling Less Than 1,500 Feet (Less Than 300 Feet)
And/Or Visibility Less Than 3 Miles (Less Than 1 Mile)

The frequency, expressed as a percent of all the hourly weather observations considered, in a specified three-hourly period during the day for a specified month in which the ceiling was observed to be less than 1,500 feet (300 feet) and/or the visibility was observed to be less than three miles (one mile).

Table F-1 (continued)

PARAMETERS FOR AIRFIELD AREA AND CLIMATIC AREA

Mean No. Days With Ceiling Equal To Or Greater Than 1,000 Feet (2,500 Feet, 6,000 Feet, etc.) and Visibility Equal To Or Greater Than 3 Miles

The average of the number of days when, at a specified hour during the day in the specified month, the ceiling was observed to be equal to or greater than 1,000 feet (2,500 feet, 6,000 feet, etc.) and the visibility was observed to be equal to or greater than three miles.

Mean No. Days With Ceiling Equal To Or Greater Than 2,000 Feet and Visibility Equal To Or Greater Than 3 Miles and Surface Wind less Than 10 knots

The average of the number of days when, at a specified hour during the day in the specified month, the ceiling was observed to be equal to or greater than 2,000 feet, the visibility was observed to be equal to or greater than three miles, and the surface wind speed less than ten knots.

Mean No. Days With Surface Wind Greater Than 16 Knots and No Precipitation

The average of the number of days when, at a specified hour during the day in the specified month, the surface wind speed was observed to be greater than 16 knots, and there was no precipitation.

Mean No. Days With Surface Wind 4-10 Knots and Temperature 33-89° F and No Precipitation

The average of the number of days when, at a specified hour during the day in the specified month, the surface wind speed was equal to or greater than four knots, but not greater than ten knots, the temperature was equal to or greater than 33° F but not greater than 89° F and there was no precipitation.

Mean No. Days With Sky Cover Less Than 0.3 and Visibility Equal To Or Greater Than 3 Miles

The average of the number of days when, at a specified hour during the day in the specified month, the portion of the sky covered with clouds was observed to be less than 0.3 and the visibility was observed to be equal to or greater than three miles.

AREA PARAMETERS (CLIMATIC AREA ONLY)

Range of Mean Daily Temperature-Degrees F

- Two temperatures for the specified month:
- (1) a representative mean daily maximum temperature observed in the area;
 - (2) a representative mean daily minimum temperature observed in the area.

Range of Mean Monthly Precipitation-Inches

- Two mean monthly precipitation amounts for the specified month:
- (1) the largest mean amount observed in the area;
 - (2) the smallest mean amount observed in the area.

Table F-2. Listing of stations for which climatological data are available from World-Wide Airfield Summaries.

ALBANIA (from U.S. Naval Weather Service, 1972). Figure F-1 shows station locations and climatic areas.

Station No.	Name	Station No.	Name
COASTAL (Climatic Area 1)		INTERIOR MOUNTAINS (Climatic Area 2)	
13600	Shkodra	13625	Gjirokastra
13615	Tirana	13629	Korca

ALGERIA (from U.S. Naval Weather Service, 1968). Figure F-2 shows station locations and climatic areas.

Station No.	Name	Station No.	Name
COASTAL (Climatic Area 1)		DESERT (Climatic Area 4)	
60355	Philippeville/Skikda	60580	Ouargla
60360	Bone-Annaba	60581	Hassi Messaoud
60379	La Reghaia-Alma	60590	El Golea
60390	Alger-Maison Blanche	60606	Timimoun
60419	Constantine-Ain	60608	Fort Flatters
60435	Blida	60625	Aoulef
60446	Telergma	60630	In Salah
60484	Bou-Sfer	60640	Fort Polignac/Illizi
60490/	Oran-La Senia	60646	Reggan
60497	Paul Cazelles	60675	Ouallen
60503	Lartigue		
60531	Tlemcen-Zenata		
ATLAS MOUNTAINS (Climatic Area 2)		SOUTHEAST HIGHLANDS (Climatic Area 5)	
60504/	Magoura	60670	Ujanet
60540	Le Kreider	60677/	In Eker
60543/	Aflou	60678	In Amquel
		60680	Tamanrasset
NORTHERN PLAINS (Climatic Area 3)			
60525	Biskra		
60545	Laghouat El Mahr		
60570/	Hammaguir		
60571	Colomb-Bechar		
60589	Meridja		
60605	Tabel Bala		
60655	Tindouf		

AUSTRIA (from U.S. Naval Weather Service, 1971a). Figure F-3 shows station locations and climatic areas.

Station No.	Name	Station No.	Name
DANUBE PLAINS (Climatic Area 1)		AUSTRIAN ALPS (Climatic Area 2)	
11010	Linz	11105	Feldkirch
11030	Vienna-Tulln	11120	Innsbruck West
11035	Wien/Hohe Warte	11146	Sonnblick
11036	Vienna/Schwechat	11150	Salzburg
14521/	Langenleibarn	11157	Aigen
		11165	Zeltweg
		11231	Klagenfurt
		11240	Graz

Table F-2 (continued)

BALEARIC ISLANDS (from U.S. Naval Weather Service, 1971a). Figure F-4 shows station locations.

Station No.	Name
08306	Palma/Son San Juan
08314	Mahon-San Luis

BULGARIA (from U.S. Naval Weather Service, 1973). Figure F-1 shows station locations and climatic areas.

Station No.	Name	Station No.	Name
LOWLANDS (Climatic Area 1)		S. W. HIGHLANDS (Climatic Area 2)	
15511	Lom	15613	Cherni
15526	Pleven	15614	Sofia
15535	Rousse	15615	Mussala
15552	Varna	15622/	Ikhtiman
15625	Plovdiv	15627	Botev Vrah
15635	Chirpan/Tchirpan	15712	Sandanski
15640	Sliven	15725	Smolyan/Raykovo
15655	Bourgas	15730	Kurdjali

CORSICA (FRANCE) (from U.S. Weather Service, 1971b). Figure F-5 shows station locations.

Station No.	Name
07761	Ajaccio/Campo Dei Oro
07765	Solenzara
07768	La Chiappa
07790	Bastia/Poretta
14529/	Ajaccio

CISTE (GREECE) (from U.S. Weather Service, 1971b). Figure F-6 shows station locations.

Station No.	Name
16746	Soudna Bay
16747	Khania
16754	Kriti/Iraklion

CYPRUS ISLAND (from U.S. Naval Weather Service, 1974a). Figure F-7 shows station locations.

Station No.	Name
17602/	Morphou Bay
17600	Paphos
17601	Akrotiri
17606	Nicosia
17611	Ayios

Table F-2 (continued)

CZECHOSLOVAKIA (from U.S. Naval Weather Service, 1973). Figure F-8 shows station locations and climatic areas.

Station No.	Name	Station No.	Name
W. HILLS PLAINS (Climatic Area 1)		EASTERN LOWLANDS (Climatic Area 2)	
11406	Cheb	11723	Brno
11448	Plzen/Dobraney	11782	Moravska/Ostrava
11518	Prague/Praha/Ruz	11816	Bratislava
11541	Ceske/Budejovice	11968	Kosice
11648	Hradek/Kralove		
11659	Pribyslav	EASTERN MOUNTAINS (Climatic Area 3)	
11735	Praded	11903	Slac
		11930	Lomnický/Štit

FRANCE (from U.S. Naval Weather Service, 1971a). Figure F-9 shows station locations and climatic areas.

Station No.	Name	Station No.	Name
PLAINS (Climatic Area 1)		PLAINS (Climatic Area 1)	
07003	Le Touquet-Paris Plage	07249	Orleans-Bricy
07015	Lille-Lesquin	07255	Bourges
07017	Cambrai-Epinoy	07257	Avord
07024	Cherbourg-Maupertus	07335	Poitiers-Biard
07027	Caen-Carpique	07354	Chateauroux
07028	Le Havre	07400	La Coubre
07038	Evreux-fauville	07412	Cognac-Chateaubernard
07053	Pontoise-Cormeilles-En-Vexin	07502	Cazaux
07055	Beauvais-Tille	07510	Bordeaux-Merignac
07057	Creil-Senlis	07602	Biarritz-Bayonne-Anglet
07070	Reims-Champagne	07603	Dax-Seyresse
07074	Suippes Gun RG	07607	Mont-De-Marsan
07109	Lanveoc-Poulmic	07610	Pau-Pont Long Uzein
07110	Brest-Guipavas	07630	Toulouse-Blagnac
07121	Brehat	07631	Toulouse-Francazai
07125	Dinard-Pleurtuit	07720	Pic Du Midi
07130	Rennes-St Jacques	07747	Perpignan-Ilabanne
07140	Chateaudun	14544/	St. Andre-De-L'eure
07141	Dreux AB	14547/	Berck Plage
07146	Toussus-Le-Noble	14548/	Cambrai/Wirgnies
07147	Villacoublay-Velizy	14550/	Coulommiers-Voisins
07148	Bretigny-Sur-Orge	14553/	Laon-Couvron
07149	Paris/Orly	14555/	Merville-Calonne
07150	Paris/Le Bourget	14558/	Orleans-Saran
07153	Melun	14559/	Roche fort
07205	Lorient-Lann Bihoue	14561/	Toulouse
07207	Letaut	14562/	Tours
07217	St Nazaire-Montoir	14564/	Valenciennes
07222	Nantes-Chateau Bougon	14565/	Villaroche
07240	Tours-St Symphorien	14566/	Vouziers-Sechault

Table F-2 (continued)

FRANCE (continued)

Station No.	Name	Station No.	Name
PLATEAU (Climatic Area 2)		RHONE VALLEY (Climatic Area 4)	
07088	Etain-Rouvres	07280	Dijon
07090	Metz-Frescaty	07480	Lyon-Bron
07169	St. Dizier-Robinson	07577	Montelimar
07170	Chaumont	07579	Orange-Caritat
07179	Toul-Rosieres	07641	Sete
07180	Nancy-Essey	07643	Montpellier Frejorgues
07181	Nancy-Ochey	07645	Nimes
07186	Phalsbourg	07646	Nimes-Garons
07190	Strasbourg-Entzheim	07647	Istres-Le Tube
07197	Colmar-Meyenheim	07648	Salon
07292	Luxeuil-St. Sauveur	07650	Marseille/Marignane
07299	Bale-Mulhouse	14546/	Avignon
07372	St. Yan	14563/	Valence-Chabeuil
14549/	Chambley	FRENCH ALPS (Climatic Area 5)	
14552/	Gros Tenquin	07491	Chambery-Aix Les Bains
14554/	Lure-Malbouhans	SOUTHEAST COAST (Climatic Area 6)	
14556/	Mirecourt	07667	Hyeres-Le Palyvestre
14557/	Montmedy-Marville	07680	Frejus-St. Raphael
14560/	Rocroi-Regniowez	07690	Nice-Cote D'Azur
CENTRAL MASSIF (Climatic Area 3)		14545/	Antibes
07374	Vichy-Charmeil	14551/	Cuers-Pierrefeu
07460	Clermont Ferrand		
07558	Millau		

GIBRALTAR (from U.S. Naval Weather Service, 1971a). Figure F-4 shows station locations.

Station No.	Name
08495	North Front
14567/	Windmill Hill

GREECE (From U.S. Weather Service, 1971b). Figure F-6 shows station locations.

Station No.	Name
14568/	Agrinion New
14569/	Provoza
16622	Thessaloniki
16625	Kavalla
16627	Alexandroupolis
16632	Kozani
16641	Kerkira
16642	Ioannina
16648	Larisa
16661	Volos
16665	Nea Anklialos
16669	Levkas
16672	Agrinion
16682	Andravida
16687	Araxos
16701	Athina-Filadelfia
16716	Athina
16718	Elefsis

Table F-2 (continued)

HUNGARY (from U.S. Naval Weather Service, 1973). Figure F-10 shows station locations.

Station No.	Name
12772	Miskolc
12812	Szombathely
12840	Budapest
12860	Szolnok
12882	Debrecen
12920	Keszthely
12940	Pecs
12982	Szeged

ISRAEL (from U.S. Naval Weather Service, 1974b). Figure F-11 shows station locations and climatic areas.

Station No.	Name	Station No.	Name
DESERT (Climatic Area 1)		COASTAL (Climatic Area 2)	
40199	Eilat	40182/	Eqron
		40185/	Hatzor
		40153	Har-Kena'an
		40154	Haifa
		40165	Ramat David
		40177	Tel Aviv
		40180	Lod
		40184	Jerusalem
		40191	Beersheva

ITALY (from U.S. Weather Service, 1971b). Figure F-5 shows station locations and climatic areas.

Station No.	Name	Station No.	Name
DOLOMITES (Climatic Area 1)		WESTERN COAST (Climatic Area 4)	
16020	Bolzano	14575/	Genova
		14577/	Napoli/Pomiglian
PO VALLEY (Climatic Area 2)		16120	Genova/Sestre
14576/	Montichiari	16122	Villanova D'Albenga
14578/	Venegono	16158	Pisa/San Giusto
16036	Aviano	16170	Florence
16044	Udine-Campoformido	16206	Grosseto
16045	Rivolto	16234	Roma/Guidonia
16061	Torino Caselle	16235	Roma/Urbe
16064	Cameri	16238	Centocelle
16066	Milano/Malpensa	16239	Roma/Ciampino
16076	Bergamo-Orio Al Serio	16242	Roma/Fiumicino
16080	Milano/Linate	16243	Latina
16084	Piacenza	16245	Pratica Di Mare
16088	Ghedì	16253	Capua-Grazzanise
16089	Verona-Boscomantico	16289	Napoli/Capodichino
16090	Villafranca-Ganfardine	APENNINES (Climatic Area 5)	
16094	Vicenza	16180	Perugia
16098	Istrana	16350	Crotone
16099	Treviso City		
16100	Venezia		
16105	Venezia-Tessera		
16106	Gorizia		
16108	Ronchi Del Legionari		
16140	Bologna		
16149	Rimini		

Table F-2 (continued)

ITALY (continued)

Station No. Name

EASTERN COAST (Climatic Area 6)

14573/	Foggia-Orta Nova
14574/	Foggia
16191	Ancona-Falconara
16230	Pescara
16261	Amendola
16270	Bari
16320	Brindisi/Campo Casale
16324	Grottaglie
16330	Taranto
16332	Lecce/San Donato

JORDAN (from U.S. Naval Weather Service, 1974b). Figure F-12 shows station locations and climatic areas.

Station No. Name

Station No. Name

WESTERN HIGHLANDS (Climatic Area 1)

EASTERN PLAINS (Climatic Area 2)

40280 Jericho

40250	H4
40265	Ma'fra
40270	Amman
40310	Ma'An

LEBANON (from U.S. Naval Weather Service, 1974b). Figure F-13 shows station locations and climatic areas.

Station No. Name

Station No. Name

COASTAL STRIP (Climatic Area 1)

HIGHLANDS (Climatic Area 2)

40100	Beirut Intl
40103	Tripoli/Kleiate

40102	Rayack
40104	Merdjayoun
40105	Les Cedres

LIBYA (from U.S. Naval Weather Service, 1968). Figure F-14 shows station locations and climatic areas.

Station No. Name

Station No. Name

COASTAL (Climatic Area 1)

DESERT (Climatic Area 3)

62007	Zuara
62010	Idris
62011	Wheelus Field
62016	Misurata
62019	Sirte
62020/	Marble Arch
62021	El Agheila

62002	Nalut
62103	Ghadames
62124	Sebha
62131	Hcn
62161	Gialo
62176	Giarabub
62259	Tazerbo
62260/	Ghat
62271	Kurfa

EASTERN COAST (Climatic Area 2)

62053	Benina
62055	Agedabia
62059	Derna
62063	El Adem

Table F-2 (continued)

MALTA (from U.S. Weather Service, 1971b). Figure F-5 shows station locations.

Station No.	Name
14200/	Hal Far
14583/	Ta Kali
16597	Luqa

MOROCCO (from U.S. Naval Weather Service, 1968). Figure F-15 shows station locations and climatic areas.

Station No.	Name	Station No.	Name
COASTAL (Climatic Area 1)		ATLAS MOUNTAINS (Climatic Area 2)	
60100	Tangier Boukhalf	60125	Touahar
60109	Saïdi Site II	60195	Midelt
60115	Oujda Angad	60265	Ouarzagate
50119/	Kenitra NAF	SOUTH COASTAL (Climatic Area 3)	
60130	Rabat Ville	60087/	Hassi Tan Tan
60135	Rabat Sale	60250	Agadir-Inezgane
60136	Sidi Siimane	INLAND PLAINS (Climatic Area 4)	
60150	Meknes	60281/	Foum El Hassane
60154/	Nouasseur		
60155	Casablanca-Anfa		
60185	Safi		
60190	Kasba-Tadla		
60204/	Ben Guerir		
60220	Essaouira		
60230	Marrakech		
60318	Tetuan-Rio Marti		
60338	Melilla		
60340	Idador Tauima		

PORTUGAL (from U.S. Naval Weather Service, 1971a). Figure F-4 shows station locations and climatic areas.

Station No.	Name	Station No.	Name
MOUNTAINS (Climatic Area 1)		PLAINS (Climatic Area 2)	
08557	Evora	08530	Cabo Carvoeiro
08566	Villa Real	08536	Lisbon/Portela
08568	Penhas Douradas	08538	Sagres-Cabo De Sao Vincente
08575	Braganca	08543	Viana Do Castelo
		08545	Porto
		18549	Coimbra
		04554	Faro
		14282/	Ota
		14591/	Alverca
		14592/	Alveiro
		14593/	Monte Roci
		14594/	Montijo
		14596/	Ovar
		14597/	Santarem
		14598/	Sintra
		14599/	Tancos

Table F-2 (continued)

RUMANIA (from U.S. Naval Weather Service, 1973). Figure F-16 shows station locations and climatic areas.

Station No.	Name	Station No.	Name
CENTRAL HIGHLANDS (Climatic Area 1)		LOWLANDS (Climatic Area 2)	
15040/	Cimpulung Moldov	15010	Satu-Mare
15120	Cluj	15080	Oradea
15230	Deva	15090	Iasi
15260	Sibiu	15150	Bacua
15280	Omurluf	15200	Arad
		15247	Timisorara
		15310	Galati
		15360	Silani
		15410	Turnu-Severin
		15420	Bucharest/Bucuresti
		15480	Constanta
		15490	Turnu-Magurele

SARDINIA (ITALY) (from U.S. Weather Service, 1971b). Figure F-5 shows station locations and climatic areas.

Station No.	Name	Station No.	Name
WESTERN COAST (Climatic Area 1)		EASTERN COAST (Climatic Area 3)	
14202/	Sassari	16506	Guardiavecchia
16520	Alghero	16530	Olbia
16539	Oristano	16550	Capo Bellavista
16546	Decimomannu	16564	Capo Carbonara
16560	Cagliari/Elmas		

INTERIOR MOUNTAINS (Climatic Area 2)

14201/	Nuoro
16524	Macomer
16538	Fonni

SICILY (from U.S. Weather Service, 1971b). Figure F-5 shows station locations.

Station No.	Name
16405	Palermo/Punta Raisi
16410	Palermo
16420	Messina
16429	Trapani-Birgi
16436	Sciacca
16450	Enna
16459	Catania-Sigonella
16460	Catania
16464	Siracusa
16470	Pantelleria
16480	Gozzo Spadaro

Table F-2 (continued)

SPAIN (From U.S. Naval Weather Service, 1971a). Figure F-3 shows station locations and climatic areas.

Station No.	Name	Station No.	Name
NORTH COAST (Climatic Area 1)		EASTERN COAST (Climatic Area 3)	
00001	San Sebastian	00135	Bouss
00002	San Sebastian	00136	Borcolene
00003	San Sebastian	00137	Valencia
00004	San Sebastian	00138	Alicante
SOUTHERN COAST (Climatic Area 2)		00139	Marsic-Alcantarilla
00005	San Sebastian	00140	San Javier
00006	San Sebastian	00141	Malaga
00007	San Sebastian	00142	Los Alamos
00008	San Sebastian	SOUTHWEST COAST (Climatic Area 4)	
00009	San Sebastian	00143	Sevilla/Tablada
00010	San Sebastian	00144	Sevilla/San Pablo
00011	San Sebastian	00145	Marea De La Frontera
00012	San Sebastian	00146	Rota
00013	San Sebastian	00147	Jerez
00014	San Sebastian		
00015	San Sebastian		
00016	San Sebastian		
00017	San Sebastian		
00018	San Sebastian		
00019	San Sebastian		
00020	San Sebastian		
00021	San Sebastian		
00022	San Sebastian		
00023	San Sebastian		
00024	San Sebastian		
00025	San Sebastian		

SWITZERLAND (From U.S. Naval Weather Service, 1971a). Figure F-3 shows station locations.

Station No.	Name
00610	Basel
00611	Basel
00612	Zurich
00613	Zurich
00614	Geneva/Coligny
00615	Geneva
00616	Lugano
00617	Samaden
00618	Geneva
00619	Geneva
00620	Geneva
00621	Geneva
00622	Geneva
00623	Geneva
00624	Geneva
00625	Geneva

Table F-2 (continued)

SYRIA (from U.S. Naval Weather Service, 1974b). Figure F-17 shows station locations and climatic areas.

Station No.	Name	Station No.	Name
COASTAL STRIP (Climatic Area 1)		DESERT INTERIOR (Climatic Area 2)	
40022	Lattakia	40001	Qamichliye
		40007	Aleppo
		40030	Hamah
		40039	Ar Raqqa
		40079	Damascus

TUNISIA (from U.S. Naval Weather Service, 1968). Figure F-18 shows station locations and climatic areas.

Station No.	Name	Station No.	Name
NORTH COASTAL (Climatic Area 1)		CENTRAL (Climatic Area 2)	
60714	Bizerte	60745	Gafsa
60714	El Aouina/Tunis Carthage	60765	Gabes
60725	Souk El Araba		
		DESERT (Climatic Area 3)	
		60775/	Remada

TURKEY (from U.S. Naval Weather Service, 1974b). Figure F-19 shows station locations and climatic areas.

Station No.	Name	Station No.	Name
BLACK SEA (Climatic Area 1)		CENTRAL PLATEAU (Climatic Area 4)	
17022	Zonguldak	17074	Kastamonu
17026	Sinop	17082	Merzifon
17030	Samsun	17090	Sivas
17038	Trabzon	17124	Eskisehir
17042	Hopa	17127	Ankara-Murad
17050	Edirne	17128	Ankara-Esenboga
17060	Yedigöller	17129	Ankara-Etimesgut
17067	Gölcük	17160	Kirsehir
		17188	Usak
AEGEAN COAST (Climatic Area 2)		17190	Afyon
17056	Tekirdag	17195	Erkilet
17112	Canakkale	17240	Isparta
17115	Bandirma	17244	Konya
17150	Balikesir		
17184	Akhisar New	EASTERN MOUNTAINS (Climatic Area 5)	
17218	Cigli	17201/	Erhac
17220	Izmir	17092	Erzincan
17296	Bodrum	17096	Erzurum
17292	Mugla	17098	Kars
		17100	Igdir
MEDITERRANEAN COAST (Climatic Area 3)		17170	Van
17300	Antalya	17200	Malatya
17330	Silifke		
17350	Adana/Incirlik	SOUTHEAST PLAINS (Climatic Area 6)	
17370	Iskenderun	17281/	Batman
		17210	Siirt
		17270	Urfa
		17280	Diyarbakir

Table F-2 (continued)

UNITED ARAB REPUBLIC (Egypt) (from U.S. Naval Weather Service, 1968). Figure F-20 shows station locations and climatic areas.

Station No.	Name	Station No.	Name
DESERT (Climatic Area 1)		NILE VALLEY (Climatic Area 2, Cont.)	
62300	Salum/Salloum	62367/	Cairo West
62306	Matruh	62370/	Inchas
62334/	Bir Gifgafa New	62371/	Cairo-Heliopolis
62335/	Gebel Libni	62372/	Cairo-Almaza
62336	El Arish	62375/	Belbeis 2
62361/	Kabrit	62378	Helwan
62412/	Daraw	62387	Minya
62414	Aswan Dam	62392/	Drrunkah
62417	Siwa	62393	Asyut/Manqabad
62420	Baharia	62405	Luxor
62432	Dakhla	62438/	Abu Suweir
62433/	El Nakhl	62441/	Ismailia
62444/	Fayid		
NILE VALLEY (Climatic Area 2)		RED SEA HILLS (Climatic Area 3)	
62312/	Dekheila	62408/	Ras Jimsah
62318	Alexandria	62413/	Ras Banas
62320/	Rumana	62459	El Tor
62333	Port Said	62462	Hurghada New
62342/	El Mansura	62465	Kosseir
62345/	Quweisna	62470/	Wadi Gimal
62355/	Kafr Daud	62471/	Daedalus
62365	Belbeis		
62366	Cairo		

YUGOSLAVIA (from U.S. Weather Service, 1971b). Figure F-6 shows station locations and climatic areas.

Station No.	Name	Station No.	Name
ADRIATIC COAST (Climatic Area 1)		DINARIC ALPS (Climatic Area 2, cont.)	
13107	Knpar	13027	Maribor
13113	Rijeka	13223	Gospic
13208	Pula	13228	Bihac
13219	Senj	13352	Sarajevo-Rajlovac
13222	Zadar	13353	Sarajevo-Butmir
13224	Zemunik	13464	Kolasin
13333	Split-Marjan	13472	Pec
13335	Hvar	13483	Skopje
13349	Mostar City	13488	Vranje
13451	Dubrovnik	13582	Bitula
13457	Hercegnovi	13584	Prilip
13462	Titograd/Intl	13590	Stip
13562	Ulcinj	13592	Demir Kapija
14032/	Mostar-Kostor	14050/	Ajdovscina
14063/	Mostar	14051/	Baono Polje
14066/	Omisalj	14054/	Celje
14069/	Rab	14056/	Golnik
14073/	Sipan	14057/	Jezersko
14074/	Split Lazarica	14058/	Kocevje
14076/	Titograd	14059/	Kosovska Mitrovica
DINARIC ALPS (Climatic Area 2)		14067/	Petrovac
13017	Ljubljana	14068/	Postojna
13018	Ljubljana/Intl	14070/	Ratece-Planina
		14071/	Ravna Gora
		14075/	Sent Jost na Kozjaku

Table F-2 (continued)

YUGOSLAVIA (continued)

Station No. Name

INTERIOR PLAINS (Climatic Area 3)

13122	Novo Mesto
13127	Zagreb-Grič
13128	Zagreb/Pleso
13150	Slavonski Brod
13156	Osijek
13123	Vrsac
3242	Banja Luka
13257	Tuzla
13261	Loznica
13266	Sremska Mitrovica
13274	Belgrade/Intl
13275	Belgrade
13285	Veliko Gradiste
13377	Kraljevo
13383	Krusevac
13388	Nis
14052/	Batajnica
14053/	Beograd-Zemun
14055/	Cerklje
14060/	Kragujevac
14061/	Lipik
14064/	Murska Sobota
14065/	Novi Sad
14072/	Senta



Figure F-1. Station locations and climatic areas in Albania and Bulgaria. WMO Station Index Numbers refer to cities listed in Table F-2 (from U.S. Naval Weather Service, 1973).

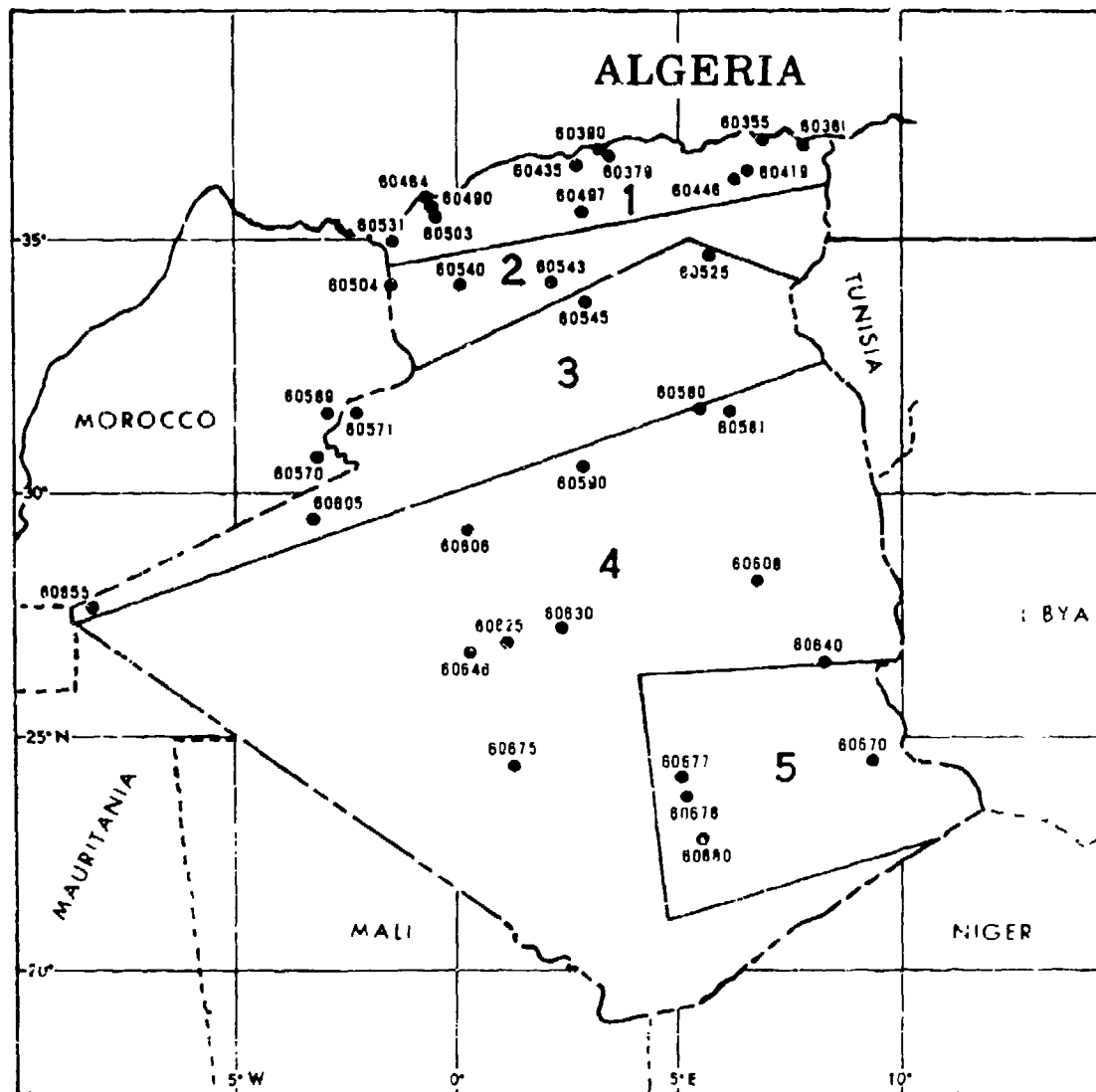


Figure F-2. Station locations and climatic areas in Algeria.
WMO Station Index Numbers refer to cities listed in
Table F-2 (from U.S. Naval Weather Service, 1968).

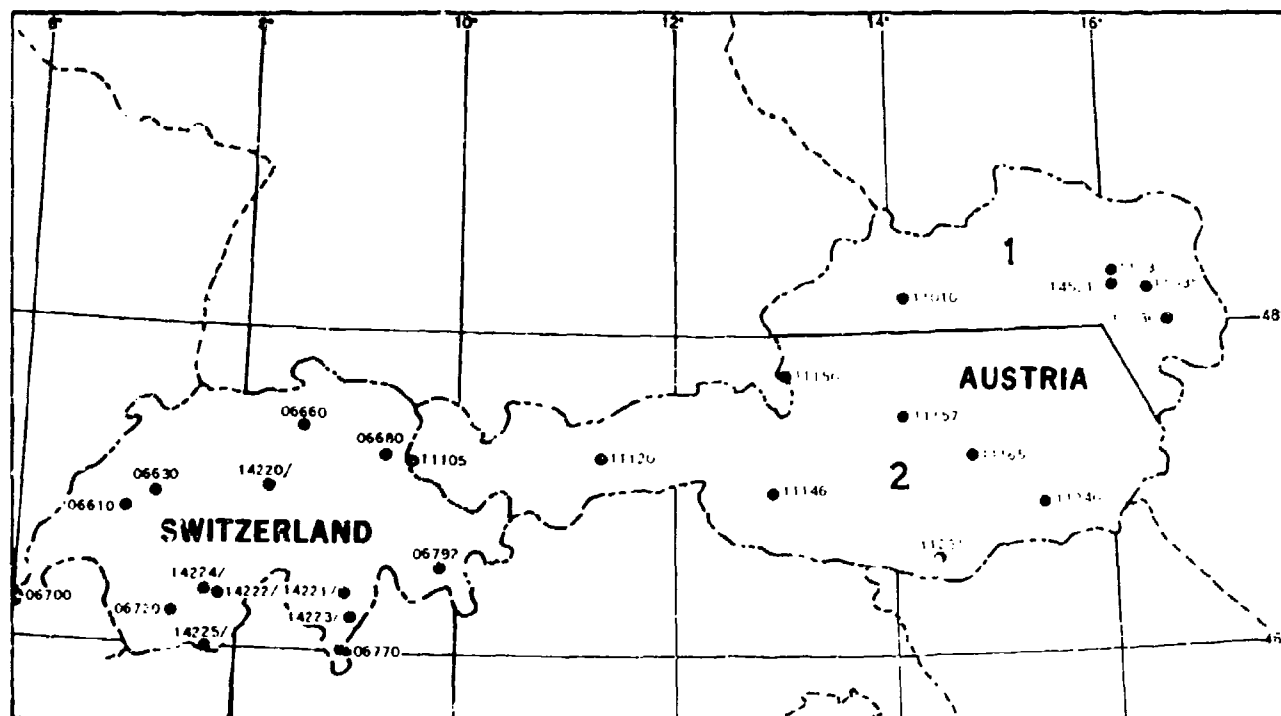


Figure F-3. Station locations and climatic areas in Austria and Switzerland. WMO Station Index Numbers refer to cities listed in Table F-2 (from U.S. Naval Weather Service, 1971a).

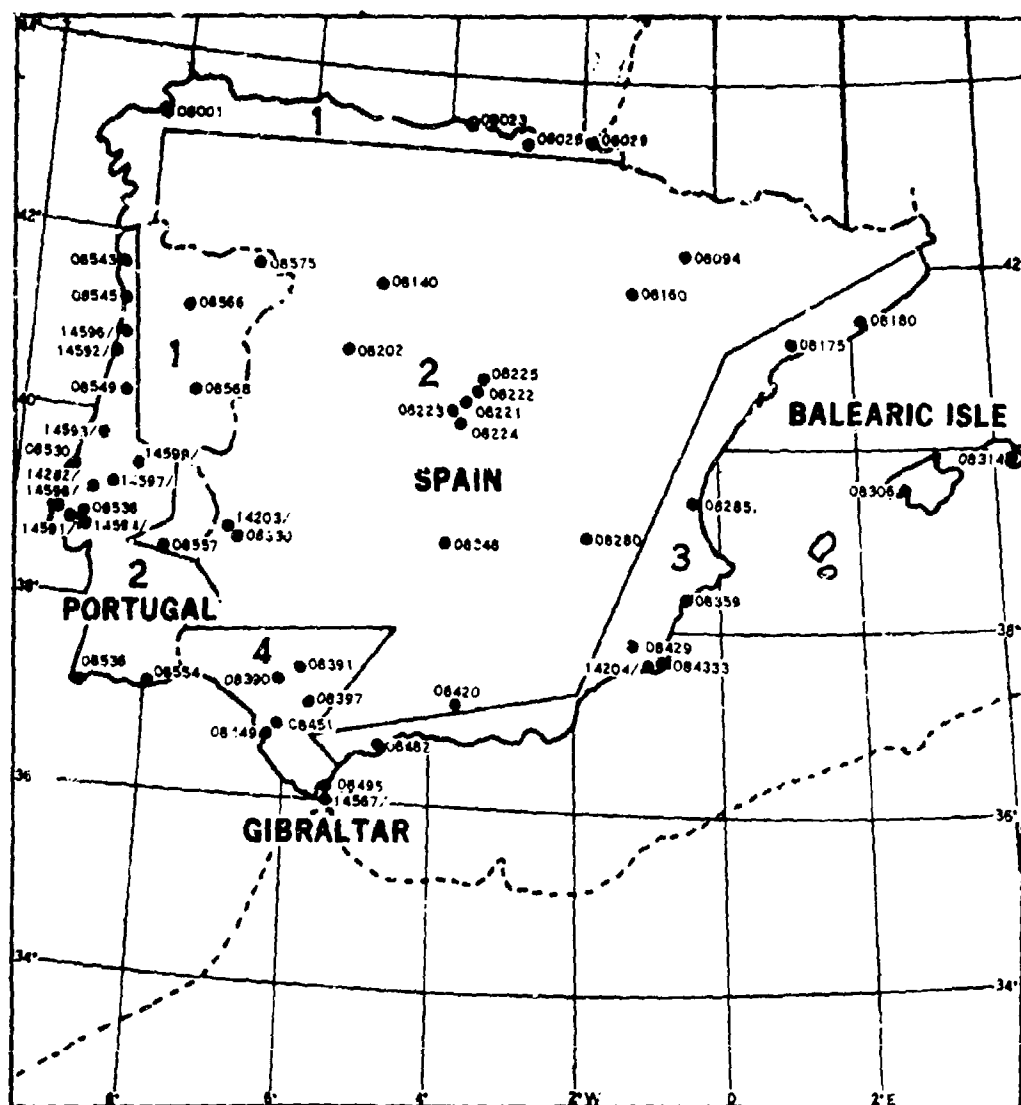


Figure F-4. Station locations and climatic areas in Balearic Islands, Gibraltar, Portugal and Spain. WMO Station Index Numbers refer to cities listed in Table F-2 (from U.S. Naval Weather Service, 1971a).



Figure F-5. Station locations and climatic areas in Corsica, Italy, Sicily, Malta and Sardinia. WMO Station Index Numbers refer to cities listed in Table F-2 (from U.S. Naval Weather Service, 1971b).

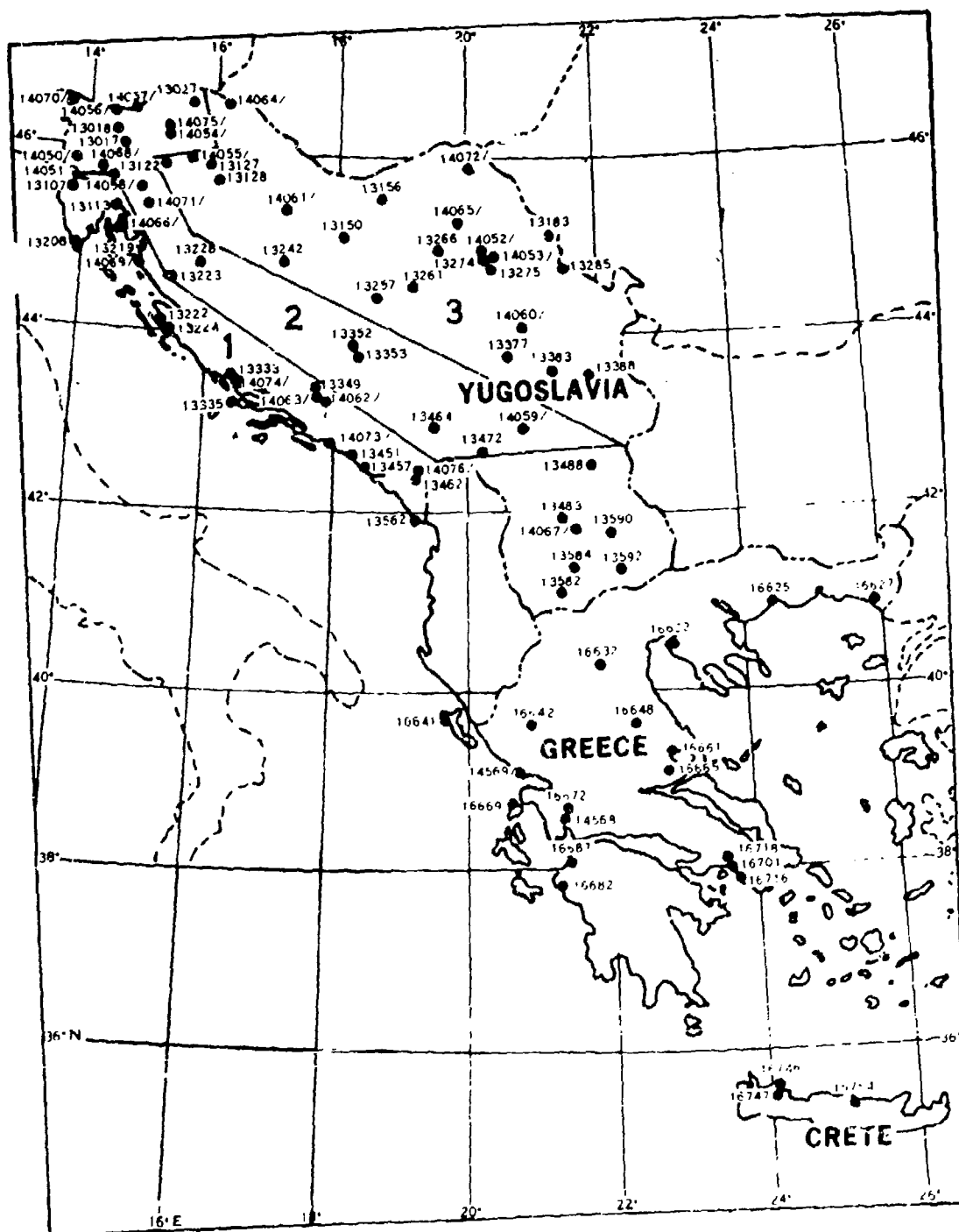


Figure F-6. Station locations and climatic areas in Crete, Greece and Yugoslavia. WMO Station Index Numbers refer to cities listed in Table F-2 (from U.S. Naval Weather Service, 1971b).

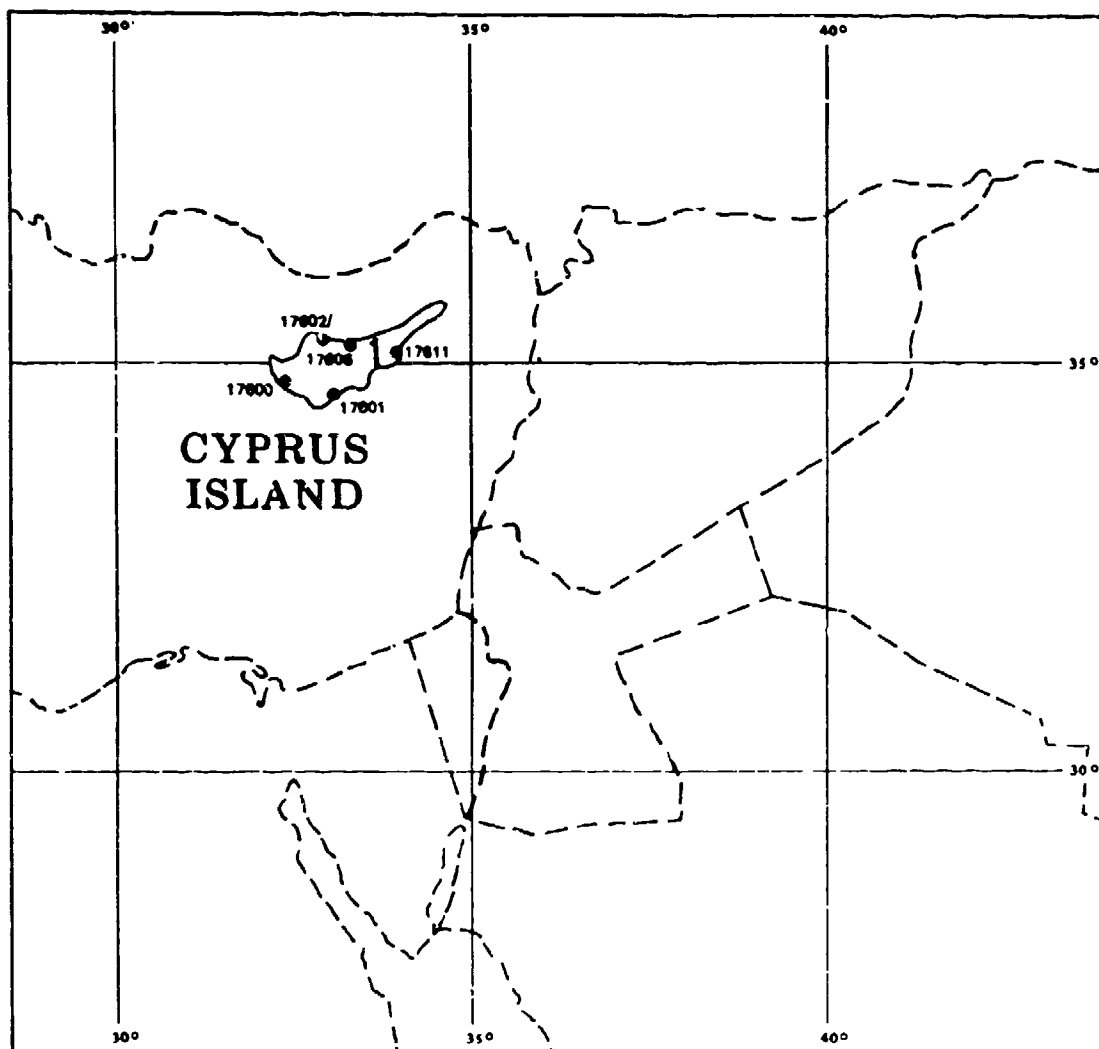


Figure F-7. Station locations in Cyprus. WHO Station Index Numbers refer to cities listed in Table F-2 (from U.S. Naval Weather Service, 1974a).



Figure F-6. Station locations and climatic areas in Czechoslovakia. WMO Station Index Numbers refer to cities listed in Table F-2 (from U.S. Naval Weather Service, 1973).

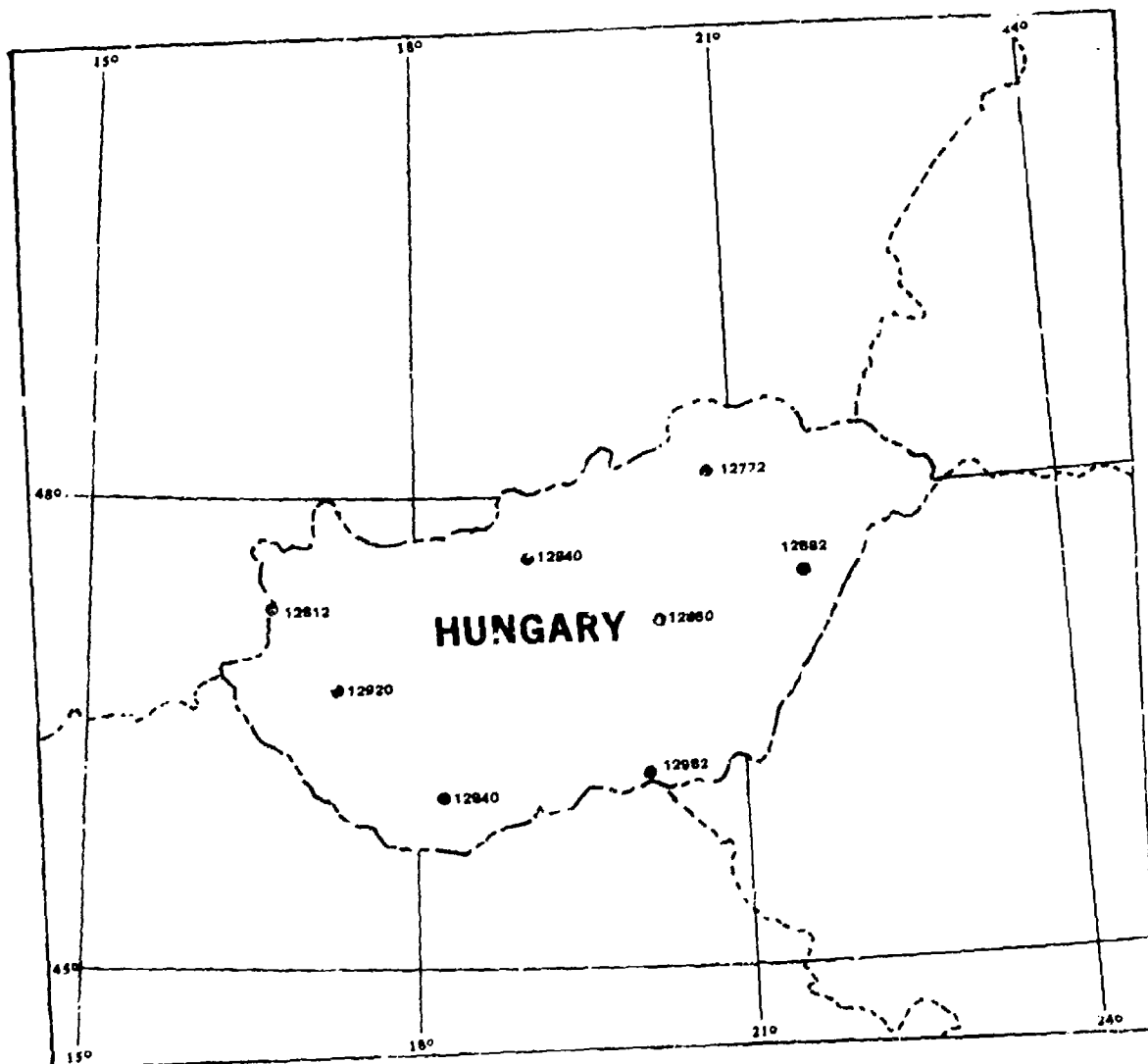


Figure F-10. Station locations in Hungary. WMO Station Index Numbers refer to cities listed in Table F-2 (from U.S. Naval Weather Service, 1973).

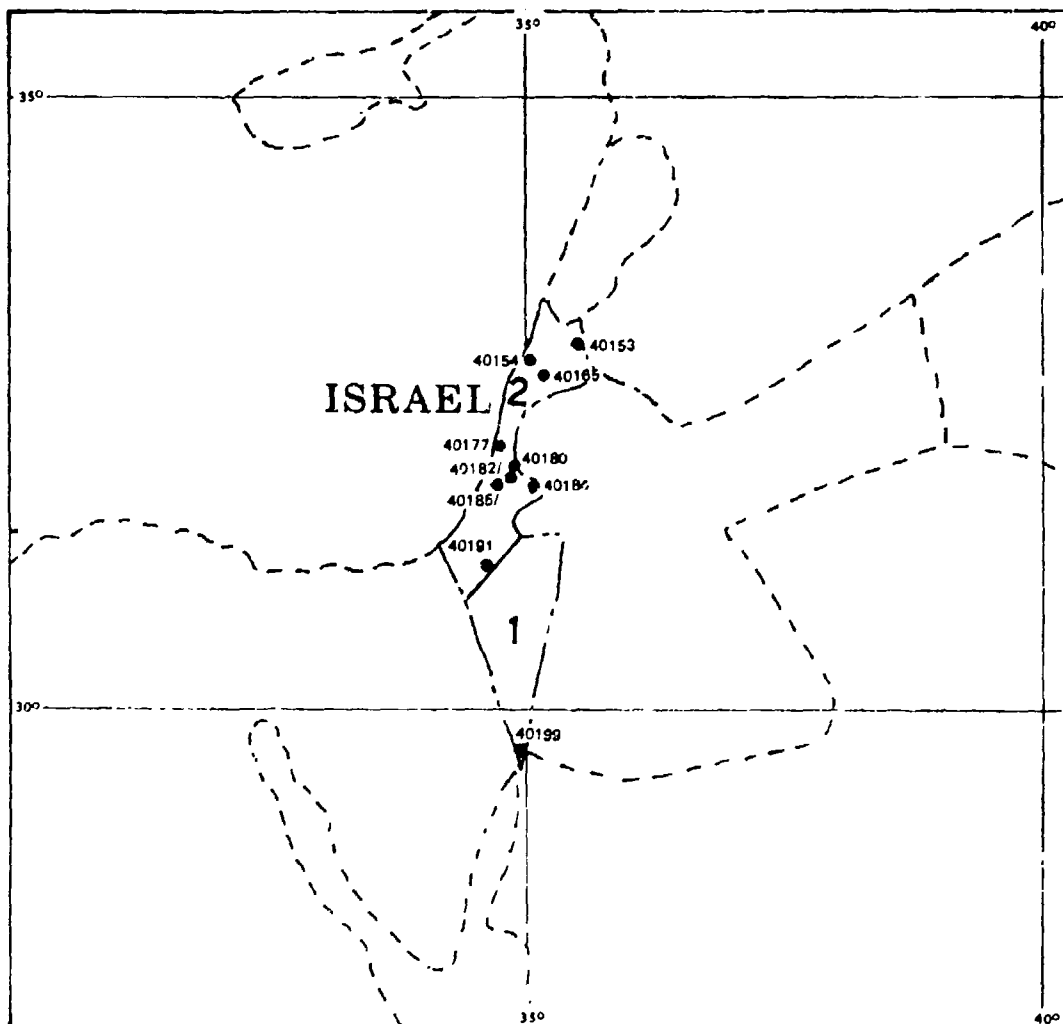


Figure F-11. Station locations and climatic areas in Israel.
WMO Station Index Numbers refer to cities in Table F-2
(from U.S. Naval Weather Service, 1974b).

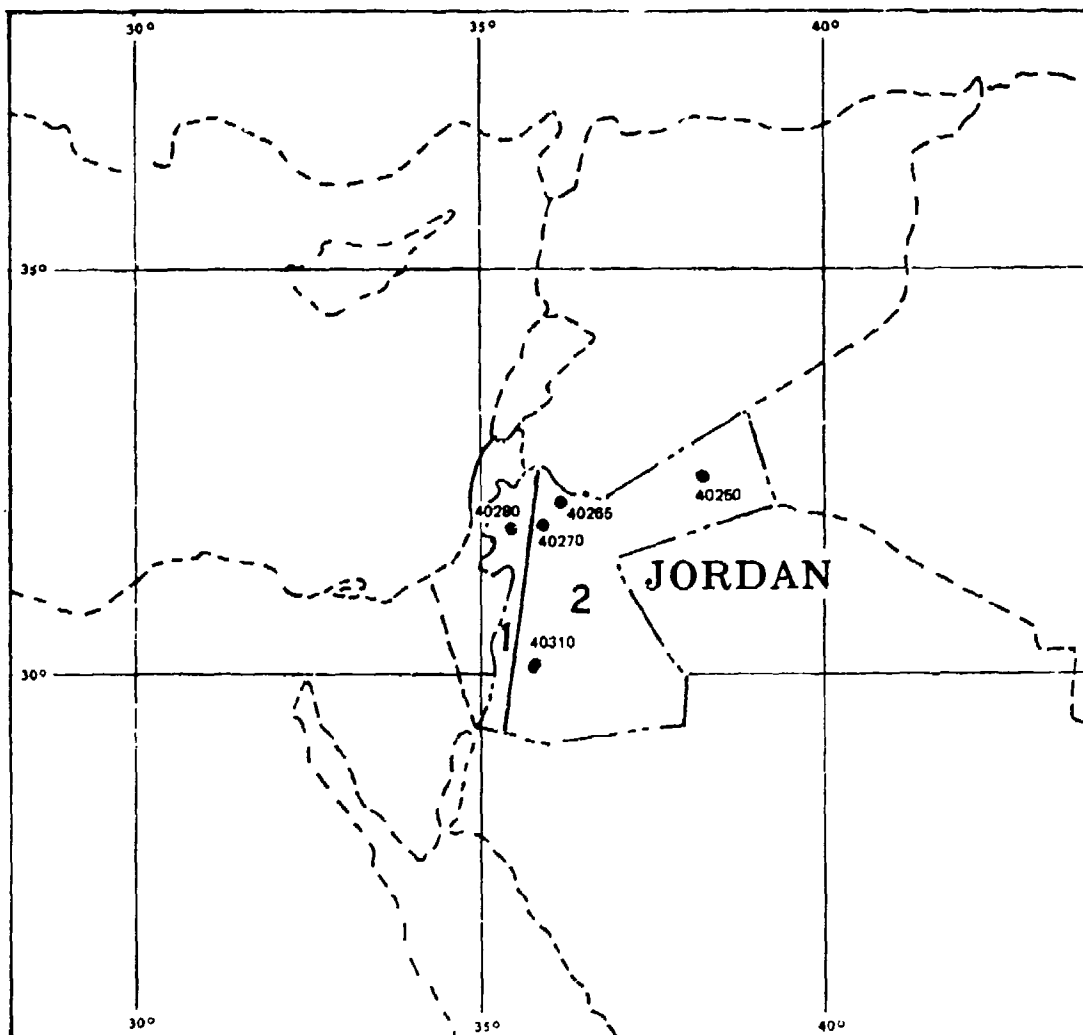


Figure F-12. Station locations and climatic areas in Jordan. WMO Station Index Numbers refer to cities listed in Table F-2 (from U.S. Naval Weather Service, 1974b).

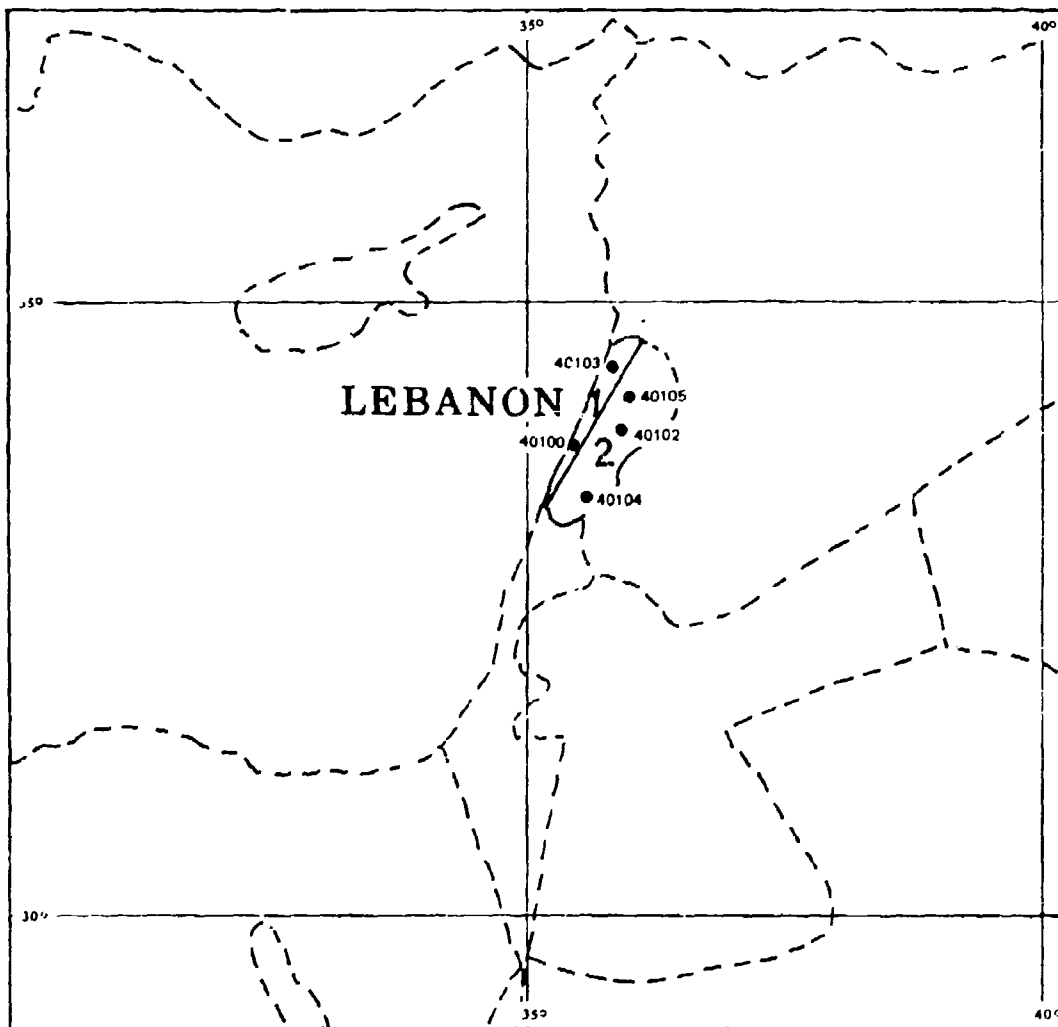


Figure F-13. Station locations and climatic areas in Lebanon. WMO Station Index Numbers refer to cities listed in Table F-2 (from U.S. Naval Weather Service, 1974b).

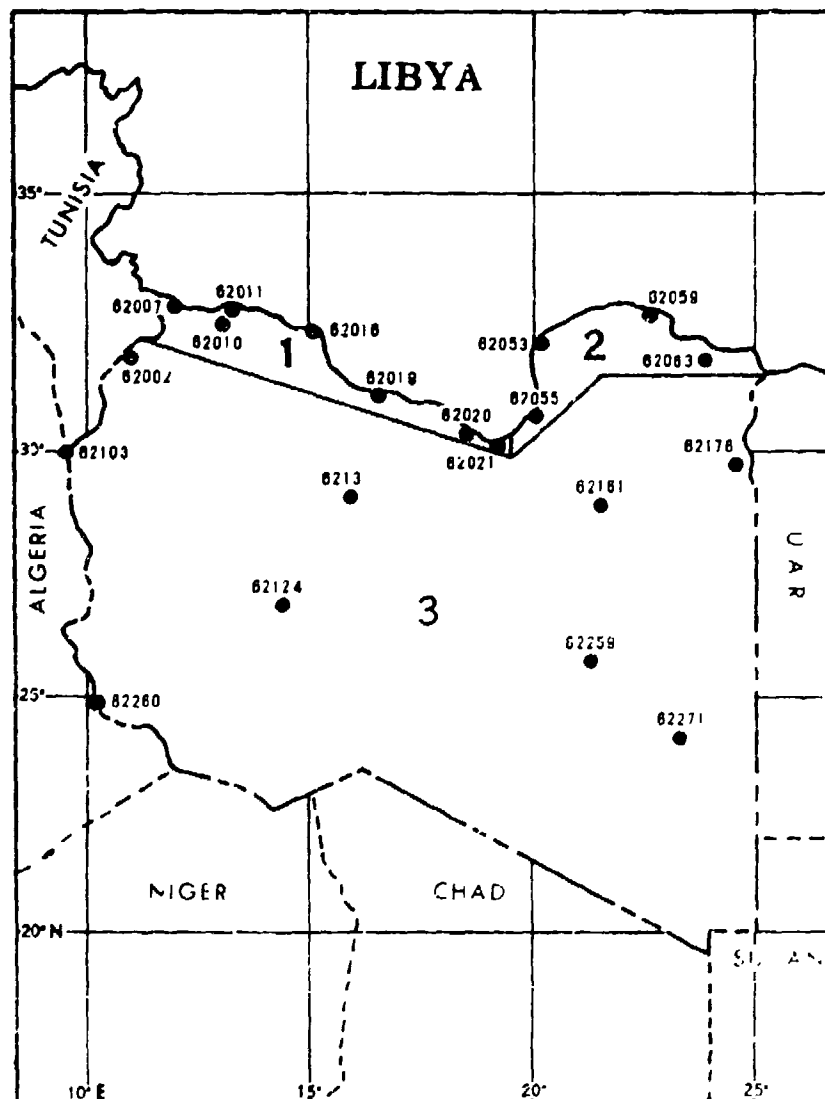


Figure F-14. Station locations and climatic areas in Libya.
WMO Station Index Numbers refer to cities listed in
Table F-2 (from U.S. Naval Weather Service, 1968).

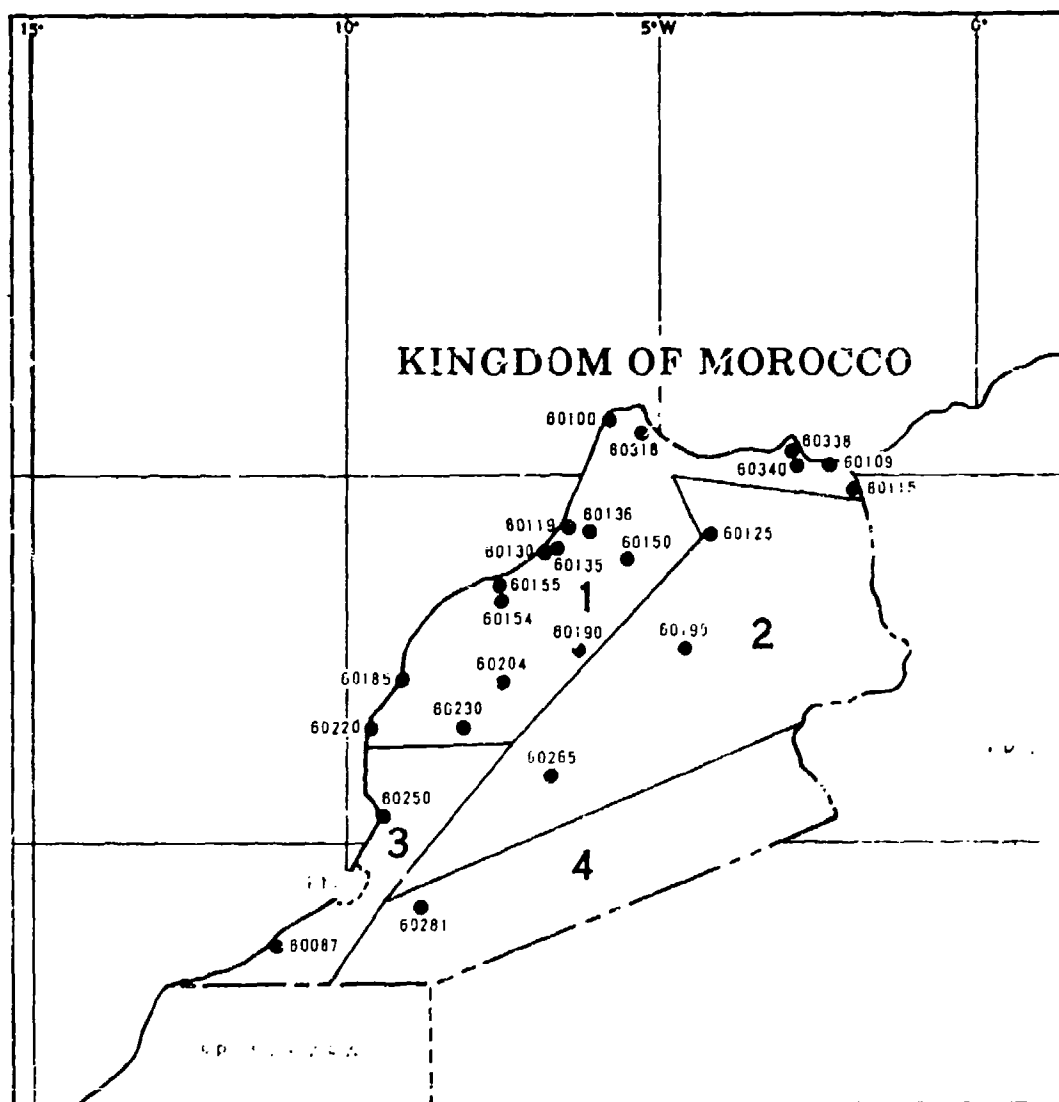


Figure F-15. Station locations and climatic areas in Morocco. WMO Station Index Numbers refer to cities listed in Table F-2 (from U.S. Naval Weather Service, 1968).

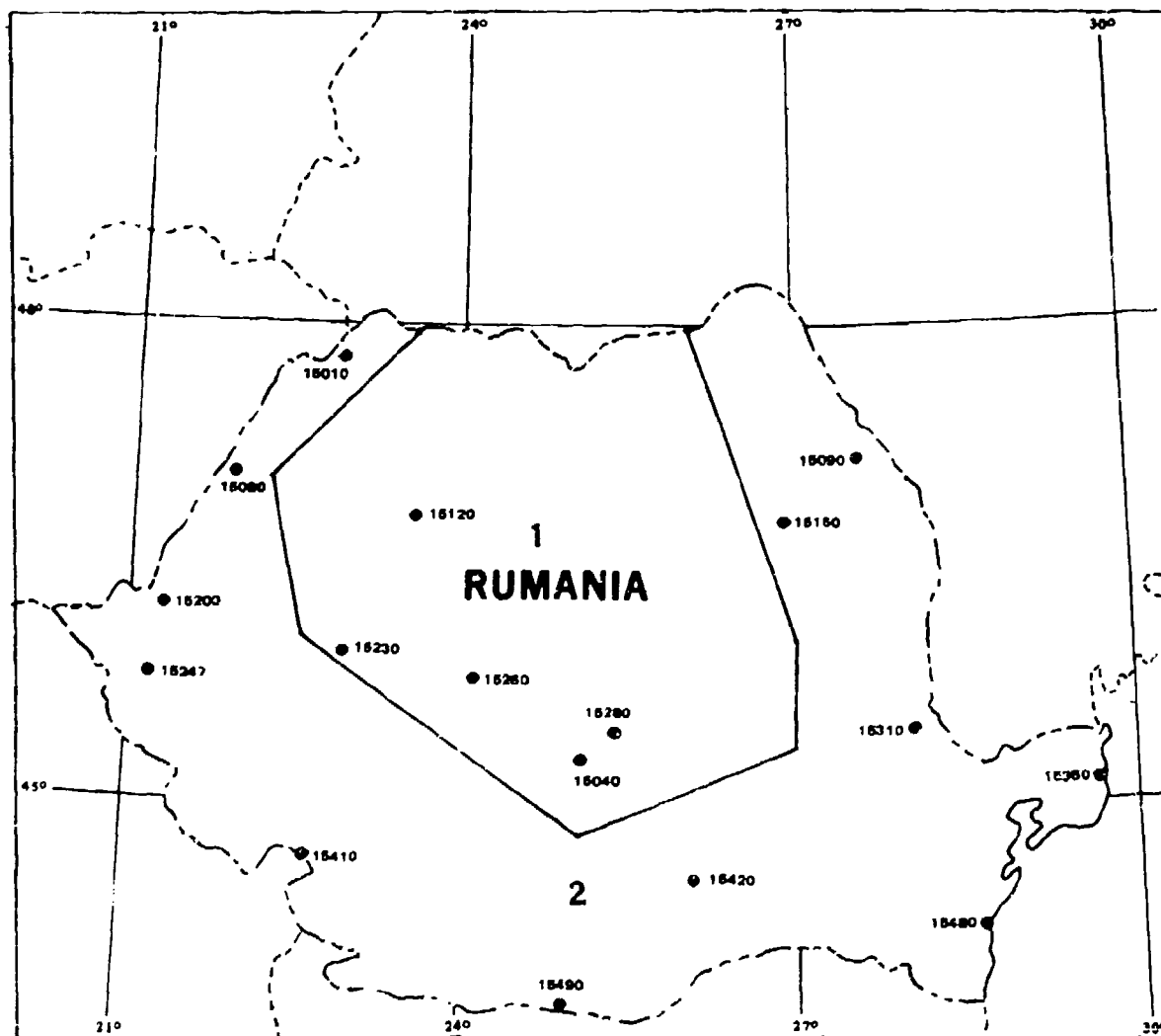


Figure F-16. Station locations and climatic areas in Rumania.
 WMO Station Index Numbers refer to cities listed in Table
 F-2 (from U.S. Naval Weather Service, 1973).

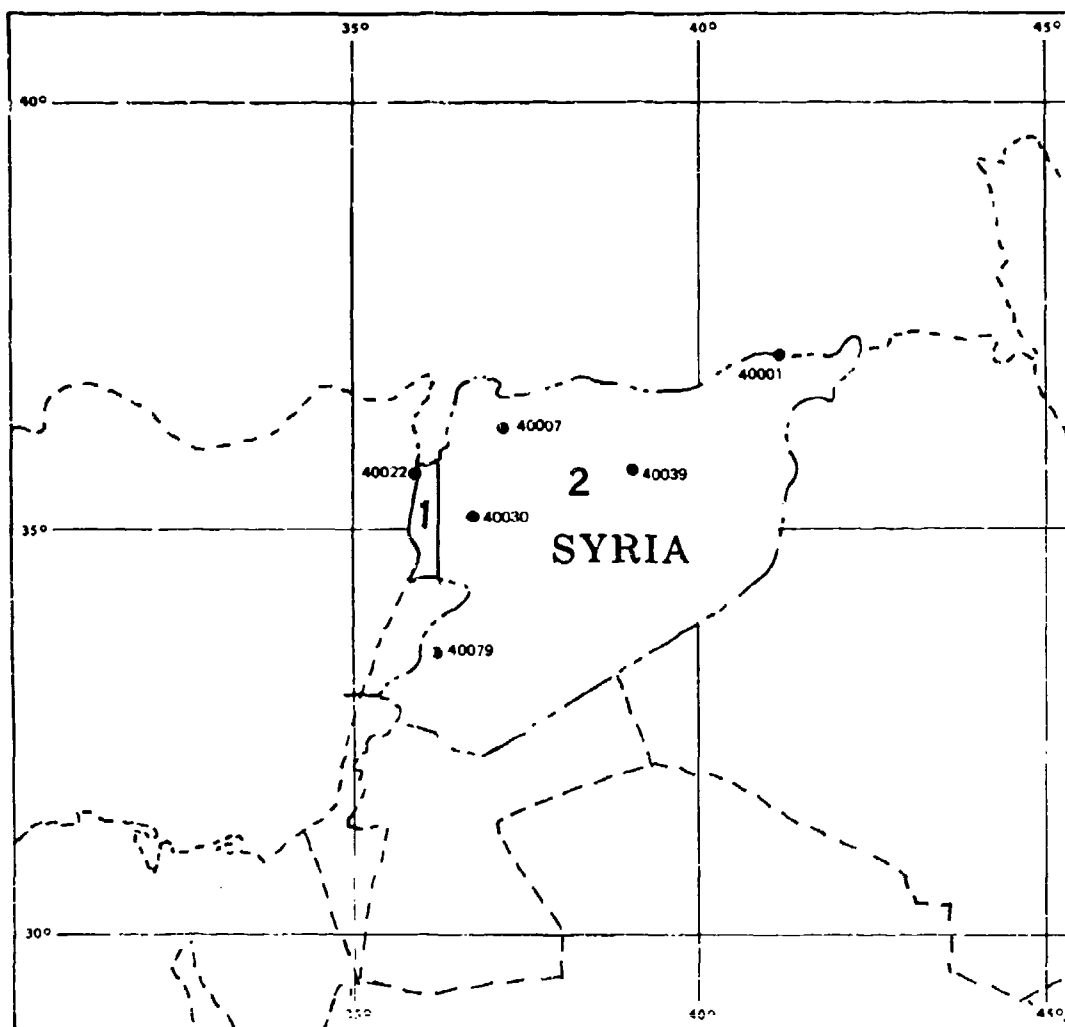


Figure F-17. Station locations and climatic areas in Syria. WMO Station Index Numbers refer to cities listed in Table F-2 (from U.S. Naval Weather Service, 19/4b).

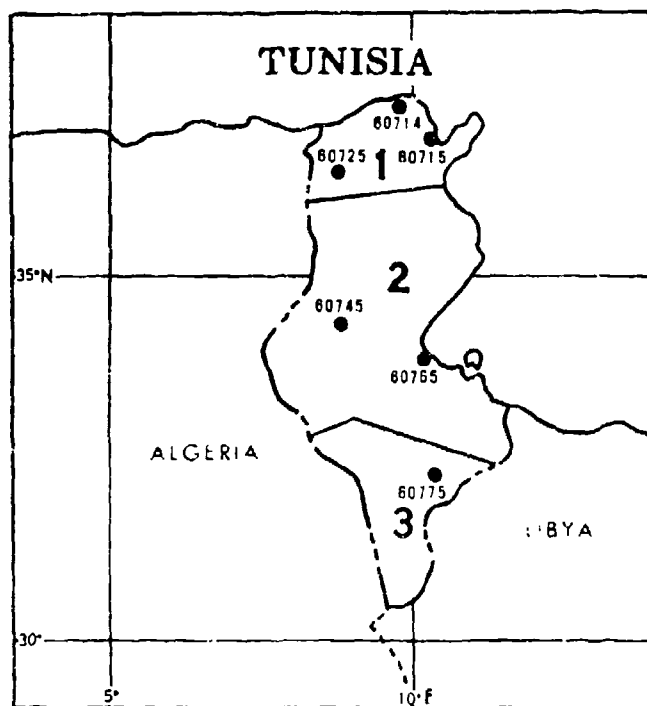


Figure F-18. Station locations and climatic areas in Tunisia.
WMO Station Index Numbers refer to cities listed in Table
F-2 (from U.S. Naval Weather Service, 1968).

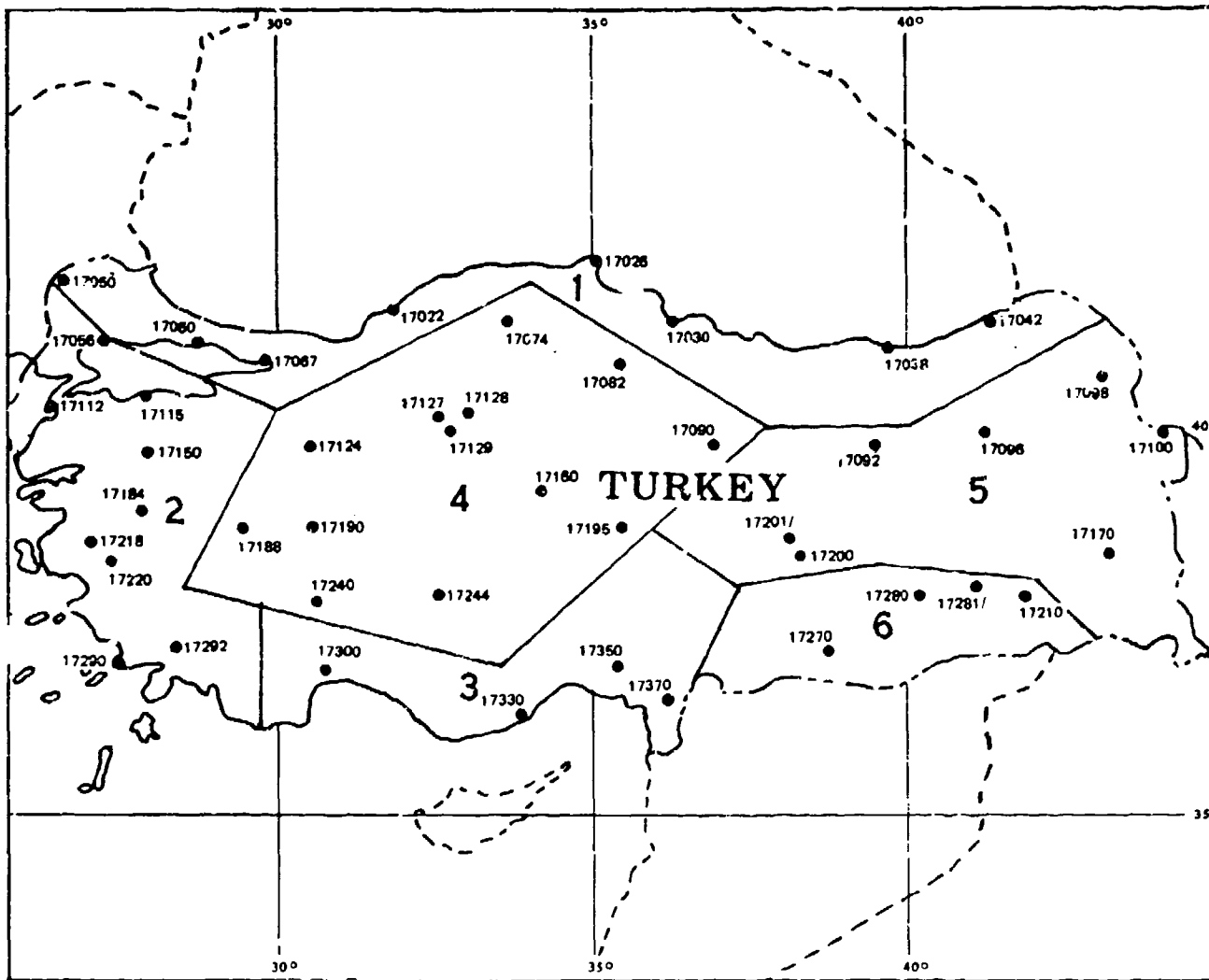


Figure F-19. Station locations and climatic areas in Turkey. WMO Station Index Numbers refer to cities listed in Table F-2 (from U.S. Naval Weather Service, 1974b).

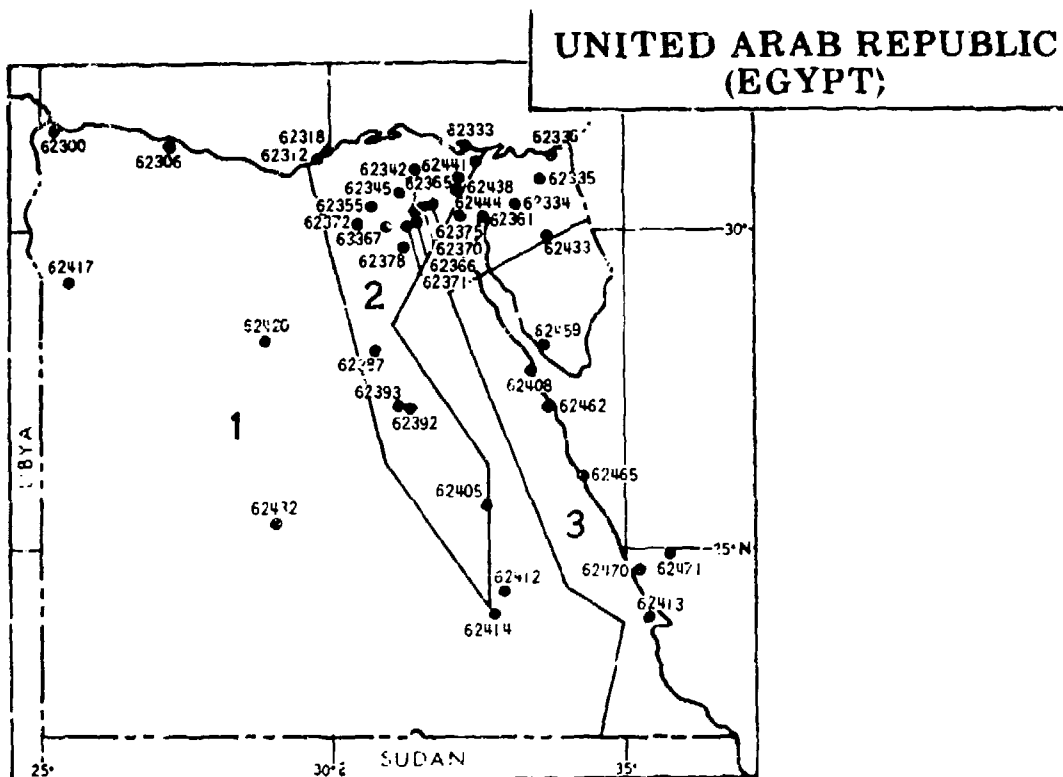


Figure F-20. Station locations and climatic areas in United Arab Republic (Egypt). WMO Station Index Numbers refer to cities listed in Table F-2 (from U.S. Naval Weather Service, 1968).

REFERENCES

- U.S. Naval Weather Service, 1968: World-wide airfield summaries, vol. IX, part 1, Africa (northern half), 559 pp. (AD-682-915).
- U.S. Naval Weather Service, 1971a: World-wide airfield summaries, vol X, part 3, Europe (Alps and S.W. Europe), 383 pp. (AD-720-708).
- U.S. Naval Weather Service, 1971b: World-wide airfield summaries, vol. X, part 4, Europe (Mediterranean), 367 pp. (AD-720-160).
- U.S. Naval Weather Service, 1973: World-wide airfield summaries, vol. XI, part 1, East Europe and U.S.S.R., 437 pp. (AD-776-611).
- U.S. Naval Weather Service, 1974a: World-wide airfield summaries, vol. II, part 1 (Revised) Middle East, 277 pp. (AD/A-002-162).
- U.S. Naval Weather Service, 1974b: World-wide airfield summaries, vol. II, part 2 (Revised), Middle East, 338 pp. (AD/A-002-163).

APPENDIX G

NORMAL PRESSURE TENDENCIES AT SYNOPTIC HOURS IN THE MEDITERRANEAN (REITER, 1971)

1. BACKGROUND

The pronounced diurnal variation of pressure in the Mediterranean and lower latitudes makes the analysis of synoptic charts and the estimation of the movement of isobaric features complicated. This variation has been analyzed in diurnal and semi-diurnal components which have been studied in detail by various authorities. The semi-diurnal component has been shown to be fairly regular at or near sea level; its amplitude decreases with increase of latitude and with altitude above MSL. The diurnal component is more pronounced inland and at high altitudes. It is also irregular and sensitive to diurnal variations of temperature and, hence, to local variations of cloudiness, rain belts and other weather factors. Over the sea, however, both components are regular, although in landlocked waters, even as extensive as the Mediterranean, seasonal fluctuations are observed.

The need has long been felt for tables or charts of representative normals of the pressure tendency at synoptic hours as an aid to forecasting. The attached maps, Figures G-1 through G-32, are designed to show representative normals of pressure tendency at all the current synoptic hours between latitudes 30N and 45N. There are four sets of eight charts, one for each season: Spring (March-May), Summer (June-August), Autumn (September-November) and Winter (December-February). Isopleths are drawn (at intervals of 0.2 mb) as dashed lines for falling tendencies and as continuous lines for rising tendencies.

2. GENERAL NOTES

The following notes give some of the principles used in the construction of the charts and explain some of the dominant features:

- (a) As a result of the large diurnal amplitude of temperature which produces a large amplitude of pressure tendency in inland areas (especially over North Africa), the isopleths, notably on the mid-day and evening charts, tend to follow the coast. The modifying influence of the sea is thus clearly apparent.

- (b) Where the coverage of observations over high ground (e.g., over N. Africa) was obviously inadequate, no attempt was made to allow for the effect of the high ground on the pressure tendency.
- (c) Inland daily tendencies are likely to be greater than normal in cloudless weather and less than normal when clouds and precipitation prevail. When using the charts for these regions, therefore, interpolation between isopleths must be carefully done.
- (d) Two stations in the Azores (08503 and 08512) for which data were available are tabled in the upper left-hand corner of the charts. Since these two stations are off the maps, they are not included in the analysis.

3. SOURCES OF DATA

The following sources of data have been used:

- (a) Gibraltar Met. Mag., 87, p. 294, 1958.
- (b) Algerian Stations Weather in the Med., Vol. III.
- (c) Marseilles, Malta Weather in the Med., Vol. I (New Editions).
- (d) Italian Stations, Sardinia Rivista di Met. Aero., XVII, No. 3, p. 3, Rome 1957.
- (e) Spanish Stations (including Mahon), Egyptian, Turkish and Levantine Stations Data worked up from Hofmeyr, W.J., Notos, 7, p. 6, Pretoria, 1958.
- (f) Sea Areas Jameson, H., M.O. Prof. Note No. 105, 1952 and Netherlands Atlas (Mediterranean).

Inconsistencies have inevitably arisen between those reports and in some cases have been difficult to resolve. It has been necessary to ignore almost completely the Dutch observations. Those from Malta were supplemented by two other sets of observations recorded in manuscript notes, but it has been difficult to fit them all into certain charts. The coverage of observations is fairly good except over the Balkans and Libya. Supplementary values for Nicosia and Tobruk have been obtained by averaging the daily tendencies recorded in Daily Weather Reports by these stations over a period of about four years.

REFERENCE

Reiter, E.R., 1971: Digest of selected weather problems of the Mediterranean. NAVWEARSCHFAC Tech. Paper No. 9-71.

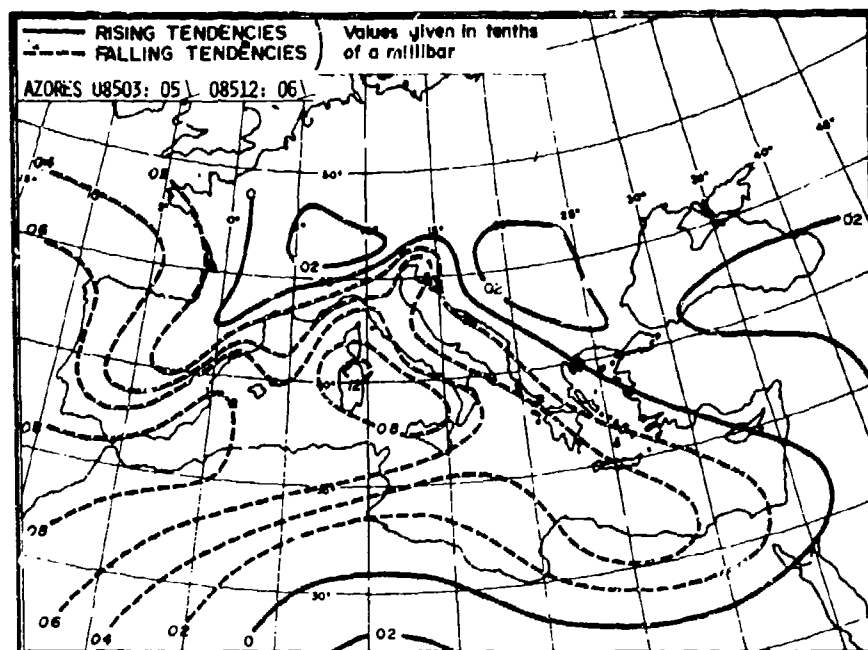


Figure G-1. Three-hourly normal pressure tendencies between 0000 GMT and 0300 GMT (valid at 0300 GMT) Spring.

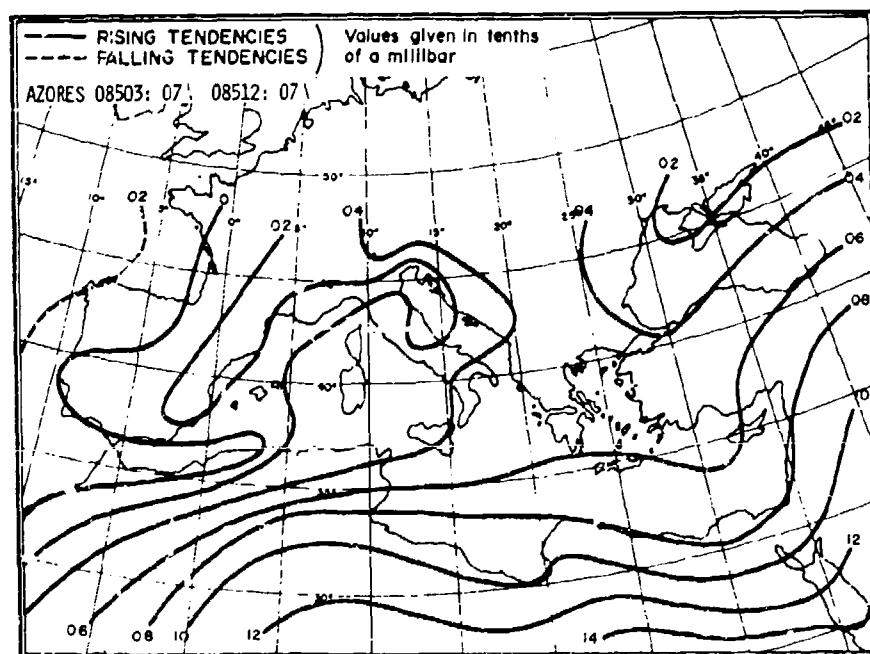


Figure G-2. Three-hourly normal pressure tendencies between 0300 GMT and 0600 GMT (valid at 0600 GMT) Spring.

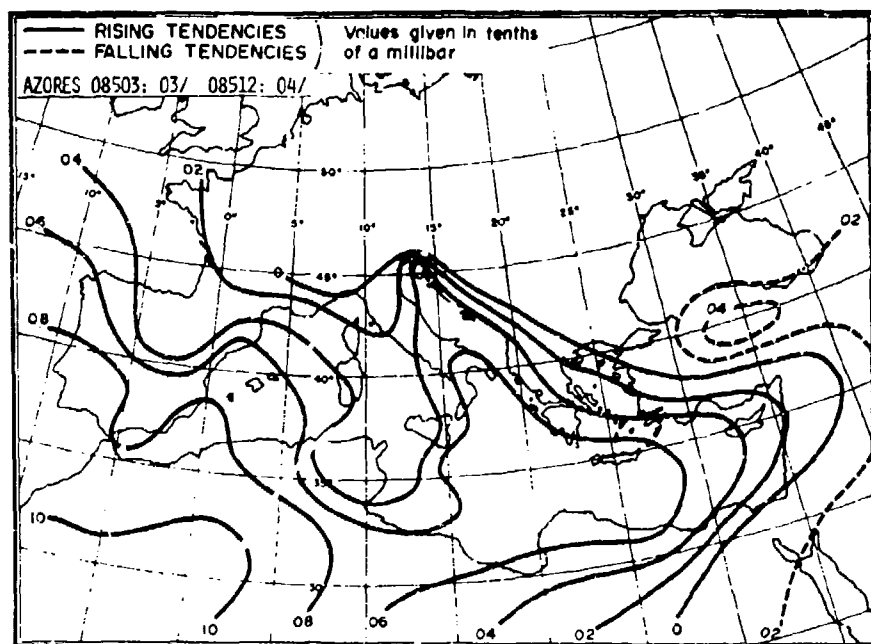


Figure G-3. Three-hourly normal pressure tendencies between 0600 GMT and 0900 GMT (valid at 0900 GMT) Spring.

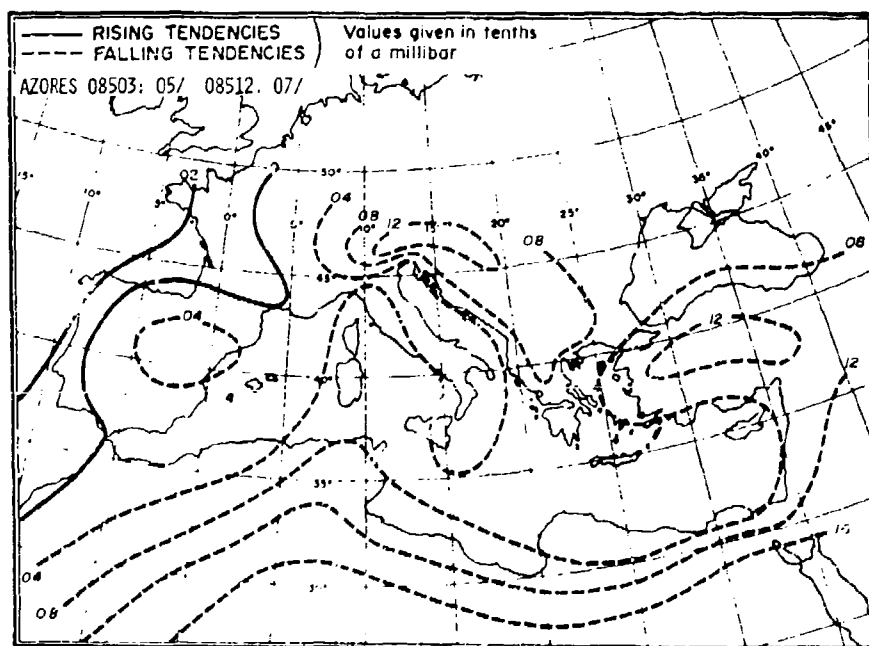


Figure G-4. Three-hourly normal pressure tendencies between 0900 GMT and 1200 GMT (valid at 1200 GMT) Spring.

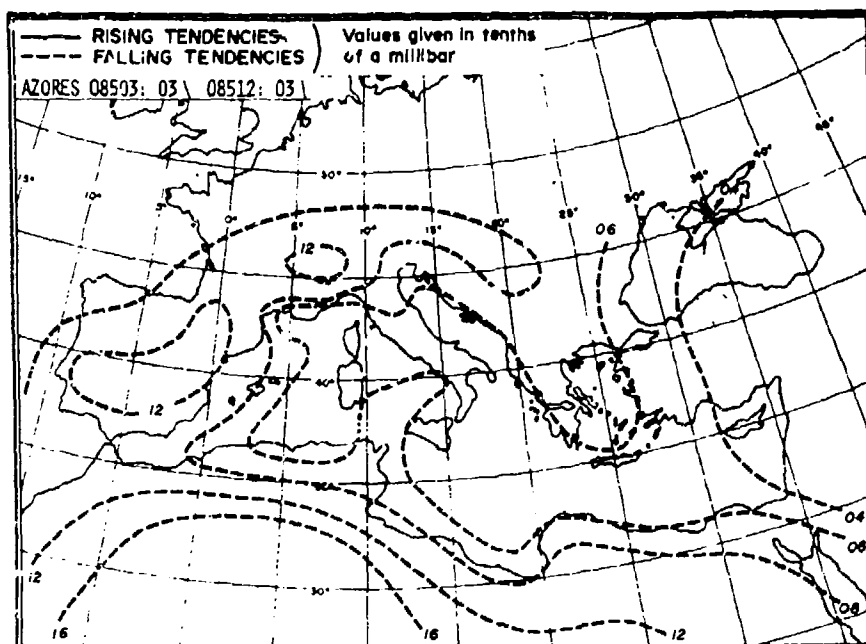


Figure G-5. Three-hourly normal pressure tendencies between 1200 GMT and 1500 GMT (valid at 1500 GMT) Spring.

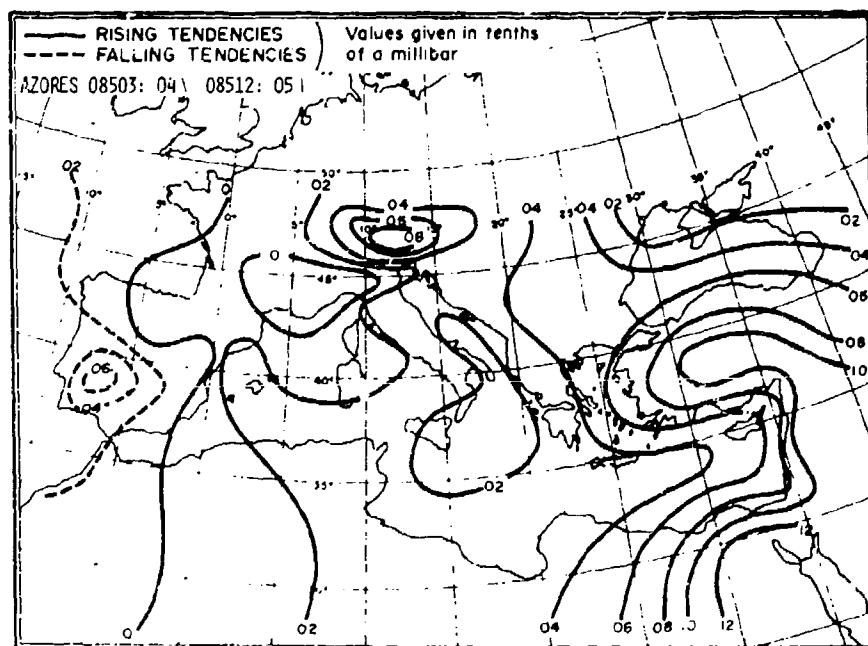


Figure G-6. Three-hourly normal pressure tendencies between 1500 GMT and 1800 GMT (valid at 1800 GMT) Spring.

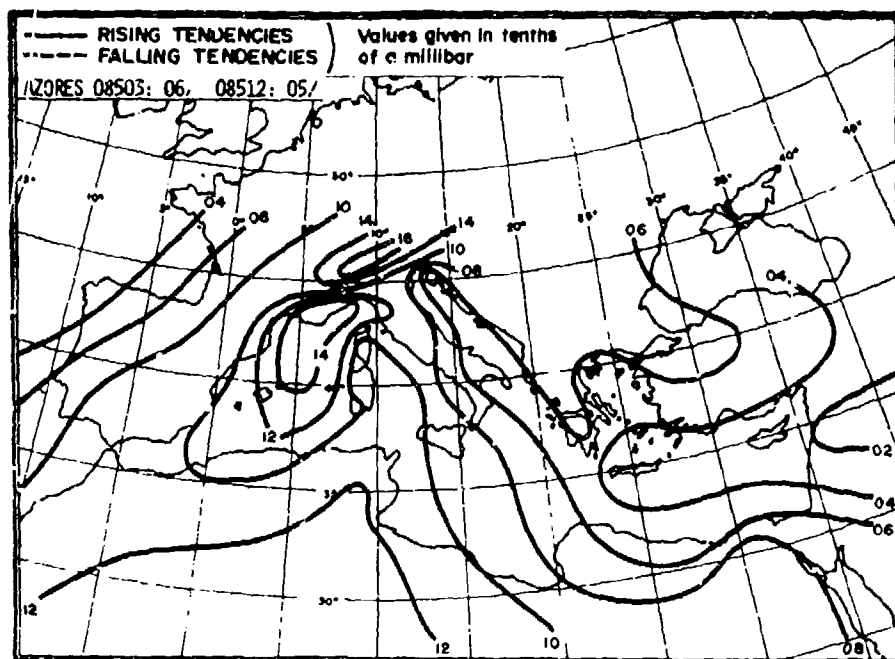


Figure G-7. Three-hourly normal pressure tendencies between 1800 GMT and 2100 GMT (valid at 2100 GMT) Spring.

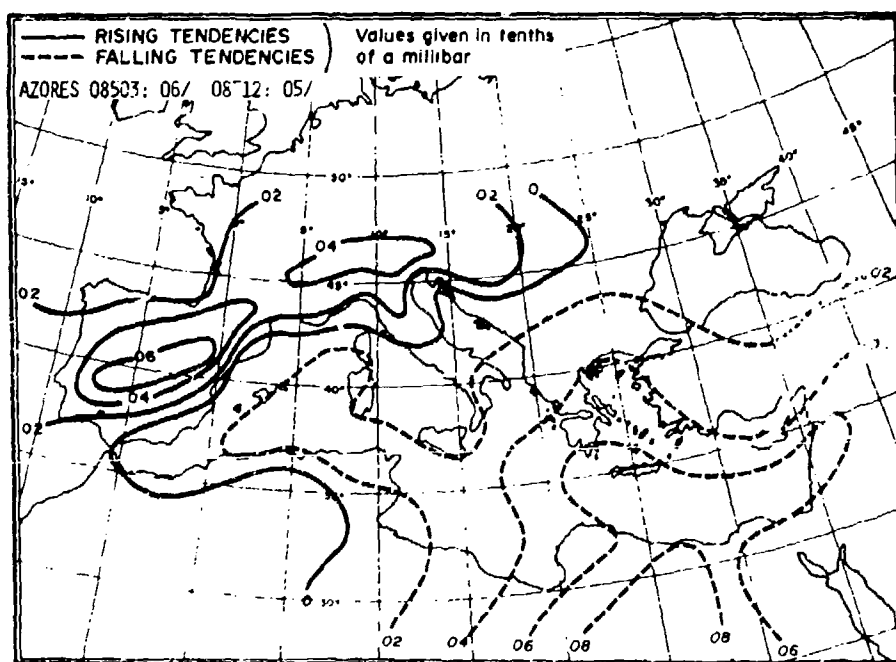


Figure G-8. Three-hourly normal pressure tendencies between 2100 GMT and 0000 GMT (valid at 0000 GMT) Spring.

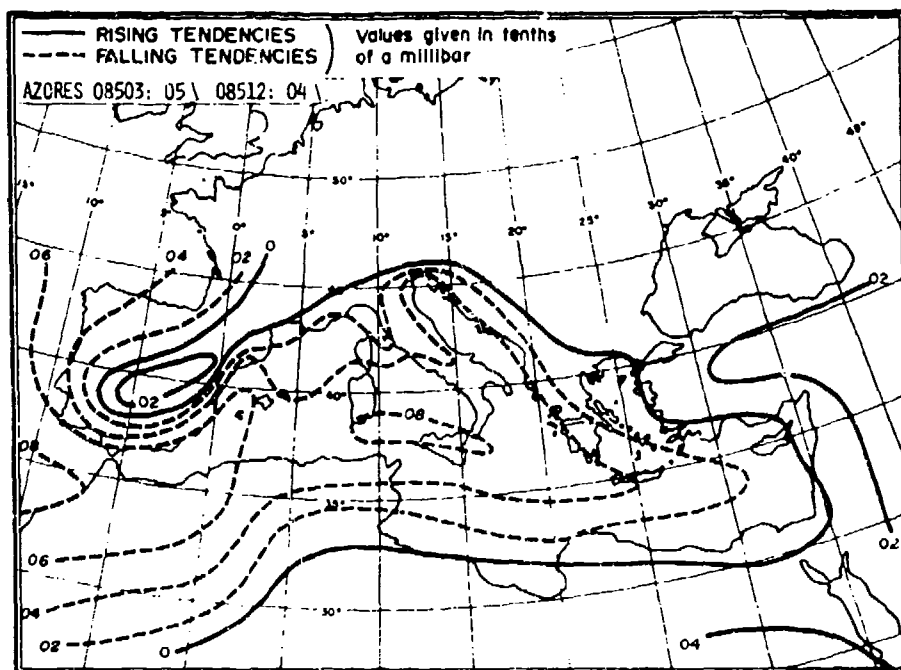


Figure G-9. Three-hourly normal pressure tendencies between 0000 GMT and 0300 GMT (valid at 0300 GMT) Summer.

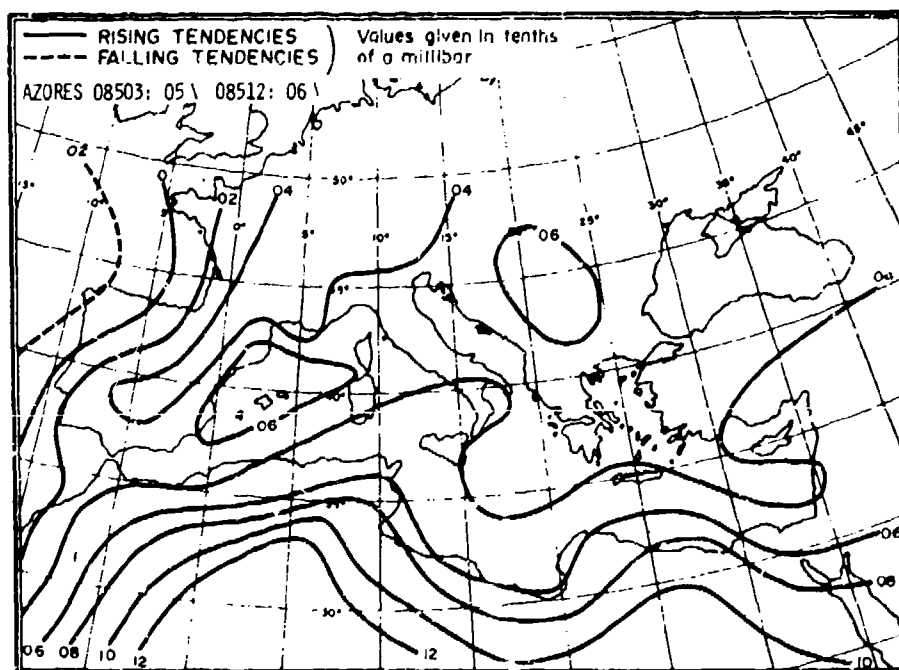


Figure G-10. Three-hourly normal pressure tendencies between 0300 GMT and 0600 GMT (valid at 0600 GMT) Summer.

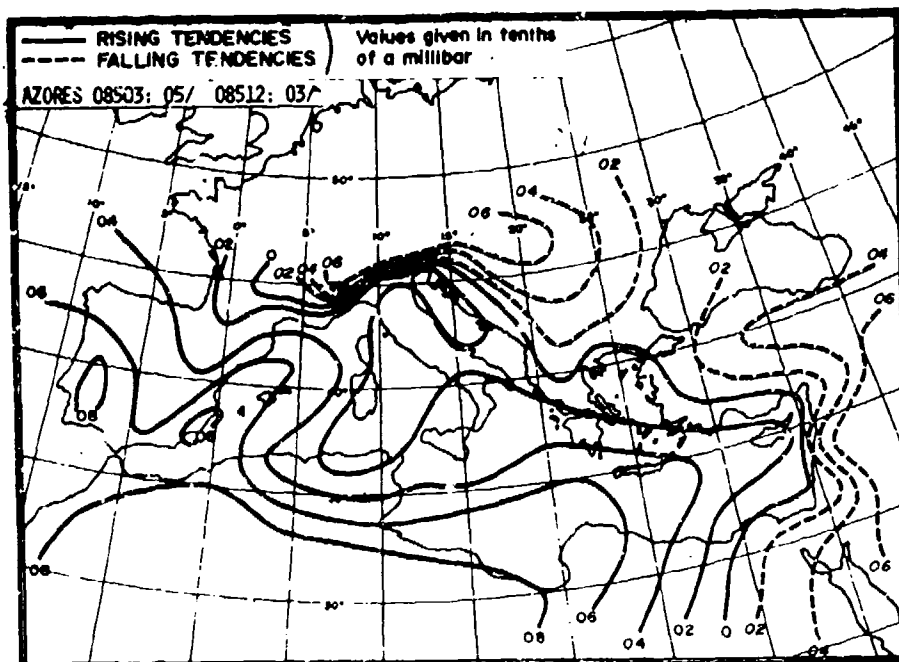


Figure G-11. Three-hourly normal pressure tendencies between 0600 GMT and 0900 GMT (valid at 0900 GMT) Summer.

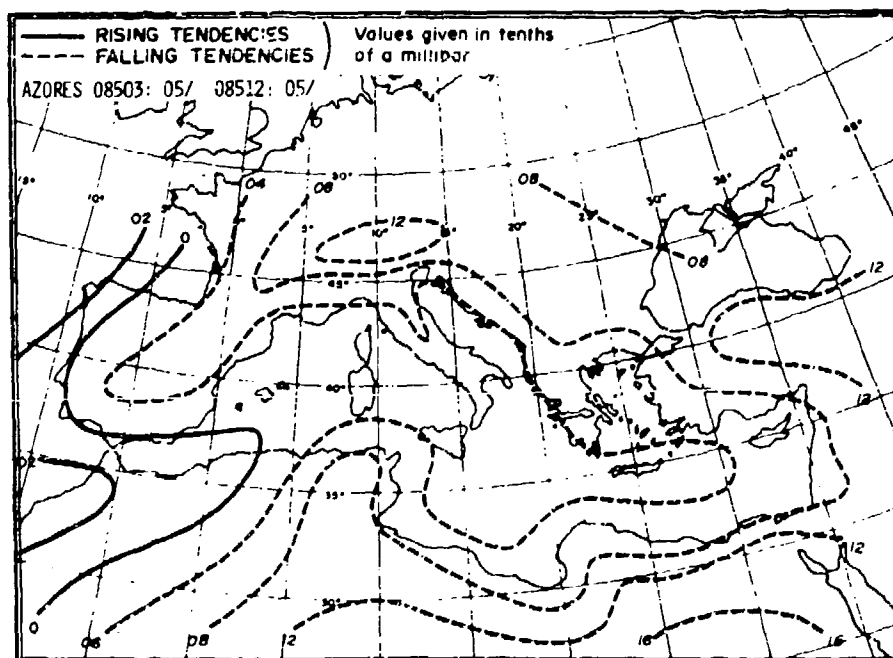


Figure G-12. Three-hourly normal pressure tendencies between 0900 GMT and 1200 GMT (valid at 1200 GMT) Summer.

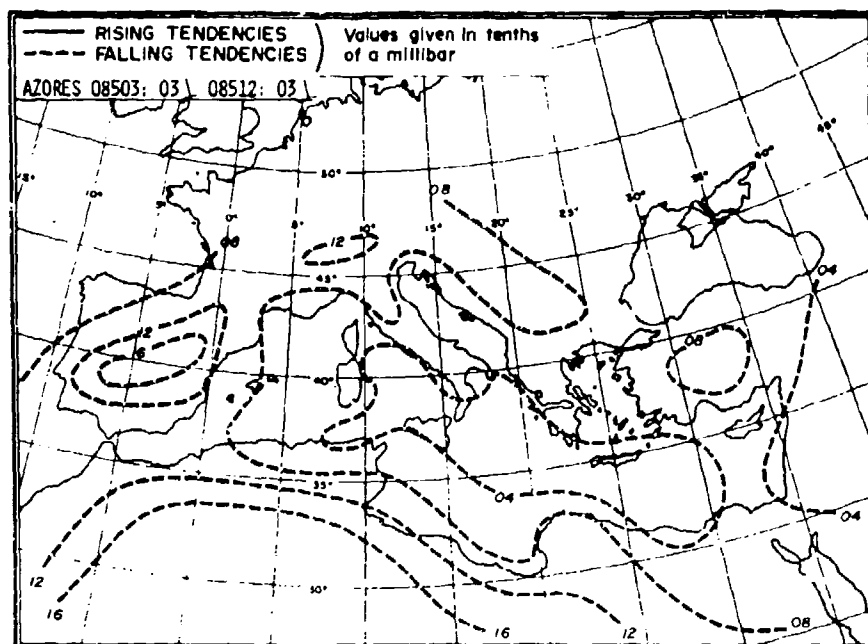


Figure G-13. Three-hourly normal pressure tendencies between 1200 GMT and 1500 GMT (valid at 1500 GMT) Summer.

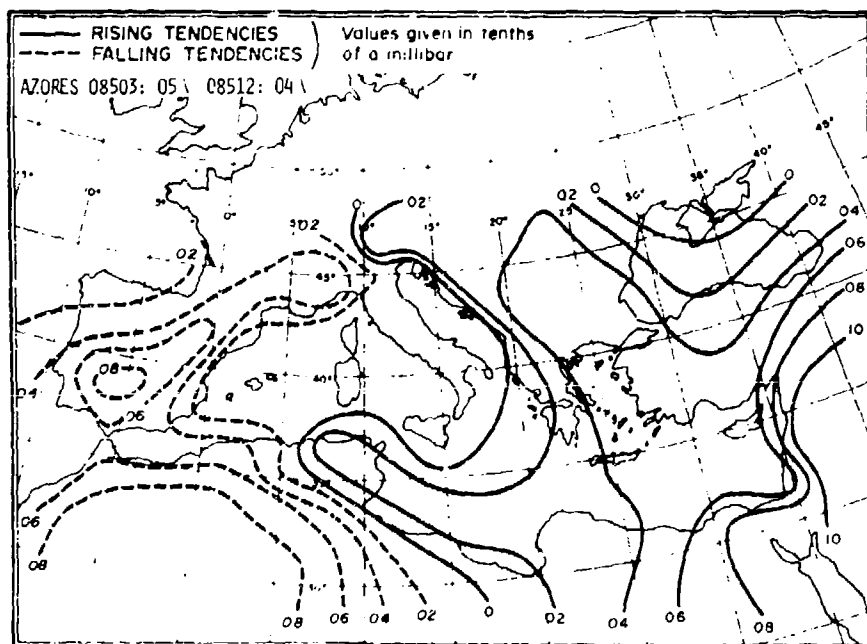


Figure G-14. Three-hourly normal pressure tendencies between 1500 GMT and 1800 GMT (valid at 1800 GMT) Summer.

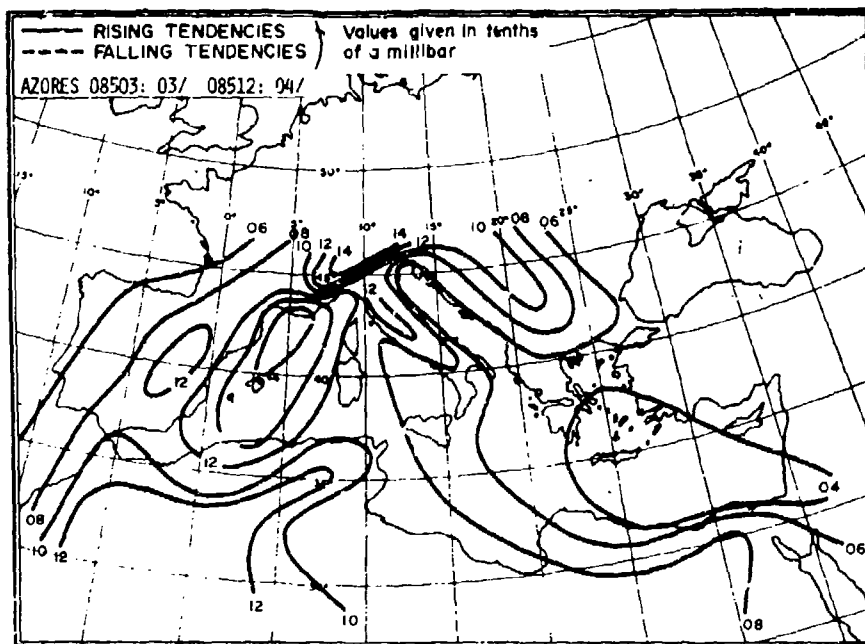


Figure G-15. Three-hourly normal pressure tendencies between 1800 GMT and 2100 GMT (valid at 2100 GMT) Summer.

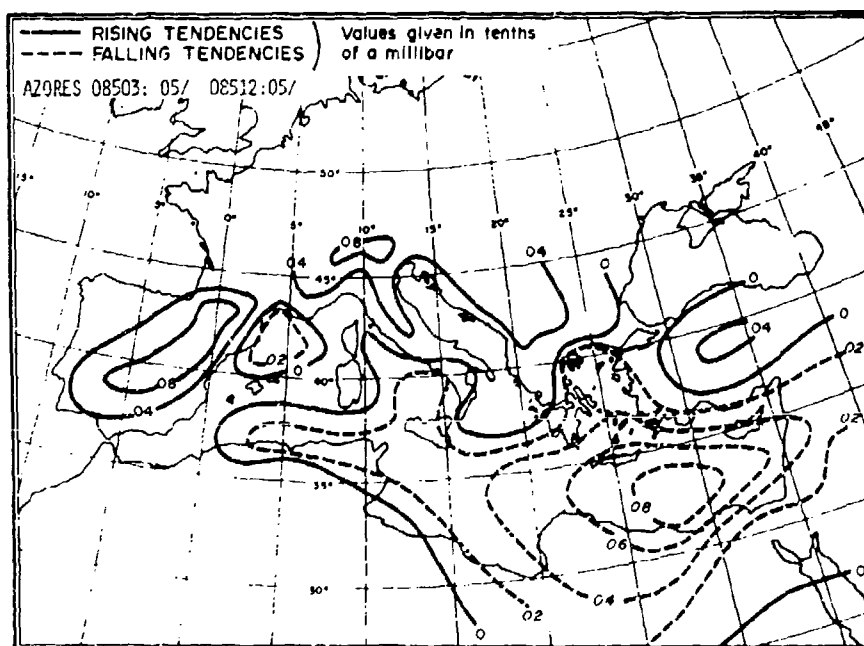


Figure G-16. Three-hourly normal pressure tendencies between 2100 GMT and 0000 GMT (valid at 0000 GMT) Summer.

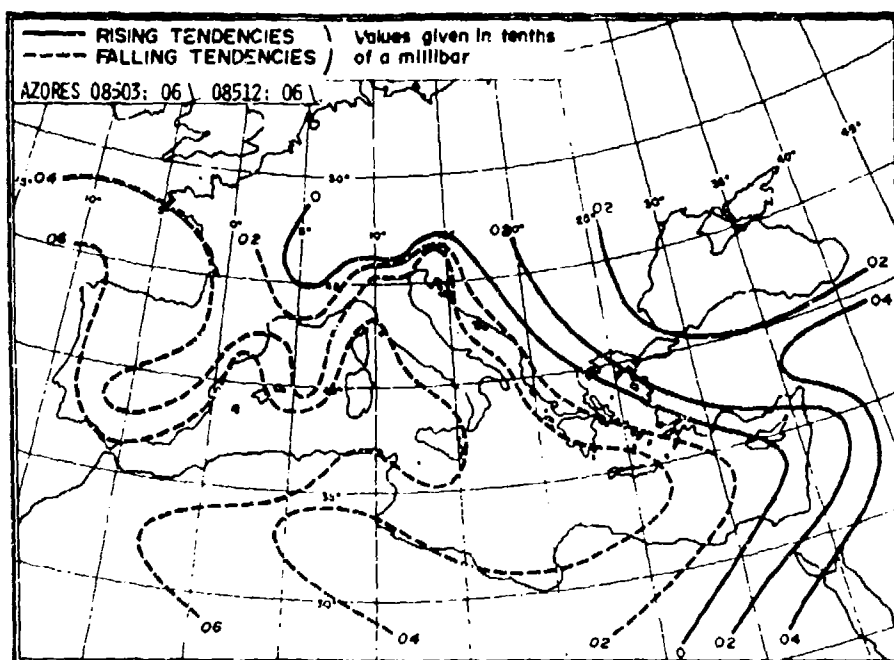


Figure G-17. Three-hourly normal pressure tendencies between 0000 GMT and 0300 GMT (valid at 0300 GMT) Autumn.

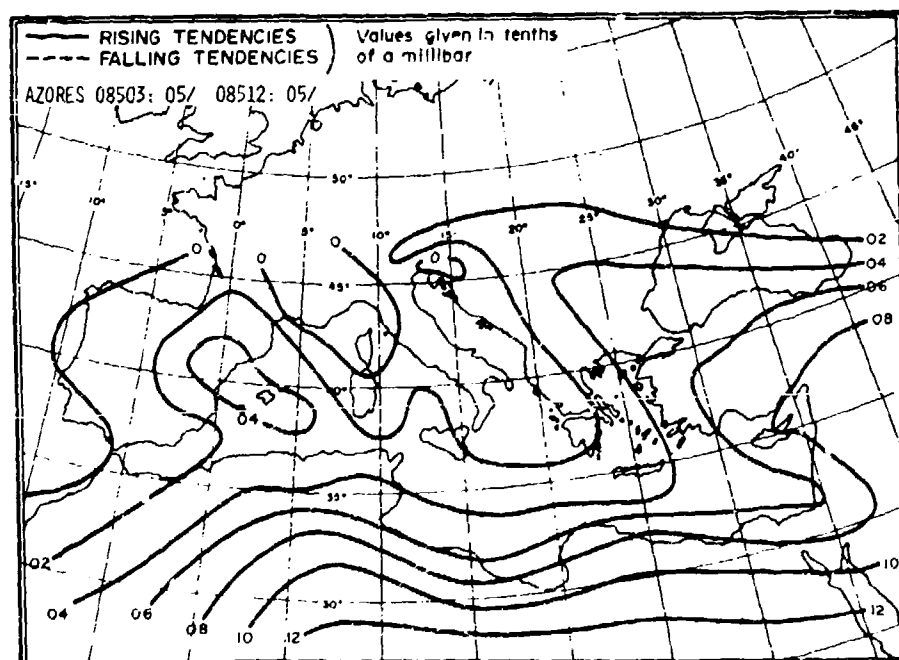


Figure G-18. Three-hourly normal pressure tendencies between 0300 GMT and 0600 GMT (valid at 0600 GMT) Autumn.

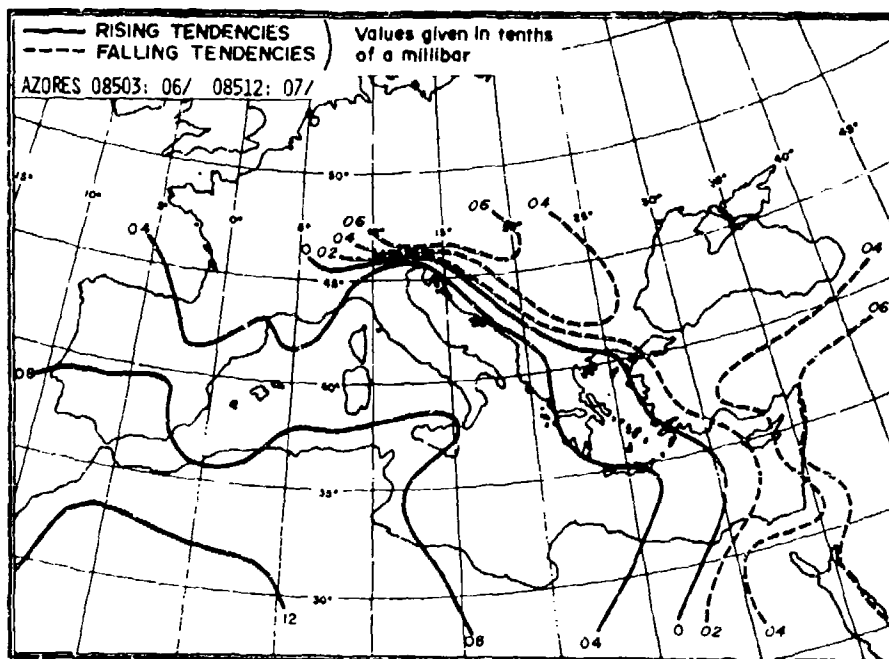


Figure G-19. Three-hourly normal pressure tendencies between 0600 GMT and 0900 GMT (valid at 0900 GMT) Autumn.

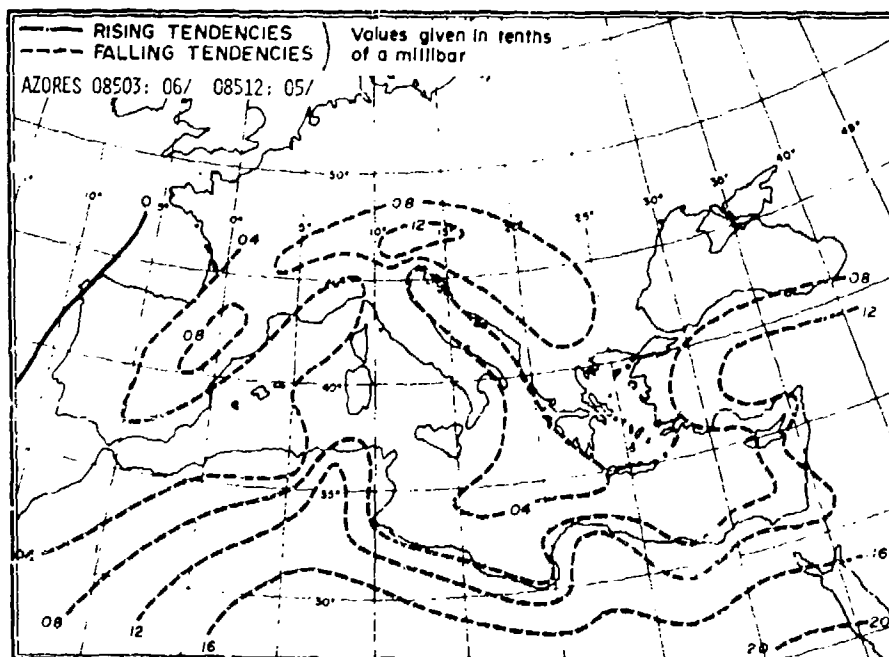


Figure G-20. Three-hourly normal pressure tendencies between 0900 GMT and 1200 GMT (valid at 1200 GMT) Autumn.

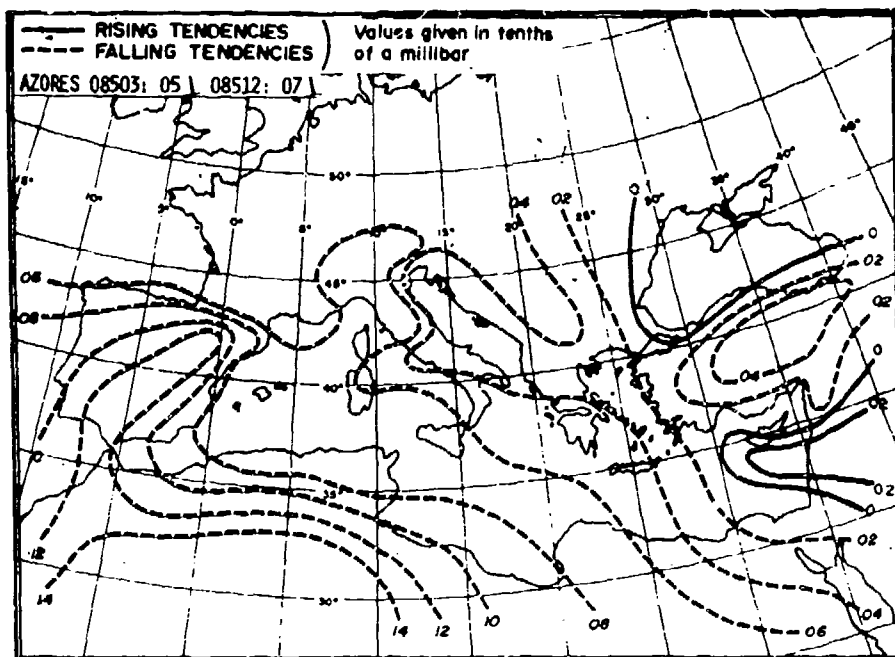


Figure G-21. Three-hourly normal pressure tendencies between 1200 GMT and 1500 GMT (valid at 1500 GMT) Autumn.

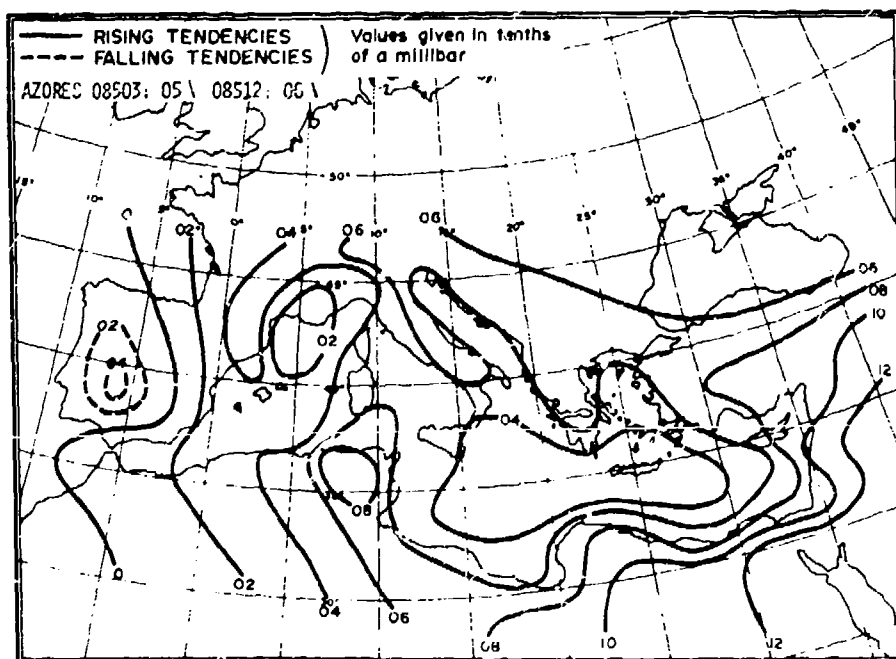


Figure G-22. Three-hourly normal pressure tendencies between 1500 GMT and 1800 GMT (valid at 1800 GMT) Autumn.

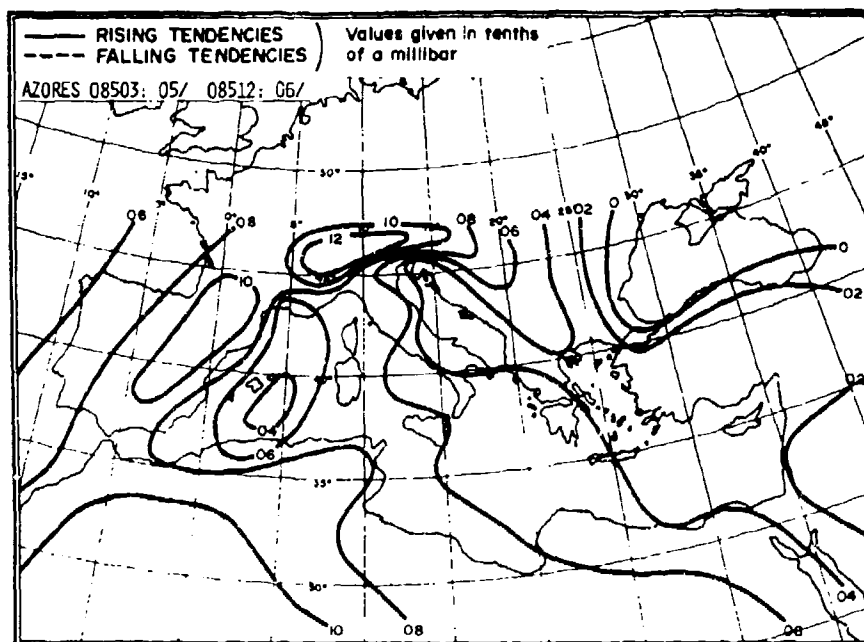


Figure G-23. Three-hourly normal pressure tendencies between 1800 GMT and 2100 GMT (valid at 2100 GMT) Autumn.

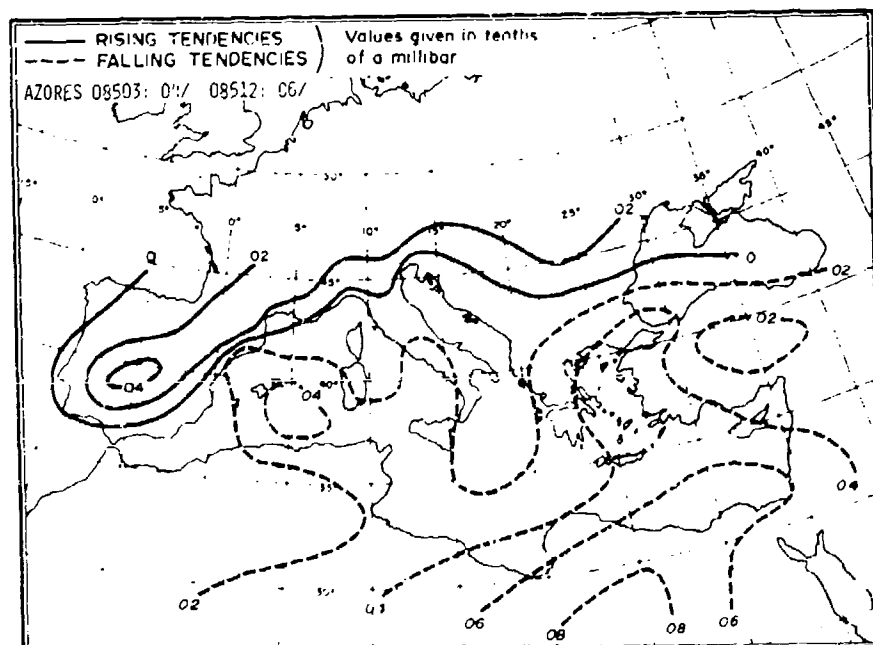


Figure G-24. Three-hourly normal pressure tendencies between 2100 GMT and 0000 GMT (valid at 0000 GMT) Autumn.

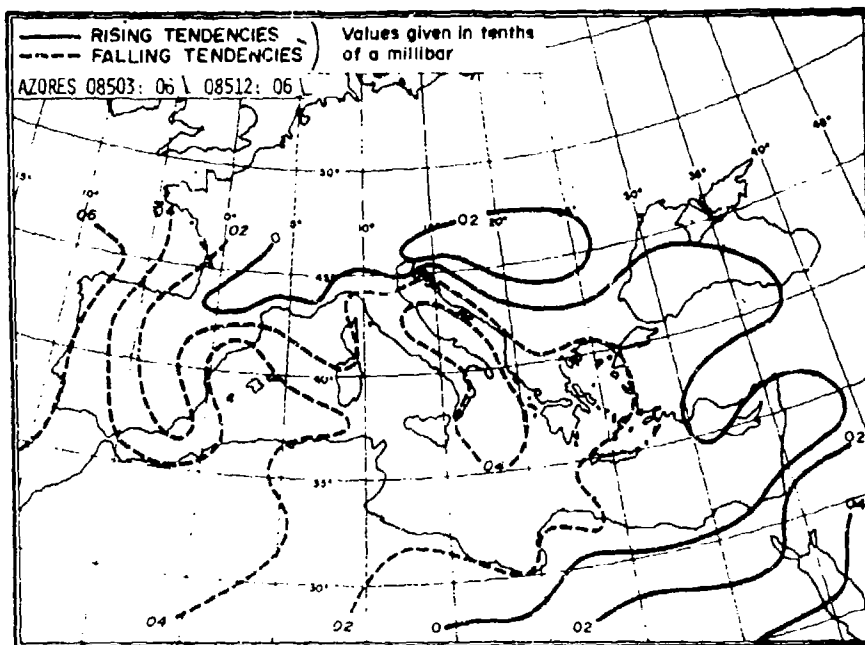


Figure G-25. Three-hourly normal pressure tendencies between 0000 GMT and 0300 GMT (valid at 0300 GMT) Winter.

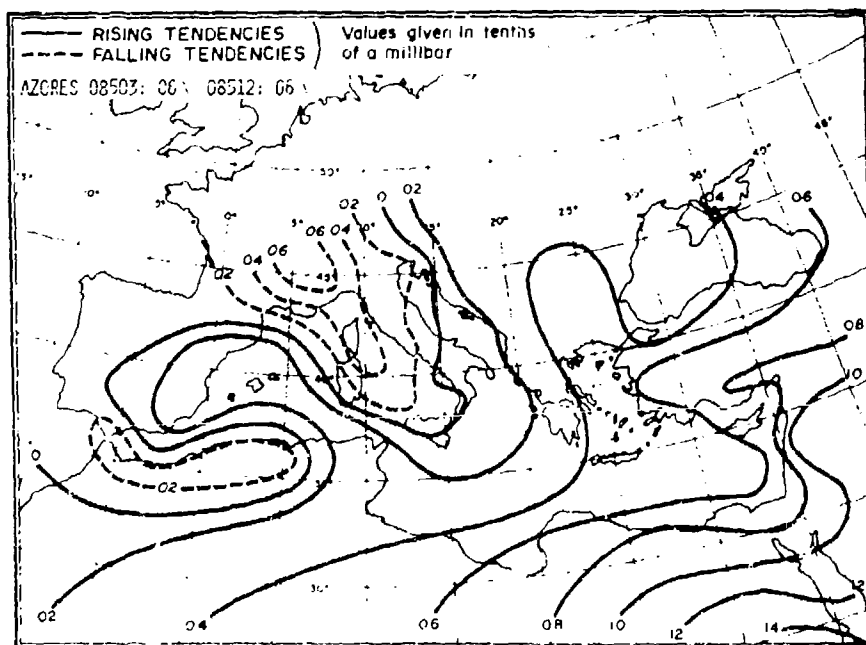


Figure G-26. Three-hourly normal pressure tendencies between 0300 GMT and 0600 GMT (valid at 0600 GMT) Winter.

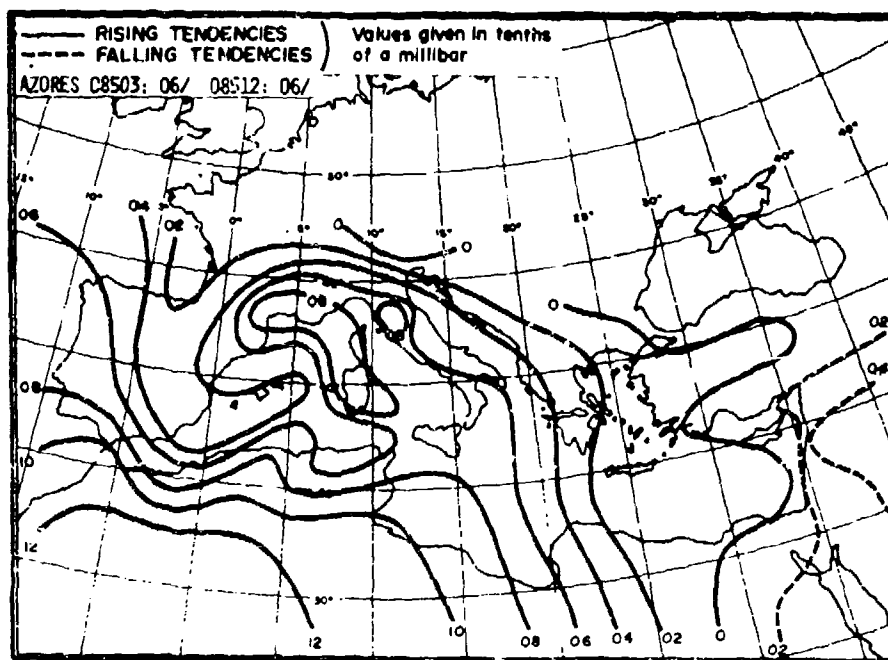


Figure G-27. Three-hourly normal pressure tendencies between 0600 GMT and 0900 GMT (valid at 0900 GMT) Winter.

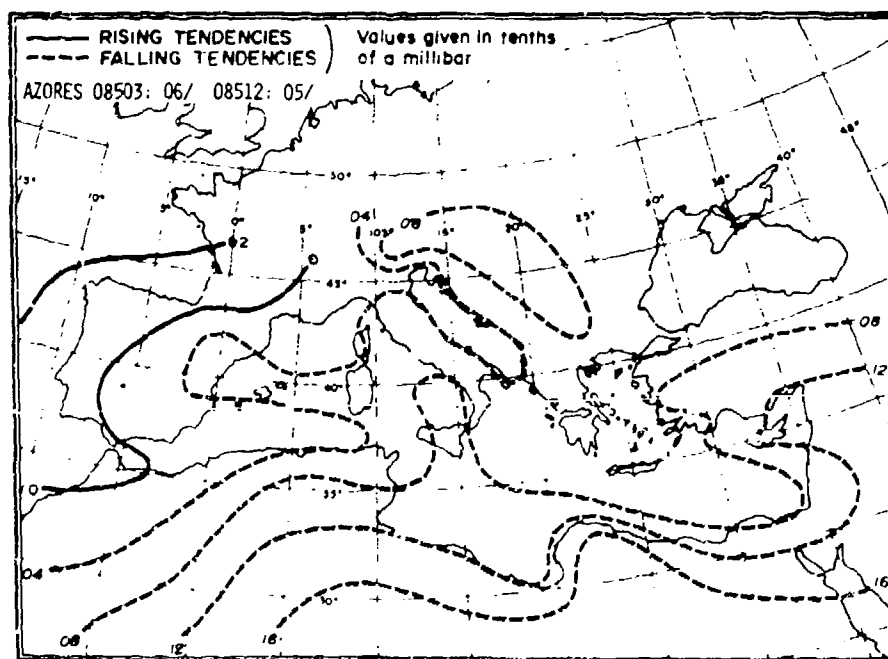


Figure G-28. Three-hourly normal pressure tendencies between 0900 GMT and 1200 GMT (valid at 1200 GMT) Winter.

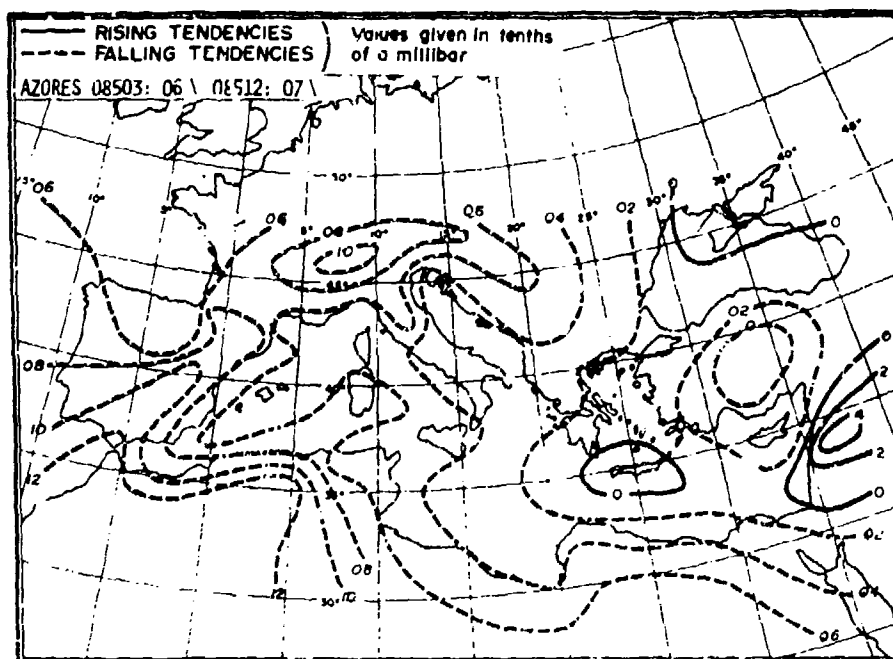


Figure G-29. Three-hourly normal pressure tendencies between 1200 GMT and 1500 GMT (valid at 1500 GMT) Winter.

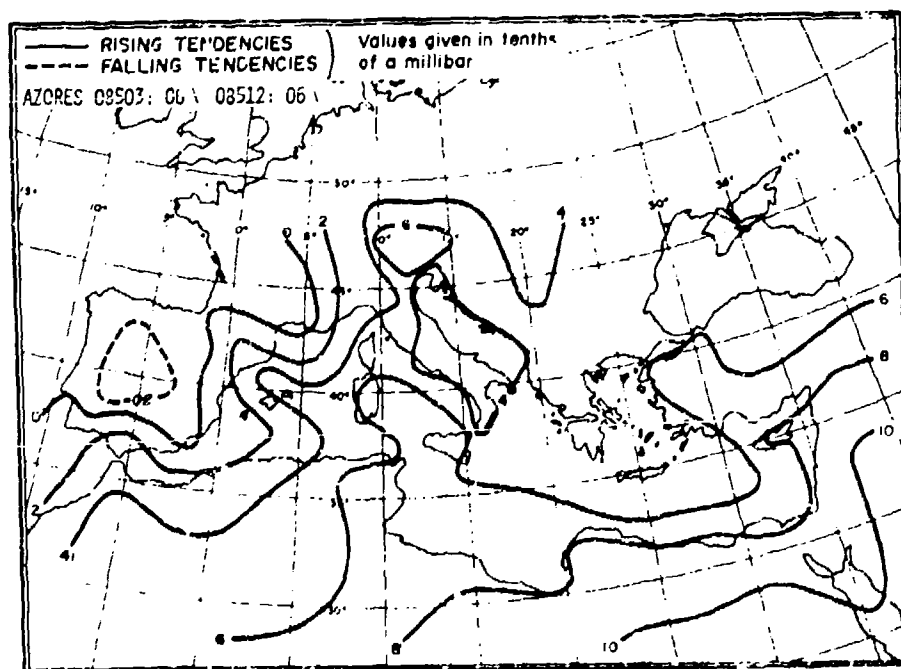


Figure G-30. Three-hourly normal pressure tendencies between 1500 GMT and 1800 GMT (valid at 1800 GMT) Winter.

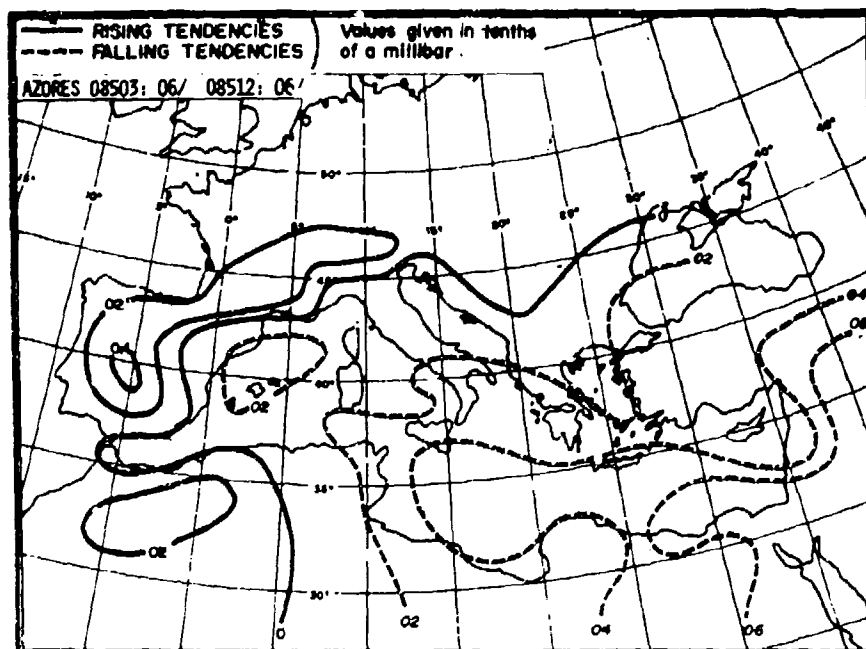


Figure G-31. Three-hourly normal pressure tendencies between 1800 GMT and 2100 GMT (valid at 2100 GMT) Winter.

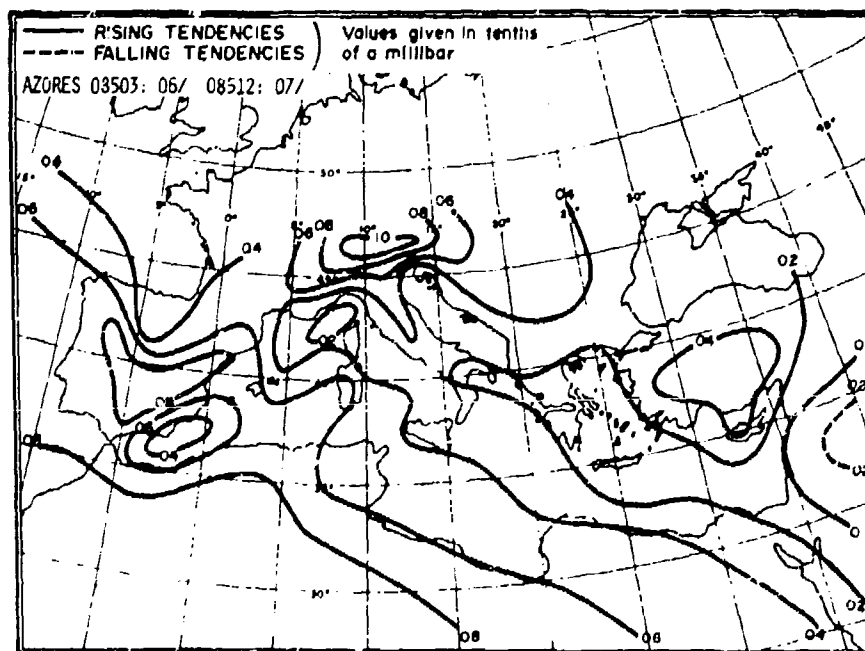


Figure G-32. Three-hourly normal pressure tendencies between 2100 GMT and 0000 GMT (valid at 0000 GMT) Winter.

APPENDIX H

METEOROLOGICAL UNITS, CONVERSION FORMULAS AND SCALES

Table H-1. Meteorological units and conversion formulas.

Current Units in Common Use		International System of Units (SI)		
Name	Symbol	Conversion Formula	Symbol	Name
<u>Temperature</u>				
degree Celsius degree Fahrenheit	°C °F	°C+273 = °K 5/9 °F+255.22 = °K	°K	degree Kelvin
<u>Pressure</u>				
bar	bar	1 bar = 10 ⁻¹ MPa = 10 ² kPa = 10 ⁵ Nm ⁻²	MPa kPa Nm ⁻²	megapascal kilopascal newton per meter squared
millibar	mb	1 mb = 10 ⁻¹ kPa = 10 ² Nm ⁻²		
standard atmosphere	atm	1 atm = 101.325 kPa		
mm mercury (Hg)	torr	1 torr = 0.133322 kPa		
inch mercury (Hg)		1 in Hg = 3.38639 kPa		
<u>Length</u>				
nautical mile	n mi	1 n mi = 1852 m	m	meter
statute mile	mi	1 mi = 1609 m		
<u>Velocity</u>				
mile per hour	mile h ⁻¹	1 mile h ⁻¹ = 1.609 km h ⁻¹	km h ⁻¹	kilometer per hour
knot	kt	1 kt = 1.852 km h ⁻¹ = 0.514 m sec ⁻¹		
meter per second	m sec ⁻¹	1 m sec ⁻¹ = 3.6 km h ⁻¹		

Table H-2. The Beaufort wind scale.

Beaufort Number	Knots	Kilometers Per Hour	Description	Effect at Sea
0	0-0.9	0-1.9	Calm	Sea like a mirror.
1	1-3	2-6	Light air	Scale-like ripples form, but without foam crests.
2	4-6	7-11	Light breeze	Small wavelets, short but more pronounced. Crests have a glassy appearance and do not break.
3	7-10	12-19	Gentle breeze	Large wavelets. Crests begin to break. Foam has glassy appearance. Perhaps scattered white horses.
4	11-16	20-30	Moderate breeze	Small waves, becoming longer. Fairly frequent white horses.
5	17-21	31-39	Fresh breeze	Moderate waves, taking a more pronounced long form. Many white horses are formed. Chance of some spray.
6	22-27	40-50	Strong breeze	Large waves begin to form. White foam crests are more extensive everywhere. Some spray.
7	28-33	51-61	Moderate gale	Sea heaps up and white foam from breaking waves begins to be blown in streaks along the direction of the wind. Spindrift begins.
8	34-40	62-74	Fresh gale	Moderately high waves of greater length. Edges of crests break into spindrift. Foam is blown in well marked streaks along the direction of the wind.
9	41-47	75-87	Strong gale	High waves. Dense streaks of foam along the direction of the wind. Sea begins to roll. Spray may affect visibility.

Table H-2 (continued)

Beaufort Number	Knots	Kilometers Per Hour	Description	Effect at Sea
10	48-55	88-102	Whole gale and/or storm	Very high waves with long overhanging crests. The resulting foam in great patches is blown in dense white streaks along the direction of the wind. On the whole, the surface of the sea takes a white appearance. The rolling of the sea becomes heavy and shocklike. Visibility is affected.
11	56-63	103-117	Storm and/or violent storm	Exceptionally high waves. Small- and medium-sized vessels might for a long time be lost to view behind the waves. The sea is completely covered with long white patches of foam lying along the direction of the wind. Everywhere, the edges of the wave crests are blown into froth. Visibility seriously affected.
12	64 or higher	118 or higher	Hurricane or typhoon	The air is filled with foam and spray. Sea is completely white with driving spray. Visibility is very seriously affected.